Doctoral theses at NTNU, 2024:54

Lucas Braakhuis

Development of Solvent Degradation Models for Amine-Based CO_2 Capture

Doctoral thesis

NTNU
Norwegian University of Science and Technology
Thesis for the Degree of
Philosophiae Doctor
Faculty of Natural Sciences
Department of Chemical Engineering

NTNU
Norwegian University of
Science and Technology

Lucas Braakhuis

Development of Solvent Degradation Models for Amine-Based CO_2 Capture

Thesis for the Degree of Philosophiae Doctor

Trondheim, February 2024

Norwegian University of Science and Technology
Faculty of Natural Sciences
Department of Chemical Engineering

NTNU
Norwegian University of
Science and Technology

NTNU
Norwegian University of Science and Technology

Thesis for the Degree of Philosophiae Doctor

Faculty of Natural Sciences
Department of Chemical Engineering

ISBN 978-82-326-7708-5 (printed ver.)
ISBN 978-82-326-7707-8 (electronic ver.)
ISSN 1503-8181 (printed ver.)
ISSN 2703-8084 (online ver.)

Doctoral theses at NTNU, 2024:54

Printed by NTNU Grafisk senter

Abstract

Carbon capture and storage can be essential for achieving short-term emission reductions to reach climate goals and realizing the decarbonization of hard-to-abate sectors in the future. Aside from logistical and political hurdles to get the CO_2 from separation to sequestration, continuous improvement of the capture technology is required to make capture processes more efficient and reliable and prevent operational and economic challenges. A good understanding of solvent degradation mechanisms and the effectiveness of solvent management strategies is essential to achieve these goals. Therefore, this thesis focuses on developing solvent degradation models for amine-based CO_2 capture and their application to predict degradation behavior in capture plants.

Lab-scale experimental data on solvent degradation is used to develop degradation models for thermal and oxidative degradation of monoethanolamine (MEA), the most well-studied and characterized solvent for amine-based carbon capture. Both models accurately reflect degradation rates, thermal degradation product formation rates, and observed trends in the experiments as a function of experimental conditions. However, the models are characterized by relatively high deviations caused primarily by high experimental uncertainty.

More detailed reporting of experimental conditions, measured or expected uncertainties, and solvent composition during the experiments is required to improve the accuracy of the models. Furthermore, typical degradation reactors are unable to accurately replicate exposure conditions in the capture process, such as high O_2 mass transfer rates and temperature swings. Therefore, a new degradation reactor, which aims to overcome these challenges, is designed, constructed, and tested. The first results of degradation experiments in this setup are promising, showing a good control of experimental conditions, and indicating increased oxidation rates.

The developed degradation models are used to make predictions of degradation rates throughout the process, which agree with observations in smaller cyclic systems and pilot plants. Oxidative degradation is the most prominent mechanism and occurs primarily in the absorber packing. Therefore, absorber intercooling, which reduces the temperature in the absorber, significantly reduces overall degradation rates. The effectiveness of other degradation-reducing process modifications, such as dissolved O_2 removal or a reduction of residence times, depends on the flue gas composition and process-specific distribution of degradation throughout the plant.

The effect of dissolved metals on oxidative degradation rates of MEA is significant but the role of these metals is unclear. Modeling studies in this work show that quantification of the catalytic effect of metals and the impact of degradation product concentration on corrosion rates and metal solubility are likely to play a significant role. Therefore, additional experimental work is required to fill these knowledge gaps.

Although this work provides new, relevant insights into solvent degradation in CO_2 capture plants, it has proven challenging to develop a framework that can accurately represent the many complexities of solvent degradation, even for a well-characterized solvent.

Acknowledgments

First of all, thank you Hanna for your expertise, guidance, and hospitality during my research and time in Trondheim. The trust and freedom you gave me right from the start have allowed me to pursue my interests and develop myself optimally. Your wit and Finnish optimism were welcoming in times of experimental struggles and always convinced me to go back to the lab and solve the challenges. I hope we stay in touch and can continue to collaborate.

I would also like to thank my colleagues and friends in the department and those in the EEART group. Your support and discussions about our research (and about topics both less and more serious than CO_2 capture and the end of the world) were a welcoming distraction from my work. The lunch, cake breaks, potlucks, and other social activities were always something I looked forward to and will miss.

I want to thank the world's best office mates, Eirini, Bahar, Karen, Maxime, and Lukas, for the time I shared with you in the office. I hope you can forgive me for all the times I distracted you from your work by asking questions voicing my complaints or talking about something completely irrelevant that just happened to cross my mind. I appreciate your input and discussions and how those also contributed to the discussions in this thesis, and I hope my help was likewise. Despite never sharing an office, special thanks go out to Vanja for always making time to answer questions and helping me out. In addition, I want to thank all the partners in the NCCS task group, especially the people at SINTEF Industry and TNO, for their support.

To the students working for an internship or on their thesis, I want to thank you for your efforts and contributions. It was a pleasure to supervise you and I appreciate all the discussions and new insight you have brought to the table. Special gratitude goes out to Trygve and Emanuele for your excellent help in building, testing, and running the new degradation setup. I would also like to acknowledge Mikael, Gøril, Merethe, Ketil, and Marius. Your help, expertise, and support are what keep the wheels turning in the department and were indispensable for my activities in the lab.

Finally, I want to express my gratitude to my parents, family, and friends for their support along the way. To my parents, Gerard and Jantine, for raising me to who I have become and supporting me regardless of my wishes and ambitions, even if that meant moving to Trondheim. To my brother, Allard, for our contact during the pandemic, the adventures during your visit to Trondheim, and for all the unfair proofreading deals. And to my friends, for the hiking/biking/skiing/swimming/fishing trips, floorball, board games, quizzes, and all other adventures in and around Trondheim. It was a pleasure sharing these moments with you.

Table of Contents

Table of Figures

Nomenclature

Constants and Variables

α	mol CO_2/mol MEA	CO_2 loading
a_{int}	m^2/m^3	interfacial area
c	mol/m^3	molar concentration
$\overline{c}$	mol/m^3	average molar concentration
$\hat{c}$	mol/m^3	modeled molar concentration
c_I	mol/m^3	liquid interface concentration
c_L	mol/m^3	liquid (bulk) concentration
ΔH_r	J/mol	enthalpy of reaction
δ_L	m	thickness of liquid mass transfer layer
D	m^2/s	diffusion coefficient
d_b	m	bubble diameter
ϵ_A	mol/m^3	expected analytical error
ϵ_L	m^3/m^3	liquid volume fraction
E_A	J/mol	activation energy
F^*	-	F-statistic
h	$m^3/kmol$	ion specific solubility parameter
f_{HSS}	-	HSS correction factor
h_G	$m^2/kmol$	gas-specific solubility parameter
h_T	$m^3/kmol/K$	temperature dependence of gas-specific parameter
Ha	-	Hatta number
Hi	-	Hinterland ratio
J	$mol/m^2/s$	mass transfer flux
k_L	m/s	liquid phase mass transfer coefficient
k_r	$(m^3/mol)^n/s$	reaction rate coefficient
k_{ref}	$(m^3/mol)^n/s$	reaction rate coefficient at T_{ref}
m	-	number of replicate sets
n	-	reaction/corrosion/solubility order
n	-	number of experimental measurements
n_r	-	number or replicate measurements
p	Pa, (atm, Eq. 4.4)	partial pressure

p	-	number of fitted parameters
P/V	W/m^3	stirring power per volume
ρ_L	kg/m^3	density of the liquid
R	mol/m^3/s	reaction rate
R_C	mol/m^2/s	corrosion rate
R_{cat}	mol/m^3/s	iron-catalyzed reaction rate
R_{id}	J/mol/K	ideal gas constant, 8.314
T	K	temperature
T_{ref}	K	reference temperature
V_L	m^3	liquid volume
V_R	m^3	reactor volume
ν	-	stoichiometric reaction coefficient
ν_L	m^2/s	kinematic viscosity of the liquid
w	-	weighing factor

Abbreviations

CCGT	combined cycle gas turbine
CCS	carbon capture and storage
COM	component object model
CSTR	continuously stirred tank reactor
DCC	direct contact cooler
EfW	energy-from-waste
GC-MS	gas chromatography and mass spectroscopy
HSS	heat-stable salts
ICP-MS	inductively coupled plasma mass spectrometry
IEA	international energy agency
IPCC	intergovernmental panel on climate change
LC-MS	liquid chromatography and mass spectroscopy
MSEP	mean pure experimental error
NCCS	Norwegian CCS research center
NDIR	non-dispersive infrared
PFR	plug flow reactor
PSO	particle swarm optimization
FTIR	Fourier transform infrared

SDR	solvent degradation rig (SINTEF)
SELOF	sum of errors due to lack of fit
SEP	sum of pure experimental errors
SMR	steam-methane reforming
SRD	specific reboiler duty
SSE	sum of square errors
TIC	total inorganic carbon
WTE	waste-to-energy

Chemical Compounds

Abbreviation	CAS registry	Name
4HEPO	23936-04-1	4-(2-hydroxyethyl)-piperazin-2-one
AEHEIA	1402137-23-8	N-(2-aminoethyl)-N'-(2-hydroxyethyl)-imidazolidinone
AMP	124-68-5	2-amino-2-methylpropanol
BHEOX	1871-89-2	N,N'-bis(2hydroxyethyl)-ethanediamide
BHEU	15438-70-7	1,3-bis(2-hydroxyethyl)-urea
DEA	111-42-2	diethanolamine
HEA	142-26-7	N-(2-hydroxyethyl)-acetamide
HEAEIA	1154942-78-5	N-[2-[(2-hydroxyethyl)amino]ethyl]imidazolidin-2-one
HEEDA	111-41-1	N-(2-hydroxyethyl)-ethylenediamine
HEF	693-06-1	N-(2-hydroxyethyl)-formamide
HEGly	5835-28-9	N-(2-hydroxyethyl)-glycine
HEI	1615-14-1	N-(2-hydroxyethyl)-imidazole
HEIA	3699-54-5	N-(2-hydroxyethyl)-2-imidazolidone
K_2CO_3	584-08-7	potassium carbonate
KOH	1310-58-3	potassium hydroxide
MDEA	105-59-9	N-methyl diethanolamine
MEA	141-43-5	monoethanolamine
$MEACOO^-$	-	MEA carbamate
MEACOOH	-	MEA carbamic acid
OZD	497-25-6	2-oxazolidinone
PZ	110-85-0	piperazine
TRIMEA	1965-29-3	N-(2-hydroxyethyl)-diethylenetriamine

Chapter 1: Introduction

This thesis is part of the Norwegian CCS Research Center (NCCS), which is an international research cooperation on CO_2 capture, transport, and storage. The work in this thesis relates to Task 2 on the development of amine-based capture solvents, which focuses on addressing challenges related to the use of solvents, including issues like degradation, reclaiming, and environmental considerations. The main objective is to develop kinetic models that describe solvent degradation in amine-based CO_2 capture plants. This is done by studying and comparing laboratory-scale degradation experiments from the literature to better understand the degradation mechanisms at play. These experimental results are then used to develop kinetic degradation models that can predict the extent of degradation in full-scale processes. In addition, this work evaluates the impact of flue gas compositions on the degradation rates throughout the process, the influence of various process modifications and the effectiveness of solvent management strategies.

The work predominantly focuses on the extensively researched 30 wt-% aqueous MEA solvent. In addition to its physical properties and CO_2 absorption kinetics, various studies explore degradation rates, catalytic effects of metals, corrosion rates, and the solubility of O_2 and metals. Therefore, the MEA solvent can serve as a case study to evaluate the overall understanding of the involved mechanisms and the predictive capabilities of degradation models. A key objective here is to identify knowledge gaps and propose further experiments to improve the understanding of degradation and the accuracy of model predictions. The MEA case study can, in turn, serve as a blueprint for other solvents, identifying the specific experimental data required for developing good predictive models.

This chapter contains a general introduction to absorption-based post-combustion capture, solvent degradation and management, and reclaiming techniques. It describes the scope of the work, gives a structured overview of the other chapters, and presents a summary of the relevant scientific contributions.

1.1 Background

Global warming and climate change pose significant challenges to the stability and sustainability of our planet as indicated by the analyses conducted by the International Energy Agency (IEA) and the Intergovernmental Panel on Climate Change (IPCC)[1,2]. At the core of these challenges is the impact of greenhouse gasses, especially CO_2. The IEA's reports emphasize the urgent necessity to reduce CO_2 emissions, particularly within the energy sector, by transitioning towards renewable and low-carbon energy sources, enhancing energy efficiency, and adopting environmentally responsible practices.

This energy transition is a time-consuming process, and with the window for effective mitigation closing rapidly, other measures must be implemented for short-term emission reduction. Carbon capture and storage (CCS) offers the potential to achieve short-term emission reductions and is predicted to play an important role in achieving climate goals. In addition, CCS can be a permanent solution for industries that are challenging to decarbonize, such as steel, cement, or waste-to-energy[2,3].

Although CO_2 can be removed using pre-combustion, post-combustion, and oxyfuel combustion capture processes, post-combustion capture is considered the most mature and is ready for wide-scale deployment[4,5]. Post-combustion systems can be installed in addition to existing industrial infrastructure with relative ease and without significant modifications to the upstream process. With a significant knowledge base and years of technical experience across the entire value chain due to related activities in natural gas and oil processing, large-scale implementation of post-combustion capture systems is technically feasible[3,6].

The dominant Industrial technology for post-combustion carbon capture is absorption with aqueous amines[5,7]. Aside from proprietary solvents, the most commonly studied amines are 2-ethanolamine (MEA), diethanolamine (DEA), n-methyl diethanolamine (MDEA), 2-amino-2-methylpropanol (AMP), piperazine (PZ) and blends of these[8,9]. These solvents are selected based on their CO_2 absorption rates, cyclic capacity, regeneration requirements, chemical stability towards degradation, and their reduced tendency to evaporate and corrode equipment in the process[8,10]. Although MEA was considered to be the benchmark solvent and is one of the most well-studied solvents, aqueous mixtures of AMP and PZ, such as CESAR1, have recently been described as the new benchmark due to their improved performance over MEA[11].

Current research is primarily focused on improving the efficiency and sustainability of the carbon capture process, while also addressing the obstacles that hinder its large-scale implementation. One of the main challenges is to extend the lifetime of the solvent by limiting losses through solvent degradation and emissions. Solvent degradation is problematic, not only because it is responsible for the majority of amine losses but also due to the generation of degradation products. These products have been observed to affect the performance of the capture plant by increasing foaming, solvent viscosity, or corrosion rates in the plant[12]. In addition, depending on the solvent, the degradation products can be volatile and toxic and may cause harm to human health and the environment. It is thus essential to gain a better understanding of the different degradation mechanisms and their impact on the process.

1.1.1 Absorption-Based Capture

A simplified overview of a typical amine-based post-combustion CO_2 capture plant is given in Figure 1.1. Pretreatment and conditioning of the flue gas may be required prior to CO_2 removal. Flue gas impurities, such as SO_x, NO_x, or heavy metals, are removed

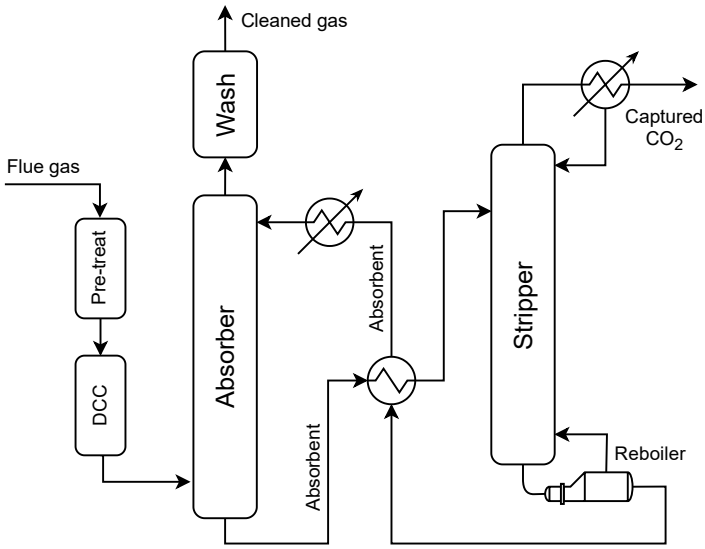

Figure 1.1: Overview of the absorption-based post-combustion capture process.

during pre-treatment in a caustic scrubber or using a wet electrostatic precipitator[5]. Next, the flue gas is typically cooled to around 40 °C using a direct contact cooler since milder temperatures thermodynamically favor absorption into the solvent.

The pre-treated flue gas enters the bottom of the absorber and travels up through the column, where it comes in counter-current contact with an aqueous amine solvent, which is distributed at the top. Generally, a random or structured packing is used to enhance the contact between the gas and liquid phases and stimulate selective absorption of CO_2. The absorption of CO_2 is exothermic and can result in a bulge in the temperature profile in the absorber. Intercooling may be applied to lower the temperature of the solvent and increase its capacity. Finally, the cleaned flue gas exits the top of the absorber and typically passes through one or more water- or acid-wash sections to remove entrained solvent, impurities, and degradation products.

The rich solvent, which is collected in the sump of the absorber and loaded with CO_2, is transported to the stripper through a cross-flow heat exchanger that preheats the rich solvent. The reboiler in the bottom of the stripper provides additional heat. The increased temperatures and production of water vapor in the stripper cause the CO_2 to desorb and regenerate the solvent. The gas leaving the top of the stripper is cooled down to condense water, and a relatively pure CO_2 product remains. The lean solvent is recycled through the cross-flow heat exchanger back to the top of the absorber.

Once dissolved into the solvent, the CO_2 can react in various ways, but the most important reversible reactions are the bicarbonate and carbamate formation reactions given in Eq. 1.1 and Eq. 1.2., respectively. Tertiary amines and sterically hindered

secondary amines cannot form carbamates and only facilitate the formation of bicarbonate. Since only one mole of amine is required to absorb one mole of CO_2, the capacity of these amines is typically higher than most primary and secondary amines. The latter are able to form carbamate but require two moles of amine per mole of CO_2. The advantage of carbamate reactions (Eq. 1.2) is their favorable reaction kinetics, which result in relatively fast absorption rates.[9,13]

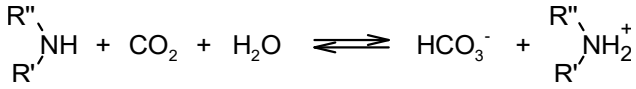

Eq. 1.1

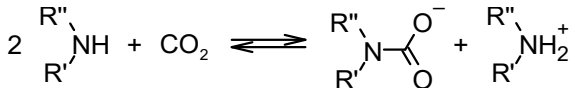

Eq. 1.2

1.1.2 Degradation of Amines

The continuous exposure of the solvent to oxidizing conditions in the absorber and increased temperatures in the stripper can cause it to degrade over time. Aside from a loss in capture capacity and plant performance, solvent degradation can also cause various operational issues, such as foaming and corrosion. In addition, solvent degradation may lead to the formation of volatile products, which can be emitted and impact human health and environmental safety[12,14]. The most common degradation mechanisms and their impact on the processes are discussed in the upcoming sections.

1.1.2.1 Thermal Degradation

The carbamate, which is formed when CO_2 reacts with the amine, may react further at elevated temperatures and form degradation products. This degradation process is commonly referred in the literature as thermal degradation with CO_2. The initial step in the thermal degradation of ethanolamine solvents involves the ring closure of the carbamate, resulting in the formation of an oxazolidinone. This intermediate is the starting point for subsequent polymerization reactions that lead to the formation of dimers and oligomers, imidazolidinones, and other cyclic compounds. In the case of MEA, this results in the formation of N-(2-hydroxyethyl)-ethylenediamine (HEEDA), 1-(2-hydroxyethyl)-2-imidazolidone (HEIA), and other products. Tertiary amines, such as MDEA and DMAE, cannot be converted to oxazolidinone directly and are generally more resistant to carbamate polymerization. Oxazolidinones formed from secondary amines, such as MAE and DEA, are relatively unstable and result in increased thermal degradation.[12,15–18]

The carbamate polymerization reaction rates are highly dependent on temperature, and most of thermal degradation occurs in high-temperature sections of the process, such as the stripper and reboiler. Lowering the temperatures in these regions can effectively

reduce the degradation rate; however, it also leads to an increase in the specific energy required for solvent regeneration[14]. Higher CO_2 loadings also increase degradation, most probably because they result in a higher concentration of carbamate[19].

The degradation products resulting from carbamate polymerization are found to have several adverse effects. They cause foaming and increase the solvent's viscosity, thereby impairing efficient mass transfer within the absorber and increasing emissions. Some of the degradation products have also been found to be corrosive, thereby damaging the equipment and increasing the concentration of dissolved metals in the solvent. Degradation of the amine will also reduce the capture capacity, however, it is worth noting that certain degradation products retain the ability to absorb CO_2. Therefore, when a fraction of the original amine degrades, it does not necessarily result in a proportional loss of CO_2 absorption capacity.[20]

1.1.2.2 Oxidative Degradation

Oxidative degradation, on the other hand, mainly occurs in the absorber. Here, oxygen in the flue gas is brought into contact with the solvent, and despite the relatively low temperatures, degradation takes place readily. Any dissolved oxygen at the bottom of the absorber is likely to react when the solvent is heated in the heat exchanger or stripper.

In contrast to carbamate polymerization, the mechanism for oxidative degradation for most amines is still relatively unclear. Two potential mechanisms are proposed: electron transfer and hydrogen abstraction. In the case of electron transfer, a free radical abstracts an electron from the lone pair of the nitrogen, whereas in the case of the hydrogen abstraction mechanism, the degradation is initiated by the abstraction of a hydrogen atom on the α-carbon or the β-carbon. In either case, the unstable amine radical readily reacts with oxygen to form a hydroperoxide, which decomposes into new radicals and a range of degradation products, including carboxylic acids, aldehydes, and ammonia.[21–25]

The role of dissolved metals in catalyzing the formation of free radicals required for initiating oxidative degradation has shown to be important. Metals, such as iron, copper and manganese, may be leached from the absorption equipment or enter the system with the flue gas in the form of fly ash[26]. Oxidative degradation products, such as organic acids, are suspected to speed up the corrosion rate and increase metal concentrations in the solvent, resulting in higher degradation rates. The rate of carbamate polymerization, however, does not appear to be influenced by the presence of dissolved metals[15]. Overall, oxidative degradation is the more dominant degradation mechanism but exact contributions are hard to quantify and depend on many process parameters[27].

1.1.2.3 Solvent Deactivation by Heat-Stable Salts

The flue gas may contain other acidic components in addition to CO_2, for example, SO_2 or HCl. Some of these acids are stronger than CO_2 and can absorb competitively. The salts, which are formed between these stronger acids and the amine, are known as heat-

stable salts (HSS) because the stronger acids do not desorb at elevated temperatures in the stripper, opposed to CO_2. As a result, a fraction of the solvent will slowly be deactivated over time, reducing the cyclic capacity and performance of the capture plant.

A second source of HSS is oxidative degradation. The oxidation of the amine can lead to the formation of organic acids, which can form covalently bonded HSS with the amine. The implications of these HSS are the same. The degree of solvent deactivation strongly depends on the flue gas conditions and the oxidative degradation rate. In the case of MEA, typical absorbent loss due to solvent deactivation is in the range of 0.6 and 1.2 kg /ton of CO_2[28]. The dissolution of strong acids in the solvent can also lead to higher solvent degradation rates, either directly or indirectly, as the result of higher dissolved metal concentrations because of increased corrosion[29].

1.1.2.4 Nitrosamines

The presence of nitrogen oxides in the flue gas can also lead to other challenges. Amines can react with dissolved NO_2, forming nitrosamine and nitramine products, which can be toxic or carcinogenic[30]. These products can escape the process through evaporation or entrainment in the flue gas and may cause danger to human health and the environment. Nitrosamines can be produced directly from both primary, secondary, and tertiary solvents but nitrosamines of primary amines, such as MEA, are generally unstable and will quickly react to form a carbocation and nitrogen. Some degradation products of primary amines, however, can react with nitrogen oxides to form more stable nitrosamines[30,31]. Although the reaction rates are insignificant with respect to the overall solvent losses, the formation of the nitrosamines should not be neglected due to their adverse effects. Sufficient monitoring of the solvent and outlet gas is required to keep emissions at acceptable levels.

1.1.2.5 Thermal Decomposition

Amine solvents have also been shown to degrade through thermal decomposition at elevated temperatures without the presence of impurities, O_2, or CO_2. However, thermal decomposition is typically not observed for most amines at conventional reboiler temperatures[16,17]. The degradation rates of the reactions involving O_2 or CO_2 are significantly higher, and most industrial experiences showed that thermal decomposition is negligible compared with these[32,33].

1.1.3 Emissions and Mitigation

Both the amine and its degradation products can exit the process with the treated flue gas through evaporation or entrainment in aerosols. The degree of evaporation depends mainly on the type of amine or degradation product and its concentration, the loading and liquid temperature in the top section of the absorber, and the pressure in the absorber[34]. Some degradation products, such as formaldehyde, acetaldehyde, and

ammonia, are more volatile than the amines they originate from. As a result, the total atmospheric emissions may increase when significant degradation occurs.

Entrainment of the amine and degradation products in aerosols is another important source of emissions. The aerosols are small liquid droplets, which are formed in the absorber, for example due to impurities in the flue gas, such as soot and H_2SO_4[35]. The conditions in the absorber, such as the temperature profile and H_2O saturation pressure gradients, control the growth of the aerosols. Larger droplets (> 10 µm) can be captured using standard demisters, but the smaller aerosols are not affected[34]. Therefore, most absorbers are equipped with a water wash section, which can reduce both volatile and aerosol amine emissions significantly. The water that is used to wash the gas flow exiting the absorber is cooler than the lean solvent and contains a low concentration of amine and degradation products. As a result, up to 95% of the solvent can be recovered by implementing a water wash system, and typical overall emissions of MEA are in the range of 1 - 6 ppmv[35–37].

1.1.4 Solvent Management

A good solvent management is imperative for the successful operation of the capture plant, and often encompasses measures for both preventing and mitigating solvent degradation and its effects on operational efficiency and environmental sustainability. These measures are described and discussed in more detail in this section. Active reclaiming is discussed in more detail in section 1.1.5.

1.1.4.1 Prevention

Preventive measures can be taken to limit solvent degradation in the process. An essential one is selecting a stable solvent, which involves screening various amines during degradation experiments. Tertiary and sterically hindered ethanolamines are generally more resilient in carbamate polymerization experiments[16], and some of these amines were found to have reduced rates of oxidative degradation and nitrosamines and nitramines formation[18]. While solvent stability is crucial, other factors, such as performance, capacity, regeneration requirements, and safety, must not be disregarded.

Pre-treatment, such as flue gas desulfurization, can reduce solvent degradation and the formation of HSS[38]. In addition, upstream process modifications that change the composition of the flue gas, for example, by lowering the O_2 concentration, can positively affect degradation rates. Modifications to the capture process, such as removing dissolved oxygen downstream of the absorber, also limit degradation[39]. Another method to restrict solvent degradation is to reduce solvent residence time in areas prone to degradation, such as the column sumps and the stripper reboiler. Good temperature control in the absorber and stripper can prevent temperature fluctuations that can lead to increased degradation rates. Finally, degradation inhibitors can be added to the solvent. These inhibitors may serve as chelating agents and interact with dissolved

metals, or they can function as oxygen scavengers to reduce oxygen solubility or interact with dissolved oxygen[40].

1.1.4.2 Symptomatic Treatment

The second type of solvent management strategy does not prevent degradation but aims to reduce or mitigate its effects. As discussed in section 1.1.2, the formation of degradation products can affect the corrosion rates in the plant or the viscosity and the surface tension of the solvent. In the case of corrosion, there are several measures one could take to limit its effects, such as the selection of appropriate materials or the application of a coating. However, if significant degradation or corrosion is not anticipated during the design phase, it might be necessary to adjust the process environment instead. This can be achieved by introducing a corrosion inhibitor, which either protects the equipment by interacting with the surface or by scavenging oxidizing agents[41].

The presence of acidic degradation products or certain corrosion inhibitors can negatively impact amine solvent foaming behavior, resulting in reduced mass transfer efficiencies in contactors and solvent loss[37]. Anti-foaming agents can be used to mitigate foaming. These agents typically have low viscosity and a strong affinity for the air-liquid interface, effectively breaking down the foam. It is important to note that these additives and inhibitors do not directly affect degradation rates, and periodic solvent makeup remains necessary. However, because fewer metallic ions are dissolved by inhibiting corrosion, the catalytic effects on oxidative degradation rates may be reduced.

1.1.4.3 Solvent Treatment and Maintenance

One of the simplest methods to maintain solvent quality is to replenish the solvent inventory. One can either periodically replace the entire inventory or gradually bleed out some of the current solvent and introduce fresh solvent as a replacement. When the solvent is replaced and discarded, it still contains a large fraction of the original amine. From both an environmental and economic perspective, this method is thus unappealing.

Moser et al. applied the bleed and feed strategy during an 18-month test run with 30-wt% MEA at the Niederaussem post-combustion capture plant[42]. The strategy successfully reduced impurity and degradation product concentrations and improved the solvent capacity. However, the degradation rates appeared to increase to the same levels before the solvent exchange shortly after feeding the new solvent. This is expected to be caused by degradation products, impurities, and dissolved metals left behind. Therefore, the bleed and feed strategy is not very effective.

Filters can also play a crucial role in solvent treatment. Mechanical filtration can remove particulates and precipitated salts that could lead to fouling or erosion issues. Meanwhile, activated carbon filters remove hydrocarbons and polar organic compounds, including surface-active components that induce foaming. They have also proven successful in

adsorbing nitrosamine contaminants[43]. The interaction of carbon filters with HSS and other impurities and degradation products is limited[44]. Mechanical filters commonly precede the carbon filters to prevent fouling. When saturated, carbon filters must be replaced[45].

Additionally, solvent treatment can involve neutralization with an alkali, like an NaOH. Amines part of an HSS are separated from the impurity, allowing them to absorb CO_2 once again. However, this method solely addresses short-term solvent deactivation and does not remove impurities from the system. If repeated periodically, the solvent can be diluted and salts can accumulate, potentially causing increased viscosity[45]. Therefore, it is not a sustainable long-term solution for maintaining solvent quality.

1.1.5 Reclaiming

The solvent that undergoes degradation either through carbamate polymerization or oxidative degradation cannot be reclaimed. However, the deactivated solvent can be treated, and the amine can be recovered by breaking up the HSS. The initial steps in this treatment typically involve CO_2 stripping and neutralization with a potent base. Stripping facilitates the desorption of CO_2 and converts most of the amine from its carbamate or protonated state back into neutral molecules. A stronger base is used to separate the remaining CO_2 and HSS from the amine. Acidic compounds exhibit a greater affinity for this base and new salts are formed. Once neutralized, the amine can be separated from contaminants using various separation techniques and then recycled back into the solvent inventory.

1.1.5.1 Thermal Reclaiming

The most well-known reclaiming technology is thermal reclaiming because of its relatively simple design and the available knowledge through its application in other gas cleaning applications, such as H_2S scrubbing. A small solvent side stream is heated in a reclaiming kettle after pretreatment and neutralization. The high volatility of the amine in comparison to the degradation products, salts, and other impurities allows it to be evaporated and separated from the mixture. Over time, degradation products and impurities are concentrated in the reclaimer, forming a sludge with an increased viscosity and boiling point. Therefore, the reclaimer is stopped periodically to dispose of the sludge.[46]

Reclaiming generally takes place at atmospheric pressures, unless higher boiling point amines, such as DEA or MDEA, are used. In such cases, significant degradation can occur at the boiling point temperature, necessitating a vacuum or steam to reduce the partial pressure of the amine in the gas phase at lower temperatures[47]. Thermal reclaiming is highly effective at eliminating a wide range of both ionic and non-ionic impurities but it is relatively energy-intensive. When impurity concentrations are low, a relatively large volume of solvent must be evaporated to achieve the same level of

impurity removal. Therefore, from an energy efficiency perspective, thermal reclaiming becomes more efficient as impurity concentrations increase.

1.1.5.2 Ion Exchange Reclaiming

After pretreatment and neutralization, ion exchange can be used to eliminate charged impurities from the solvent. These charged impurities, some of which were part of an HSS prior to neutralization, adhere to the resin, displacing it with another ion, such as OH^-. Over time, the resin becomes saturated and must be regenerated. Anion exchange resins interact with negatively charged impurities, and regeneration often involves using an alkali like NaOH. In cases where continuous ion exchange is required, multiple beds may be needed to operate in parallel. Moreover, for the removal of both cationic and anionic impurities, beds with different types of resins must be used.

The resin adsorbs not only ionic impurities that form HSS but also the ions introduced during the neutralization phase, such as sodium or potassium. Excessive neutralization can consequently reduce the removal efficiency. The ion exchange process has low energy requirements compared with thermal reclaiming and electrodialysis. However, its environmental water and chemicals footprint is considerably larger because washing and regeneration of the resins can demand substantial quantities of these resources. Furthermore, another limitation of ion exchange is its inability to remove uncharged impurities since they do not interact with the resins.[48]

1.1.5.3 Electrodialysis Reclaiming

Electrodialysis can also be used for removing charged impurities. This method employs a series of alternating cation- and anion-exchange membranes, allowing the removal of anions and cations. The contaminated solvent passes in between the membranes, alternated by electrolyte solution. When an electric potential is applied, ions migrate across the membranes toward the electrolyte solution, resulting in a concentrate, while the concentration of ions and HSS decreases in the solvent. Electrodialysis, however, is ineffective in addressing uncharged contaminants, such as some thermal degradation products, as they do not respond to the applied electric potential.[45,49]

The process is characterized by its large electrical energy usage, which scales with the concentration of charged components in the solvent and can contribute significantly to the overall reclaiming costs[50]. Since electrical energy makes up most of the total energy requirements, it is relatively easy to make the process sustainable or carbon neutral, by shifting to renewable electricity sources. The concentration of impurities cannot easily be concentrated up to the levels of the thermal reclaiming wastes, resulting in larger waste volumes. To address this, several electrodialysis stacks can be placed in series to obtain a more concentrated waste and reduce to total waste volume[51].

The exchange membranes are susceptible to fouling, and proper filtration up to 1µm is usually required. The high alkaline conditions of the neutralized solvent can be

problematic for the stability and long-term lifespan of some types of membranes[50]. An advantage of membrane processes, on the other hand, is the relatively simple scale-up from lab scale to pilot plants and industrial plants. Therefore, lab-scale processes can give a good approximation of the final performance.

1.1.5.4 Reclaimer Waste Disposal

The discussed reclaiming processes produce waste, and it is necessary to consider the costs related to the handling and disposal of this waste. Electrodialysis and ion exchange processes produce a relatively large volume of aqueous waste, whereas thermal reclaiming yields a more concentrated waste. This waste is often corrosive due to its high concentrations of impurities and must be treated as hazardous waste[52]. The waste can be incinerated on-site if a suitable boiler and permissions are available, but otherwise, it will have to be transported and disposed of or incinerated off-site. The latter can be expensive and might make up more than half of the total reclaiming costs[53].

Wastewater treatment plants can be used to treat dilute wastes. The cost of this treatment is case-specific and strongly depends on the exact composition of the waste, but is less than those of hazardous waste treatment[53]. Given the significant impact of waste treatment costs on overall expenses, it should be a primary factor in the decision-making process when selecting a reclamation method. Furthermore, research into the exact compositions and classification of the wastes can be interesting to provide more details and give better estimates.

1.2 Layout of the Thesis

Chapter 2 presents Article I: “Modeling the Formation of Degradation Compounds during Thermal Degradation of MEA” (https://doi.org/10.1021/acs.iecr.1c04496), which has been published in Industrial & Engineering Chemistry Research in February 2022. This article aims to compare experimental data on the thermal degradation of MEA, analyze discrepancies in results, statistically quantify experimental uncertainty, and develop a comprehensive degradation model predicting solvent losses and degradation product formation under different process conditions. Chapter 3 continues the work presented in the article and discusses several additional aspects of the thermal degradation model, such as expanding its complexity and the potential role of MEA carbamate in the degradation reactions and reaction rate equation.

Chapter 4 presents Article II: “Predicting solvent degradation in absorption-based CO_2 capture from industrial flue gases” (https://doi.org/10.1016/j.ces.2023.118940), which has been published in Chemical Engineering Science in September 2023. In this article, shortcomings of experimental setups to measure oxidative degradation of the solvent are identified and a new setup design is proposed to provide data that is more useful for degradation modeling. Chapter 5 continues the work in this article and discusses several additional aspects, such as validation of the models and additional case studies. In

section 5.7, the degradation models are applied to evaluate degradation in capture processes featuring high capture efficiencies. The work in this section is performed in collaboration with the University of Edinburgh and Sheffield (D. Mullen and Prof. M. Lucquiaud), and, although a complete draft is not available at the time of writing, a joint publication is planned in the future.

Chapter 6 delves into the application of conventional degradation setups and their constraints in relation to the development of degradation models. A novel setup design, intended to examine degradation under conditions that more accurately reflect the actual process, is introduced and explored. The challenges and insights associated with the assembly, testing, and operation of the setup are detailed, and preliminary testing outcomes are presented.

Chapter 7 explores the catalytic role of iron in oxidative solvent degradation and proposes an extension to the existing oxidative degradation model. Various hypothetical scenarios, including corrosion rate limitations, iron solubility constraints, and O_2 mass transfer limitations in the absorber packing, are considered and included in the degradation model. The predicted outcomes are compared with pilot plant observations, and knowledge gaps are identified. In addition, the effectiveness of continuous reclaiming is evaluated based on the extended degradation model.

1.3 Articles and Dissemination

1.3.1 Journal Publications

L. Braakhuis, K. K. Høisæter, and H. K. Knuutila, 'Modeling the Formation of Degradation Compounds during Thermal Degradation of MEA', *Ind. Eng. Chem. Res.*, Feb. 2022, doi: 10.1021/acs.iecr.1c04496.

L. Braakhuis and H. K. Knuutila, 'Predicting solvent degradation in absorption–based CO_2 capture from industrial flue gases', *Chemical Engineering Science*, vol. 279, p. 118940, Sep. 2023, doi: 10.1016/j.ces.2023.118940.

1.3.1.1 Other Journal Publications Not Part of this Thesis

K. K. Høisæter, S. J. Vevelstad, L. Braakhuis, and H. K. Knuutila, 'Impact of Solvent on the Thermal Stability of Amines', *Ind. Eng. Chem. Res.*, vol. 61, no. 43, pp. 16179–16192, Nov. 2022, doi: 10.1021/acs.iecr.2c01934.

1.3.2 Conference Contributions

L. Braakhuis and H. K. Knuutila, 'Modelling and Evaluating Carbamate Polymerization of Monoethanolamine in Post-Combustion Carbon Capture', Trondheim Carbon Capture & Storage Conference 11 (TCCS-11), in *SINTEF*

Proceedings, Trondheim, Jun. 2021. https://sintef.brage.unit.no/sintef-xmlui/handle/11250/2785872

V. Andersen, H. K. Knuutila, L. Braakhuis, E. H. Myrhaug, K. E. Einarsrud, and G. Tranell, 'CO2 Capture for the Silicon Process-Effects of Flue Gas', presented at the Infacon XIV, Trondheim, Sep. 2021. doi: https://dx.doi.org/10.2139/ssrn.3926089.

L. Braakhuis and H. K. Knuutila, 'Modelling the Formation of Degradation Compounds during Thermal Degradation of MEA', presented at the Post Combustion Capture Conference 6 (PCCC-6), London, Oct. 2021.

L. Braakhuis and H. K. Knuutila, (poster) 'Evaluation of Solvent Degradation in Amine-Based Post-Combustion Capture Process Simulations.', at the 16th Greenhouse Gas Control Technologies Conference 2022 (GHGT-16), Oct. 2022. doi: 10.2139/ssrn.4274973.

L. Braakhuis and H. K. Knuutila, 'The Impact of Process Modifications on Solvent Degradation in Amine-Based Post-Combustion Capture Systems', presented at the Trondheim Conference on Carbon Capture, Transport and Storage 12 (TCCS-12), Jun. 2023.

L. Braakhuis, H. K. Knuutila, and E. A. Scelzo, (poster) 'New Apparatus to Measure Solvent Degradation for Degradation Model Development', presented at the Post Combustion Capture Conference 7 (PCCC-7), Pittsburgh, Sep. 2023.

1.3.3 Other Dissemination

L. Braakhuis, H. K. Knuutila, Overview of reclaiming technologies and their application in post combustion carbon capture (29.04.2021). Norwegian CCS Research Centre (NCCS) Webinar.

L. Braakhuis, H. K. Knuutila, Task 2: Impact of process design on degradation: a modeling study, November 2022. Norwegian CCS Research Centre (NCCS) Consortium days presentation.

L. Braakhuis, H. K. Knuutila, Task 2: The Impact of Process Modifications on Solvent Degradation, November 2023. Norwegian CCS Research Centre (NCCS) Consortium days presentation.

1.4 References

(1) International Energy Agency. *World Energy Outlook 2023*; Paris, 2023. https://www.iea.org/reports/world-energy-outlook-2023.

(2) *Climate Change 2023: Synthesis Report. Contribution of Working Groups I, II and III to the Sixth Assessment Report of the Intergovernmental Panel on*

Climate Change; The Intergovernmental Panel on Climate Change (IPCC): Geneva, Switzerland, 2023.
(3) Bui, M.; Adjiman, C. S.; et al. Carbon Capture and Storage (CCS): The Way Forward. *Energy Environ. Sci.* **2018**, *11* (5), 1062–1176. https://doi.org/10.1039/C7EE02342A.
(4) Liang, Z. (Henry); Rongwong, W.; et al. Recent Progress and New Developments in Post-Combustion Carbon-Capture Technology with Amine Based Solvents. *International Journal of Greenhouse Gas Control* **2015**, *40*, 26–54. https://doi.org/10.1016/j.ijggc.2015.06.017.
(5) de Meyer, F.; Jouenne, S. Industrial Carbon Capture by Absorption: Recent Advances and Path Forward. *Current Opinion in Chemical Engineering* **2022**, *38*, 100868. https://doi.org/10.1016/j.coche.2022.100868.
(6) Feron, P. H. M. *Absorption-Based Post-Combustion Capture of Carbon Dioxide*; Feron, P. H. M., Ed.; Woodhead Publishing, 2016. https://doi.org/10.1016/B978-0-08-100514-9.00001-9.
(7) Kearns, D.; Liu, H.; et al. Technology Readiness and Costs of CCS. *Global CCS institute* **2021**, *3*.
(8) Solrun Johanne Vevelstad. CO2 Absorbent Degradation. Doctoral thesis, Norwegian University of Science and Technology, Trondheim, 2013.
(9) Buvik, V. Stability of Amines for CO2 Capture. Doctoral thesis, NTNU, 2021. https://ntnuopen.ntnu.no/ntnu-xmlui/handle/11250/2777358 (accessed 2023-01-23).
(10) Puxty, G.; Conway, W.; et al. 4 - Liquid Absorbent Selection Criteria and Screening Procedures. In *Absorption-Based Post-combustion Capture of Carbon Dioxide*; Feron, P. H. M., Ed.; Woodhead Publishing, 2016; pp 69–100. https://doi.org/10.1016/B978-0-08-100514-9.00004-4.
(11) Feron, P. H. M.; Cousins, A.; et al. An Update of the Benchmark Post-Combustion CO2-Capture Technology. *Fuel* **2020**, *273*, 117776. https://doi.org/10.1016/j.fuel.2020.117776.
(12) Reynolds, A. J.; Verheyen, T. V.; et al. Degradation of Amine-Based Solvents. In *Absorption-Based Post-combustion Capture of Carbon Dioxide*; Elsevier, 2016; pp 399–423. https://doi.org/10.1016/B978-0-08-100514-9.00016-0.
(13) Puxty, G.; Maeder, M. 2 - The Fundamentals of Post-Combustion Capture. In *Absorption-Based Post-combustion Capture of Carbon Dioxide*; Feron, P. H. M., Ed.; Woodhead Publishing, 2016; pp 13–33. https://doi.org/10.1016/B978-0-08-100514-9.00002-0.
(14) Vega, F.; Sanna, A.; et al. Degradation of Amine-Based Solvents in CO2 Capture Process by Chemical Absorption. *Greenhouse Gases: Science and Technology* **2014**, *4* (6), 707–733. https://doi.org/10.1002/ghg.1446.
(15) Léonard, G. Optimal Design of a CO2 Capture Unit with Assessment of Solvent Degradation. Doctoral thesis, Université de Liège, 2013.
(16) Lepaumier, H.; Picq, D.; et al. New Amines for CO_2 Capture. I. Mechanisms of Amine Degradation in the Presence of CO_2. *Ind. Eng. Chem. Res.* **2009**, *48* (20), 9061–9067. https://doi.org/10.1021/ie900472x.

(17) Reza, J.; Trejo, A. Degradation of Aqueous Solutions of Alkanolamine Blends at High Temperature, Under the Presence of CO2 and H2S. *Chemical Engineering Communications* **2006**, *193* (1), 129–138. https://doi.org/10.1080/009864490923592.
(18) Mazari, S. A.; Si Ali, B.; et al. An Overview of Solvent Management and Emissions of Amine-Based CO2 Capture Technology. *International Journal of Greenhouse Gas Control* **2015**, *34*, 129–140. https://doi.org/10.1016/j.ijggc.2014.12.017.
(19) Davis, J. D. Thermal Degradation of Aqueous Amines Used for Carbon Dioxide Capture. Doctoral thesis, The University of Texas, Austin, 2009. https://repositories.lib.utexas.edu/handle/2152/6581.
(20) Zoannou, K.-S.; Sapsford, D. J.; et al. Thermal Degradation of Monoethanolamine and Its Effect on CO2 Capture Capacity. *International Journal of Greenhouse Gas Control* **2013**, *17*, 423–430. https://doi.org/10.1016/j.ijggc.2013.05.026.
(21) Voice, A. K.; Rochelle, G. T. Inhibitors of Monoethanolamine Oxidation in CO $_2$ Capture Processes. *Ind. Eng. Chem. Res.* **2014**, *53* (42), 16222–16228. https://doi.org/10.1021/ie500996z.
(22) Parks, C.; Alborzi, E.; et al. DFT Studies on Thermal and Oxidative Degradation of Monoethanolamine. *Industrial and Engineering Chemistry Research* **2020**, *59* (34), 15214–15225. https://doi.org/10.1021/acs.iecr.0c03003.
(23) Goff, G. S.; Rochelle, G. T. Monoethanolamine Degradation: O $_2$ Mass Transfer Effects under CO $_2$ Capture Conditions. *Ind. Eng. Chem. Res.* **2004**, *43* (20), 6400–6408. https://doi.org/10.1021/ie0400245.
(24) Lepaumier, H.; Picq, D.; et al. New Amines for CO $_2$ Capture. II. Oxidative Degradation Mechanisms. *Ind. Eng. Chem. Res.* **2009**, *48* (20), 9068–9075. https://doi.org/10.1021/ie9004749.
(25) Sexton, A. J.; Rochelle, G. T. Reaction Products from the Oxidative Degradation of Monoethanolamine. *Ind. Eng. Chem. Res.* **2011**, *50* (2), 667–673. https://doi.org/10.1021/ie901053s.
(26) Dhingra, S.; Khakharia, P.; et al. Understanding and Modelling the Effect of Dissolved Metals on Solvent Degradation in Post Combustion CO2 Capture Based on Pilot Plant Experience. *Energies* **2017**, *10* (5), 629. https://doi.org/10.3390/en10050629.
(27) Lepaumier, H.; da Silva, E. F.; et al. Comparison of MEA Degradation in Pilot-Scale with Lab-Scale Experiments. *Energy Procedia* **2011**, *4*, 1652–1659. https://doi.org/10.1016/j.egypro.2011.02.037.
(28) Veltman, K.; Singh, B.; et al. Human and Environmental Impact Assessment of Postcombustion CO2 Capture Focusing on Emissions from Amine-Based Scrubbing Solvents to Air. *Environmental Science and Technology* **2010**, *44* (4), 1496–1502. https://doi.org/10.1021/es902116r.
(29) Supap, T.; Idem, R.; et al. Kinetics of Sulfur Dioxide- and Oxygen-Induced Degradation of Aqueous Monoethanolamine Solution during CO2 Absorption

from Power Plant Flue Gas Streams. *International Journal of Greenhouse Gas Control* **2009**, *3* (2), 133–142. https://doi.org/10.1016/j.ijggc.2008.06.009.
(30) da Silva, E. F.; Booth, A. M. Emissions from Postcombustion CO2 Capture Plants. *Environ. Sci. Technol.* **2013**, *47* (2), 659–660. https://doi.org/10.1021/es305111u.
(31) Dai, N.; Mitch, W. A. Effects of Flue Gas Compositions on Nitrosamine and Nitramine Formation in Postcombustion CO2 Capture Systems. *Environ. Sci. Technol.* **2014**, *48* (13), 7519–7526. https://doi.org/10.1021/es501864a.
(32) da Silva, E. F.; Lepaumier, H.; et al. Understanding 2-Ethanolamine Degradation in Postcombustion CO_2 Capture. *Ind. Eng. Chem. Res.* **2012**, *51* (41), 13329–13338. https://doi.org/10.1021/ie300718a.
(33) Bedell, S. A. Oxidative Degradation Mechanisms for Amines in Flue Gas Capture. In *Energy Procedia*; Elsevier, 2009; Vol. 1, pp 771–778. https://doi.org/10.1016/j.egypro.2009.01.102.
(34) Raghu, Amrutha. Quantification of Amine Loss in the Post Combustion CO2 Capture Process. Thesis, University of Regina, 2012.
(35) Khakharia, P.; Brachert, L.; et al. Investigation of Aerosol Based Emission of MEA Due to Sulphuric Acid Aerosol and Soot in a Post Combustion CO2 Capture Process. *International Journal of Greenhouse Gas Control* **2013**, *19*, 138–144. https://doi.org/10.1016/j.ijggc.2013.08.014.
(36) Karl, M.; Wright, R. F.; et al. Worst Case Scenario Study to Assess the Environmental Impact of Amine Emissions from a CO2 Capture Plant. *International Journal of Greenhouse Gas Control* **2011**, *5* (3), 439–447. https://doi.org/10.1016/j.ijggc.2010.11.001.
(37) Reynolds, A. J.; Verheyen, T. V.; et al. Towards Commercial Scale Postcombustion Capture of CO2 with Monoethanolamine Solvent: Key Considerations for Solvent Management and Environmental Impacts. *Environmental Science and Technology* **2012**, *46* (7), 3643–3654. https://doi.org/10.1021/es204051s.
(38) Garg, B.; Haque, N.; et al. Techno-Economic Evaluation of Amine-Reclamation Technologies and Combined CO2/SO2 Capture for Australian Coal-Fired Plants. *International Journal of Greenhouse Gas Control* **2020**, *98*, 103065. https://doi.org/10.1016/j.ijggc.2020.103065.
(39) V. Figueiredo, R.; Srivastava, T.; et al. Impact of Dissolved Oxygen Removal on Solvent Degradation for Post-Combustion CO2 Capture. *International Journal of Greenhouse Gas Control* **2021**, *112*, 103493. https://doi.org/10.1016/j.ijggc.2021.103493.
(40) Fytianos, G.; Vevelstad, S. J.; et al. Degradation and Corrosion Inhibitors for MEA-Based CO2 Capture Plants. *International Journal of Greenhouse Gas Control* **2016**, *50*, 240–247. https://doi.org/10.1016/j.ijggc.2016.05.003.
(41) Wattanaphan, Pathamaporn. Studies and Prevention of Carbon Steel Corrosion and Solvent Degradation During Amine-Based CO2 Capture from Industrial Gas Streams. Doctoral thesis, University of Regina, 2012.
(42) Moser, P.; Wiechers, G.; et al. Results of the 18-Month Test with MEA at the Post-Combustion Capture Pilot Plant at Niederaussem – New Impetus to

Solvent Management, Emissions and Dynamic Behaviour. *International Journal of Greenhouse Gas Control* **2020**, *95*, 102945. https://doi.org/10.1016/j.ijggc.2019.102945.

(43) Widger, L. R.; Combs, M.; et al. Selective Removal of Nitrosamines from a Model Amine Carbon-Capture Waterwash Using Low-Cost Activated-Carbon Sorbents. *Environ. Sci. Technol.* **2017**, *51* (18), 10913–10922. https://doi.org/10.1021/acs.est.7b02806.

(44) ElMoudir, W.; Supap, T.; et al. Part 6: Solvent Recycling and Reclaiming Issues. *Carbon Management* **2012**, *3* (5), 485–509. https://doi.org/10.4155/cmt.12.55.

(45) Cummings, A. L.; Smith, G.; et al. Advances in Amine Reclaiming. **2007**. https://www.digitalrefining.com/article/1000267/advances-in-amine-reclaiming.

(46) Kentish, S. E. Reclaiming of Amine-Based Absorption Liquids Used in Post-Combustion Capture. In *Absorption-Based Post-combustion Capture of Carbon Dioxide*; Elsevier, 2016; pp 425–438. https://doi.org/10.1016/B978-0-08-100514-9.00017-2.

(47) Kohl, A. L.; Nielsen, R. B. Alkanolamines for Hydrogen Sulfide and Carbon Dioxide Removal. In *Gas Purification*; Elsevier, 1997; pp 40–186. https://doi.org/10.1016/B978-088415220-0/50002-1.

(48) Dumée, L.; Scholes, C.; et al. Purification of Aqueous Amine Solvents Used in Post Combustion CO2 Capture: A Review. *International Journal of Greenhouse Gas Control* **2012**, *10*, 443–455. https://doi.org/10.1016/j.ijggc.2012.07.005.

(49) Strathmann, H. Electrodialysis, a Mature Technology with a Multitude of New Applications. *Desalination* **2010**, *264* (3), 268–288. https://doi.org/10.1016/j.desal.2010.04.069.

(50) Wang, T.; Hovland, J.; et al. Amine Reclaiming Technologies in Post-Combustion Carbon Dioxide Capture. *Journal of Environmental Sciences (China)* **2015**, *27* (C), 276–289. https://doi.org/10.1016/j.jes.2014.06.037.

(51) Grushevenko, E. A.; Bazhenov, S. D.; et al. Two-Step Electrodialysis Treatment of Monoethanolamine to Remove Heat Stable Salts. *Russ J Appl Chem* **2018**, *91* (4), 602–610. https://doi.org/10.1134/S1070427218040110.

(52) Sexton, A.; Dombrowski, K.; et al. Evaluation of Reclaimer Sludge Disposal from Post-Combustion CO2 Capture. *Energy Procedia* **2014**, *63*, 926–939. https://doi.org/10.1016/j.egypro.2014.11.102.

(53) Sexton, A. J.; Fisher, K.; et al. Evaluation of Amine Reclaimer Operation and Waste Disposal from Post-Combustion CO2 Capture. In *Laurance Reid Gas Conditioning Conference*; Norman, Oklahoma USA, 2016.

Chapter 2: Article I: Thermal Degradation of MEA

Solvent degradation primarily results from oxidative and thermal degradation. Extensive studies have been conducted on the thermal degradation of monoethanolamine (MEA) through degradation experiments and the development of degradation models[1–5]. While there is a consensus on most of the degradation mechanisms, minor differences and distinctions exist.

The experimental procedure for the degradation experiments is similar across various works in the literature. However, variations exist in experiment durations, temperature ranges, and used CO_2 loadings. Various analytical methods are employed to measure the concentrations of MEA, CO_2, and degradation products. While the concentration of MEA is consistently measured, different sets of degradation products have been analyzed. The degradation experiments are characterized by significant uncertainty. This uncertainty is especially evident when comparing the results of different studies, but also when comparing experimental runs from the same study. Two different authors have developed degradation models[1,2]; however, the data used to fit these models is limited to their own experimental results. Consequently, the variations in the experimental results are reflected in the models[6].

In this chapter, Article I is presented, as published in Industrial & Engineering Chemistry Research. The article's objective is to collect and combine all available experimental data on MEA's thermal degradation to develop a degradation model that aligns with all data. Differences in the experimental results are analyzed, and the experimental uncertainty is discussed and quantified statistically. The kinetic rate equations are selected based on the mechanisms proposed in the literature. The resulting model aims to predict solvent losses and the formation of degradation products over time and under various process conditions, including temperature and loading.

Chapter 3 continues the work presented in the article and discusses several additional aspects of the thermal degradation model. The use of additional reaction rate parameters and the inclusion of reversible reaction is considered and more insights on uncertainties and possible model improvements are given. Finally, the role of the MEA carbamic acid in the degradation mechanism and the effect of its protonation on the degradation rate are discussed.

Modeling the Formation of Degradation Compounds During Thermal Degradation of MEA

Lucas Braakhuis, Karen Karolina Høisæter, Hanna K. Knuutila*

Department of Chemical Engineering, Norwegian University of Science and Technology (NTNU), NO-7491 Trondheim, Norway

*Corresponding author: hanna.knuutila@ntnu.no

DOI: https://doi.org/10.1021/acs.iecr.1c04496

DOI of correction: https://doi.org/10.1021/acs.iecr.3c00760

2.1 Abstract

A kinetic model has been developed to predict thermal degradation of aqueous solutions of monoethanolamine (MEA) in carbon capture. The model focusses on both the degradation rate of the amine and the formation rates of selected degradation products as a function of time, temperature, and loading. Experimental literature data on thermal degradation of MEA were used to develop, fit, and evaluate the model. The model was found to have an average relative deviation of 17.5%, most of which was caused by uncertainty in experimental data. The degradation model was also compared to a cyclic degradation campaign. The concentration of 1-(2-hydroxyethyl)-2-imidazolidinone (HEIA), one of the more stable thermal degradation products, is well predicted with the thermal degradation model. However, the results also indicate that oxidative and thermal degradation mechanisms interact and that this interaction influences the concentration of several thermal degradation products.

2.2 Introduction

A reduction in carbon emissions is essential in reaching climate goals. One of the most promising processes for reducing these emissions in the short term is amine-based post-combustion carbon capture, as it is a process that can be retrofitted to current industrial installations. The flue gas, which contains the CO_2, is brought into contact with an aqueous amine solvent in an absorber, where it is selectively removed. The loaded solvent is then heated and introduced into the stripper. The higher temperatures in the stripper cause the CO_2 to desorb, regenerating the solvent.[7]

Current research mainly focuses on improving the effectiveness and sustainability of the process, making it more attractive for implementation. One of the main challenges is extending the lifetime of the solvent by limiting losses through vaporization, entrainment, or solvent degradation and deactivation. Solvent degradation is problematic as it is responsible for a significant fraction of the amine losses but also because of the production of degradation products. These products have been shown to influence the

performance of the capture plant by increasing foaming and viscosity or leading to higher corrosion rates in the plant[8].

One of the degradation mechanisms is carbamate polymerization, often referred to as thermal degradation with CO_2. This form of degradation occurs at elevated temperatures in the capture process, for example, in the stripper and reboiler. A reduction in temperature at these locations can significantly reduce the degradation rate but can, at the same time, lead to higher specific energy requirements for regeneration[9]. A good understanding of the degradation rates and mechanisms and the impact of degradation products on the process is thus essential for efficient operation and the protection and maintenance of equipment[9,10].

In this work, the thermal degradation of MEA is studied in more detail. Aqueous solutions of MEA are commonly used in carbon capture processes, and substantial data are available on degradation under typical process conditions. Several degradation models have been proposed to predict thermal degradation rates of MEA[1,2]. The role of these models is to predict not only solvent losses in the process but also the formation of degradation products. This information is valuable for obtaining a better understanding of the effects of different solvent management strategies and the influence of degradation inhibitors.

However, the degradation models in the literature are often not in agreement, as a result of different model reactions and rate equations or the use of different data sets, which are often limited to experimental measurements by the authors themselves. Therefore, this work collects experimental data on the thermal degradation of MEA, which is then used to develop, fit, and evaluate a new degradation model. The developed model aims to predict quantitatively the solvent losses and degradation product formation as a function of time and other process conditions, such as temperature and loading.

2.2.1 Degradation Mechanism

An overview of the suggested degradation reactions is given in Figure 2.1 and the relevant compounds are listed in Table 2.1. The carbamate formed when CO_2 reacts with MEA is susceptible to degradation, and at increased temperatures, it undergoes ring closure and is dehydrated to form 2-oxazolidinone (OZD). OZD is sensitive to nucleophilic attacks and reacts with MEA, leading to the formation of dimers and oligomers, imidazolidinones, and other cyclic compounds. The cyclization of the carbamate leading to the formation of OZD is the rate-limiting reaction. This rate was found to be dependent on both temperature and CO_2 loading. Higher CO_2 loadings have been shown to increase degradation rates, possibly either by forming more of the carbamate or by increasing the availability of proton donors, which can catalyze the dehydration.[9]

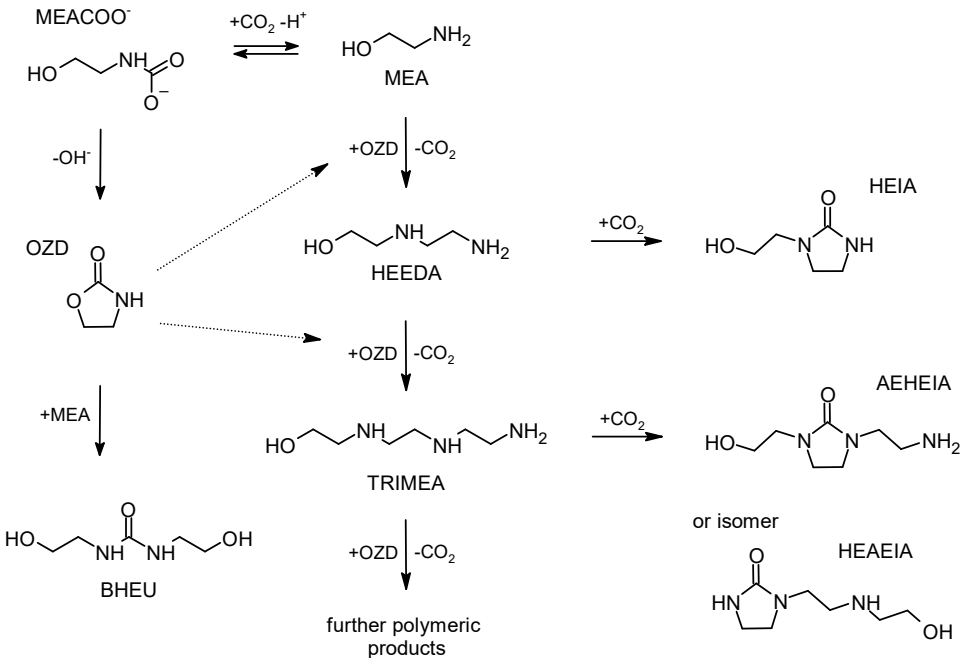

Figure 2.1: Overview of degradation reactions for the carbamate polymerization of MEA as suggested by Davis[1] and Lepaumier et al.[5].

The degradation mechanism of MEA has been discussed in the literature[1,4–6,11,12]. Polderman et al.[6] suggested a polymerization mechanism in which OZD reacted with MEA to form 1-(2-hydroxyethyl)-2-imidazolidione (HEIA). Subsequently, HEIA was suggested to react with water to form N-(2-hydroxyethyl)-ethylenediamine (HEEDA) while expelling a molecule of CO_2. This was thought to be an equilibrium reaction that is influenced by temperature and the concentration of CO_2.

Davis[1] later showed that the formation of HEEDA from HEIA is very limited under stripper conditions, whereas HEEDA readily reacts with CO_2 to form imidazolidone. HEIA is a relatively stable compound due to its five-ring structure, and experimental degradation results show that the compound accumulates in the solution over time. After an initial increase, the concentration of HEEDA remains more or less constant for the rest of the experiments, confirming its role as an intermediate. This mechanism was also suggested by Lepaumier et al.[5].

Additionally, Davis[1] found that HEEDA could react with OZD to form a trimer, N-(2-hydroxyethyl)-diethylenetriamine (TRIMEA), and further polymeric compounds. TRIMEA can react with CO_2 and form a cyclic urea through internal condensation. Depending on which amine group reacts with CO_2, two different isomers can be formed: N-(2-aminoethyl)-N'-(2-hydroxyethyl)imidazolidinone (AEHEIA) or N-[2-[(2-hydroxyethyl)amino] ethyl]imidazolidin-2-one (HEAEIA)[1,4,13]. Because the isomers are

similar in structure and no commercial standard was available, no consensus has been reached as to which isomer is the most likely product[4].

Another common degradation product is the urea of MEA, also known as 1,3-Bis(2-hydroxyethyl)urea (BHEU). The formation of this product was reported by Yazvikova et al.[14]. A mixture of MEA and OZD was heated to 200 °C in the absence of water and the urea was observed as the only degradation product. The reaction mechanisms for BHEU and HEEDA are similar, and the exact route depends on where the cleavage of the OZD ring occurs. Lepaumier et al.[13] also proposed another mechanism for the formation of BHEU. In this case, MEA directly reacts with the carbamic acid of MEA to form the urea. However, under aqueous conditions, the ion pair of the protonated MEA and the MEA carbamate is more stable than the carbamic acid, so this reaction is unlikely to occur in an aqueous MEA solvent[13].

Table 2.1: Amines and thermal degradation compounds considered in the degradation model.

Compound name	**Abbreviation**	**Molecular Formula**	**M_W (g/mol)**	**CAS Registry**
Monoethanolamine	MEA	C_2H_7NO	61.08	141-43-5
2-oxazolidinone	OZD	$C_3H_5NO_2$	78.08	497-25-6
N-(2-hydroxyethyl)-ethylenediamine	HEEDA	$C_4H_{12}N_2O$	104.15	111-41-1
1-(2-hydroxyethyl)-2-imidazolidinone	HEIA	$C_5H_{10}N_2O_2$	130.15	3699-54-5
N-(2-hydroxyethyl)-diethylenetriamine	TRIMEA	$C_6H_{17}N_3O$	147.14	1965-29-3
N-(2-aminoethyl)-N'-(2-hydroxyethyl)imidazolidinone	AEHEIA	$C_7H_{15}N_3O_2$	173.22	1402137-23-8
N-[2-[(2-hydroxyethyl)amino] ethyl]imidazolidin-2-one	HEAEIA	$C_7H_{15}N_3O_2$	173.22	1154942-78-5
1,3-Bis(2-hydroxyethyl)urea	BHEU	$C_5H_{12}N_2O_3$	148.16	15438-70-7

2.2.2 Kinetic Degradation Models in Literature

Kinetic models to describe thermal degradation of MEA have been developed by Davis[1] and Léonard et al.[2]. Léonard et al.[2] used HEIA as a surrogate for all the intermediates and degradation products but only analyzed the concentration of MEA. The degradation rate was determined by multiplying the reaction rate coefficient with the initial concentration of CO_2. The concentration of MEA has not been included in the rate equation because it is not considered to be limiting. The temperature dependence of the reaction rate coefficient was modeled using the Arrhenius equation.

The kinetic model by Davis[1] is more extensive, including most of the degradation products, except for OZD and BHEU. No reliable experimental data were available on the concentration of OZD at the time, and Davis[1] suggested that even if analytical methods would be improved, some of the OZD is likely to convert back to MEA carbamate during the cooling and handling of the samples. It was assumed that the concentration of OZD was in equilibrium with carbamate, which itself is directly related to the CO_2 concentration. At loadings below 0.5, it was assumed that the vast majority of CO_2 in the solution would be present in the form of carbamate, and as such, the concentration of CO_2 was used as a surrogate for OZD.

Analyses of degradation samples by Davis[1] showed that the trimer was not an end product and could react with OZD and CO_2 to form other polymeric compounds and imidazolidones. The concentrations were significantly lower than those of other modeled compounds. Due to the sparse data on these compounds, they were not modeled directly but grouped together as further polymeric products. The reactions from the oligomers (HEEDA and TRIMEA) to the imidazolidones (HEIA and HEAEIA) were modeled as rate-limited equilibrium reactions.[1]

Davis[1] used the Arrhenius equation to describe the temperature dependency of the reactions and the pre-exponential factor and activation energy were fitted for each reaction. The pre-exponential factor and activation energy for the reaction from HEAEIA to TRIMEA could not be determined due to insufficient experimental data of HEAEIA and is estimated instead. The activation energy for the initial degradation reaction, describing the consumption of MEA, is comparable to the activation energy fitted by Léonard et al.[2].

2.3 Methodology

2.3.1 Model Development and Assumptions

The model in this work is an adapted version of the model by Davis[1] and the following degradation reactions are taken into account:

$$2\ \mathrm{MEA} \rightarrow \mathrm{HEEDA} + \mathrm{H_2O} \qquad R_1 = k_1[\mathrm{MEA}][\mathrm{CO_2}] \qquad \text{Eq. 2.1}$$

$$\mathrm{MEA} + \mathrm{HEEDA} \rightarrow \mathrm{TRIMEA} \qquad R_2 = k_2[\mathrm{HEEDA}][\mathrm{CO_2}] \qquad \text{Eq. 2.2}$$

$$\mathrm{HEEDA} + \mathrm{CO_2} \rightarrow \mathrm{HEIA} \qquad R_3 = k_3[\mathrm{HEEDA}][\mathrm{CO_2}] \qquad \text{Eq. 2.3}$$

$$\mathrm{TRIMEA} + \mathrm{CO_2} \rightarrow \mathrm{AEHEIA} \qquad R_4 = k_4[\mathrm{TRIMEA}][\mathrm{CO_2}] \qquad \text{Eq. 2.4}$$

$$2\ \mathrm{MEA} + \mathrm{CO_2} \rightarrow \mathrm{BHEU} + \mathrm{H_2O} \qquad R_5 = k_5[\mathrm{MEA}][\mathrm{CO_2}] \qquad \text{Eq. 2.5}$$

The equilibrium reactions from HEEDA and TRIMEA to the imidazolidones HEIA and AEHEIA are assumed to be irreversible. This assumption is based on degradation experiments, which showed that the reaction rate for the production of HEIA from HEEDA was significantly larger than the reverse reaction[1]. Furthermore, concentration profiles of degradation products from experimental studies used in this work (see Table 2.2) also suggest that rate limitations are predominant, since an increase in concentration of HEIA showed no immediate effect on the concentration of HEEDA[4]. The model was tested by including these reverse and equilibrium reactions, but no improvements were observed.

Davis[1] used the concentration of CO_2 as a surrogate for the carbamate and OZD concentrations. However, at higher loadings ($\alpha \approx 0.5$), nearly all of the MEA is saturated and a fraction of CO_2 will be present as carbonates and bicarbonates. The MEA carbamate concentration is thus lower than expected in these cases, and as a result, the degradation rate is expected to be overpredicted. In an attempt to include this behavior in the model, speciation models in AspenPlus and CO2SIM (in-house software) were used to predict the carbamate concentrations in the solutions. These were then used in the degradation model as a surrogate for the OZD concentration. The resulting degradation model, however, clearly underpredicted degradation in the experiments with a loading of 0.5.

The use of the total CO_2 concentration as a surrogate was also tested and gave a much better result. Intuitively, this is difficult to understand as one would expect the carbamate concentration to be directly proportional to the formation rate of OZD and thus the overall degradation rate. An explanation could be that the dehydration of the carbamate is the rate-limiting step. The availability of protons (e.g. in the shape of $MEAH^+$) could then be rate determining. Finally, it was decided to continue to use the total concentration of CO_2 as a surrogate for the OZD concentration.

The cyclic urea that is formed when TRIMEA reacts with CO_2 has been identified in the literature as AEHEIA[4] or HEAEIA[1,15]. Huang et al.[16] reported to have identified and quantified both isomers in the degradation samples, but methods for identification are not elaborated and commercial standards of either of the isomers were not used. Because of the uncertainty, the model considers only one of the isomers, AEHEIA. Compounds that are identified as HEAEIA are assumed to be AEHEIA instead. Since the concentration of the isomers is low compared with the other degradation product, there should not be a significant error in the model if both isomers are formed in reality.

The collection of experimental data used in this work includes liquid chromatography and mass spectroscopy (LC-MS) measurements of BHEU[16,17], which makes it possible to include the urea in the model. Where the formation of OZD is a the result of an intramolecular reaction of the MEA-carbamate, BHEU is expected to be formed through an intermolecular reaction of MEA and carbamate[12]. The concentration of CO_2 is used as a surrogate for the carbamate concentration in this reaction as well. It is assumed that

the urea is a stable end product and reverse reactions are not considered. Since all but one of the measured concentrations of BHEU were from experiments at 135 °C, temperature dependence is not considered for this reaction, and the activation energy is set at zero.

2.3.2 System of Equations

In the model, the change in concentration of a compound over time is described using Eq. 2.6. The change is equal to the sum of production and consumption in all the reactions (n_r). The degree of change in each reaction is the product of the stoichiometric coefficient ($v_{i,r}$), the reaction rate coefficient (k_r), and the reactant concentrations (c_j) in mol/m^3. Here, n_j is the number of reactants.

$$\frac{dc_i}{dt} = \sum_{r=1}^{r=n_r} \left(v_{i,r}\, k_r \cdot \prod_{j=1}^{j=n_j} c_j \right) \qquad \text{Eq. 2.6}$$

The reaction rate coefficient is defined using an adjusted form of the Arrhenius equation, see Eq. 2.7. Here k_{ref} is the reaction rate coefficient at the reference temperature (T_{ref}). This temperature was chosen to be 400 K as it was close to the average temperature of the degradation experiments. E_A is the activation energy in J/mol, and R is the ideal gas constant in J·K^{-1}·mol^{-1}.

$$k_r = k_{\text{ref}} \cdot \exp\left(\frac{-E_A}{R_{id}} \left(\frac{1}{T} - \frac{1}{T_{\text{ref}}} \right) \right) \qquad \text{Eq. 2.7}$$

This form of the Arrhenius equation yields the same results as the conventional form but changes the interaction between the pre-exponential factor and the activation energy. For example, a change in activation energy will have no influence on the reaction rate coefficient for a reaction at reference temperature. This allows the parameters to be changed more independently and simplifies the optimization.

2.3.3 Objective Function

To find the reaction rate parameters for the degradation model, an objective function is defined. This objective function describes the quality of the fit as a function of the parameter estimates. An optimization algorithm can then be used to search for the optimal reaction rate parameters. The objective function should be designed such that the contribution of each deviation from experimental data is representable to the expected accuracy of this data. Measurements with higher analytical uncertainty are more likely to result in a larger deviation between the modeled and experimental values and should be weighted accordingly.

This work uses data of various reactants and products from different sources, obtained using a range of analytical methods, including LC-MS, gas chromatography and mass spectroscopy (GC-MS), and titration. Detailed information on the used analytical equipment and its accuracy, use of duplicates, dilution factors, and other extensive error analyses is in most cases not provided. Therefore, it is not easy to evaluate the accuracy and precisions of the different analytical techniques and it is assumed that the deviations are the same for all measurements.

A root-mean-square error objective function was initially used to fit the kinetic parameters, but the mean average error of the model was found to be nearly ten times larger than the analytical error observed in in-house LCMS calibration measurements. This indicates that other factors could play a significant role and influence the results of the degradation experiments. Furthermore, the concentration and absolute deviations of the degradation products and intermediates were found to be proportional. Both are thus a consequence of an increased degradation rate. The deviations of MEA and CO_2 were found to be less correlated with the rate of degradation. However, since the concentration of these compounds is higher, more dilution is required prior to analysis. As more dilution will lead to higher uncertainty, it is expected that the uncertainty is also proportional to the concentration for these compounds.

Since the error's exact nature is unknown, there is no clear reason to penalize more significant outliers using a root-mean-square function. Instead, a mean absolute error function was used, as given in Eq. 2.8. To account for the proportionality of the error, a weighing factor (w_i) is used, which is equal to the inverse experimental concentration (c_i). In the case the concentration of the products is low, however, the weighing factor can become unrealistically high and distort the results. If the experimental concentration is below the expected analytical error (ϵ_A), the inverse of this expected error is used as the weighing factor instead. From in-house LC-MS measurements, the analytical error is found to be in the range of 25-50 mol/m^3 depending on the compound, so the expected analytical error is set at a value of 50 mol/m^3.

$$f(x) = \sum_{i=1}^{i=n} w_i \cdot |\widehat{c_i} - c_i| \qquad \text{Eq. 2.8}$$

$$w_i = \min\left(\frac{1}{c_i}, \frac{1}{\epsilon_A}\right) \qquad \text{Eq. 2.9}$$

2.3.4 Optimization

Optimization of the objective function can be challenging, especially when the number of parameters (reaction rate coefficients and activation energies) is increased. The

complexity of the model may cause local optimization algorithms, such as Newton's method, to have problems finding a global minimum. For this reason, the optimization in this work is done using the particle swarm optimization (PSO) algorithm as implemented in MATLAB (R2019a). The PSO algorithm uses a swarm of particles which are distributed throughout the search space and evaluates the objective function at their location. The particles will then move through the search space based on the location of their own historical minimum and the location of the global minimum. Over time, the particles converge at a solution.

Global optimization algorithms such as PSO are generally better suited for multivariable optimization because they can overcome local minima. The default PSO algorithm settings were used as they provided satisfactory results. The number of particles was increased to 50 particles per model parameter as the optimization was not computationally demanding and this increased the accuracy of the optimization.

In the first step, the model was optimized using a constant activation energy of 100 kJ/mol for all the reactions. This provided a good estimation of the reaction rate coefficients at reference temperature, so the parameter ranges for the optimization of the complete system could be determined. Next, all the parameters were optimized. The optimization was run several times and the parameter boundaries as well as the initial guesses were adjusted to check if the same solution was obtained.

2.3.5 Repeatability and Lack of Fit F-test

The sum of residual errors describes the deviation between the model and the experimental data. This deviation is the result of two factors: the variance of the measurements and the limitations of the model. These variances can be quantified and compared to test if the model is adequate or if there is a lack of fit.

The data set used in this work contains 24 sets of experiments that share the same model parameters (initial concentration, loading, temperature, and duration). These can give an insight in the repeatability of the degradation experiments and can be used to calculate the sum of pure experimental errors (SEP) using Eq. 2.10. For every set of replicates (i, n_s), the experimental measurements in the set (j, n_r) are compared to the average concentration of the set $(\overline{c_i})$. Note that the same weighting factor $(w_{i,j})$ as for the objective function (see Eq. 2.9) is used in this equation.

$$SEP = \sum_{i=1}^{i=n_s} \sum_{j=1}^{j=n_r} w_{i,j} \cdot \left| c_{i,j} - \overline{c_i} \right| \qquad \text{Eq. 2.10}$$

The sum of errors due to lack of fit (SELOF) makes up the rest of the residual error and is equal to the difference of sum of residual errors and the SEP. An F-statistic (F^*) is then determined by taking the ratio between the mean error due to lack of fit and the

mean pure error (see Eq. 2.11). Here, n is the total number of experimental measurements, n_r is the number of replicate values, p is the number of fitted parameters (coefficients and activation energies), and m is the number of replicate sets.

	$F^* = \frac{\frac{SELOF}{n-p-(n_r-m)}}{\frac{SEP}{n_r-m}} \rightarrow F_{0.95,(n-p-n_r+m),(n_r-m)}$	Eq. 2.11

The statistical significance of the F-statistic is then compared to an F-distribution at 95% confidence, with the corresponding degrees of freedom. In the case the F-statistic is smaller than the fence value of the F-distribution, there is no significant lack of fit. If the F-statistic is larger, on the other hand, the contribution of the error due to lack of fit is statistically significant and the model is inadequate. Or in other words, the error between the model and experimental data cannot primarily be explained by the deviations in experimental results.

2.3.6 Experimental Data from the Literature

An overview of the available experimental data on carbamate polymerization is given in Table 2.2. Although some of the experiments are conducted below or around the conventional stripper temperature of 120 °C, most experiments are run at higher temperatures, as illustrated in Figure 2.2. The conditions cause the degradation rate to increase and reduce the time required to observe significant degradation and product formation. This is done under the assumption that only the reaction rates change with temperature, but the reaction mechanism remains the same. Similarly, some of the experiments are run at high loadings to increase the degradation rate. These loadings are higher than commonly found in the stripper and reboiler and thus not representable.

The majority of the experimental data consist of measurements of MEA, HEEDA, and HEIA as these are the most prominent compounds. Less data are available on CO_2, OZD, and AEHEIA as those compounds are less commonly analyzed. The data on TRIMEA have only been reported by Davis[1], most likely because the concentration of this compound is relatively low. Finally, limited data are available for BHEU and except from the single measurement by Huang et al.[16], all experiments where BHEU was measured were conducted at 135 °C. This, in combination with the relatively short degradation time of the experiments by Huang et al.[16], makes it difficult to evaluate the temperature dependency of the BHEU formation rate.

2.3.7 Experimental Procedures and Analytical Methods

The experimental data in Table 2.2 are from similarly performed degradation studies. In general, a solution of MEA and water was prepared, which was then loaded with CO_2. The loaded solvent was then placed inside a stainless-steel cylinder, which was hereafter

closed. The cylinders were placed inside an oven at the specified temperature, without being stirred or agitated. After a specified time, the cylinders were removed from the oven and cooled down, after which the solvent was analyzed.

Table 2.2: Overview of thermal degradation data from literature. *The concentration of OZD was measured using gas chromatography and possibly also contains MEA-urea (see analytical methods).

				No. experimental measurements								
Ref.	**Temp. (°C)**	**Loading**	**Days**	MEA	CO_2	OZD	HEEDA	HEIA	TRIMEA	HEAEIA	AEHEIA	BHEU
([3])	105 – 135	0.1 – 0.4	7 – 35	9	12	9	9	-	-	-	-	-
([4])	135	0.1 – 0.5	7 – 35	25	20	5*	5	5	-	-	5	-
([1])	100 – 150	0.1 – 0.5	2 – 112	24	-	-	24	24	24	24	-	-
([2])	120 – 140	0.44	7 – 21	6	-	6*	6	6	-	-	-	-
([15])	135	0.4	7 – 56	8	-	-	8	-	-	8	-	-
([16])	125 – 145	0.4	0.6 – 7	3	-	1	1	1	-	1	1	1
([18])	160	0.19 – 0.37	14 – 56	6	-	6*	6	6	-	-	-	-
([17])	135	0.1 – 0.4	7 – 35	7	9	7	7	7	-	-	-	7
Total	**100 – 160**	**0.1 – 0.5**	**0.6 – 112**	**88**	**41**	**34**	**66**	**49**	**24**	**33**	**6**	**8**

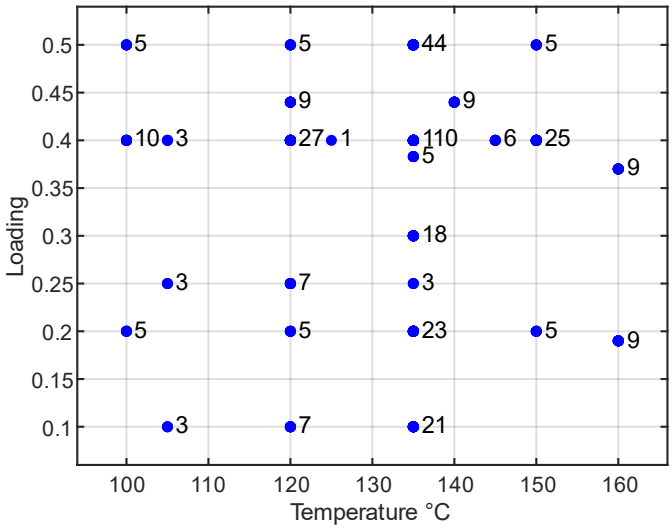

Figure 2.2: Overview of the number of data points at a given condition. The data points represent measurements of all components in all publications.

In the experiments by Zoannou et al.[18] a larger vessel with more solvent was used. The solvent and pure CO_2 were introduced into the vessel and a total organic carbon analyzer was used to monitor the loading. When the specified loading was reached, the gas valve was closed and any CO_2 that was not absorbed was vented. The vessel was then sealed and placed in a convection oven for the duration of the experiment. The preparations and experimental conditions are thus similar to the cylinder experiments. However, the measurements at 160 °C showed unrealistically high degradation, to the point where nearly all MEA was consumed, so this data has been excluded from the dataset.

Several analytical methods have been used to determine the concentrations of MEA, CO_2, and degradation products in the literature studies. Titration methods are used to determine the concentration of CO_2 and sometimes also that of the amine.[3,4,15] However, a downside of amine titration is that some of the intermediates and products, for example, HEEDA, can interact similar to the main amine and give a displaced representation of the actual concentration of MEA. Therefore, although titration is a relatively quick and inexpensive analytical method, the results are less accurate, and titration measurements have not been used for model fitting.

As alternatives to titration, liquid and ion chromatography are used to analyze the concentration of MEA and also some of the degradation products.[2,4,16,17] These analytical methods give a better representation of the actual concentration of MEA, since the compounds in the solution are separated before quantification.

GC-MS is also used to identify and quantify degradation products.[4,18] In-house analytical experience has shown that OZD and BHEU are hard to separate and identify individually using GC-MS. Although not explicitly reported, there are some indications that other works face similar challenges, as significantly higher concentrations of OZD are reported by studies that analyze using GC-MS[4,18] compared with the results obtained in studies where LC-MS is used.[3,16,17] This could indicate that the OZD which is analyzed with GC-MS is in reality the sum of OZD and BHEU. Additionally, the formation of BHEU was not reported in any of the GC-MS studies.

2.4 Results

2.4.1 Optimized Model Parameters

The optimized parameters are given in Table 2.3. Although the rate coefficients are significantly lower for reactions 1 and 5, the reaction rate is in the same order of magnitude for all the reactions. The reason for this is that both reactions 1 and 5 have MEA as a reagent, which is present in much higher concentrations compared with the other compounds.

Table 2.3: Optimized parameters for the carbamate polymerization model.

Reaction	k_{ref} **[m^3·mol^{-1}·s^{-1}]**	E_A **[kJ/mol]**
1 (MEA to HEEDA)	$1.599 \cdot 10^{-11}$	151.1
2 (HEEDA to TRIMEA)	$1.117 \cdot 10^{-10}$	121.5
3 (HEEDA to HEIA)	$3.054 \cdot 10^{-10}$	142.6
4 (TRIMEA to AEHEIA)	$2.839 \cdot 10^{-10}$	136.2
5 (MEA to BHEU)	$1.281 \cdot 10^{-12}$	-

2.4.2 Lack of Fit F-test

An overview of the variations for the data set and the fitted results is given in Table 2.4. In total, there are 24 sets of replicates with mostly 2, 3, or 4 replicates each. The total number of distinct replicate values, and thus the degrees of freedom for the SEP is 31. The mean deviation in the replicates is 18.2%, which is roughly similar to the mean deviation of the model. The results from the F-test also show that the lack of fit is not significant as the F-statistic is lower than the 95% F-distribution fence.

Table 2.4: Overview of the variations and the lack of fit evaluation.

Variation source	**Total variation**	**Mean variation**	**Degrees of freedom**	**F-statistic**	**F-fence**
SE	50.0	0.175	286 $(n-p)$	0.96	1.63
SEP	5.65	0.182	31 (n_r-m)		
SELOF	44.4	0.174	255 $(n-p-n_r+m)$		

The variation in experimental results is also illustrated in the top left plot of Figure 2.3. All the experimental observations in this figure describe degradation of a 30 wt-% solution of MEA, with a loading of 0.4 and at a temperature of 135 °C. Although the experiments are identical on paper, there is still a significant deviation in the measured amine concentrations, which explains the substantial pure experimental error. Similar observations are made for the degradation products (e.g., Figure 2.4).

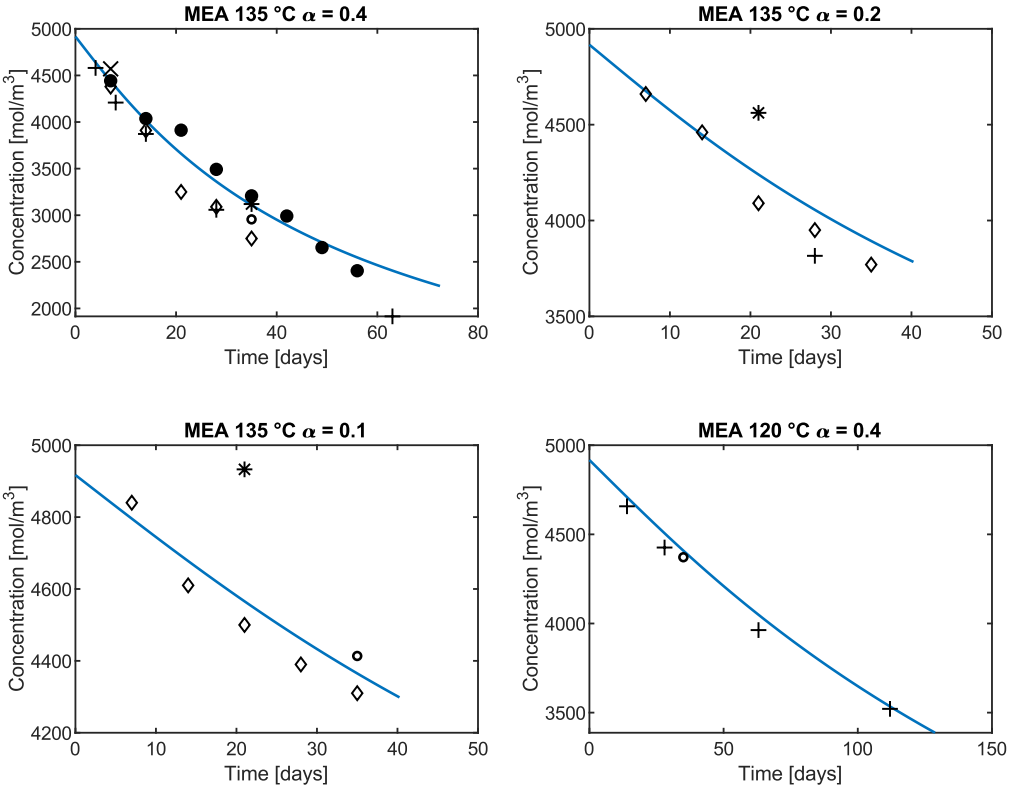

Figure 2.3: Modeled concentrations of MEA as a function of time for various loadings and temperatures compared to experimental measurements from literature (∗ Høisæter et al.[17], + Davis[1], ◊ Eide-Haugmo[4], o Grimstvedt et al.[3], × Huang et al.[16], • Zhou et al.[15]).

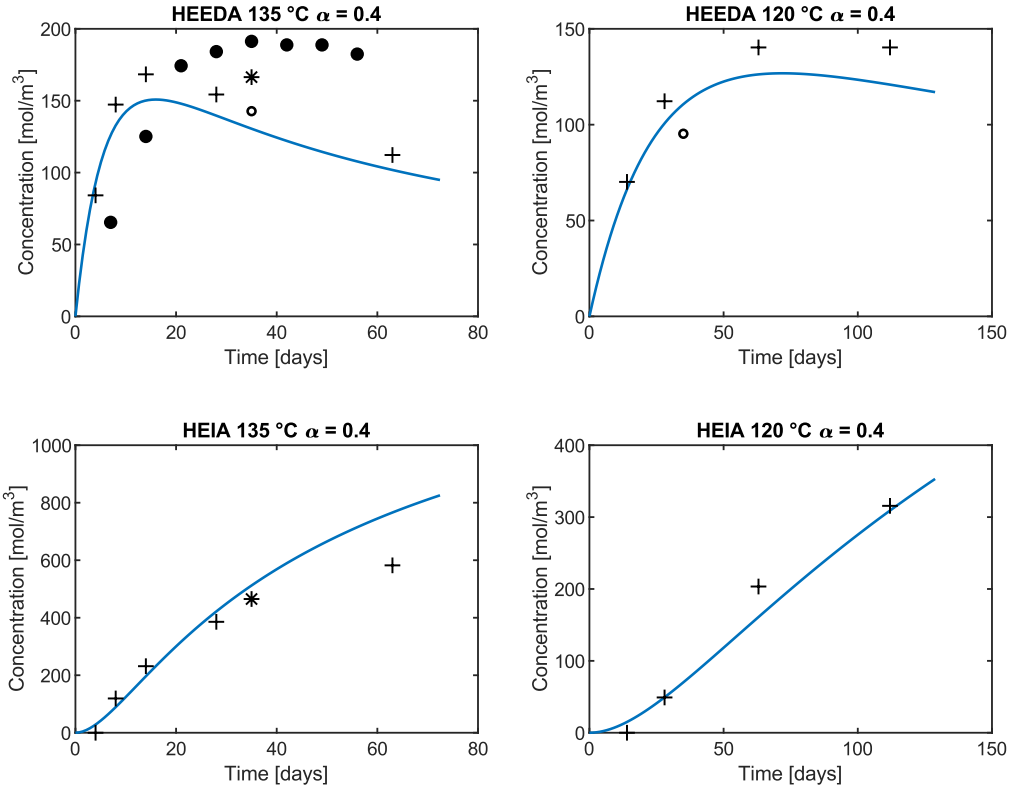

Figure 2.4: Modeled concentrations of the degradation products HEEDA and HEIA as a function of various loadings and temperatures compared to experimental measurements from literature (∗ Høisæter et al.[17], + Davis[1], o Grimstvedt et al.[3], • Zhou et al.[15]).

2.4.3 Model Deviations and Trends

An overview of the relative deviations for each component is given in Figure 2.5. The mean relative deviation is 17.5%. The components have deviations that roughly average out around zero. The majority of the deviations are located around the average and only a few points show significant relative deviation, primarily for HEEDA, HEIA, or AEHEIA. Further inspection shows that these high relative deviations are caused by low absolute concentrations. Although the object function was designed to address this issue by limiting the weight of these points using a minimal analytical error, it is not entirely successful. It is possible that the analytical errors were more significant than expected for some of the measurements or that other errors were at play. Nevertheless, the contribution of the few high relative deviations is limited.

Figure 2.6 shows the model's relative deviations in MEA concentration for each of the experimental works. The model appears to overpredict the concentration of MEA for some of the experiments (e.g., Davis[1] and Eide-Haugmo[4]). This means that the degradation in these experiments is relatively high with respect to the rest of the experiments. The experimental results by Léonard et al.[2], on the other hand, show less degradation than predicted. The figure thus illustrates that there are potentially some systematic errors at play. This agrees with the observations in Figure 2.3 and Figure 2.4. Since the experimental methods for each of the studies are nearly identical, the reason

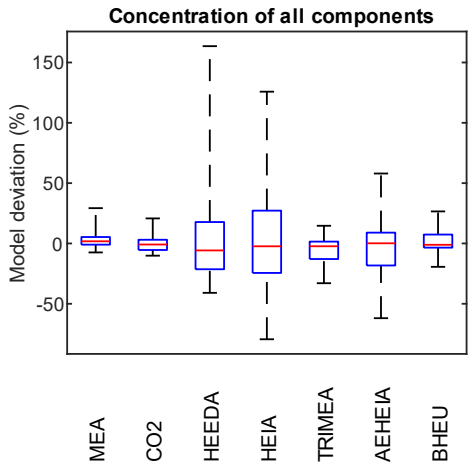

Figure 2.5: Box plot of the weighted deviations of the model in comparison to the experimental results for each of the components.

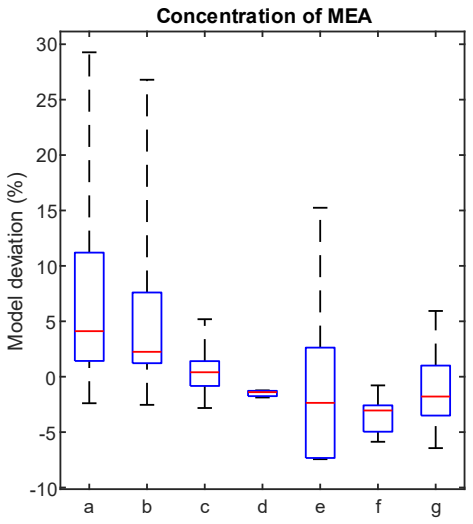

Figure 2.6: Box plot of the weighted deviations of the model for MEA in comparison to the experimental results for each of the experimental works (a:Davis[1], b:Eide-Haugmo[4], c:Grimstvedt et al.[3], d:Huang et al.[16], e:Høisæter et al.[17], f:Léonard et al.[2], g:Zhou et al.[15].

for the discrepancies is unknown. The absolute and relative deviations for HEIA as a function of several parameters are given in Figure 2.7 and Figure 2.8, respectively. Figure 2.7 shows that the absolute deviations increase as the extent of degradation increases through higher temperatures, loadings, or longer durations. However, the last points (at 112 days) give low deviations as these experiments were performed at low loadings and/or temperatures leading to only a small amount of degradation. By applying weights according to Eq. 2.8 and Eq. 2.9, the contributions of the measurements are more balanced (see Figure 2.8). A similar behavior was observed for HEEDA and the other degradation products.

The absolute and relative model deviations for MEA are given in Figure 2.9 and Figure 2.10. The relative deviation is smaller for MEA compared with the other degradation compounds. Figure 2.10 shows that the predictions of the model are accurate for higher concentrations of MEA, in which case the degradation is limited. In the case of high temperature or/and a high loading leading to more degradation, the model tends to overpredict the concentration of MEA, which means there is more degradation in the experiments than predicted.

One potential reason for the overprediction at high temperatures could be related to the formation rate of BHEU. Since there was not enough experimental data at different temperatures (experimental data for this compound were mainly available at 135 °C), the reaction rate was assumed to be temperature-independent. Experiments at higher temperatures could therefore produce more BHEU and consume more MEA, which could explain why the model shows less degradation at high temperatures.

At a loading of 0.5, the overprediction of MEA corresponds with an underprediction of several degradation products, for example, HEIA (see Figure 2.7 and Figure 2.8). The results thus suggest that there is more degradation than the model is able to represent at high loadings. However, it is important to note that the deviations for MEA are in the same order of magnitude as the pure experimental error (18.2%). Experiments with significant degradation were found to deviate considerably from each other. Although there appears to be a trend that higher degradation leads to larger deviations in the model, it is important to consider that this could be the result of experimental uncertainty.

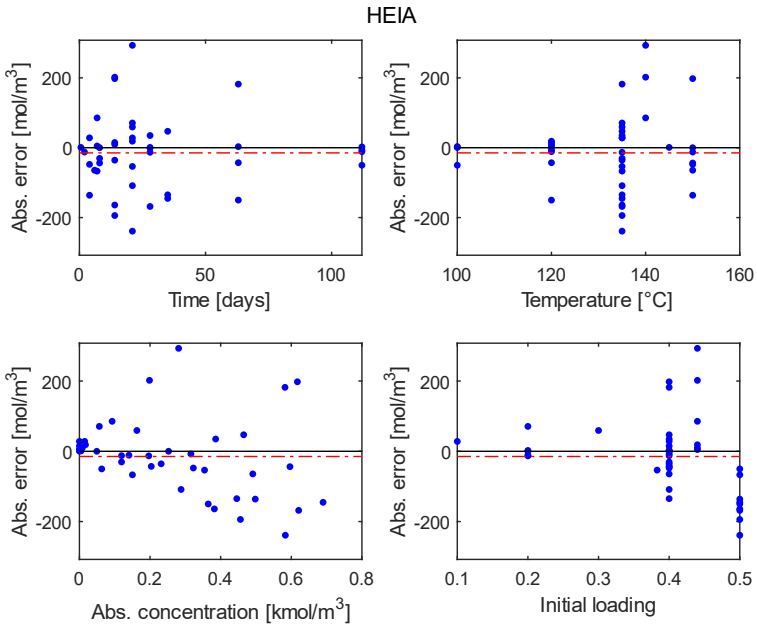

Figure 2.7: Absolute deviations for HEIA as a function of time, temperature, experimental HEIA concentration, and initial loading. The red line indicates the average deviation.

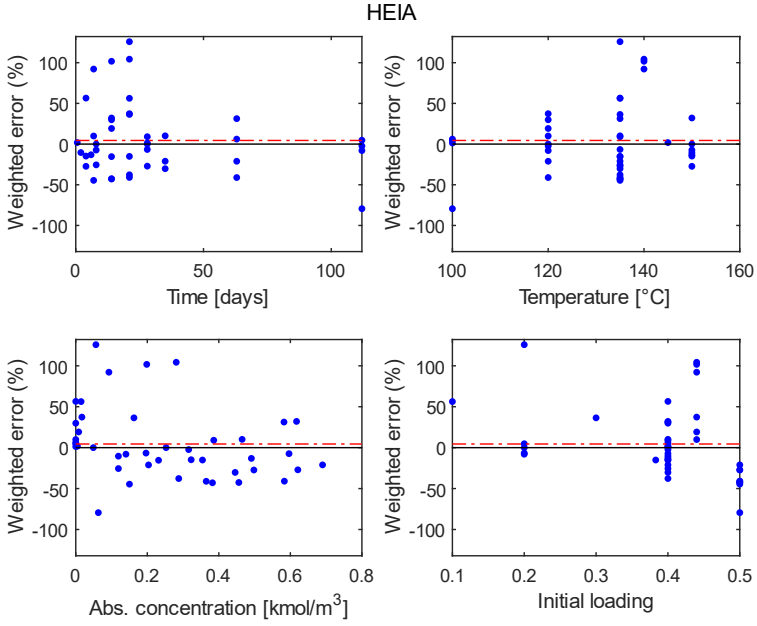

Figure 2.8: Relative deviations for HEIA as a function of time, temperature, experimental HEIA concentration, and initial loading.

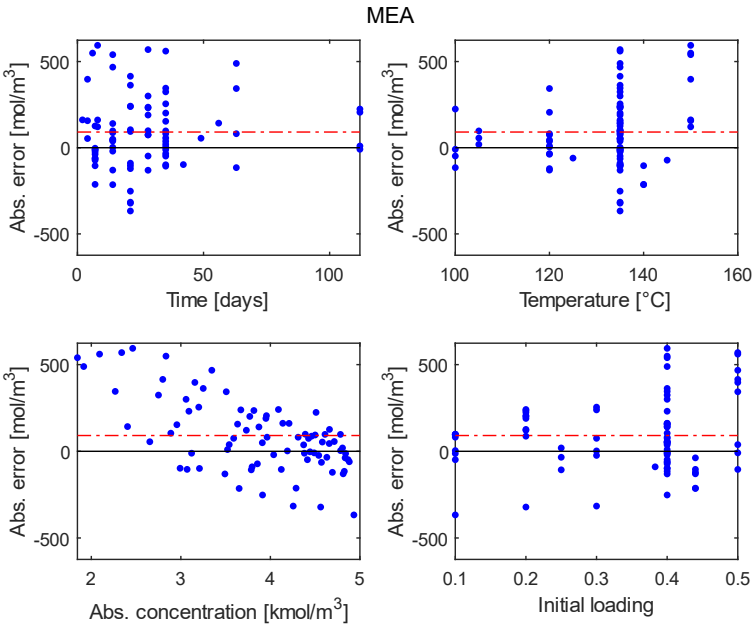

Figure 2.9: Absolute deviations for MEA as a function of time, temperature, experimental MEA concentration, and initial loading.

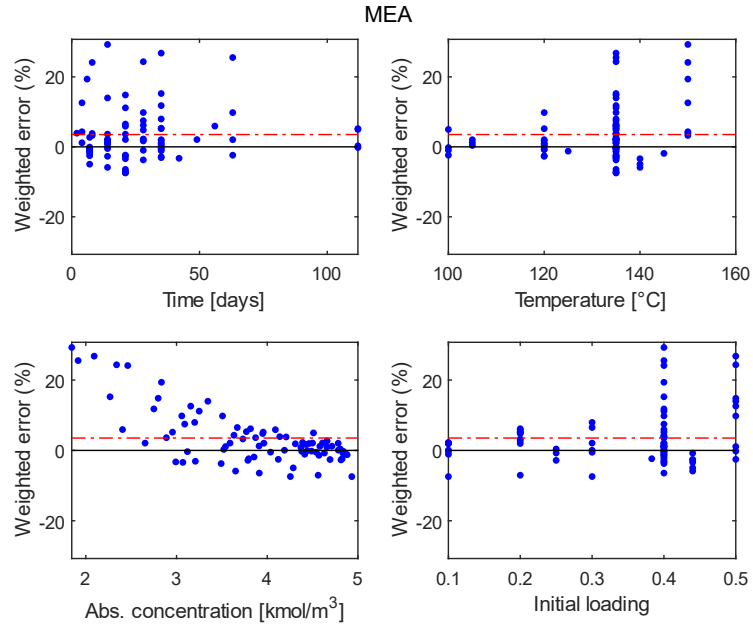

Figure 2.10: Relative deviations for MEA as a function of time, temperature, experimental MEA concentration, and initial loading.

2.4.4 Comparison with Literature Models

The models of Davis[1] and Léonard et al.[2] have been implemented and were used to compare and evaluate the model developed in this work. The models were run starting with a fresh 30 wt% MEA solution loaded with CO_2 and under the specified conditions. The models were then assessed on their initial degradation rate and the total consumption rate of MEA at the beginning of the run. The model of Davis[1], which also contained reaction rate equations for the formation of degradation products, was also used to evaluate the production rate of HEIA. The model by Léonard et al.[2] does not go in further detail on the formation of degradation products. First, the models were evaluated for a range of temperatures in the case of a rich solvent at a loading of 0.4. The results of the comparison are given in Figure 2.11 and Figure 2.12.

The figures show the high temperature dependency of the reaction rates, which is a result of significant activation energies in the Arrhenius equation. This dependency has been

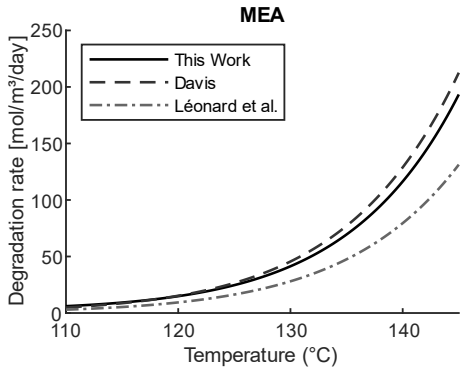

Figure 2.11: Comparison of the initial degradation rates of the models at a loading of 0.4, (Davis[1] and Léonard et al.[2]).

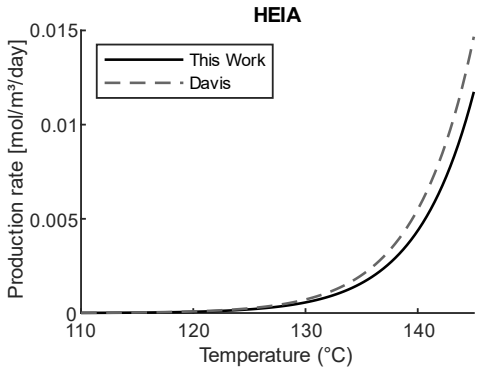

Figure 2.12: Comparison of the initial production rates of HEIA of the models at a loading of 0.4, (Davis[1])

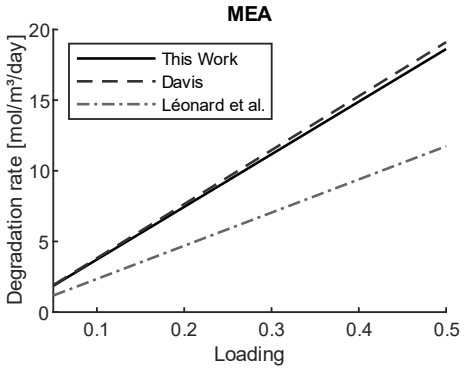

Figure 2.13: Comparison of the initial degradation rates of the models at 120 °C, (Davis[1] and Léonard et al.[2])

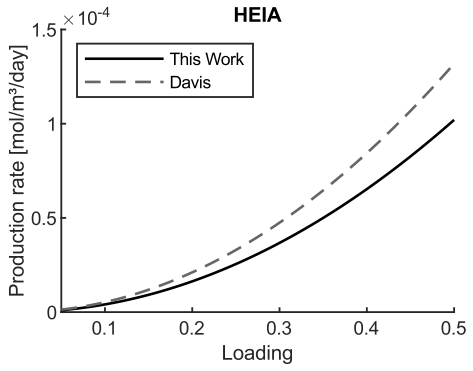

Figure 2.14: Comparison of the initial production rates of HEIA of the models at 120 °C, (Davis[1])

reported in the literature before[19,20]. At lower temperatures, the model developed in this work predicts relatively high degradation rates. However, due to limited degradation under these conditions, the absolute differences remain limited. As the temperature and degradation rate increase, the model by Davis[1] predicts similar MEA losses as the current model. The model by Léonard et al.[2], on the other hand, deviates more significantly from the current model and predicts lower degradation rates throughout the entire temperature range. At a temperature of 120 °C, the degradation rate is predicted to be 14.5 mol/m^3/day. At this temperature, the model by Davis[1] predicts a degradation rate of 15.6 mol/m^3/day (+7.7%) and the model by Léonard et al.[2] predicts a rate of 9.57 mol/m^3/day (-34.0%).

With regard to HEIA, the model by Davis[1] predicts significantly higher concentrations. At higher temperatures, the relative deviation appears to decrease, but at 135 °C, this deviation is still +40%. This is in agreement with the observation that the experimental concentrations of HEIA reported by Davis[1] were slightly higher than measured by other researchers. The deviations between the models for the other degradation products were roughly in the same order of magnitude.

The models were then also evaluated at a constant temperature of 120 °C, which is the typical temperature of the reboiler in the stripper of the capture plant. The results of this comparison are given in Figure 2.13 and Figure 2.14. The degradation rate and formation rate of HEIA show a more linear dependency on loading. As a result, the found model deviations are relatively constant as a function of temperature. At 120 °C, the model by Davis[1] predicts a slightly higher consumption of MEA, whereas the model by Léonard et al.[2] predicts a significantly lower degradation rate. More HEIA is predicted to be formed by the model of Davis[1].

2.4.4.1 Lack of Fit F-test for Literature Models

The models by Davis[1] and Léonard et al.[2] have been evaluated using all the data shown in Table 2.2, and the results are given in Table 2.5. The mean variation for the model by Davis[1] was found to be 18.5%, which is slightly higher than the model from this work, but the F-statistic is still within the F-fence. This indicates that there is no significant lack of fit for the model. Since the model by Léonard et al.[2] does not quantify the formation of degradation products, it is evaluated only using data of MEA measurements. The same has been done for the other models to be able to compare the results. The mean relative deviation of the model by Davis[1] is the lowest, followed by the model from this work and the model by Léonard et al[2]. The lower mean relative deviations indicate that the uncertainty for the degradation products is high compared with the uncertainty in the MEA measurements. In addition, the mean pure experimental error (MSEP) of the MEA replicates is 7.1%, which is also significantly lower than the MSEP of the complete replicate data set. Therefore, also in this case, it appears that the experimental error limits the accuracy of the model. None of the models appear to have a lack of fit.

Table 2.5: Variances and lack of fit F-test of the compared models (this work, model by Davis[1], and model by Léonard et al.[2]) for the entire dataset and for the measurements of MEA only.

Model	Mean rel. error (%)	Number of Experiments	Number of Replicates	F-statistic	F-fence
This work	17.5	295	55	0.96	1.64
Davis[1]	18.5	295	55	1.01	1.64
Léonard et al.[2] (MEA only)	8.1	82	25	1.17	2.16
This work (MEA only)	6.1	82	25	0.81	2.16
Davis[1] (MEA only)	5.0	82	25	0.62	2.16

2.4.5 Experimental Uncertainty

The model deviations and the pure experimental error are more significant than the expected analytical error, which was also used in the objective function (see Eq. 2.8 and Eq. 2.9). Only for less abundant components, such as the intermediate HEEDA, can the experimental uncertainty be explained by analytical deviations. The source of the uncertainty is thus expected to be experimental rather than analytical.

Despite the similarities of the experimental methods across the investigated works, there are some differences that could result in experimental uncertainty. In some experiments[4,5], glass containers were used to prevent metallic ions from leaching into the solvent. Nevertheless, this was not found to have significant effect on degradation.[4,5] Also, in the error analysis of this work, no trends were observed with regard to the use of glass cylinders.

Furthermore, the temperature in the degradation ovens could potentially deviate and fluctuate during the experiments. In general, however, temperature control in degradation ovens is good and the deviations in the degradation model as a result of the expected temperature fluctuations were negligible compared with the model's error with respect to the experimental data. Another parameter that is important in the experiments is the loading of the solution. In-house experience has shown that it can be challenging to accurately load a solvent gravimetrically and deviations up to 0.03 mol CO_2/mol MEA are not uncommon. Eide-Haugmo[4] measured the CO_2 concentrations of the initial solutions in her work, which were found to deviate between 0.005 and 0.025 mol CO_2/mol MEA from the targeted loading. Other experimental works[1–3,15,16] only report the targeted loading, while analytical results of the initial loaded solutions are often not given. Also, there could be a loss of CO_2 while transferring the solution during

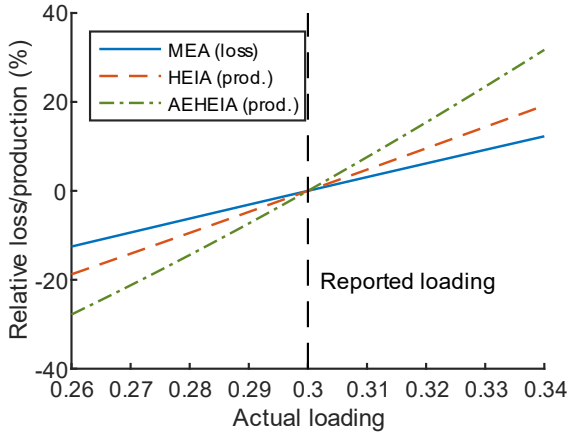

Figure 2.15: Effect of inaccurate initial loadings on the loss of MEA and production of HEIA and AEHEIA in modeled degradation experiments at 130 °C for 5 weeks.

preparation of the degradation cylinders. Although not quantified, we expect this loss to be insignificant.

To assess the impact of a deviation in loading, the degradation model is used to simulate degradation experiments at 130 °C and around a loading of 0.3, which is approximating the average of the experimental dataset. The initial loading is varied and the loss of MEA and production of HEIA and HEEDA are compared to the reference values at a loading of 0.3. The sensitivity of the model with respect to the initial loading is shown in Figure 2.15. The figure shows that a deviation in the initial loading of 0.03 mol CO_2/mol MEA can have a significant effect on the solvent consumption and the production of degradation products, both of which are under or overpredicted by 10 to 20%. This deviation is comparable with the pure experimental error and the mean relative deviation of the model, given in Table 2.4. Furthermore, the variations in the initial loading have a higher impact on the production of HEIA and AEHEIA than on the consumption of MEA, which is in line with the higher experimental uncertainty of degradation products observed in Figure 2.5.

The deviations in the solvent loading are thus expected to be the main cause of the observed experimental uncertainty. This can be reduced by analyzing and reporting the initial CO_2 loading instead of only providing the target loading. To get a loading closer to the target value, one could aim slightly higher during the gravimetrical loading, measure the CO_2 concentration, and compensate for the difference by adding some unloaded solvent. Given the strong influence of the loading, it remains important to weigh the cylinders before and after degradation and to be critical towards leakages.

2.4.6 Model Performance for Circulative Degradation Rig and Pilot Operation

Vevelstad et al. investigated solvent degradation of a 40 wt-% aqueous MEA solvent in the solvent degradation rig (SDR)[21]. The setup simulates an absorption/desorption system and uses a synthetic flue gas with 3 vol% CO_2, 12 vol% O_2, and 10 ppmv NO_x. During the 8 week campaign, the concentration of NO_x and reboiler temperature were varied. NO_x was increased to 100 ppmv from week 4 up to and including week 7. The stripper temperature was generally kept at 120 °C but was increased to 140 °C during weeks 5 and 6 to evaluate the degree of degradation at higher temperatures.

The conditions in different process parts and solvent volumes in them are given in Table 2.6. In the desorber sump, the CO_2 has been stripped from the solvent and the temperatures are equal to the reboiler temperature. The overflow of the reboiler sump was collected in a buffer vessel before passing through the heat exchanger. The temperature in this vessel is observed to be roughly 10 °C lower than the reboiler temperature due to heat losses to the environment.

The rich inlet temperature was observed to be 75 °C with a reboiler temperature of 120 °C and around 95 °C in the case of a reboiler temperature of 140 °C. For the plate heat exchanger, both the rich and lean flows were considered, and the holdup volume on each side was reported to be around 0.61 L. The temperature of the lean inlet was assumed to be 10 °C higher than the rich outlet temperature. The temperature corresponding with the average degradation rate in the heat exchanger was assumed to be 5 °C lower than the maximum temperature on each side, and this was used in the model.

Table 2.6: Overview of the estimated degradation volumes and conditions in the SDR equipment. [1]The level in the lean buffer vessel was not reported but it was assumed to be 50% of the total volume.

	Desorber sump	**Lean buffer vessel**	**Rich inlet**	**Heat exchanger**
Temperature (°C)	120/140	110/130	75 – 95	40 – 105
Holdup volume (L)	0.27 (5.4%)	0.29 (5.8%)[1]	0.02 (0.4%)	1.22 (24.4%)
Loading	0.24 – 0.26	0.24 – 0.26	0.46 – 0.49	± 0.25 and 0.48

Since the degradation experiment in the SDR was aimed at studying both oxidative and thermal degradation, as well as degradation by NO_x, the observed consumption of MEA is larger than that predicted using the degradation model, which only considers the thermal contribution. It is thus not possible to evaluate the thermal degradation model using these results. However, three of the thermal degradation products were also analyzed in the SDR experiment: HEEDA, HEIA, and BHEU. The model considers the formation rate of BHEU to be independent of the temperature because all but one of the measurements for this compound were at 135 °C. With most temperatures in the SDR setup well below this temperature, the thermal degradation model predicts a three times

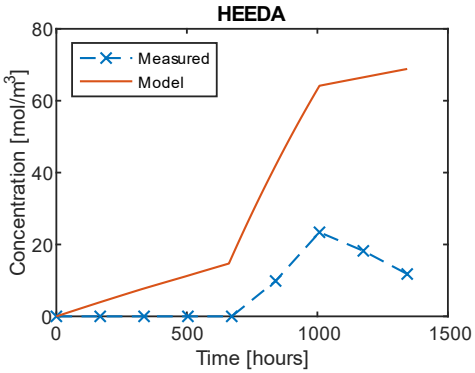

Figure 2.16: Modeled and experimental concentration profile of HEEDA during the SDR campaign[21].

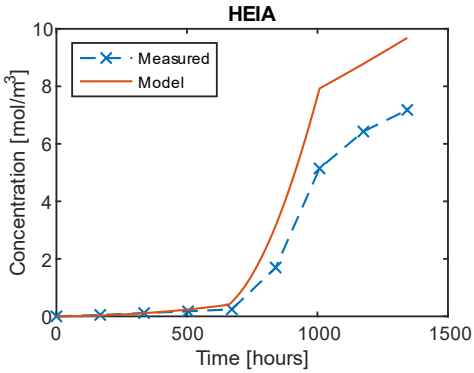

Figure 2.17: Modeled and experimental concentration profile of HEIA during the SDR campaign[21].

higher concentration of BHEU at the end of the experimental campaign. This also illustrates that the formation of BHEU is temperature-dependent and experimental data at different temperatures are needed.

Figure 2.16 shows that the concentration of HEEDA is over-predicted by the model. The measured concentrations in the first 4 weeks were negligible. Only when the stripper temperature was increased to 140 °C for the next 2 weeks, the formation of HEEDA was observed. The rate at which the concentration increases is lower compared with the model prediction. This can be caused by either a lower production rate or additional consumption of the intermediate. This difference is expected to be caused by oxidative degradation, due to the presence of oxygen in the flue gas of the degradation rig.

Vevelstad et al.[22] invested thermal degradation of MEA with an already oxidatively degraded solvent, from which they concluded that the same degradation products were formed and solvent loss was comparable to thermal degradation with a fresh solvent. Therefore, instead of oxidative degradation influencing thermal degradation, it is more likely that HEEDA partakes in oxidative degradation. This also explains the absence of HEEDA in the first weeks of the campaign, and also the decrease in concentration during the final 2 weeks when the stripper temperature is reduced again.

Lepaumier et al.[23] showed that HEEDA is susceptible to oxidative degradation, so it is a possibility that it reacts with the dissolved oxygen in the absorber. Generally, however, the concentration of HEEDA is relatively low and the oxidative degradation reactions are probably not selective due to their radical nature, so the loss of HEEDA through oxidative degradation is expected to be limited.

A more probable alternative is the reaction between HEEDA and oxidative degradation products. Lepaumier et al.[23] suggested that HEEDA reacts with glycolic acid, which is followed by an intramolecular dehydration to form piperazinones, such as 4-(2-hydroxyethyl)piperazin-2-one (4HEPO). Gouedard[12] proposes an alternative

mechanism, in which HEEDA reacts with glyoxal to form a vicinal diol that can be dehydrated to form the piperazinones. 4HEPO was also found to be a significant degradation product in the circulative degradation rig[21]. The results thus suggest that HEEDA is consumed for the production of piperazinones when exposed to oxidative degradation products.

Furthermore, Huang et al.[16] investigated the impact of flue gas contaminants on thermal degradation of MEA. It was found that the addition of 5000 ppm of nitrite significantly increased the production of HEEDA. Huang et al. proposed a slightly adjusted pathway for the degradation of MEA in which the nitrite reacts with a hydroxyl group on the MEA, after which this intermediate can react with another MEA and form HEEDA through an intermolecular substitution to cleave nitrite. Therefore, the NO_x in the flue gas of the SDR, which forms nitrite upon dissolution, could have increased the formation of HEEDA. This effect is not directly visible in the SDR results since a higher concentration of HEEDA would be expected in that case. The effect is possibly reduced by the relatively low concentration of NO_x in the flue gas and may be overshadowed by the consumption of HEEDA through reactions with oxidative degradation products. It would be interesting to see and compare the concentration profiles of the degradation products without the addition of NO_x.

The concentration of HEIA, on the other hand, seems to be well-predicted, as illustrated in Figure 2.17. Initially, at a normal stripper temperature, the formation of HEIA is limited and the degradation model is in line with the experimental results. When the stripper temperature is increased, both show an increase in HEIA production, with a slightly higher concentration for the model at the end of week 6. For the remainder of the experiment, the increase in HEIA concentration appears to be similar for both, with a difference of around 2 mol/m^3. The formation of HEIA is considered to be a function of the concentration of HEEDA and CO_2 in the degradation model, and in the literature, it has been confirmed that HEEDA is a predecessor of HEIA. Since the concentration of CO_2 is controlled in the SDR, an overestimation of HEEDA is thus expected to also result in also a similar overestimation of HEIA. However, this is not the case.

The model results also show that most of the thermal degradation takes place in the reboiler sump and the rich side of the heat exchanger, the latter mostly due to relatively high volumes in the heat exchanger. According to the degradation model, the thermal degradation rate in a typical reboiler (α = 0.2, 120 °C) is nearly twice as large as the rate in a typical rich stripper inlet (α = 0.5, 100 °C). This combined with a relatively large retention time in the reboiler causes it to be one of the main contributing locations of thermal degradation. When the stripper temperature is increased, this effect will become even more pronounced. A higher stripper temperature will have an effect on the temperature in the other parts of the plant, but due to the strong temperature dependency of the degradation reaction, the increase in degradation will be more substantial in the

reboiler. In the case of the SDR, around 60% of the thermal degradation is expected to take place in the reboiler sump at a stripper temperature of 140 °C.

Degradation of a 30 wt% MEA solvent was also investigated in a post-combustion capture pilot plant by Moser et al. in an 18-month test at Niederaussem[24]. For the first 335 days, the capture plant was operated without applying solvent management strategies or active reclaiming. The accumulated data for this period on degradation product concentrations can be used to evaluate the degradation model.

Solvent degradation of MEA in the Niederaussem plant was found to be lower compared with other capture plants and this is also reflected on the measured concentrations of HEEDA and HEIA. Like the comparison with SDR data, HEEDA is overpredicted substantially using the model, possibly due to the same reasons discussed previously.

The measured and modeled concentrations of HEIA over the course of the pilot run are shown in Figure 2.19. For the first 50 days, the concentration of HEIA seems to be well-predicted by the degradation model. Afterward, however, the growth in HEIA concentration stagnates in the capture plant, whereas the model predicts an increase. HEIA is considered to be a stable degradation compound and is expected to accumulate in the solution. The results at Niederaussem, however, suggest that either the formation of HEIA is slowed down or HEIA is consumed in consecutive reactions through, for example, polymerization or precipitation. It is hard to find a clear reason for this behavior since it is not observed in the laboratory-scale studies.

It is important to consider that the duration of the laboratory-scale experiments, on which the degradation model is based, is limited and in most cases below 100 days. There could thus be a change in the degradation mechanisms or rates after extended exposure, and it would be interesting to investigate if a similar behavior is observed in laboratory-scale experiments over an extended period.

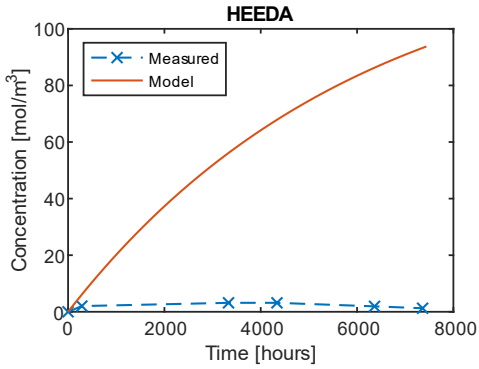

Figure 2.18: Modeled and experimental concentration profile of HEEDA during the Niederaussem campaign[24].

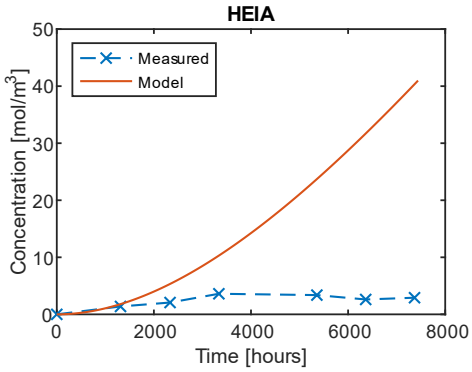

Figure 2.19: Modeled and experimental concentration profile of HEIA during the Niederaussem campaign[24].

2.5 Conclusions

In this work, a model describing carbamate polymerization of aqueous MEA solutions was developed and fitted using a collection of experimental data from the literature. The model has an average relative deviation of 17.5%, most of which is a result of high experimental uncertainty and limited reproducibility. In comparison with the developed model, the degradation model by Davis[1] slightly overpredicts degradation, whereas the model by Léonard et al.[2] underpredicts degradation for the majority of conditions.

The current model overpredicted the concentration of MEA for experiments with high loadings. The reason for this behavior is unclear. However, analysis of experimental variances in replicates showed that the observed deviations are still in the same magnitude of the expected experimental variance. Since degradation under these conditions is often not encountered in post-combustion capture plants, more research could help to clarify the observed behavior, but model improvements will probably be limited.

The degradation model was able to predict the formation of HEIA in the SDR campaign accurately and the degradation product is shown to be a promising indicator of thermal degradation. The concentration of HEIA is usually low in comparison with other degradation products, so it is not a good indicator for the quality of the solvent but rather may help to quantify the degree of thermal degradation. Concentrations of HEIA in the Niederaussem capture plant were found to differ substantially from the model predictions. The low degradation rates during the campaign and the concentration profile of HEIA are unexpected and the data should be investigated in more detail as it is possible that other factors influenced the degradation mechanism or reaction rates.

The observed concentrations of HEEDA in the campaigns were not in agreement with the predictions from the degradation model. The conditions in the pilot plant campaigns are not as controlled as the laboratory-scale experiments and the presence of oxygen can influence the degradation mechanisms. The carbamate polymerization reactions are likely to interact with oxidative degradation reactions, which would explain the unexpected concentration profiles of HEEDA. Future research should therefore focus on clarifying this interaction between oxidative and thermal degradation as details on these mechanisms could be valuable for further development of the degradation model.

Finally, the use of more consistent experimental methodologies and more elaborate reporting of experimental conditions, assumptions and calculations, and analytical methods are required to improve the quality of the experimental results. This should lead to better reproducibility and more accurate model development.

Acknowledgments

This publication has been produced with support from the NCCS Research Centre, performed under the Norwegian research program Centres for Environment-friendly

Energy Research (FME). The authors acknowledge the following partners for their contributions: Aker Carbon Capture, Allton, Ansaldo Energia, Baker Hughes, CoorsTek Membrane Sciences, Equinor, Fortum Oslo Varme, Gassco, KROHNE, Larvik Shipping, Lundin Norway, Norcem, Norwegian Oil and Gas, Quad Geometrics, Stratum Reservoir, Total, Vår Energi, Wintershall DEA, and the Research Council of Norway (257579/E20). We acknowledge Solrun Johanne Vevelstad for reading the manuscript before submission and providing valuable input on the degradation mechanisms and Vanja Buvik for suggestions regarding the degradation mechanisms and analytical methods and their uncertainties.

2.6 References

(1) Davis, J. D. Thermal Degradation of Aqueous Amines Used for Carbon Dioxide Capture. Doctoral thesis, The University of Texas, Austin, 2009. https://repositories.lib.utexas.edu/handle/2152/6581.

(2) Léonard, G.; Toye, D.; et al. Experimental Study and Kinetic Model of Monoethanolamine Oxidative and Thermal Degradation for Post-Combustion CO 2 Capture. *International Journal of Greenhouse Gas Control* **2014**, *30*, 171–178. https://doi.org/10.1016/j.ijggc.2014.09.014.

(3) Grimstvedt, A.; Falck da Silva, E.; et al. Thermal Degradation of MEA, Effect of Temperature and CO2 Loading; SINTEF Materials and Chemistry, Trondheim, TCCS-7, 2013.

(4) Eide-Haugmo, I. Environmental Impacts and Aspects of Absorbents Used for CO2 Capture. Doctoral thesis, Norwegian University of Science and Technology, Trondheim, 2011.

(5) Lepaumier, H.; Picq, D.; et al. New Amines for CO_2 Capture. I. Mechanisms of Amine Degradation in the Presence of CO_2. *Ind. Eng. Chem. Res.* **2009**, *48* (20), 9061–9067. https://doi.org/10.1021/ie900472x.

(6) L. D. Polderman; Dillon, C. P.; et al. Why Monoethanolamine Solution Breaks down in Gas-Treating Service. *Oil & Gas Journal* **1955**, *54* (2), 180–183.

(7) Nakao, S.; Yogo, K.; et al. CO2 Capture with Adsorbents. In *Advanced CO2 Capture Technologies: Absorption, Adsorption, and Membrane Separation Methods*; Springer International Publishing: Cham, 2019; pp 45–63. https://doi.org/10.1007/978-3-030-18858-0_4.

(8) Reynolds, A. J.; Verheyen, T. V.; et al. Degradation of Amine-Based Solvents. In *Absorption-Based Post-combustion Capture of Carbon Dioxide*; Elsevier, 2016; pp 399–423. https://doi.org/10.1016/B978-0-08-100514-9.00016-0.

(9) Vega, F.; Sanna, A.; et al. Degradation of Amine-Based Solvents in CO2 Capture Process by Chemical Absorption. *Greenhouse Gases: Science and Technology* **2014**, *4* (6), 707–733. https://doi.org/10.1002/ghg.1446.

(10) Reynolds, A. J.; Verheyen, T. V.; et al. Towards Commercial Scale Postcombustion Capture of CO2 with Monoethanolamine Solvent: Key Considerations for Solvent Management and Environmental Impacts. *Environmental Science and Technology* **2012**, *46* (7), 3643–3654. https://doi.org/10.1021/es204051s.

(11) Strazisar, B. R.; Anderson, R. R.; et al. Degradation Pathways for Monoethanolamine in a CO_2 Capture Facility. *Energy Fuels* **2003**, *17* (4), 1034–1039. https://doi.org/10.1021/ef020272i.
(12) Gouedard, C. Novel Degradation Products of Ethanolamine (MEA) in CO2 Capture Conditions: Identification, Mechanisms Proposal and Transposition to Other Amines. Doctoral thesis, Université Pierre et Marie Curie, 2014.
(13) Lepaumier, H. Étide des mécanismes de dégradation des amines utilisées pour le captage du CO2 dans les fumées. Doctoral thesis, L'université de Savoie, 2008.
(14) Yazvikova, N. V.; Zelenskaya, L. G.; et al. Mechanism of Side Reactions during Removal of Carbon Diocide Froma Gases by Treatment with Monoethanolamine. *Zhurnal Prikladnoi Khimii* **1975**, *48* (3), 674–676.
(15) Zhou, S.; Wang, S.; et al. Thermal Degradation of Monoethanolamine in CO_2 Capture with Acidic Impurities in Flue Gas. *Ind. Eng. Chem. Res.* **2012**, *51* (6), 2539–2547. https://doi.org/10.1021/ie202214y.
(16) Huang, Q.; Thompson, J.; et al. Impact of Flue Gas Contaminants on Monoethanolamine Thermal Degradation. *Ind. Eng. Chem. Res.* **2014**, *53* (2), 553–563. https://doi.org/10.1021/ie403426c.
(17) Høisæter, K. K.; Vevelstad, S. J.; et al. Impact of Solvent on the Thermal Stability of Amines. *Ind. Eng. Chem. Res.* **2022**, *61* (43), 16179–16192. https://doi.org/10.1021/acs.iecr.2c01934.
(18) Zoannou, K.-S.; Sapsford, D. J.; et al. Thermal Degradation of Monoethanolamine and Its Effect on CO2 Capture Capacity. *International Journal of Greenhouse Gas Control* **2013**, *17*, 423–430. https://doi.org/10.1016/j.ijggc.2013.05.026.
(19) Davis, J.; Rochelle, G. Thermal Degradation of Monoethanolamine at Stripper Conditions. *Energy Procedia* **2009**, *1* (1), 327–333. https://doi.org/10.1016/j.egypro.2009.01.045.
(20) da Silva, E. F.; Lepaumier, H.; et al. Understanding 2-Ethanolamine Degradation in Postcombustion CO_2 Capture. *Ind. Eng. Chem. Res.* **2012**, *51* (41), 13329–13338. https://doi.org/10.1021/ie300718a.
(21) Vevelstad, S. J.; Grimstvedt, A.; et al. Evaluation of Results from SDR Campaigns and Pilot Data. In *Trondheim Carbon Capture and Storage Conference (TCCS-11)*; Trondheim, 2021.
(22) Vevelstad, S. J.; Grimstvedt, A.; et al. Thermal Degradation on Already Oxidatively Degraded Solutions. *Energy Procedia* **2013**, *37*, 2109–2117. https://doi.org/10.1016/j.egypro.2013.06.090.
(23) Lepaumier, H.; Picq, D.; et al. New Amines for CO_2 Capture. II. Oxidative Degradation Mechanisms. *Ind. Eng. Chem. Res.* **2009**, *48* (20), 9068–9075. https://doi.org/10.1021/ie9004749.
(24) Moser, P.; Wiechers, G.; et al. Results of the 18-Month Test with MEA at the Post-Combustion Capture Pilot Plant at Niederaussem – New Impetus to Solvent Management, Emissions and Dynamic Behaviour. *International Journal of Greenhouse Gas Control* **2020**, *95*, 102945. https://doi.org/10.1016/j.ijggc.2019.102945.

Chapter 3: Article I: Additional Considerations

3.1 Reversible Reactions

The degradation model in the paper assumes the irreversible formation of the imidazolidones, HEIA, and AEHEIA. The degradation mechanism originally proposed by Polderman[1], considers HEIA to be the initial degradation product, which can then react to form HEEDA. However, Davis[2] showed that the formation of HEEDA from HEIA is very limited in loaded solutions at 135 °C, even at significant concentrations of HEEDA. Despite this, the degradation model by Davis[2] includes a reverse reaction from HEIA to HEEDA and from the imidazolidone TriHEIA to Trimer (MEA trimer). This results in 7 rate equations with a total of 14 fitting parameters.

The inclusion of these two additional rate equations to the model discussed in the article in Chapter 2 led to marginally improved fitting results. However, given that the model with irreversible reactions for the imidazolidones and 10 parameters showed no lack of fit, the additional reaction rate parameters may lead to overfitting. Although the model may perform well on the training data, it is less generalized and may yield less accurate predictions for new measurements or those from alternative reactors and systems. Another disadvantage of including the reverse reactions is the increased complexity of the system of equations, leading to a challenging optimization of the parameters. The forward and reverse reactions and the reaction rate parameters are highly dependent. This can cause optimization to be more time-consuming and makes it more challenging to locate the global optimum.

3.2 Uncertainty and Model Improvements

Instead of trying to improve the performance of the model by increasing the complexity of the reaction rate equations, addressing the uncertainty of the degradation experiments is likely to yield the most significant improvements in accuracy. Several authors have shown that the deviations found between analytical duplicates are significantly lower than those found for experimental duplicates[3,4]. Therefore, uncertainty in the analytical methods is not expected to play a significant role in the overall uncertainty of the measurements. However, it would be interesting to analyze the same degradation samples using various analytical methods and apparatuses employed in distinct studies and compare the results. It could be that differences in analytical methodology or the utilization of diverse standards contribute to some of the observed deviations.

Experimental uncertainties are likely to play a more important role because the error plots in the paper show a correlation between the extent of degradation and the model deviation. Slight experimental irregularities, such as small leakages, the reuse of degradation cylinders, or fluctuations in the oven temperature, may change the

degradation rate, which increases the absolute deviation with respect to the mean over time.

However, it is challenging to quantify these uncertainties because the documentation of the experimental methods is often limited. The limited reporting of the initial CO_2 loading of the solutions is a good example and was discussed in more detail in the article, in section 2.4.5. This loading is often reported with only 1 decimal of accuracy, whereas both preparation and subsequent analysis of the carbon content can be performed with higher accuracies. Deviations that arise from this were estimated, using the degradation model, to be around 10% for the concentration of MEA and up to 30% for the concentration of the degradation products. In addition, CO_2 loadings were often not reported during or after the experiments, whereas a significant decrease is typically observed over time[3,5].

Therefore, the quality of the experimental results can be improved by more elaborate reporting of solution preparation, experimental conditions, and calculations and assumptions. This should lead to better reproducibility and more accurate model development. In addition, the rate equation for the formation of BHEU can be improved. Since the only quantitative measurements of BHEU were performed on samples from experiments at 135 °C, it was not possible to investigate the temperature dependence of this reaction. It would thus be recommended to perform additional experiments and include data on BHEU at different temperatures.

3.3 Potential Role of MEA Carbamic Acid

Thermal degradation occurs through the rate-limiting ring closure of the MEA carbamate, forming 2-oxazolidinone (OZD). Therefore, the concentration of the carbamate is expected to be proportional to the degradation rate. However, an interesting finding in the paper was that the use of the carbamate concentration in the rate equation resulted in an under-prediction of degradation at higher loadings. At these loadings, the MEA is close to saturation and a larger fraction of the CO_2 will be dissolved as bicarbonate (HCO_3^-). The total CO_2 concentration, on the other hand, which was linearly proportional to the CO_2 loading, was finally used as a surrogate and gave much better fitting results. However, it is difficult to explain how the presence of bicarbonate can contribute to increased degradation.

Consider a hypothesis, in which not the MEA carbamate ion, but its protonated conjugate, the carbamic acid, is a rate-determining compound. In this case, the concentration of CO_2 has a direct influence on the concentration of the carbamate, as well as an indirect influence by altering the pH of the solution. Even though the formation of additional carbamate is limited at higher loadings due to saturation of the MEA, the addition of CO_2 can still cause the pH to decrease and yield more carbamic acid at equilibrium.

This effect can be illustrated by the reaction mechanism for the formation of OZD in Figure 3.1, as proposed by Lepaumier[6]. The oxygen in the β-position from the nitrogen acts as a nucleophile and attacks the carboxyl, leading to dehydration and ring closure. The carbamate ion is not susceptible to nucleophilic attacks and therefore protonation of the carbamate is required to facilitate the reaction.

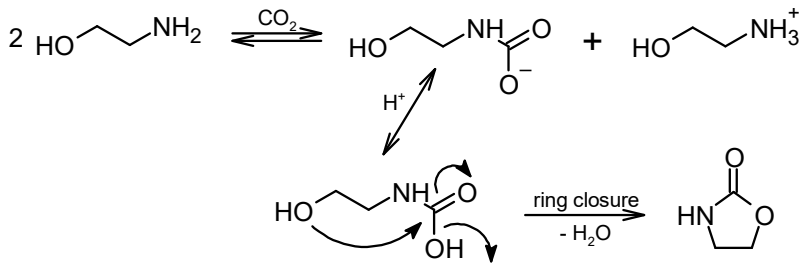

Figure 3.1: Reaction scheme of 2-oxazolidinone formation from the MEA carbamic acid, as proposed by Lepaumier et al.[7]

It is challenging to make accurate estimations of the concentration of carbamic acid because speciation models are generally fitted using data at relatively low temperatures and the carbamic acid is often not included in those models[8]. Despite this, an attempt is made to predict the concentration of the carbamic acid to evaluate the hypothesis. The speciation of the solvent at different loadings is first estimated using an in-house CO2SIM speciation model at 120 °C, a typical stripper temperature. The predicted mole fraction of the MEA carbamate is then assumed to be the sum of the carbamate and the carbamic acid. The equilibrium between these has been studied by McCann et al.[9]. The equilibrium reaction is given in Eq. 3.1, where K_{eq} was determined to be $3.09 \cdot 10^7$ at 30 °C.

$$\mathrm{MEACOO^-} + \mathrm{H^+} \overset{K_{eq}}{\longleftrightarrow} \mathrm{MEACOOH} \qquad \text{Eq. 3.1}$$

The predicted speciation at varying loading is shown in Figure 3.2. In this figure, MEACOO (tot) represents the sum of the mole fraction of the carbamate as predicted by the CO2SIM speciation model. As the loading increases, the mole fractions of $MEAH^+$ and MEACOO (tot) start to diverge because more of the dissolved CO_2 will be present as bicarbonate. The concentration of the carbamic acid is low initially but increases at higher loadings as the pH is decreased. The CO_2 loading and mole fraction of MEACOOH are almost linearly proportional and using the concentration of the acid in the rate equation for the degradation reaction should yield similar results to those in the paper, where the total CO_2 concentration was used.

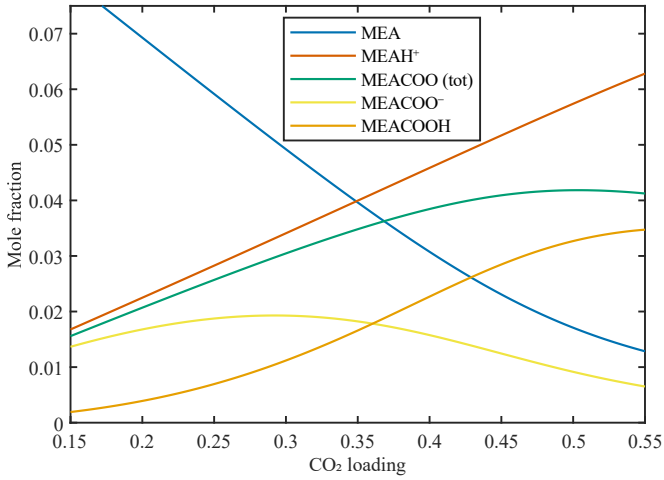

Figure 3.2: Predicted speciation of an aqueous solution with 30 wt% MEA at 120 °C at various CO_2 loadings.

The equilibrium constant for the protonation of the carbamate ion was determined only at 30 °C by McCann et al.[9], whereas the thermal degradation experiments were performed at higher temperatures. The equilibrium constant for higher temperatures can be estimated using the Van 't Hoff equation, of which the definitive integral between two temperatures is given in Eq. 3.2. However, the reaction enthalpy, that is used in this equation, is unknown at these temperatures.

But given that a protonation reaction is typically endothermic, the reaction enthalpy should be positive, and the equilibrium constant is expected to increase with temperature. This would shift the equilibrium towards the formation of the carbamic acid. It would be interesting to improve the speciation model by overcoming technical challenges and collecting experimental data on the concentration of species, equilibrium constants, and the pH of the solution at increased temperature to better reflect the composition of the solvent at stripper conditions.

$$\ln\left(\frac{K_2}{K_1}\right) = \frac{\Delta H_r}{R_{id}}\left(\frac{1}{T_1} - \frac{1}{T_2}\right) \qquad \text{Eq. 3.2}$$

Furthermore, Høisæter et al.[10] studied the thermal degradation of MEA in closed batch cylinders at various concentrations of MEA. In these experiments, the CO_2 loading was kept at a constant concentration. Therefore, the solutions with a lower concentration of MEA had a higher CO_2 loading and the solvent was close to saturation. As a result, a larger fraction of the CO_2 is expected to be present as bicarbonate, and the concentration of the MEA carbamate is expected to be lower than in the solutions where a surplus of

MEA is available. This behavior is illustrated in Figure 3.3, where the speciation of the solutions is predicted using the CO2SIM speciation model.

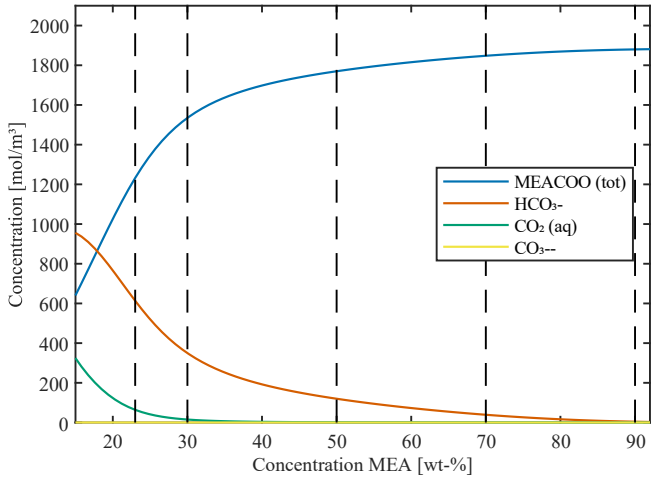

Figure 3.3: Predicted speciation of aqueous solutions with a varying concentration of MEA at 135 °C with a constant concentration of CO_2 (0.19 mol/100 g unloaded solution). Dotted lines represent the starting solutions in the experiments by Høisæter et al.[10].

Figure 3.4 shows the results from the degradation study by Høisæter et al.[10], where the concentration of MEA was analyzed using amine titration. The results show that the absolute degradation rate appears to be similar for all the investigated solutions, regardless of their amine concentration. If the concentration of the MEA carbamate would be proportional to the degradation rate, one would expect the solutions with a lower MEA concentration to degrade less. The constant concentration of total CO_2 and therefore perhaps the availability of protons could, therefore, play a role in the degradation mechanism.

Additional experiments could be performed to investigate the role of pH on the thermal degradation of MEA. Loaded solutions of the solvent can be modified by adding a selection of different acids, to artificially decrease the pH. Changes in degradation rate could indicate that protonation of the carbamate plays an important role in the mechanisms. This could then be of interest for understanding degradation in the process, as degradation products from oxidative degradation, such as organic acids, may turn out to have an influence on thermal degradation rates.

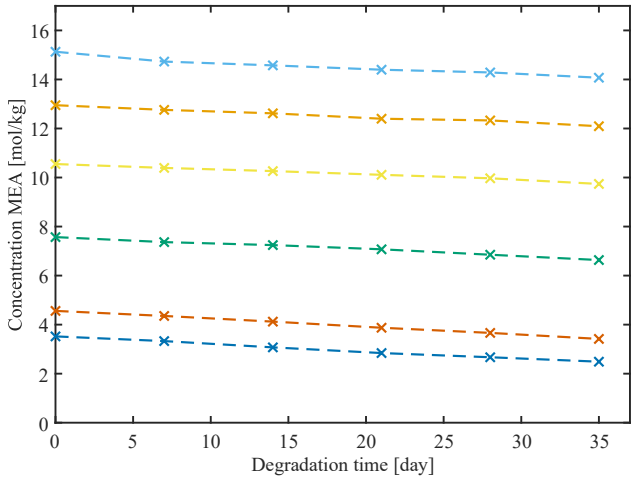

Figure 3.4: Thermal degradation experiments with various concentrations of MEA (23 wt-% to 100 wt-%) at 135 °C but a constant concentration of CO_2 (0.19 mol/100 g unloaded solution), by Høisæter et al.[10]

3.4 References

(1) L. D. Polderman; Dillon, C. P.; et al. Why Monoethanolamine Solution Breaks down in Gas-Treating Service. *Oil & Gas Journal* **1955**, *54* (2), 180–183.

(2) Davis, J. D. Thermal Degradation of Aqueous Amines Used for Carbon Dioxide Capture. Doctoral thesis, The University of Texas, Austin, 2009. https://repositories.lib.utexas.edu/handle/2152/6581.

(3) Eide-Haugmo, I. Environmental Impacts and Aspects of Absorbents Used for CO2 Capture. Doctoral thesis, Norwegian University of Science and Technology, Trondheim, 2011.

(4) Léonard, G. Optimal Design of a CO2 Capture Unit with Assessment of Solvent Degradation. Doctoral thesis, Université de Liège, 2013.

(5) Grimstvedt, A.; Falck da Silva, E.; et al. Thermal Degradation of MEA, Effect of Temperature and CO2 Loading; SINTEF Materials and Chemistry, Trondheim, TCCS-7, 2013.

(6) Lepaumier, H. Étide des mécanismes de dégradation des amines utilisées pour le captage du CO2 dans les fumées. Doctoral thesis, L'université de Savoie, 2008.

(7) Lepaumier, H.; Picq, D.; et al. New Amines for CO ₂ Capture. I. Mechanisms of Amine Degradation in the Presence of CO ₂. *Ind. Eng. Chem. Res.* **2009**, *48* (20), 9061–9067. https://doi.org/10.1021/ie900472x.

(8) Jakobsen, J. P.; Krane, J.; et al. Liquid-Phase Composition Determination in CO2−H2O−Alkanolamine Systems: An NMR Study. *Ind. Eng. Chem. Res.* **2005**, *44* (26), 9894–9903. https://doi.org/10.1021/ie048813+.

(9) McCann, N.; Phan, D.; et al. Kinetics and Mechanism of Carbamate Formation from CO_2 (Aq), Carbonate Species, and Monoethanolamine in Aqueous Solution. *J. Phys. Chem. A* **2009**, *113* (17), 5022–5029. https://doi.org/10.1021/jp810564z.
(10) Høisæter, K. K.; Vevelstad, S. J.; et al. Impact of Solvent on the Thermal Stability of Amines. *Ind. Eng. Chem. Res.* **2022**, *61* (43), 16179–16192. https://doi.org/10.1021/acs.iecr.2c01934.

Chapter 4: Article II: Solvent Degradation in the Process

The aim of this article is to describe and predict the overall degradation in a capture process, which involves both thermal and oxidative degradation. The thermal degradation model for MEA was already developed in Chapter 2, while oxidative degradation and the development of a kinetic rate model for MEA are discussed here.

Oxidative degradation is a complex process that depends on the solubility of O_2 in the solvent, the mass transfer of O_2 from the interface to the bulk of the solvent, and the sequential liquid phase reaction of dissolved O_2 with the amine. It is challenging to isolate the reaction kinetics from the other mechanisms with the current experimental designs, which is a problem because the conditions in bench scale setups are very different from those in the actual process. Therefore, it is important to carefully consider and correct the model for these differences to obtain accurate predictions. Many of the existing oxidative degradation models in literature do not meet these requirements and have shortcomings in one or more of the following aspects:

- Consideration of experimental mass transfer resistances of dissolved O_2
- Solubility model for O_2 that includes the effect of CO_2 loading
- Consistent use of the O_2 solubility model for both development and application of the degradation model

In this chapter, Article II is presented, as published in Chemical Engineering Science. This article presents the modeling work that aims to develop a degradation model that takes all these points into account. As a result, a more generalized reaction rate equation can be derived that should give a more representative reflection of the actual degradation in a capture process. A thorough evaluation of degradation rates throughout the entire process, and not only selected unit operations, should provide a good overview of the extent and distribution of degradation. Furthermore, the effectiveness of proposed mitigation strategies can be investigated and their impact on the overall degradation in the process can be evaluated.

Chapter 5 continues the work presented in the article and discusses several additional aspects of the oxidative degradation model and predictions in the capture processes. Aside from the validation of the degradation framework, this chapter will show the effects of various other process configurations and modifications. At the end of this chapter (section 5.7), work performed in collaboration with the University of Edinburgh and Sheffield (D. Mullen and Prof. M. Lucquiaud), who are the main authors, is presented. This work aims to simulate capture processes with a high capture efficiency and evaluate the extent and distribution of solvent degradation. An overview of the capture cases is given and the degradation results are discussed in more detail. The work will be continued, and a joint publication is under preparation.

Predicting Solvent Degradation in Absorption-Based CO_2 Capture from Industrial Flue Gases

Lucas Braakhuis, Hanna K. Knuutila*

Department of Chemical Engineering, Norwegian University of Science and Technology (NTNU), NO-7491 Trondheim, Norway

*Corresponding author: hanna.knuutila@ntnu.no

DOI: https://doi.org/10.1016/j.ces.2023.118940

4.1 Abstract

This work aims to predict solvent degradation rates in absorption-based CO_2 capture processes using a 30 wt% aqueous monoethanolamine (MEA) solvent. A degradation model for MEA is developed and used to predict solvent degradation in full-scale capture processes. Mass transfer resistances and the solubility of O_2 are considered to obtain a generalized and consistent degradation model. Degradation is evaluated for the capture process for flue gasses with typical industrial compositions; a natural gas-fired power plant, a waste-to-energy plant, a coal-fired power plant, and a cement plant. The impact of process modifications, such as absorber intercooling, dissolved O_2 removal, a reduction in solvent residence times, and increased stripper pressures on degradation is evaluated.

The predicted degradation rate in the capture processes is approximately 90 to 150 g MEA/ton CO_2 captured, and the composition of the flue gas was found to have a significant influence on the distribution of degradation throughout the process. Modifications to the process can significantly affect the overall degradation rate. Both absorber intercooling and removal of dissolved O_2 may reduce the overall degradation by up to 40%, depending on the composition of the flue gas. A reduction in solvent residence times or pressure in the stripper has limited effects on the degradation in the case of MEA, because of the amine's relatively low stability towards oxidative degradation. However, these process modifications look promising for more stable solvents.

4.2 Introduction

Carbon capture processes using amine-based absorbents can play an essential role in reducing carbon emissions from industrial plants, not only in the short term but also in the future in case of hard-to-abate industries, such as waste-to-energy and the production of metals, cement, and silicon[1]. A good absorbent for CO_2 capture is not only characterized by favorable capture properties, such as fast kinetics, a high capacity, a low viscosity, and a low regeneration energy requirement but also by good stability and

resistance towards degradation.[2] Solvent degradation results in the formation of degradation products and can reduce the solvent's capture capacity. These degradation compounds cause various operational issues, such as reduced capture performance, increased emissions, corrosion of equipment, and additional degradation.[3–5] Therefore, it is crucial to consider degradation and possible mitigation and solvent treatment technologies, when designing a capture plant and developing operational strategies. Aside from a good understanding of the degradation mechanisms, solvent degradation models that can predict degradation and product formation rates are important for developing these strategies.

Although several solvents have received more interest in recent years, MEA is still one of the most researched solvents on both a laboratory and industrial scale.[6] Significant information is available on the physical and chemical properties of the solvent, the solubility of O_2, and degradation both in lab-scale reactors[6,7] and industrial capture pilots and plants[8]. For these reasons, this work will primarily focus on MEA. However, the conclusions of this work may also apply to other solvents or solvent blends.

The most prominent solvent degradation mechanisms are oxidative and thermal degradation. Oxidative degradation is caused by the presence of O_2 in flue gas and thermal degradation occurs at increased temperatures. Various works in the literature have studied these types of degradation for MEA solvents. Thermal degradation is often studied by exposing the loaded solvent to high temperatures in closed batch reactors[9–12], whereas oxidative degradation is typically studied in open or semi-open systems where O_2 is added to compensate for the O_2 consumed during the degradation[12–16]. In some cases, degradation models have been developed based on the results from the lab scale degradation experiments[10,12,17–19].

Some of these kinetic models have been used to evaluate solvent degradation in a full-scale capture process, such as in the works by Léonard et al.[20] and Dhingra et al.[21]. However, the assumptions and decisions that were made when developing the kinetic model using the lab-scale experiments are not always valid or logical with respect to the full-scale process. This includes neglecting mass transfer resistances in the experiments or the inconsistent use of O_2 solubility models. Therefore, the predictions made for the full-scale process are likely inaccurate.

This work aims to develop a degradation model for MEA and use it to predict solvent degradation in full-scale capture processes. The degradation model is developed such that it is consistent and applicable for both lab-scale experiments and full-scale plants. Degradation is evaluated for the capture process for flue gasses with typical industrial compositions; a natural gas-fired power plant, a waste-to-energy plant, a coal-fired power plant, and a cement plant. The impact of process modifications, such as absorber intercooling, dissolved O_2 removal, a reduction in solvent residence times, and increased stripper pressures on degradation is evaluated. The degradation model is connected to

Aspen Plus, where steady-state process simulations were performed to get process data for the degradation model.

The degradation model presented here will primarily focus on the solvent loss through degradation and not on the type and quantity of the formed degradation products. The degradation model is limited to thermal and oxidative degradation as these degradation mechanisms are responsible for the majority of solvent degradation in most capture processes[22]. Thermal degradation is described using a previously developed model[17], whereas a new oxidative degradation model is constructed in this work. This oxidative model takes into account the mechanisms for solubility and mass transfer of O_2 for oxidative degradation and is therefore applicable to both the degradation experiments and the full-scale processes.

The lack of experimental data on the corrosion of stainless steels in the presence of degradation products, along with the solubility of corroded metals and their influence on degradation rate, makes it difficult to accurately model these effects. Therefore, this study does not address accelerated degradation as a result of these factors[23–25]. Although the predictions in this work may not always fully correspond with observations in real-life processes, the work still offers needed insights into the extent and distribution of degradation and the effect of mitigation strategies.

4.2.1 Oxidative Degradation Modeling

Oxidative degradation is a complex process that involves both the transfer of O_2 from the gas to the liquid phase and a sequential liquid phase reaction of the dissolved O_2 with the amine. The observed amine degradation rate is thus a function of O_2 solubility, mass transfer resistances, and kinetic reaction parameters[5,16]. Relevant process parameters, such as temperature, O_2 partial pressure, MEA concentration, and CO_2 loading, influence each of these mechanisms. It can be challenging to isolate, quantify, and model these mechanisms individually. As a result, models developed using specific experimental setups may be inaccurate when evaluating degradation in industrial equipment with a different geometry.

In a typical capture plant, oxidative degradation can be classified into two types: direct and indirect oxidative degradation. Direct oxidative degradation occurs when the solvent is in direct contact with the flue gas. The dissolved O_2 in the solvent can be replenished to some degree with O_2 from the flue gas as the degradation reactions consume it. This type of oxidative degradation occurs, for example, in the absorber packing. Indirect oxidative degradation, on the other hand, occurs when there is no direct contact with the flue gas but due to the presence of dissolved O_2. This type of degradation occurs in the piping and heat exchanger when the rich solvent is transported from the absorber to the stripper. The increased temperatures in some of these equipment may accelerate the degradation, up until the point at which all the dissolved O_2 is consumed.

A kinetic model for the oxidative degradation of MEA was developed by Uyanga et al.[19] and Supap et al.[18] using experiments in a semi-batch autoclave reactor. The temperatures of the experiments range from 100 °C to 120 °C, which is higher than those typically found in the absorber. Degradation in the presence of SO_2 was also investigated. However, this kinetic model doesn't distinguish between degradation through O_2, SO_2, or thermal degradation with CO_2, and only considers the total consumption of MEA. Further, the concentration of dissolved O_2 was assumed to be in equilibrium and was calculated using the correlation by Rooney et al.[26]. This correlation does not consider the effect of CO_2 loading on the solubility of O_2.

Léonard et al.[12,27] also studied oxidative degradation of MEA and developed a kinetic model. Aside from a single experiment at 55 °C, the experiments were run at temperatures above 100 °C. The experiments were performed in a degradation reactor similar to the one used by Supap et al.[18], but a gas entrainment impeller was used to enhance the contact between the gas and liquid phases. Léonard[27] showed a linear relationship between the agitation rate and degradation experiments in their experimental work, indicating that mass transfer resistances play an important role in this type of degradation experiments. In a similar setup, Goff et al.[16] also observed increased degradation rates at higher agitation speeds.

In the kinetic model, Léonard et al.[12] used Henry's law for O_2 in water to determine the concentration of O_2. Mass transfer limitations and the impact of the CO_2 loading on the solubility of O_2 were not considered, and the regressed kinetic constants may thus be underestimated. In the following work on predicting degradation in a capture process by Léonard et al.[28], Henry's constant was also used to predict the concentration of O_2 in the solvent. Although this is consistent with the experimental modeling, the mass transfer mechanisms in the degradation experiments are different from those in the absorber, which could lead to inaccuracies in the results.

Additional modeling of solvent degradation in absorption-based capture processes was done by Dhingra et al.[21], where the extent of degradation in pilot plants was investigated and modeled. The oxidative reaction kinetics by Léonard et al.[12] were used in combination with an O_2 solubility model that was fitted using experimental data by Wang et al.[29]. This data, however, contains measurements of the O_2 solubility in loaded aqueous solutions of MEA and are thus not consistent with the used degradation model. Furthermore, the relatively high residence times in the pilot plants allow for flexibility in operation but are not representative of full-scale capture plants.

Oxidative degradation was studied at lower temperatures by Vevelstad et al.[14], with experiments ranging from 55 °C to 75 °C. The experimental setup is similar to the one used by Léonard et al.[12] but featured a gas recycle that allowed a higher gas flow rate and increased contact between the gas and liquid phase. Aside from the consumption of MEA, the formation of a broad set of degradation products was measured and quantified.

Pinto et al.[30] used the experimental data by Vevelstad et al.[14] to develop a multicomponent kinetic model, including the formation of degradation products. The complexity of oxidative degradation makes it challenging to describe the reaction pathways and identify the role of each of the components in the reaction rate equations. Assumptions regarding the reaction mechanisms had to be made by Pinto et al.[30] and these are likely to have caused the observed uncertainties in the predictions of the model, especially for the degradation products. The predictions for MEA consumption were more accurate. However, the correlation by Rooney et al.[26] was also used in this work to calculate the solubility of O_2, thus not taking into account the effect of CO_2.

The CO_2 loading of the solvent plays a key role in the degradation experiments as it is found to decrease the oxidative degradation rate in several experimental works. Léonard[27] observed a significant inhibiting effect of CO_2 loading compared with an unloaded solvent, but the degree of CO_2 loading appeared to have no effect. Supap et al.[18] and Kasikamphaiboon et al.[31] observed a similar inhibiting effect in the autoclave experiments, but the authors did observe increased inhibition at higher CO_2 loadings. The decrease in degradation may be the effect of a reduced O_2 solubility since the presence of CO_2 in the solvent has been found to lower the O_2 solubility[29,32].

The CO_2 can also increase the viscosity of the solvent, thereby reducing the diffusivity and mass transfer coefficient of O_2[33]. In the case oxidative degradation is limited by mass transfer, a reduction in degradation is observed. The differences between the observations on the role of CO_2 may be explained by the different experimental reactor designs and their associated mass transfer resistances.

4.3 Methodology

4.3.1 Degradation Framework

Solvent degradation is a gradual process that has little to no direct impact on the capture plant. It is the accumulation of degradation products and solvent consumption over time that changes the properties and performance of the solvent. It is, therefore, not necessary to implement a dynamic model that describes both kinetics of absorption/desorption and solvent degradation rates, but instead, a pseudo-steady state model can be used.

In the pseudo-steady state model, process conditions of the steady state simulation that are used to evaluate solvent degradation are assumed to be constant for a specific period of time. Changes in solvent composition as a result of degradation in this period are calculated, after which the solvent in the simulation is updated and the simulation is run again to obtain a new steady state. These steps are repeated for the duration of the entire modeled operational period. The time step size is chosen such that the difference in process conditions of consecutive simulations does not lead to significant changes in the degradation reaction rates.

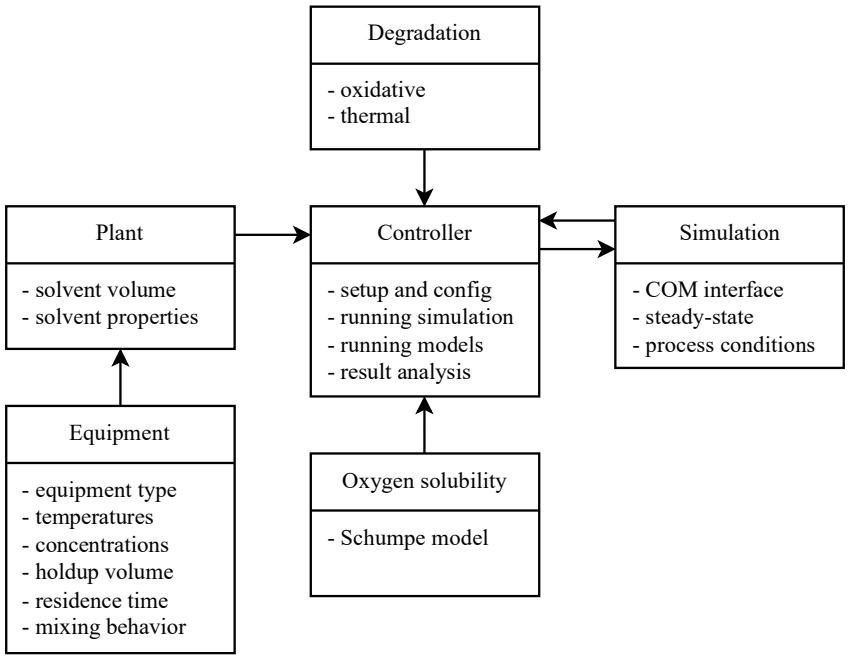

Figure 4.1: Overview of the degradation framework and the corresponding modules.

An overview of the degradation framework that is used in this work is given in Figure 4.1. The heart of the framework is the *Controller* module, which controls communication between all the other modules. The module opens a simulation and constructs an interface to communicate with the simulation software. From here, simulation parameters can be changed, the simulation can be executed, and simulation results can be retrieved.

The controller module uses the simulation results to construct a *Plant* object, which is a simplified model of the simulation that contains general information on the quality of the solvent as well as a set of *Equipment* objects. Each of the *Equipment* objects stores the simulation results of the corresponding equipment, so these can be used to evaluate the O_2 solubility or degradation models. For example, the *Equipment* object for a column stores process information (e.g., temperatures, partial pressures, liquid concentrations, and volumes) for various parts of the column, such as the packing, condenser, reboiler, or sump.

The *Controller* module uses the stored process information in each of the *Equipment* objects to evaluate the O_2 solubility and degradation models and calculate the predicted solvent consumption and degradation product formation for that *Equipment* object. These results are then stored in the objects themselves and combined to determine the overall degradation in the plant. The composition of the solvent in the process

simulation can then be updated to evaluate the impact of the degradation on the capture process.

The modular structure of the framework allows for good customizability since new degradation modules or modules for other solvents can seamlessly replace the current ones. Additionally, new modules can be added seamlessly. Future extension modules could contain models on viscosity, corrosion, entrainment and evaporation, or reclaiming of the solvent.

4.3.2 Thermal Degradation of MEA

Thermal degradation of the aqueous MEA solvent is described using a degradation model from one of our previous works[17]. The model was designed and fitted using experimental data on the concentrations of MEA and its degradation products when exposed to increased temperatures in closed cylinders. The data were collected from several independent works and contained results for aqueous solutions with 30 wt% of MEA at loadings between 0.1 and 0.5 mol CO_2/mol MEA and temperatures from 100 to 160 °C. The proposed degradation reactions, rate equations, and corresponding kinetic parameters for the model are given in Table 4.1. The reaction rate coefficient (k_r) is described using an alternative notation of the Arrhenius equation in Eq. 4.1, which was used to simplify the fitting of the model parameters. The reference temperature (T_{ref}) for the coefficients is 400 K.

Table 4.1: Proposed degradation reactions, reaction rate equations, and kinetic parameters for the thermal degradation model.[17] The reference temperature (T_{ref}) is 400 K.

No.	Reaction	Reaction rate [mol·m^{-3}·s^{-1}]	k_{ref} [m^3·mol^{-1}·s^{-1}]	E_A [J/mol]
1	$2\,\mathrm{MEA} \rightarrow \mathrm{HEEDA} + \mathrm{H_2O}$	$R_1 = k_{r,1}[\mathrm{MEA}][\mathrm{CO_2}]$	$1.599 \cdot 10^{-11}$	$1.511 \cdot 10^{5}$
2	$\mathrm{MEA} + \mathrm{HEEDA} \rightarrow \mathrm{TRIMEA}$	$R_2 = k_{r,2}[\mathrm{HEEDA}][\mathrm{CO_2}]$	$1.117 \cdot 10^{-10}$	$1.215 \cdot 10^{5}$
3	$\mathrm{HEEDA} + \mathrm{CO_2} \rightarrow \mathrm{HEIA}$	$R_3 = k_{r,3}[\mathrm{HEEDA}][\mathrm{CO_2}]$	$3.054 \cdot 10^{-10}$	$1.426 \cdot 10^{5}$
4	$\mathrm{TRIMEA} + \mathrm{CO_2} \rightarrow \mathrm{AEHEIA}$	$R_4 = k_{r,4}[\mathrm{TRIMEA}][\mathrm{CO_2}]$	$2.839 \cdot 10^{-10}$	$1.362 \cdot 10^{5}$
5	$2\,\mathrm{MEA} \rightarrow \mathrm{BHEU} + \mathrm{H_2O}$	$R_5 = k_{r,5}[\mathrm{MEA}][\mathrm{CO_2}]$	$5.170 \cdot 10^{-13}$	$1.511 \cdot 10^{5}$

$$k_r = k_{\mathrm{ref}} \cdot \exp\left(\frac{-E_A}{R_{\mathrm{id}}}\left(\frac{1}{T} - \frac{1}{T_{\mathrm{ref}}}\right)\right) \qquad \text{Eq. 4.1}$$

The activation energy for reaction no. 5 for the formation of 1,3-Bis(2-hydroxyethyl)urea (BHEU) could not be determined due to insufficient data for this compound at different temperatures. It is, however, expected to be comparable to the activation energy of reaction no. 1, because the reaction mechanisms are similar.[17] Therefore, in this work, the same activation energy is used for reaction no. 5. Regardless of the temperature, the contribution of this reaction to the consumption of MEA is limited

because the reaction rate coefficient is nearly two orders of magnitude smaller. The model can be safely extrapolated for temperatures below 100 °C since the predicted reaction rates are insignificant at these conditions.

4.3.3 Oxidative Degradation of MEA

4.3.3.1 Oxygen Solubility

The concentration of dissolved O_2 in the solvent is predicted using the gas solubility model for electrolyte solution by Schumpe et al.[34], see Eq. 4.2 and Eq. 4.3. This model considers the effects of temperature and the concentration of ionic species in the solvent. Reduced O_2 solubility due to carbamate and carbonate species from CO_2 absorption can thus be modeled. The ion-specific model parameters for a loaded aqueous MEA solvent are taken from the work by Buvik et al.[32]. The authors determined the ion-specific parameters for protonated MEA and the MEA carbamate using experimental data for the solubility of N_2O. In addition, the authors validated the model using experimental data and concluded that the modeling results were realistic[32].

The parameters for the solubility model are given in Table 4.2. The solubility of O_2 in pure water was determined using the correlation proposed by Benson et al.[35], see Eq. 4.4. The same correlation is also used in this work. The concentrations of the protonated MEA and the MEA carbamate are assumed to be equal to the concentration of dissolved CO_2. A small fraction of the absorbed CO_2 will be present as carbonate or bicarbonate, but the concentrations of these species are low compared with the carbamate, especially at lower loadings.[36] In addition, the ion-specific parameter for bicarbonate is similar to the parameter for the carbamate, so significant deviations in O_2 solubility are not expected.

$$\log_{10}\left(\frac{c_{O_2,H_2O}}{c_{O_2,l}}\right)=\sum_{i=1}^{i=n}(h_i+h_{G,O_2})c_{i,l} \qquad \text{Eq. 4.2}$$

$$h_{G,O_2}=h_{G,O_2,0}+h_{T,O_2}(T-298.15) \qquad \text{Eq. 4.3}$$

$$c_{O_2,H_2O}=\frac{55.56\,p_{O_2}}{\exp\left(3.71814+\frac{5596.17}{T}+\frac{1049668}{T^2}\right)-p_{O_2}} \qquad \text{Eq. 4.4}$$

Table 4.2: Model parameters for the solubility of O_2 in loaded aqueous MEA solvents.[32,34] The h_{T,O_2} parameter is valid from 273 K to 353 K.

Parameter	Unit	Value	Reference
h_{MEAH^+}	$m^3 \cdot kmol^{-1}$	0.0133	Buvik et al.[32]
h_{MEACOO^-}	$m^3 \cdot kmol^{-1}$	0.1284	Buvik et al.[32]
$h_{HCO_3^-}$	$m^3 \cdot kmol^{-1}$	0.0967	Schumpe et al.[34]
$h_{G,O_2,0}$	$m^3 \cdot kmol^{-1}$	0	Schumpe et al.[34]
h_{T,O_2}	$m^3 \cdot kmol^{-1} \cdot K^{-1}$	-0.000334	Schumpe et al.[34]

4.3.3.2 Oxidative Degradation Kinetics

The experimental dataset on oxidative degradation of MEA in a stirred open batch reactor by Vevelstad et al.[14] is used in this work to develop a degradation model. For the experiments, the reactor was filled with the loaded aqueous MEA solvent and exposed to O_2 through the bubbling of an artificial flue gas at atmospheric conditions. The concentration of O_2 in the dry gas varied from 6 vol% to 98 vol%, whereas the concentration of CO_2 was kept constant at 2 vol%, to keep the solution loaded. Most of the gas was recycled, and a small purge and make-up were used to control the gas composition. The purge gas was led through a cooler to condense volatile compounds. The temperature in the experiments varied from 55 to 75 °C.

The correlation for gas bubbles in a stirred tank by Cussler[37] is used to estimate the liquid phase mass transfer coefficient (k_{L,O_2}). The correlation is given in Eq. 4.5, where D_{O_2} is the diffusivity of O_2, d_b the bubble diameter, P/V the stirring power per volume, ρ_L the density, and ν_L the kinematic viscosity of the solvent. The dynamic viscosity and density of the loaded aqueous MEA solvent are calculated using the correlation by Weiland et al.[33], and the diffusivity of O_2 has been estimated using the Wilke-Chang correlation[38]. Other experimental parameters, such as reactor volume (1.0 L), stirring power (12.5 W), and average bubble diameter (8 mm), were determined by analyzing the setup by Vevelstad et al.[14].

The mass transfer resistance for O_2 in the gas phase is assumed to be negligible, as gas absorption processes are commonly controlled by mass transfer in the liquid[37]. In addition, the concentration of O_2 in the gas bubble is assumed to be constant.

$$k_{L,O_2} = \frac{0.13 D_{O_2}}{d_b} \left(\frac{(P/V) d_b^{\,4}}{\rho_L \nu_L^3} \right)^{\frac{1}{4}} \left(\frac{\nu_L}{D_{O_2}} \right)^{\frac{1}{3}} \qquad \text{Eq. 4.5}$$

The equilibrium loadings were determined given the experimental temperature and CO_2 partial pressure in the wet gas using the equilibrium data by Aronu et al.[39]. For the experiments at 55 °C, 65 °C, and 75 °C the loading was calculated to be 0.43, 0.37, and 0.30 respectively.

The proposed reaction rate for the degradation of MEA is given in Eq. 4.6. The solvent is nearly always loaded to some degree in industrial capture plants and the experiments by Vevelstad et al.[14], so it is not necessary to consider unloaded solvent. The CO_2 loading is assumed to influence the O_2 solubility, viscosity, and mass transfer resistance for O_2 but not the degradation kinetics. The concentration of MEA was found to influence the degradation rate [13,31,40], and is thus included in the kinetic rate equation. Although no significant changes in MEA concentration are expected in the capture process due to solvent make-up, a decrease in MEA is observed during the semi-batch experiments. Therefore, the concentration of MEA should be considered when developing the model.

The oxidative degradation products are not considered in this work. The oxidative reaction mechanisms and interactions between intermediates are complex and not fully understood. Without a better understanding of these mechanisms, it is hard to develop a generalized model that can make accurate predictions of degradation product concentrations regardless of the experimental setup or process geometry. An oxidative kinetic model based on partially incorrect reaction mechanisms may perform well with respect to the data it is regressed with but may give inaccurate results when applied in a capture process, for example through the interactions between oxidative and thermal degradation products of MEA.

Instead, the consumption of MEA and O_2 is investigated. Léonard et al.[12] proposed a weighted overall reaction balance for the oxidative degradation of MEA, in which 1.3 mol of O_2 are consumed per mole of MEA. Goff[23] also estimated the O_2 stoichiometry for degradation of MEA using experimental results by Rooney et al.[41]. They estimated the O_2 stoichiometry for loaded MEA (0.25 mol CO_2 per mol MEA) to be 1.44, which is comparable with the findings by Léonard et al.[12]. The developed degradation model in this work will assume a stoichiometry of 1.3. The reaction rate for the consumption of O_2 is then given in Eq. 4.7.

$$R_{\mathrm{MEA}} = k_r \, c_{\mathrm{MEA}} \, c_{\mathrm{O_2},L}^{n} \qquad \text{Eq. 4.6}$$

$$R_{\mathrm{O_2}} = 1.3 \cdot k_r \, c_{\mathrm{MEA}} \, c_{\mathrm{O_2},L}^{n} \qquad \text{Eq. 4.7}$$

4.3.3.3 Objective Function and Optimization

The accumulation of dissolved O_2 in the liquid bulk is equal to the transport from the gas-liquid interface minus the consumption by the degradation reaction, as expressed in Eq. 4.8. At steady state, the concentration of O_2 in the liquid bulk is constant and the

expression can be simplified to Eq. 4.9, which can then be solved for $c_{O_2,L}$. The concentration of MEA in the reactor over time can then be described by Eq. 4.10, where the reaction rates for MEA and O_2 are given in Eq. 4.6 and Eq. 4.7, respectively. The reaction rate coefficient at the reaction temperature is set using Eq. 4.1. The variables that are optimized are the reaction rate coefficient at a reference temperature of 338.15 K (k_{ref}), the activation energy (E_A), and the reaction order of O_2 (n).

$$V_R \frac{dc_{O_2,L}}{dt} = a_{int} J_{O_2} V_R - \epsilon_L R_{O_2} V_R \qquad \text{Eq. 4.8}$$

$$0 = k_L a_{int} \left(c_{O_2,I} - c_{O_2,L}\right) - \epsilon_L R_{O_2} \qquad \text{Eq. 4.9}$$

$$\frac{dc_{MEA}}{dt} = R_{MEA} \qquad \text{Eq. 4.10}$$

The sum of square errors (SSE) with respect to the experimental results was used as the objective function. The kinetic parameters for the reaction are determined by minimizing this objective function using the particle swarm optimization implementation in MATLAB. This is a global optimizer suitable for multi-variable non-linear objective functions. The optimization was run multiple times while changing the optimization settings and initial particle distribution, and similar results were obtained each time.

4.3.4 Capture Plant Simulations

A process flow diagram of the carbon capture simulations is given in Figure 4.2. The flue gas is brought in contact with the solvent in the absorber, where CO_2 is selectively removed. The rich solvent is then heated in a heat exchanger, and the CO_2 is desorbed in the stripper. The reboiler supplies the additional heat that is required for desorption. The solvent is then cooled in the heat exchanger and subsequent cooler and recycled to the absorber.

The columns are filled with a structured packing to facilitate extensive interfacial contact between the liquid and the gas. Both columns have two liquid distributors, one at the top of the packing and another one midway through. Although the distributors are not simulated, they are included in the plant model in the degradation framework. Since emissions are outside the scope of this work, water washes have not been simulated. Make-up streams ensure that volatile emissions of water or solvent in the treated flue gas or the CO_2 product are replaced.

Aspen Plus V10 is used in this work to simulate the capture plants. The RadFrac column model with rate-based calculations is used to simulate the absorber and stripper. Mass transfer and liquid holdup are modeled with the mass transfer correlation for structured packing by Bravo et al. (Brf-92) with reactions in the film layer. Heat transfer was

modeled using the Chilton and Colburn method. The vapor is modeled as a plug flow, whereas the liquid phase is considered to be ideally mixed at each segment (VPlug). This is done to simulate maldistribution of the liquid and the effect of axial dispersion. The gas phase, on the other hand, typically maintains a uniform distribution throughout the packing[42]. Different segment heights were tested and finally, a height of 0.4 m was selected. This height yielded the most satisfactory result during the validation of the simulations using the data by Tobiesen et al.[43,44].

A plate heat exchanger was selected to facilitate heat exchange between the lean and rich solvent. The exchanger was simulated using the shortcut method with a temperature approach of 7 °C. The optimum approach temperature of heat exchangers for process streams usually lies in the range of 10 – 30 °C, but plate heat exchangers are capable of achieving lower approach temperatures[45]. The calculated exchange area is used in combination with typical dimensions for plate heat exchangers[45], to determine the liquid holdup and residence time for the exchanger. A shell and tube heat exchanger was also tested, resulting in comparable residence times.

The solvent residence times in other parts of the process can vary from plant to plant but have been based on recommendations for the specific process equipment[46]. Residence times in piping in between process equipment have been determined using a fluid velocity of 1.0 m/s and estimated required pipe lengths. The residence times and other simulation parameters for the investigated cases are given in

Table 4.3. Typical flue gas specifications from the literature are used to estimate the flue gas composition for a natural gas-fired power plant[47,48], a waste-to-energy plant[49,50], a coal-fired power plant[51,52], and a cement plant[53]. All flue gasses were assumed to be saturated with water when entering the absorber. Other process parameters, such as solvent inlet temperatures, lean loading, and column pressures, have been estimated using typical values found in literature[54–57].

To be able to compare degradation between the capture simulation, some process parameters have been fixed. The packing heights for the absorber and stripper were kept constant, as well as the CO_2 loading of the lean solvent and the percentage of CO_2 removed. For each flue gas case, the lean solvent flow rate was adjusted to ensure 90% of the CO_2 was removed from the flue gas in the absorber. The stripper duty was then adjusted to strip the solvent down to the specified lean loading. The simulations are not optimized for the specified flue gas because the column height and lean loading were fixed for all cases, and as a result, the energy requirements are slightly higher than those for the optimized processes.

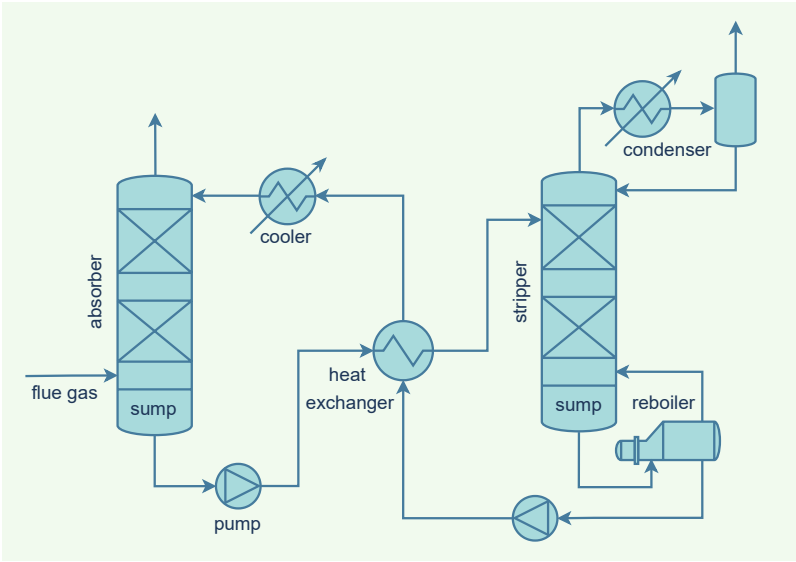

Figure 4.2: Process flow diagram of the simulated carbon capture plants.

Table 4.3: Simulation parameters for the investigated industrial base cases.

	Unit	Natural gas	Waste-to-energy	Coal	Cement
Absorber					
Packing	-	Mellapak 250Y	Mellapak 250Y	Mellapak 250Y	Mellapak 250Y
Packing height	m	12.0	12.0	12.0	12.0
Pressure top	bar	1.1	1.1	1.1	1.1
Sump residence time	s	180	180	180	180
Temp. liquid inlet	°C	40.0	40.0	40.0	40.0
Temp. liquid outlet	°C	41.4	42.8	45.2	51.7
Temp. gas inlet	°C	40.0	40.0	40.0	40.0
Liquid-gas ratio	wt/wt	0.91	1.63	2.46	3.83
Flue gas CO_2	vol%	4.2	8.0	12.0	20.2
Flue gas O_2	vol%	11.8	10.5	5.0	8.6
Flue gas H_2O	vol%	6.7	6.7	6.7	6.7
Flue gas N_2	vol%	77.3	74.8	76.3	64.5
Lean loading	mol/mol	0.19	0.19	0.19	0.19
Rich loading	mol/mol	0.52	0.53	0.54	0.54

Stripper					
Packing	-	Mellapak 250Y	Mellapak 250Y	Mellapak 250Y	Mellapak 250Y
Packing height	m	10.0	10.0	10.0	10.0
Pressure condenser	bar	1.8	1.8	1.8	1.8
Sump residence time	s	180	180	180	180
Reboiler residence time	s	240	240	240	240
Temp. reboiler	°C	119.0	119.0	119.0	119.0
Reboiler duty	MJ/kg CO_2	3.62	3.50	3.46	3.47

Heat exchanger					
Exchanger type	-	Plate	Plate	Plate	Plate
Temp. approach	°C	7.0	7.0	7.0	7.0
Residence time (side)	s	30	30	30	30

4.3.5 Oxygen Solubility and Mass Transfer in the Absorber

The O_2 solubility model by Buvik et al.[32] used for the regression of the oxidative degradation reaction kinetics from the experimental degradation results, is also used to determine the concentration of O_2 in the capture process. Similar to in the degradation experiments, mass transfer limitations for O_2 in the absorber packing may reduce the degradation rate. The impact of these mass transfer limitations was evaluated using the correlation by Billet et al. [58] for the liquid phase mass transfer coefficients in structured packings on the coal-fired flue gas capture case.

Figure 4.3 shows the calculated volumetric liquid-phase mass transfer coefficient as a function of the packing depth and Figure 4.4 shows the influence of the mass transfer resistance on the concentration of O_2 in the absorber packing. Although, the relatively high temperatures at the top of the absorber packing lead to an increase in the mass transfer coefficient, the increase in degradation rate is even larger. Therefore, the difference between the equilibrium concentration of O_2 at the interface and the bulk concentration of O_2 is increased slightly. However, the difference between both concentrations is small throughout the column, and the bulk concentration is at least 95% of the equilibrium. Therefore, mass transfer resistances in the absorber packing can be neglected and the equilibrium solubility can be used to determine the concentration of O_2.

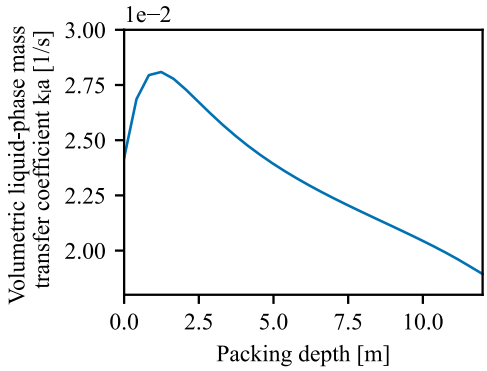

Figure 4.3: Volumetric mass transfer coefficient for the liquid phase in the absorber packing as a function of the packing depth for the coal-fired power plant case.

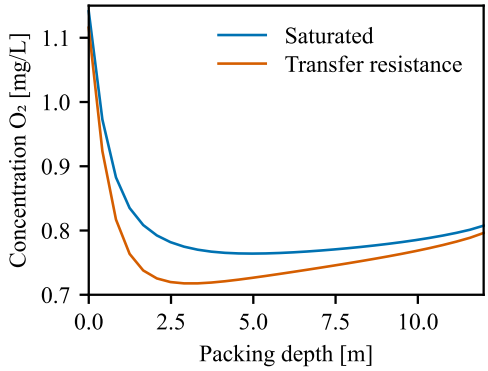

Figure 4.4: Concentration of dissolved O_2 in the liquid bulk with and without considering mass transfer limitations in the liquid phase as a function of the packing depth for the coal-fired power plant case.

4.3.6 Case Studies

The coal-fired power plant case presented in section 4.3.4 was used as the starting point for all case studies, focusing on the impact of process and solvent modifications on the predicted MEA degradation rate. The coal-fired power plant case was chosen as a

reference case because the degradation in the coal case was diverse, with significant contributions from direct oxidative degradation, degradation by dissolved O_2, and thermal degradation. The case studies and the assumptions made are described briefly in the sections below.

4.3.6.1 Intercooled and Isothermal Absorbers

The absorber packing is expected to be one of the locations where oxidative degradation occurs since the solvent is in direct contact with O_2 from the flue gas. The exothermic nature of CO_2 absorption causes the temperatures in the absorber to increase and leads to a temperature bulge. The magnitude of this bulge is dependent on a number of factors, including the solvent, the CO_2 content of the flue gas, and the liquid-to-gas ratio, and absorber bulge temperatures up to 70 – 80 °C are not uncommon for processes with MEA.[59] Given the temperature dependence of the oxidative degradation reactions, the elevated temperatures in the packing are expected to lead to increased degradation.

Temperature control in the absorber packing in the form of intercooling is thus a potential degradation mitigation strategy. In this case study, the solvent is intercooled once at 2.4 m from the top of the packing, as this resulted in the lowest peak temperature in the packing. Although packings with in-situ intercooling are under development[60], the solvent is typically collected and removed from the column to be cooled down, after which it is returned. This case study initially focuses on the application of instantaneous in-situ intercooling that does not require additional solvent holdup but also discusses the effect of the additional solvent holdup in the external recycle loop for in-and-out intercooling. To investigate the potential of additional cooling, degradation in an isothermal absorber at 40 °C is also considered and evaluated.

Lower absorber temperatures can also lead to more efficient CO_2 absorption, and thus lower requirements for the column height, solvent flow rate, and/or reboiler duty. These effects have not been modeled. The column height, reboiler duty, solvent flow rate, and lean loading have thus been set according to the values in the reference case.

4.3.6.2 Dissolved Oxygen Removal

Oxidative degradation can occur even when the solvent is no longer exposed to O_2 in the flue gas. The rich solvent may contain O_2 that was dissolved in the absorber, which can lead to indirect oxidative degradation of the solvent. This type of degradation is expected to occur in the absorber sump, heat exchanger, and piping until the O_2 is desorbed in the stripper. The extent of this type of degradation depends on the O_2 content of the flue gas, the solubility of O_2, and the oxidative degradation rate. The removal of dissolved O_2 from the solvent may be an effective method for reducing this indirect degradation[61].

This removal of dissolved O_2 can be achieved using membrane contactors. Figueiredo et al.[61] investigated the potential of such a removal technology and concluded that removal efficiencies up to 90% are feasible using a dense layer membrane with a 30 wt% MEA

solvent. Alternatively, dissolved O_2 can be removed by sparging the rich solvent with nitrogen in the absorber sump or right after the absorber in a separate column. Bench-scale experiments by Nielsen showed that nitrogen sparging could reduce oxidative degradation of piperazine (PZ) by 50%.[62] Modeling work by Wu[63] showed that removal efficiencies up to 90% are feasible when applying nitrogen stripping in 5 mol/kg piperazine.

This case study investigates the potential of dissolved O_2 removal to mitigate degradation. The concentration of dissolved O_2 is reduced by 90% before the solvent enters the absorber sump. It is likely that the concentration of O_2 is higher in some parts of the sump in case of nitrogen sparging, or that additional holdup volume is required for O_2 removal using membranes, but these effects are not considered in the case study.

4.3.6.3 Change in Capture Efficiency

Amine-based capture processes can operate with various CO_2 capture efficiencies, and operation at lower or higher capture efficiencies than 90% is possible. Therefore, in this case study, the reference case was modified to remove both 95% and 85% of the CO_2 in the flue gas. For the 95% efficiency case, the packed height was increased from 12 to 15 m, and an additional solvent redistributor was added. In addition, the solvent flow rate was increased by 5.6% to ensure the same amount of solvent is available per mole of captured CO_2 and the rich loading is the same as in the reference case. For the process with an 85% capture efficiency, the packed height was reduced to 10 meters and the solvent flow rate was reduced by 5.6%.

4.3.6.4 Stripper Pressure

The energy that is required for stripping the CO_2 is supplied in the reboiler in the form of pressurized steam. The energy is used for sensible heating, producing water vapor, and driving the endothermic CO_2 desorption reaction. The pressure in the stripper typically is between 1.5 bar and 2.0 bar[64], and the base case simulations in this work are run with a pressure of 1.8 bar. An increase in stripper pressure will lead to an increase in operating temperature. Higher temperatures favor the desorption of CO_2 and result in higher partial pressures of CO_2 at the same loading. Therefore, less water vapor is needed to facilitate the desorption and less energy is required in the reboiler[64,65]. A downside of higher temperatures in the stripper, especially in the sump and reboiler, is the increased rate of thermal degradation.

In this case study, the reboiler pressure is varied between 1.3 bar and 3.0 bar. The reboiler duty is adjusted to ensure 90% of CO_2 is stripped, and the lean loading and solvent flow rate remain unchanged. Since the volumetric flow rate of the gas changes with pressure, the diameter of the stripper is adjusted to ensure that the stripper is operated at 75% flooding.

4.3.6.5 Reduced Solvent Residence Times

Solvent holdup is required throughout the process to facilitate mass and heat transfer, and buffer tanks are required for stable operation of the capture plant. The sump, for example, collects the solvent that exits the packing, forms an inventory buffer for the pump, and prevents it from running dry. The residence time can, from a degradation perspective, also be regarded as an exposure time in which the solvent is exposed to increased temperatures or environments containing O_2. A reduction of this exposure time may thus reduce degradation. Therefore, several of the equipment residence times have been reduced by 50% in this case study. An overview of the default and reduced residence times is given in Table 4.4. Solvent degradation is then predicted and evaluated.

Table 4.4: Default and reduced residence times in the capture plant equipment.

Equipment	Default residence time [s]	Reduced residence time [s]
Column distributor	15	7.5
Column sump	180	90
Reboiler	240	120
Heat exchanger	30	15
Pump	10	5
Heater and cooler	30	15

4.3.6.6 Oxygen Content in the Flue Gas

The concentration of O_2 in the flue gas is expected to influence the oxidative degradation rates in the process since the solubility of O_2 is proportional to its partial pressure in the gas phase. The studied industrial flue gasses given in Table 4.3 have different concentrations of O_2 and CO_2. The concentration of CO_2 has a significant impact on process conditions, such as rich loadings or the temperature profile in the absorber, and will thus influence the degradation rate. This case study aims to isolate and study the effect of the O_2 concentration in the coal-fired flue gas of the reference case. The concentration of O_2 is varied from 0.1% to 12%, while the concentration of CO_2 and H_2O are kept constant. The remainder of the gas is set to be N_2.

4.3.6.7 Reduced Oxidative Degradation Rate

In the context of solvent degradation, MEA is the most tested and studied amine.[6] Despite its wide-spread interest and use, the amine is not known for its stability towards oxidative degradation and other solvent candidates have been found to be more resilient, for example, MDEA, PZ, and AMP.[66] However, experimental data on degradation of these alternative solvents is limited. Extended datasets that are similar in size and detail to the dataset by Vevelstad et al. on 30 wt% MEA are not available, making it more challenging to develop kinetic degradation models for these solvents. Therefore, in this

case study, the kinetic parameters in the oxidative degradation model for MEA are varied, and the effect on degradation in the process is investigated.

Besides the resilience towards oxidative degradation, there are more differences in the properties of solvents used for carbon capture. These properties can significantly influence process parameters such as temperatures in the absorber, solvent capacity and flow rates, and O_2 solubility. This case study does not consider these effects and thus only gives a hypothetical overview of the expected behavior of more stable solvents.

4.3.7 Validation of the Simulations

The simulations in Aspen Plus are validated using experimental data by Tobiesen et al.[43,44] on the CO_2 capture performance of a Mellapak 250Y packing in the packed absorber and desorber sections. The experimental data were obtained from a 3-month

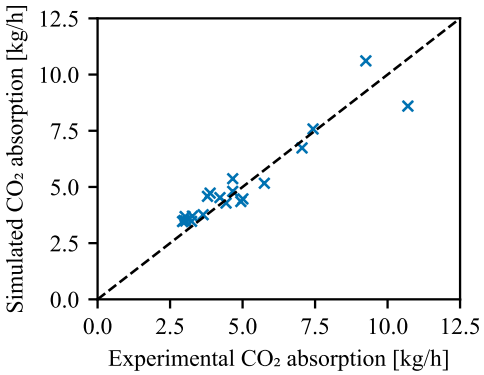

Figure 4.5: Parity plot of the experimental and simulated CO_2 absorption rate.

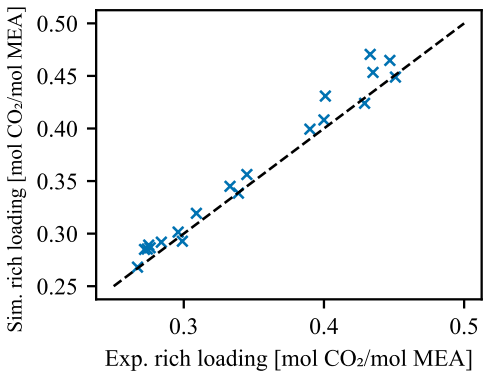

Figure 4.6: Parity plot of the experimental and simulated rich loading of the exiting solvent.

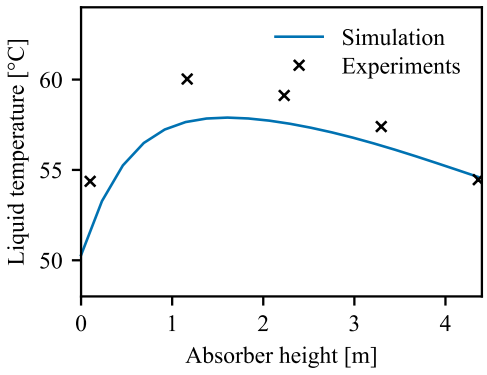

Figure 4.7: Comparison between the liquid phase absorber temperature profile simulated in this work and experimental data for run 12 by Tobiesen et al.[43].

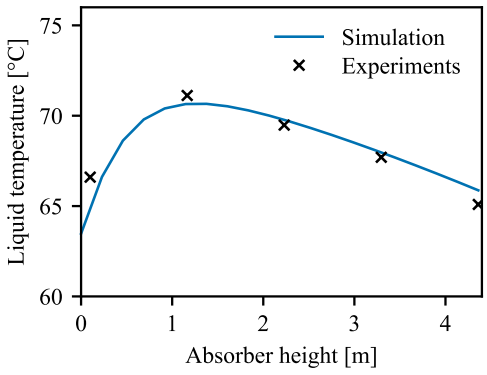

Figure 4.8: Comparison between the liquid phase absorber temperature profile simulated in this work and experimental data for run 15 by Tobiesen et al.[43].

campaign in a laboratory pilot plant. Although the columns were relatively small, 4.36 m for the absorber and 3.89 m for the stripper, experiments were conducted with varying temperatures, flow rates, and lean and rich loadings to simulate the different operating conditions in the various sections of the packed columns.

For the absorber, the simulations give an accurate representation of the experiments, as can be seen in the parity plots for the absorption rate and rich loading in Figure 4.5 and Figure 4.6. The mean average deviations were 6.0% and 3.3% for the absorption rate and rich loading, respectively. These deviations are of the same magnitude as the deviations observed by Tobiesen et al.[43]

The simulated temperature profiles in the absorber also correspond well with the experimental results, as shown in Figure 4.7 and Figure 4.8. In some cases, there was a slight over or under-prediction of the temperature profile, even though the absorption

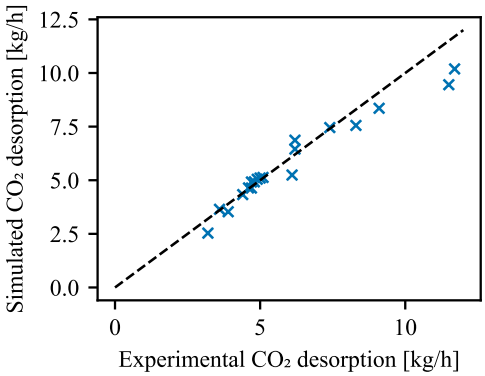

Figure 4.9: Parity plot of the simulated CO_2 desorption rate and the experimental results by Tobiesen et al.[44]

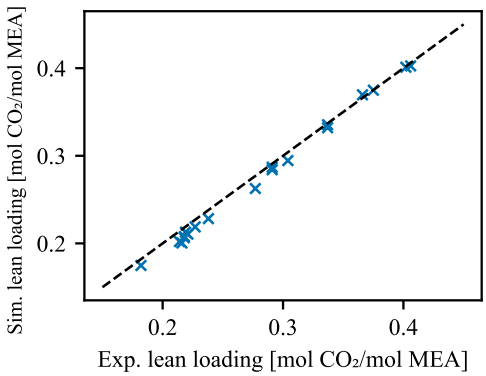

Figure 4.10: Parity plot of the simulated lean CO_2 loading and the experimental results by Tobiesen et al.[44]

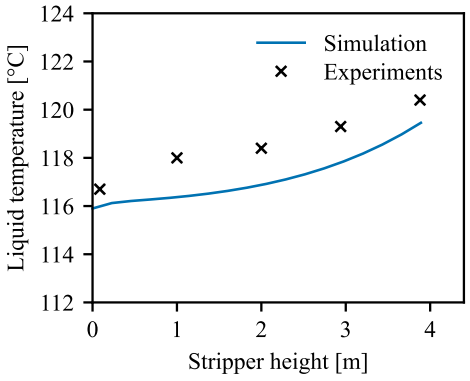

Figure 4.11: Comparison between the liquid phase stripper temperature profile simulated in this work and experimental data for run 2 by Tobiesen et al.[44].

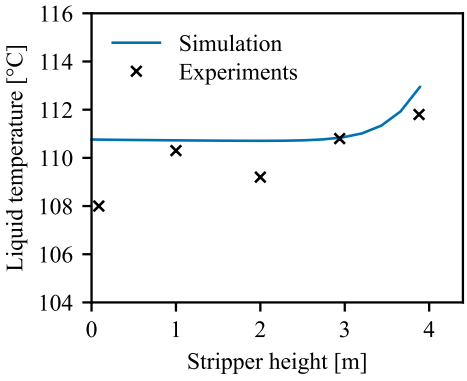

Figure 4.12: Comparison between the liquid phase stripper temperature profile simulated in this work and experimental data for run 18 by Tobiesen et al.[44].

rate corresponded well. An example of this is the temperature profile of run 12 in Figure 4.7. A reason for this deviation may be the water content of the gas, which was not analyzed in the experiments. Tobiesen et al.[43] showed that a difference in water content can significantly change the temperature profile through changes in water evaporation rates and CO_2 partial pressure, because the dry gas composition was analyzed.

The parity plots for the performance of the desorber section are given in Figure 4.9 and Figure 4.10. These show that there is also a good agreement between the simulation and the experimental results for the desorber. Deviations were in the same order of magnitude as for the absorber and are considered to be acceptable.

A pair of simulated and experimental temperature profiles in the desorber is given in Figure 4.11 and Figure 4.12. The temperature in the stripper was difficult to measure and led to possible uncertainties in the experimental results. Firstly, it is not known which phase is in contact with the temperature sensor at any time. Also, Tobiesen et al.[44] suspect that in the case of high loadings, some of the liquid may flash before entering the stripper column, underestimating the enthalpy content of the flow. Despite some slight deviations in temperature, the simulations correspond relatively well with the experimental data.

4.4 Results

4.4.1 Oxidative Degradation Model Fitting Results

The fitted reaction rate coefficients and their 95% confidence intervals are given in Table 4.6. The reaction order with respect to O_2 is fractional, which indicates that oxidative degradation is most likely a chemical chain reaction.[67] This is in agreement with mechanisms discussed by Goff et al.[16] and Sexton[68], in which free radicals derived from O_2 play a role as intermediates in oxidative degradation reactions.

Table 4.5: Degradation reactions and reaction rate equations for the oxidative degradation model. The reference temperature for the oxidative rate coefficients is 338.15 K.

Reaction	**Reaction rate [mol/m^3/s]**	**Reaction rate coefficient**
$\mathrm{MEA} + 1.3\mathrm{O}_2 \rightarrow \mathrm{Prod.}$	$R = k_r[\mathrm{MEA}][\mathrm{O}_2]^n$	$k_r = k_{\mathrm{ref}} \cdot \exp\left(\frac{-E_A}{R_{\mathrm{id}}}\left(\frac{1}{T} - \frac{1}{T_{\mathrm{ref}}}\right)\right)$

Table 4.6: Regressed reaction rate parameters for the oxidative degradation model.

Parameter	**Unit**	**Value**	**95% confidence interval**
k_r	$(\mathrm{m}^3/\mathrm{mol})^n/\mathrm{s}$	$6.790 \cdot 10^{-7}$	$[0.588 \cdot 10^{-7} – 0.784 \cdot 10^{-7}]$
E_A	J/mol	$7.908 \cdot 10^4$	$[6.952 \cdot 10^4 – 8.997 \cdot 10^4]$
n	-	0.469	[0.405 – 0.533]

The activation energy for the reaction is higher than those regressed by other works in the literature, which are 41.7 kJ/mol by Léonard et al.[12] and 29.4 kJ/mol by Supap et al.[18]. This difference may be the results of both literature works assuming that the concentration of dissolved O_2 was in equilibrium, neglecting the mass transfer resistance of O_2. The importance of this mass transfer resistance depends on the reaction rate in the liquid phase and thus on the temperature. At increased temperatures, the mass transfer can cause the actual liquid bulk concentration of O_2 to drop below the equilibrium concentration. If this is not considered, the reaction rate coefficient is underestimated, and the temperature dependency of the apparent reaction rate coefficient is smaller.

This effect can be amplified by the reaction order of O_2 since a change in O_2 concentration will result in a larger change in reaction rate coefficient if the reaction order is high. The regressed reaction orders were reported to be 1.46 by Léonard et al.[12] and 2.91 by Supap et al.[18]. The temperatures in the degradation experiments by Vevelstad et al.[14] were low compared with the typical temperatures used by Léonard et al.[12] and Supap et al.[18]. Therefore, it is also a possibility that a difference in reaction mechanism at increased temperatures leads to a lower temperature dependency of the reaction. The difference in reaction order for O_2 and the use of different O_2 solubility models makes it challenging to compare reaction rate coefficients between these studies and the current work.

The experiment at 55 °C and 21 vol% O_2 was run three times by Vevelstad et al.[14], and the replicate measurements can give an insight into the uncertainty of the experiments. The absolute differences between the three runs are limited, and the standard deviation of the measured concentration of MEA is only 132.0 mol/m^3. However, it is expected that the uncertainty in the experiments is proportional to the extent of degradation, which was also the case for thermal degradation experiments[17]. The standard deviation of the experiments with more degradation will thus likely be higher.

One could consider the error to be proportional and evaluate the standard deviation with respect to the measured degradation, but this is also challenging due to limited degradation at 55 °C. The standard deviation for the replicates is, on average 49.7% of the measured degradation of MEA. This high error is a result of the relatively large size of the analytical error and deviations in the mass balance with respect to the measured degradation. The impact of these uncertainties will be lower for experiments with more degradation, resulting in a lower relative error.

It is thus challenging to estimate the uncertainty of the experimental data and evaluate the quality of the fit. The residual plots for the fitted model with respect to the experimental data are given as a function of the temperature, partial pressure of O_2, degradation time, and the initial and final concentration of MEA in Figure 4.13 through Figure 4.17. The standard deviation of the model with respect to the experimental data is 248.8 mol/m^3, which is, on average 23.7%, with respect to measured degradation. Despite the deviation, the model appears to give a good representation of the

experimental data, and no significant residual trends were observed. The use of additional parameters in the rate equation, for example, a reaction order for MEA, did not significantly improve the fitting results.

Figure 4.18 shows the degree of saturation for O_2 in the liquid bulk with respect to the solubility at the bubble interface, where the gas and liquid phases are assumed to be in equilibrium. At lower temperatures, consumption of O_2 by the degradation reactions is relatively low, and degradation is not limited by mass transfer. As a result, the bulk concentration of O_2 is close to the equilibrium concentration. At higher temperatures, O_2 consumption in the liquid is increased, and more O_2 has to be transferred to the liquid phase. A more significant driving force is needed across the boundary layer, which causes the bulk concentration of O_2 to decrease. In these conditions, the degradation rate is partially limited by mass transfer.

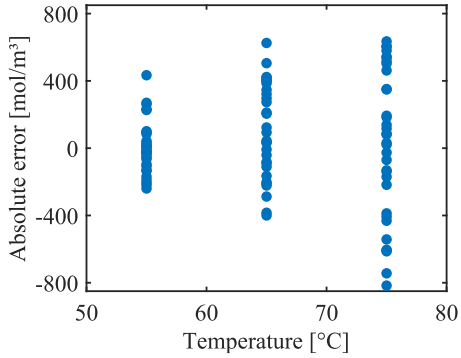

Figure 4.13: Residuals of the modeled MEA concentrations with respect to the experimental values as a function of temperature.

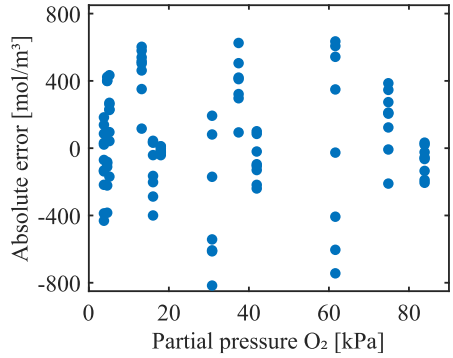

Figure 4.14: Residuals of the modeled MEA concentrations with respect to the experimental values as a function of partial pressure of O2.

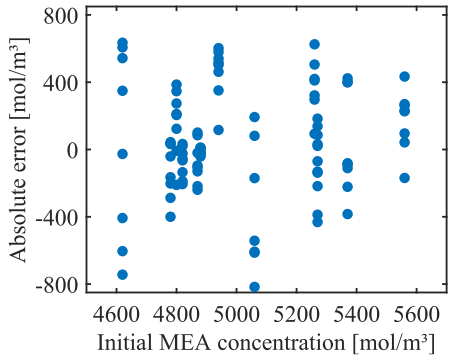

Figure 4.15: Residuals of the modeled MEA concentrations with respect to the experimental values as a function of the initial concentration of MEA.

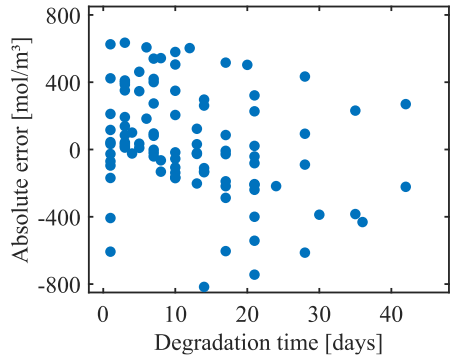

Figure 4.16: Residuals of the modeled MEA concentrations with respect to the experimental values as a function of degradation time.

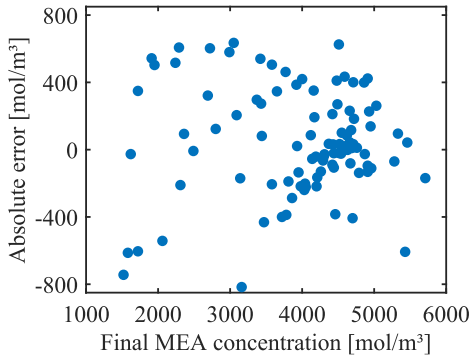

Figure 4.17: Residuals of the modeled MEA concentrations with respect to the experimental values as a function of the final concentration of MEA.

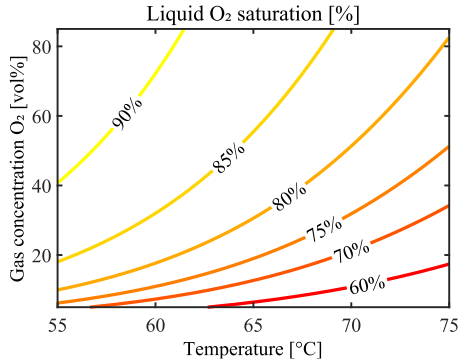

Figure 4.18: Estimated liquid-phase O_2 saturation (bulk over interfacial concentration) in the experiments by Vevelstad et al.[14] at various temperatures and gas-phase O_2 concentrations.

Experiments with lower O_2 partial pressures are also more mass transfer limited. This is an effect of the reaction order of O_2 in the degradation reaction. The fitted reaction order is 0.47, so an increase in the concentration of dissolved O_2 will have a progressively smaller impact on the degradation rate. The O_2 solubility and the driving force over the mass transfer film, on the other hand, scale more linearly with the partial pressure of O_2 in the gas.

4.4.2 Predicted Degradation in the Industrial Flue Gas Cases

The predicted solvent degradation for the industrial flue gas cases is given in Figure 4.19. Note that the degradation rates are normalized with respect to the amount of CO_2 captured, so the absolute degradation rates are more significant for the cases with higher CO_2 concentrations in the flue gas. The degradation rates and process conditions in the absorber packing are given in Figure 4.20 to Figure 4.24. Degradation in the collectors and distributors is not displayed in these profiles but has been included under the absorber packing category in the bar plot in Figure 4.19. The total degradation rates for the natural gas and waste-to-energy are comparable, at around 110 g MEA/ton CO_2. Degradation in the cement case was relatively high, at 150 g MEA/ton CO_2, and the lowest degradation was observed in the coal case, at 89.1 g MEA/ton CO_2.

In comparison, the total solvent losses in the capture pilot plant at Niederaussem for a coal-fired power plant, which had a similar coal flue gas composition as the case simulated in this work, were around 210 g MEA/ton CO_2 at the start of the campaign[52]. Moser et al.[52] reported that losses of MEA in the gas downstream of the absorber were negligible with respect to the overall solvent losses and that degradation was the main cause. The predicted degradation rate is thus significantly lower than the observed degradation. This may be a result of differences in the process, for example, an increased

solvent holdup, higher temperatures in the absorber ,or a higher stripper pressure. In addition, the catalytic effect of dissolved iron on oxidative degradation is not modeled. Although the concentrations of iron were low at the start of the campaign[52], the catalytic effect of iron can still be significant[25].

Oxidative degradation seen in this work constitutes around 80% to 90% of the total degradation. The remainder is caused by thermal degradation. This is in line with the observations on degradation of MEA in experimental works and pilot plant reports in literature [52,69,70]. Thermal degradation primarily takes place in the stripper sump and reboiler and only approximately 10% of the thermal degradation is predicted to occur in the packing and distributors in the stripper.

Léonard et al.[20] predicted degradation in the pilot plant campaign by Knudsen et al.[71]. The composition of the flue gas was similar to the composition of the flue gas for the coal-fired power plant in this work. The concentration of CO_2 and O_2 were 14 vol% and 6 vol%, respectively. The total degradation in the pilot plant was predicted to be 79.5 g MEA/ton CO_2, which is close to the degradation predicted in this work. Léonard et al.[20] predicted slightly more degradation in the absorber compared with the current work. This is due to increased solvent holdup since a packed height of 20 m was used, in contrast to the 12 m used in this work.

The predictions for thermal degradation by Léonard et al.[20] are several orders of magnitude smaller. This is unexpected because the used rate equations for thermal degradation of MEA are comparable to the ones used in this work[17]. It could be that the stripper sump and or reboiler have not been considered in the model by Léonard et al.[20], but even when just considering thermal degradation in the stripper packing, significantly more degradation is predicted in this study.

Degradation in the absorber is primarily oxidative and makes up a significant fraction of the total degradation for each of the processes. Higher temperatures in the absorber packing lead to more degradation. This applies to the cement case, where the high concentration of CO_2 in the flue gas leads to increased temperatures in the absorber. Based on the oxidative degradation kinetics, a stronger temperature dependence is expected, but a reduction of O_2 solubility at higher temperatures reduces the actual impact.

A higher concentration of O_2 in the flue gas also results in increased degradation. This applies to the natural gas case, in which there is significant degradation in the packing, regardless of the milder temperatures. The combination of these effects leads to comparable degradation rates in the absorber packing for the natural gas, waste-to-energy, and coal cases, despite different flue gas compositions. This can be seen in Figure 4.24. The impact of CO_2 loading on O_2 solubility is illustrated in Figure 4.23. At the top of the absorber packing, the solvent is relatively lean, and the concentration of dissolved O_2 is high. The solubility is reduced as the temperature rises in the top part of

the absorber packing and the CO_2 loading is increased, thereby increasing the concentrations of the protonated MEA, MEA carbamate, and carbonate ions. After the temperature peak, the concentration of dissolved O_2 is relatively constant. Here, the decrease in temperature and increase in CO_2 loading roughly balance each other out.

The liquid holdup per cubic meter of total absorber volume for each of the investigated cases is shown in Figure 4.21. The flue gas flow rates are identical across all cases, resulting in equivalent column diameters and total internal volumes. Flue gasses with a higher CO_2 content, such as in the cement and waste-to-energy cases, require higher liquid flow rates to achieve the required capture efficiency, which results in increased liquid holdup in the packing. The liquid holdup is relatively constant throughout the absorber packing. The CO2 loading in the absorber is shown in Figure 4.22.

Most of the degradation in the heat exchanger is on the rich side through indirect oxidative degradation. Although there is no direct source of O_2 in the heat exchanger, O_2 that is dissolved in the absorber reacts with the amine when the temperature is increased. A high O_2 solubility is therefore associated with more degradation in the heat exchanger. This is observed in the natural gas case, where indirect degradation in the sump and heat exchanger accounts for around 40% of the total degradation. Oxygen consumption in the rich solvent is shown in Figure 4.25. It should be noted that the reaction kinetics are extrapolated to evaluate degradation at temperatures above 75 °C, which could lead to uncertainty. However, even when degradation in the hot rich stream is evaluated at 75 °C, complete consumption of dissolved O_2 is observed, so the results should not change significantly.

Because all of the dissolved O_2 has reacted before the rich solvent enters the stripper, there is no oxidative degradation in the stripper. The extent of degradation in the stripper is approximately the same for each case, due to comparable process conditions in the stripper. The holdup volumes in the stripper and reboiler, and thus also the degradation of MEA, are proportional to the amount of CO_2 removed. A slightly higher relative degradation rate is observed in the stripper for the natural gas capture process. This is caused by the relatively low concentration of CO_2 in the flue gas, which results in a lower rich loading and a reduced cyclic capacity, as the lean loading is fixed. As a result, the solvent flow rate and, thus, the solvent holdup volumes are increased slightly. Degradation in other parts of the plant, such as the pumps and piping, is negligible for all the studied base cases.

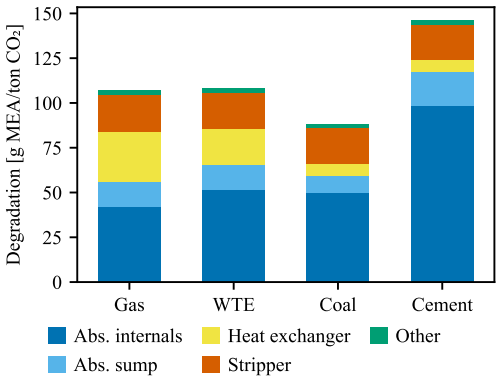

Figure 4.19: Predicted MEA degradation in different parts of the capture plant for the industrial flue gasses.

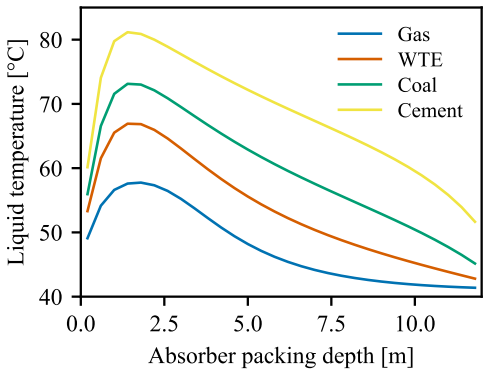

Figure 4.20: The liquid temperature profiles in the absorber packing for the studied flue gas cases.

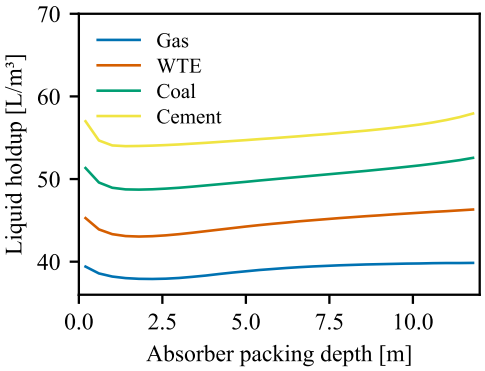

Figure 4.21: Liquid holdup profiles in the absorber packing per m^3 of total column volume for the studied flue gas cases.

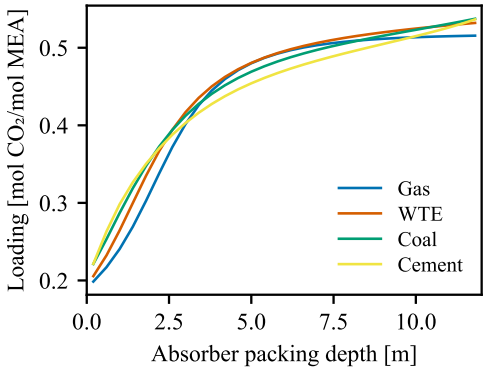

Figure 4.22: Loading in the absorber packing for the three base cases.

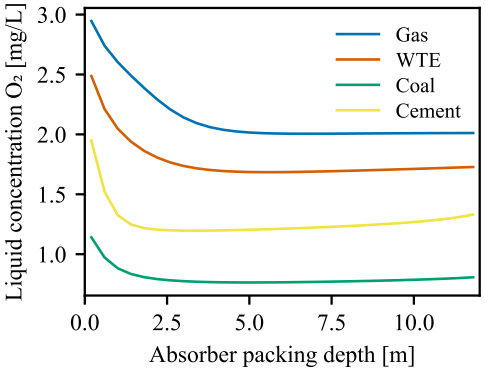

Figure 4.23: Dissolved O_2 in the absorber packing for the three base cases.

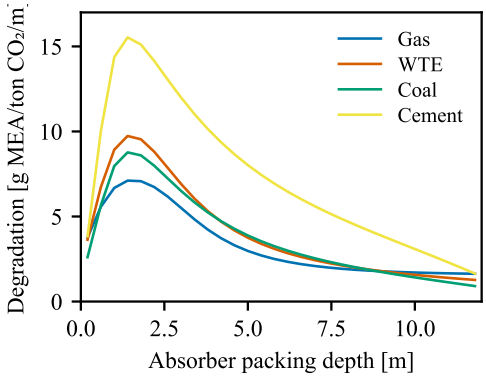

Figure 4.24: Predicted MEA degradation in the absorber packing per meter of packing for the three base cases.

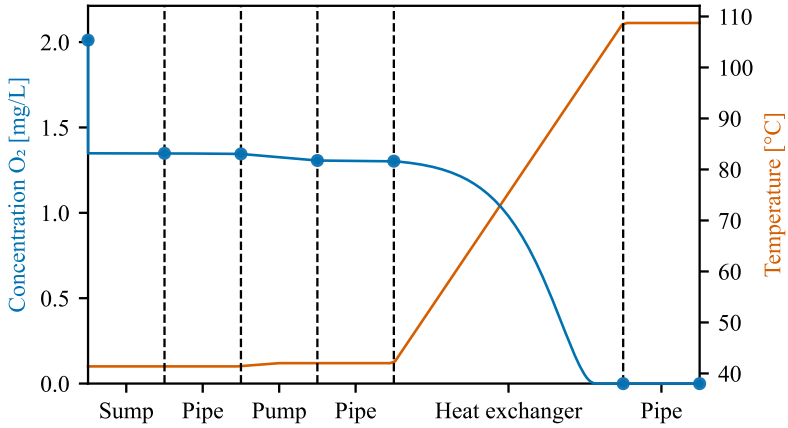

Figure 4.25: Liquid temperature and predicted concentration of dissolved O_2 in the rich solvent from the absorber sump to the inlet of the stripper for the natural gas-fired power plant capture case.

4.4.3 Impact of Process Modifications

The predicted degradation of MEA for each of the process modifications is given in Figure 4.26. The degradation in the coal-fired power plant base case is used as a reference. Each case is discussed in more detail below.

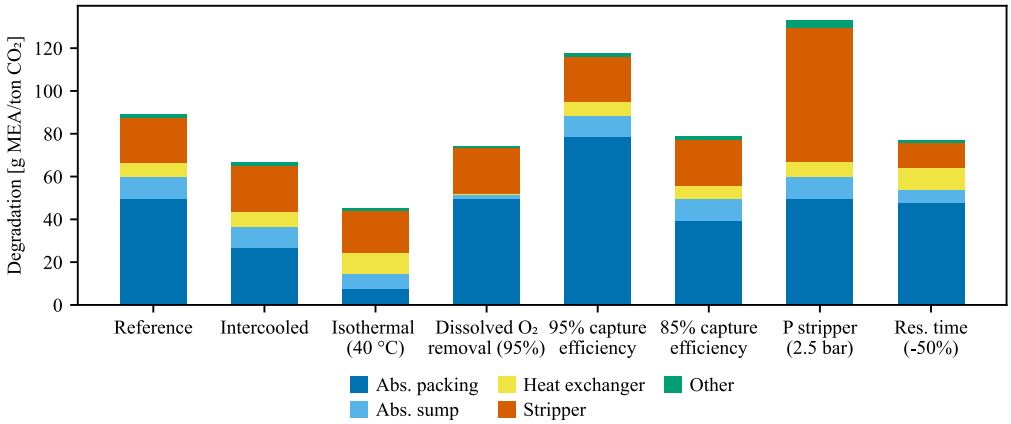

Figure 4.26: Predicted degradation of MEA for the process modifications to the coal-fired power plant base case, which is given here as a reference.

4.4.3.1 Intercooled and Isothermal Absorber

Figure 4.26 shows that the predicted degradation is significantly lower for the in-situ intercooled and isothermal cases. The largest reduction in degradation is observed in the absorber packing. The temperature profiles and degradation rate profiles in the absorber

packing for the reference, intercooled, and isothermal cases are given in Figure 4.27 and Figure 4.28, respectively. Intercooling in the absorber is an effective method to reduce both the peak temperature and the overall temperatures in the absorber packing. As a result, the degradation in the packing is reduced by 44%. Additional heat removal from the absorbent influences the degradation rates significantly, since the isothermal case shows an 71% reduction in degradation in the entire absorber compared with the reference case.

The loading profiles and the concentration profiles of dissolved O_2 in the absorber packing are shown in Figure 4.29 and Figure 4.30, respectively. The isothermal case shows that the CO_2 loading has a significant impact on the solubility O_2. Although the CO_2 loadings in the isothermal absorber packing are generally higher, the concentrations of dissolved O_2 are also higher. This indicates that the effect of temperature is more

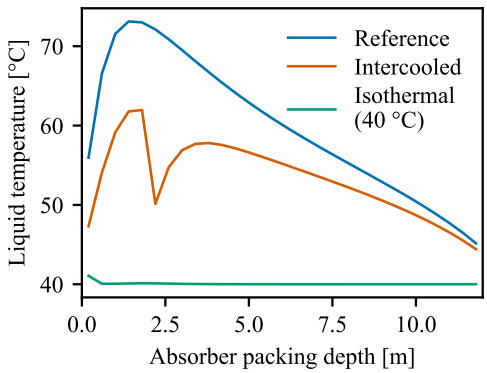

Figure 4.27: Liquid temperature in the absorber packing for the reference, intercooled, and isothermal cases.

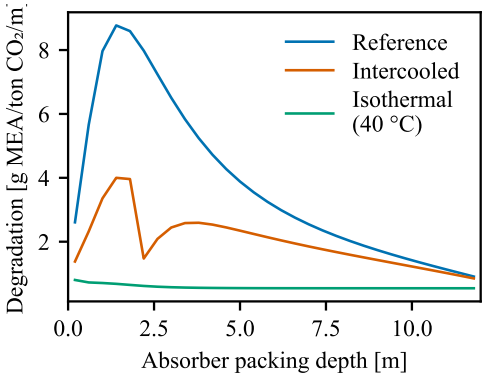

Figure 4.28: Degradation rate per ton of CO_2 captured per meter of packing height in the absorber packing for the reference, intercooled, and isothermal cases.

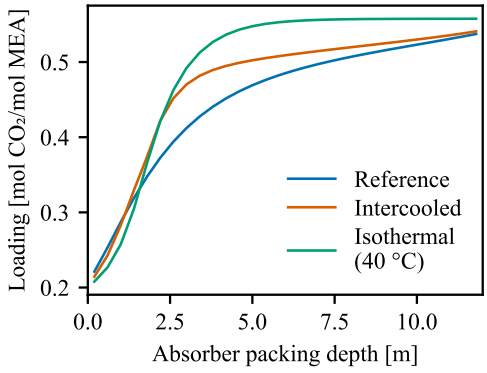

Figure 4.29: Liquid CO_2 loading in the absorber packing for the reference, intercooled, and isothermal cases.

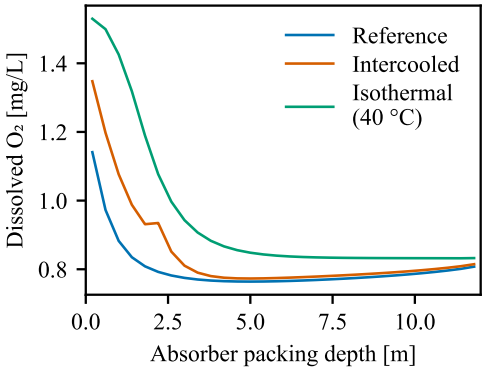

Figure 4.30: Liquid O_2 concentration in the absorber packing for the reference, intercooled, and isothermal cases.

prominent. The lower temperature in the bottom of the absorber for the isothermal case reduces the degradation rate in the sump. The remaining dissolved O_2 now reacts in the heat exchanger instead, resulting in an increase in degradation in this part of the plant. The total amount of degradation as a result of dissolved O_2 is increased slightly due to a higher O_2 solubility in the sump.

In this comparison, the column height, solvent flow rate, lean loading, and reboiler duty remain unchanged. In reality, increased absorption rates due to intercooling may impact some of these process parameters. For example, shorter columns may be used to capture the same amount of CO_2, thus reducing the solvent holdup and exposure time in the absorber packing. Alternatively, intercooling may lead to higher rich loadings and increase the cyclic capacity. This would lead to lower solvent flow rates and reduced holdups not only in the absorber but also in the stripper and other parts of the plant.

In the more realistic scenario of in-and-out intercooling, where the solvent is temporarily removed from the column, additional solvent holdup is expected to be required. The solvent has to be collected, transported, cooled, transported, and redistributed in the absorber again. To study the impact of this addition to the process, the simulation is adjusted to include the intercooling loop, as shown in Figure 4.31. Solvent is removed at a height of around 10 m in this case and is transported to the ground to be cooled in a heat exchanger and re-entered into the absorber at approximately the same height as the outlet. The residence time of the intercooling loop is estimated to be around 40 s.

The solvent is saturated with O_2 when leaving the column, and some of the dissolved O_2 is consumed in the intercooling loop. This can be seen in Figure 4.32, which shows the concentration of O_2 and the temperature of the solvent in the intercooling loop. Some of the dissolved O_2 is consumed by the oxidative degradation reactions, in particular before the solvent is cooled. After cooling, degradation is limited.

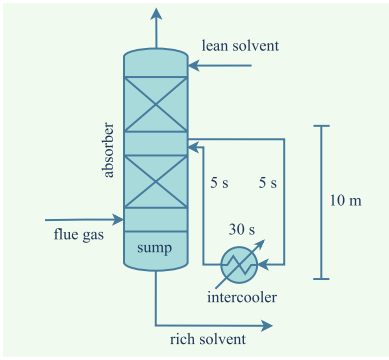

Figure 4.31: Process flow diagram of in-and-out intercooling in the absorber.

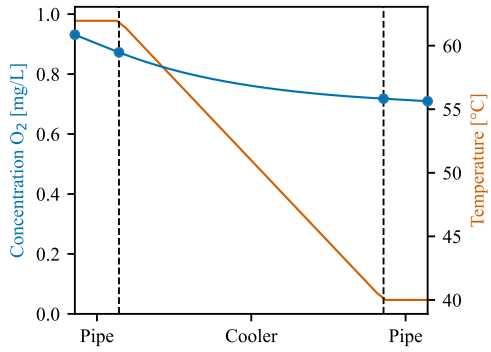

Figure 4.32: Liquid temperature and predicted concentration of dissolved O_2 in the in-and-out intercooling loop.

An overview of the predicted degradation rates in the simulated processes for the reference and intercooled cases is given in Table 4.7. The initial case study on ideal intercooling is predicted to have a degradation rate of 36.7 g MEA/ton CO_2 in the absorber, which is a reduction of 39.0% with respect to the reference case. The total degradation in the entire process is reduced by 25.0%. The implementation of in-and-out intercooling is predicted to add 9.3 g MEA/ton CO_2 of additional degradation, resulting in a total degradation of 76.1 g MEA/ton CO_2, which is only a reduction of 14.6% with respect to the base case. This shows that there is a significant potential for intercooling to reduce degradation, but that the implementation is important, and that additional solvent holdup and residence times have to be minimized.

Table 4.7: Predicted degradation in the absorber and intercooling loop for the reference case for the coal-fired power plant flue gas, the ideal intercooled case with no additional holdup, and the realistic intercooled case with the intercooling loop and additional distribution.

Degradation [g MEA/ton CO_2]	**Reference case**	**Intercooled (in-situ)**	**Intercooled (in-and-out)**
Absorber	59.9	36.7	39.5
Structured packing	→ 45.3	→ 23.8	→ 23.8
Collectors/distributors	→ 4.6	→ 3.1	→ 5.8
Sump	→ 10.0	→ 9.9	→ 9.9
Intercooling loop	-	-	6.6
Total (process)	89.1	66.8	76.1

4.4.3.2 Dissolved Oxygen Removal

The 90% removal of dissolved O_2 before the solvent enters the absorber sump effectively reduces degradation rates in the stripper and heat exchanger as is shown in Figure 4.26. Degradation in the other parts of the process is unchanged. The predicted overall degradation for this case study is 74.1 g MEA/ton CO_2, which is a reduction of 16.8%.

The overall impact of dissolved O_2 removal is limited for MEA since a large fraction of oxidative degradation occurs in the absorber. Solvents that are more stable towards oxidative degradation at typical absorber temperatures are still expected to degrade oxidatively as the temperature increases in the heat exchanger. Degradation as a result of dissolved O_2 is expected to play a larger role for these solvents, and dissolved O_2 removal can have a larger impact.

It is important to study oxidative degradation at heat exchanger conditions for these solvents, as the reaction order of O_2 can play an important role. For example, if the dependency of the reaction rate on the concentration of O_2 is relatively low, the degradation rate will not change by removing dissolved O_2. The impact of dissolved O_2

removal may then be limited if the amount of O_2 left behind is larger than the amount of O_2 consumed by degradation.

4.4.3.3 Change in Capture Efficiency

Increasing the capture rate to 95%, increases the degradation rate per ton of CO_2 in the absorber packing and distributors by 57.7%, due to the additional packing height and the added collector and distributor (Figure 4.26). The solvent flow rate was increased by 5.6%, which causes the degradation in the other parts of the process to increase slightly. However, since more CO_2 is captured in this case study, the degradation rate relative to the amount of CO_2 captured is unchanged. Since most of the degradation is caused by direct oxidative degradation in the packing, mitigation strategies that aim at reducing thermal degradation or indirect oxidative degradation through dissolved O_2 will be less effective at increased capture efficiencies.

A capture process with a reduced capture efficiency of 85% was also investigated. Apart from a marginal reduction in degradation in the absorber packing and distributors (-20.9%), similar degradation is expected in the other parts of the process. However, as the degradation rates are normalized to the CO_2 captured, the absolute degradation in the process would be lower.

4.4.3.4 Stripper Pressure

The predicted degradation for the case study with a stripper pressure of 2.5 bar is shown in Figure 4.26. Thermal degradation in this case study is increased by 200% with respect to the reference case, because at this pressure, the temperatures in the stripper are higher, especially in the sump and reboiler. Aside from a slight increase in thermal degradation in the heat exchanger, degradation in the rest of the simulated process is the same. The overall degradation rate is predicted to be 133.2 g MEA/ton CO_2.

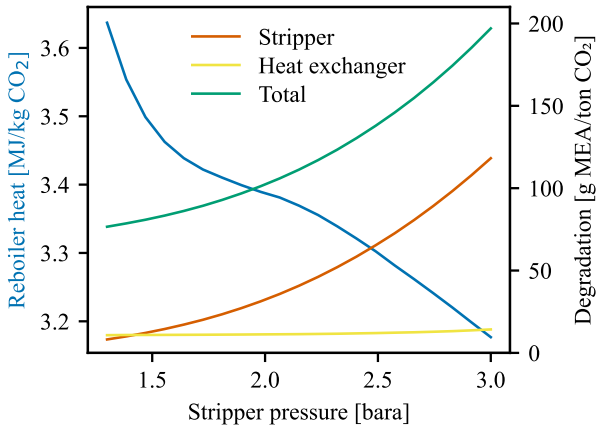

Figure 4.33: Impact of stripper pressure on required reboiler heat and solvent degradation.

Léonard et al.[20] also investigated the effect of increased stripper pressures on the total degradation but observed a significantly smaller increase. However, the contribution of thermal degradation was negligible in the predictions by Léonard et al.[20], so although an increase in thermal degradation was observed, the total degradation was not influenced significantly.

The thermal and total degradation rate as a function of the stripper pressure is shown in Figure 4.33. At a constant solvent flow rate, the energy duty in the reboiler that is required to capture 90% CO_2 in the process decreases as the stripper pressure increases. At a stripper pressure of 3.0 bar, the temperature in the stripper reboiler is 134 °C. At this point, the total predicted degradation is 188.7 g MEA/ton CO_2, which is more than double the degradation in the reference case. More than half of the degradation at a stripper pressure of 3.0 bar is due to thermal degradation in the stripper.

A good operating strategy would thus select a stripper pressure that benefits from the reduced energy requirements, without the occurrence of significant thermal degradation. However, as degradation causes other operational problems, potentially increased emission mitigation requirements, and increased costs, optimizing the reboiler pressure is in reality a complex design problem.

4.4.3.5 Reduced Solvent Residence Times

A 50% reduction in solvent residence time of the equipment, as specified in Table 4.4, reduces degradation by 13.7%, for a total of 76.9 g MEA/ton CO_2. Degradation in the packing is reduced only slightly and this shows that only a small fraction of degradation is occurring in the collectors and distributors. Most of the degradation is taking place in the packing itself, where the residence time is not changed.

Even though degradation in the absorber sump is reduced, the unreacted dissolved O_2 is now consumed in the heat exchanger. The residence time in this equipment is also reduced, but the low stability of MEA at increased temperatures causes all of the O_2 to still be consumed. A reduction in residence times may be more effective for solvents that are more stable toward oxidative degradation. In those solvents, complete depletion of O_2 in the heat exchanger may not occur and exposure time is more important.

Degradation in the stripper sump and reboiler is halved. Since this thermal degradation only makes up a limited percentage of the total degradation, the effects here are limited. However, if thermal degradation is more prominent, a reduction of residence time could be valuable. This could be the case for solvents that are more resistant toward oxidative degradation, for processes with flue gasses with a low O_2 content, or in case the stripper pressure is increased. Residence times in the stripper may be reduced for example by combining the sump and reboiler. Finally, degradation in the pumps and cooler is limited and the effect of reduced residence times on the overall degradation is negligible.

4.4.3.6 Oxygen Concentration in the Flue Gas

Figure 4.34 shows that oxidative degradation is expected to be the dominant degradation mechanism for post-combustion capture processes. Thermal degradation is predicted to be dominant, only in case the flue gas contains less than 1 vol% of O_2. The extent of indirect oxidative degradation appears to be linearly proportional to the concentration of O_2 in the flue gas. This is caused by the linear dependency of the solubility of O_2 on the partial pressure of O_2 at absorber conditions and the fact that all of the dissolved O_2 will react. This means that a change in the solubility of O_2 will have a similar effect on degradation as a change in O_2 partial pressure.

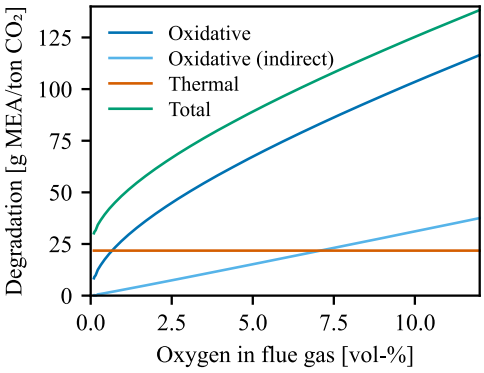

Figure 4.34: Predicted oxidative and thermal degradation in the reference case as a function of the concentration of O_2 in the flue gas, also showing the contribution of indirect oxidative degradation through dissolved O_2.

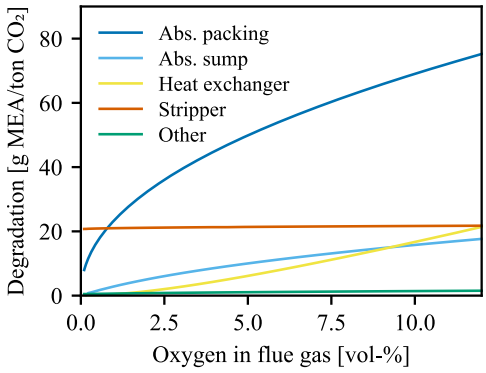

Figure 4.35: Predicted degradation for equipment in the reference case as a function of the concentration of O_2 in the flue gas.

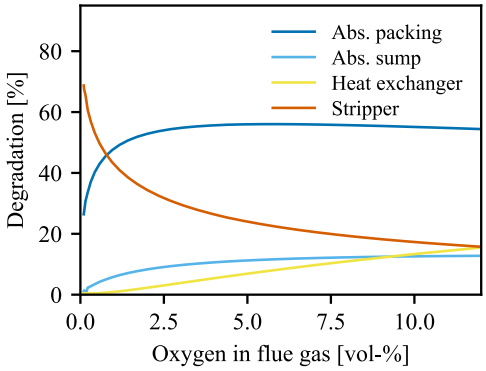

Figure 4.36: Predicted distribution of degradation for equipment in the reference case as a function of the concentration of O_2 in the flue gas.

The distribution of the degradation in the various parts of the process is shown in Figure 4.35 and Figure 4.36. Higher O_2 concentrations in the flue gas lead to an increase in direct oxidative degradation in the absorber packing. The increase is more prominent at lower O_2 concentrations, which is a result of the reaction order for O_2 in the rate equation (n=0.47). An increase in degradation is observed in the heat exchanger at higher O_2 concentrations since more dissolved O_2 remains in the rich solvent exiting the absorber sump. There is no oxidative degradation in the stripper and thermal degradation in equipment other than the stripper is limited. Therefore, the extent of degradation in the stripper remains unchanged. Degradation in other parts of the process is limited.

4.4.3.7 Reduced Oxidative Degradation Rate

The effects of a reduction in oxidative degradation rate on the overall oxidative and thermal degradation and degradation in various parts of the process are shown in Figure 4.37 and Figure 4.38, respectively. Degradation in the absorber packing is linearly proportional to the degradation rate coefficient. A small reduction in the oxidative degradation rate has no impact on the amount of degradation through dissolved O_2. Oxidative degradation in the sump is reduced, but the remaining O_2 is now consumed in the heat exchanger.

At around 30% of the initial degradation rate, full consumption of O_2 in the heat exchanger no longer occurs and the remaining dissolved O_2 is consumed in the sequential pipe leading up to the stripper inlet. Degradation in this pipe is responsible for the majority of the degradation labeled as "Other" in Figure 4.38. When the oxidative degradation is reduced to 10% of the initial rate, there is a breakthrough of dissolved O_2 into the stripper. This behavior is illustrated in Figure 4.39, where all of the initially dissolved O_2 is just consumed. A significant part of the dissolved O_2 is consumed in the

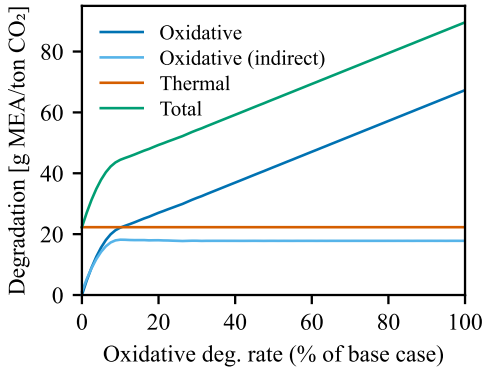

Figure 4.37: Predicted oxidative and thermal degradation in the reference case as a function of the oxidative degradation rate, also showing the contribution of indirect oxidative degradation through dissolved O_2.

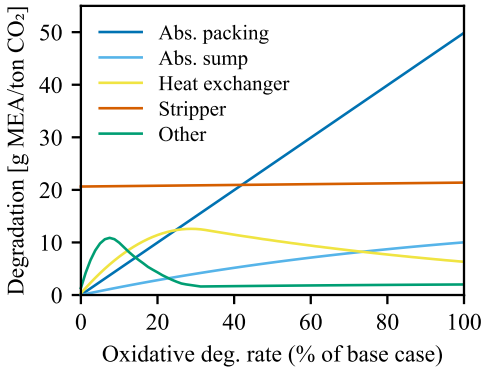

Figure 4.38: Predicted degradation for equipment in the reference case as a function of the oxidative degradation rate. By far the largest contribution to Other is degradation in the pipe from the heat exchanger to the stripper.

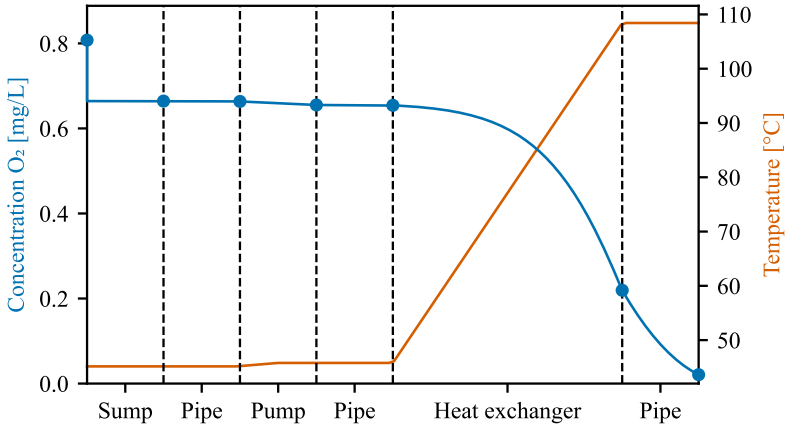

Figure 4.39: Liquid temperature and predicted concentration of dissolved O_2 in the rich solvent from the absorber sump to the inlet of the stripper at an oxidative degradation rate of 10% the rate of the reference case.

pipe leading up to the stripper, even though the residence time in this pipe is only 20 s. A higher liquid velocity in this pipe, leading to a lower residence time may be an effective way of reducing degradation in such a case.

The more stable a solvent is towards oxidative degradation, the larger the relative contributions of degradation by dissolved O_2 and thermal degradation will be. Mitigation strategies that aim at reducing these types of degradation, such as a reduction in residence times or stripper pressure, or removal of dissolved O_2, will thus be more effective for these stable solvents.

4.5 Conclusions

This work focused on solvent degradation in absorption-based CO_2 capture processes using a 30 wt% aqueous MEA solvent. A degradation model for MEA was developed and used to predict solvent degradation in full-scale capture processes. Degradation in the base case capture processes for the investigated flue gasses was predicted to be 90 to 150 g MEA/ton CO_2, which is lower than typically observed in pilot plants. In these plants, however, iron and other metals are expected to dissolve and catalyze the degradation. The degradation model in this work does not take this accelerated degradation into account and this is the most likely cause of the underprediction. Additional experimental data is required to accurately model the catalyzed reactions and the rate equations that describe corrosion and dissolved metal concentrations, which should then be included in future iterations of degradation models.

The high CO_2 content of the flue gas for the coal and cement cases leads to increased temperatures in the absorber and relatively high degradation rates. The natural gas and

WTE cases, on the other hand, are characterized by more indirect oxidative degradation, due to the relatively high concentration of O_2 in the flue gas and rich solvent. The degree of thermal degradation is similar for all the cases, accounting for approximately 10% to 20% of the total degradation.

Modifications to the base case capture process for a coal-fired power plant can have a significant effect on the degradation. A reduction of temperatures in the absorber packing can reduce degradation up to 84.6% if an isothermal absorber would be implemented. A single in-situ intercooling stage at the peak of the temperature bulge reduces the total degradation in the process by 25.0%. However, the additional solvent holdup and exposure as a result of implementing the intercooling may negate some of these benefits. An in-and-out intercooler placed at ground level generates additional degradation and is estimated to only lead to a 14.6% net reduction in the overall degradation.

Dissolved O_2 removal can be effective at reducing indirect oxidative degradation. However, due to the relatively small contribution of this type of degradation to the total degradation in the coal-fired flue gas case, the overall impact is limited for 30 wt% MEA. The extent of indirect oxidative degradation will be more significant in processes with higher concentrations of O_2 in the flue gas or for solvents that are more stable towards oxidative degradation at absorber temperatures. Timely removal of the dissolved O_2 may play an important role here. An increase in stripper pressure is found to both decrease heat requirements and increase degradation significantly. More information about the impact of degradation and the degradation products on, for example, the performance of the process or the costs of reclaiming is required to select the optimal operating point.

The impact of reduced residence times in the column sumps and reboilers, heat exchanger, pumps, and piping is limited for the process with MEA as a solvent. Despite a smaller exposure time for the rich solvent on its way to the stripper, all of the dissolved O_2 is still consumed. The effect will be more significant in case the stability of the solvent is higher and some of the dissolved O_2 does not react. For similar reasons, an increase in solvent stability or a reduction in the oxidative degradation rate has initially little effect on the extent of indirect oxidative degradation. Only the direct oxidative degradation in the absorber packing is reduced. At an oxidative degradation rate that is lower than 17.5% the rate for MEA, a fraction of the dissolved O_2 is not consumed and enters the stripper. This results in less indirect oxidative degradation and a larger reduction in the overall degradation.

The liquid phase mass transfer limitations of O_2 in the absorber packing have been estimated and are found to be negligible, so the solvent is saturated with O_2 in the packing. This is, however, not always the case for oxidative degradation experiments. Experiments in an agitated bubble reactor are likely to involve significant liquid phase mass transfer resistances, especially at the higher temperatures that are typical for the absorber. In this work, these resistances have been considered and a rate equation for the consumption of MEA has been fitted using the experimental data by Vevelstad et al.[14].

The deviations of the oxidative degradation model were significant, but no clear trends were observed in the residuals. The experimental uncertainty is expected to play an important role in the uncertainty of the model but could not be quantified accurately.

To develop more accurate oxidative degradation models, the degradation kinetics should be separated from mass transfer resistances. Correlations used to estimate mass transfer resistances can be uncertain because they rely on a generalization of mass transfer processes. In addition, the quantification of the process parameters, such as the bubble diameter or stirring power, can be challenging. Oxidative degradation reactors should therefore be designed to eliminate mass transfer resistances so that the observed degradation is directly related to the reaction kinetics. This can be achieved by for example increasing the interfacial area or reducing the liquid volume fraction in the reactor. Alternatively, if the elimination of mass transfer resistances is not feasible, the degradation reactor should be designed such that these can be quantified accurately.

The solubility of O_2 and its temperature dependency are important parameters to evaluate oxidative degradation since the concentration of dissolved O_2 can be directly proportional to the extent of degradation in the absorber sump, cross-heat exchanger, and related piping. Therefore, accurate quantification of this solubility is valuable. But this may be hard to achieve because of consumption by the degradation reactions. Alternatively, solubility models can be used to develop degradation models, but these degradation models should not be used independently or combined with other solubility models, and the impact of the CO_2 loading on the solubility of O_2 should be considered.

Acknowledgments

This publication has been produced with support from the NCCS Research Centre, performed under the Norwegian research programme Centre for Environment-friendly Energy Research (FME). The authors acknowledge the following partners for their contributions: Aker BP, Aker Carbon Capture, Allton, Ansaldo Energia, Baker Hughes, CoorsTek Membrane Sciences, Elkem, Eramet, Equinor, Gassco, Hafslund Oslo Celsio, KROHNE, Larvik Shipping, Norcem Heidelberg Cement, Offshore Norge, Quad Geometrics, Stratum Reservoir, TotalEnergies, Vår Energi, Wintershall DEA and the Research Council of Norway (257579/E20).

4.6 References

(1) Rogelj, J.; Shindell, D.; et al. Mitigation Pathways Compatible with 1.5°C in the Context of Sustainable Development; Intergovernmental Panel on Climate Change, 2018.

(2) Reynolds, A. J.; Verheyen, T. V.; et al. Degradation of Amine-Based Solvents. In *Absorption-Based Post-combustion Capture of Carbon Dioxide*; Elsevier, 2016; pp 399–423. https://doi.org/10.1016/B978-0-08-100514-9.00016-0.

(3) Kohl, A. L.; Nielsen, R. B. Alkanolamines for Hydrogen Sulfide and Carbon Dioxide Removal. In *Gas Purification*; Elsevier, 1997; pp 40–186. https://doi.org/10.1016/B978-088415220-0/50002-1.
(4) Martin, S.; Lepaumier, H.; et al. New Amines for CO2 Capture. IV. Degradation, Corrosion, and Quantitative Structure Property Relationship Model. *Ind. Eng. Chem. Res.* **2012**, *51* (18), 6283–6289. https://doi.org/10.1021/ie2029877.
(5) Vega, F.; Sanna, A.; et al. Degradation of Amine-Based Solvents in CO2 Capture Process by Chemical Absorption. *Greenhouse Gases: Science and Technology* **2014**, *4* (6), 707–733. https://doi.org/10.1002/ghg.1446.
(6) Gouedard, C.; Picq, D.; et al. Amine Degradation in CO2 Capture. I. A Review. *International Journal of Greenhouse Gas Control* **2012**, *10*, 244–270. https://doi.org/10.1016/j.ijggc.2012.06.015.
(7) Fredriksen, S. B.; Jens, K. J. Oxidative Degradation of Aqueous Amine Solutions of MEA, AMP, MDEA, Pz: A Review. *Energy Procedia* **2013**. https://doi.org/10.1016/j.egypro.2013.06.053.
(8) Buvik, V.; Høisæter, K. K.; et al. A Review of Degradation and Emissions in Post-Combustion CO2 Capture Pilot Plants. *International Journal of Greenhouse Gas Control* **2021**, *106*, 103246. https://doi.org/10.1016/j.ijggc.2020.103246.
(9) Eide-Haugmo, I. Environmental Impacts and Aspects of Absorbents Used for CO2 Capture. Doctoral thesis, Norwegian University of Science and Technology, Trondheim, 2011.
(10) Davis, J. D. Thermal Degradation of Aqueous Amines Used for Carbon Dioxide Capture. Doctoral thesis, The University of Texas, Austin, 2009. https://repositories.lib.utexas.edu/handle/2152/6581.
(11) Grimstvedt, A.; Falck da Silva, E.; et al. Thermal Degradation of MEA, Effect of Temperature and CO2 Loading; SINTEF Materials and Chemistry, Trondheim, TCCS-7, 2013.
(12) Léonard, G.; Toye, D.; et al. Experimental Study and Kinetic Model of Monoethanolamine Oxidative and Thermal Degradation for Post-Combustion CO 2 Capture. *International Journal of Greenhouse Gas Control* **2014**, *30*, 171–178. https://doi.org/10.1016/j.ijggc.2014.09.014.
(13) Supap, T.; Idem, R.; et al. Kinetics of the Oxidative Degradation of Aqueous Monoethanolamine in a Flue Gas Treating Unit. *Ind. Eng. Chem. Res.* **2001**, *40* (16), 3445–3450. https://doi.org/10.1021/ie000957a.
(14) Vevelstad, S. J.; Johansen, M. T.; et al. Extensive Dataset for Oxidative Degradation of Ethanolamine at 55–75°C and Oxygen Concentrations from 6 to 98%. *International Journal of Greenhouse Gas Control* **2016**, *50*, 158–178. https://doi.org/10.1016/j.ijggc.2016.04.013.
(15) Lepaumier, H.; Picq, D.; et al. New Amines for CO $_2$ Capture. II. Oxidative Degradation Mechanisms. *Ind. Eng. Chem. Res.* **2009**, *48* (20), 9068–9075. https://doi.org/10.1021/ie9004749.

(16) Goff, G. S.; Rochelle, G. T. Monoethanolamine Degradation: O_2 Mass Transfer Effects under CO_2 Capture Conditions. *Ind. Eng. Chem. Res.* **2004**, *43* (20), 6400–6408. https://doi.org/10.1021/ie0400245.
(17) Braakhuis, L.; Knuutila, H. K. Modelling and Evaluating Carbamate Polymerization of Monoethanolamine in Post-Combustion Carbon Capture. In *Trondheim Carbon Capture and Storage Conference (TCCS-11)*; Trondheim, 2021.
(18) Supap, T.; Idem, R.; et al. Kinetics of Sulfur Dioxide- and Oxygen-Induced Degradation of Aqueous Monoethanolamine Solution during CO2 Absorption from Power Plant Flue Gas Streams. *International Journal of Greenhouse Gas Control* **2009**, *3* (2), 133–142. https://doi.org/10.1016/j.ijggc.2008.06.009.
(19) Uyanga, I. J.; Idem, R. O. Studies of SO2- and O2-Induced Degradation of Aqueous MEA during CO2 Capture from Power Plant Flue Gas Streams. *Ind. Eng. Chem. Res.* **2007**, *46* (8), 2558–2566. https://doi.org/10.1021/ie0614024.
(20) Léonard, G.; Crosset, C.; et al. Influence of Process Operating Conditions on Solvent Thermal and Oxidative Degradation in Post-Combustion CO2 Capture. *Computers & Chemical Engineering* **2015**, *83*, 121–130. https://doi.org/10.1016/j.compchemeng.2015.05.003.
(21) Dhingra, S.; Khakharia, P.; et al. Understanding and Modelling the Effect of Dissolved Metals on Solvent Degradation in Post Combustion CO2 Capture Based on Pilot Plant Experience. *Energies* **2017**, *10* (5), 629. https://doi.org/10.3390/en10050629.
(22) Veltman, K.; Singh, B.; et al. Human and Environmental Impact Assessment of Postcombustion CO2 Capture Focusing on Emissions from Amine-Based Scrubbing Solvents to Air. *Environmental Science and Technology* **2010**, *44* (4), 1496–1502. https://doi.org/10.1021/es902116r.
(23) Goff, G. S. Oxidative Degradation of Aqueous Monoethanolamine in CO2 Capture Processes: Iron and Copper Catalysis, Inhibition, and O2 Mass Transfer. Doctoral thesis, 2005.
(24) Léonard, G.; Voice, A.; et al. Influence of Dissolved Metals and Oxidative Degradation Inhibitors on the Oxidative and Thermal Degradation of Monoethanolamine in Postcombustion CO_2 Capture. *Ind. Eng. Chem. Res.* **2014**, *53* (47), 18121–18129. https://doi.org/10.1021/ie5036572.
(25) Chi, S. Oxidative Degradation of Monoethanolamine. Thesis, University of Texas Austin, 2000.
(26) Rooney, P. C.; Daniels, D. D. Oxygen Solubility in Various Alkanolamine/Water Mixtures. *Petroleum Technology Quarterly* **1998**, 97–101.
(27) Léonard, G. Optimal Design of a CO2 Capture Unit with Assessment of Solvent Degradation. Doctoral thesis, Université de Liège, 2013.
(28) Léonard, G.; Toye, D.; et al. Assessment of Solvent Degradation within a Global Process Model of Post-Combustion CO2 Capture. In *Computer Aided Chemical Engineering*; Elsevier, 2014; Vol. 33, pp 13–18. https://doi.org/10.1016/B978-0-444-63456-6.50003-X.

(29) Wang, M. H.; Ledoux, A.; et al. Oxygen Solubility Measurements in a MEA/H2O/CO2 Mixture. *J. Chem. Eng. Data* **2013**, *58* (5), 1117–1121. https://doi.org/10.1021/je301077y.
(30) Pinto, D. D. D.; Brodtkorb, T. W.; et al. Modeling of Oxidative MEA Degradation. *Energy Procedia* **2014**, *63*, 940–950. https://doi.org/10.1016/j.egypro.2014.11.103.
(31) Kasikamphaiboon, P.; Chungsiriporn, J.; et al. Degradation Kinetics of Monoethanolamine during CO2 and H2S Absorption from Biogas. **2015**, 9.
(32) Buvik, V.; Bernhardsen, I. M.; et al. Measurement and Prediction of Oxygen Solubility in Post-Combustion CO2 Capture Solvents. *International Journal of Greenhouse Gas Control* **2021**, *104*, 103205. https://doi.org/10.1016/j.ijggc.2020.103205.
(33) Weiland, R. H.; Dingman, J. C.; et al. Density and Viscosity of Some Partially Carbonated Aqueous Alkanolamine Solutions and Their Blends. *J. Chem. Eng. Data* **1998**, *43* (3), 378–382. https://doi.org/10.1021/je9702044.
(34) Weisenberger, S.; Schumpe, A. Estimation of Gas Solubilities in Salt Solutions at Temperatures from 273 K to 363 K. *AIChE Journal* **1996**, *42* (1), 298–300. https://doi.org/10.1002/aic.690420130.
(35) Benson, B. B.; Krause, D.; et al. The Solubility and Isotopic Fractionation of Gases in Dilute Aqueous Solution. I. Oxygen. *J Solution Chem* **1979**, *8* (9), 655–690. https://doi.org/10.1007/BF01033696.
(36) Jakobsen, J. P.; Krane, J.; et al. Liquid-Phase Composition Determination in CO2−H2O−Alkanolamine Systems: An NMR Study. *Ind. Eng. Chem. Res.* **2005**, *44* (26), 9894–9903. https://doi.org/10.1021/ie048813+.
(37) Cussler, E. L.; Cussler, E. L. *Diffusion: Mass Transfer in Fluid Systems*; Cambridge University Press, 2009.
(38) Geankoplis, C. J.; Hersel, A. A.; et al. *Transport Processes and Separation Process Principles*; Prentice Hall, 2018.
(39) Aronu, U. E.; Ghondal, S.; et al. Equilibrium in the H2O-MEA-CO2 System: New Data and Modeling. In *Post Combustion Capture Conference (PCCC1)*.
(40) Bello, A.; Idem, R. O. Comprehensive Study of the Kinetics of the Oxidative Degradation of CO2 Loaded and Concentrated Aqueous Monoethanolamine (MEA) with and without Sodium Metavanadate during CO2 Absorption from Flue Gases. *Ind. Eng. Chem. Res.* **2006**, *45* (8), 2569–2579. https://doi.org/10.1021/ie050562x.
(41) Rooney, P. C.; Dupart, M. S.; et al. Oxygen's Role in Alkanolamine Degradation. *Hydrocarbon Processing* **1998**, *77*, 109–113.
(42) Strigle, R. F. *Packed Tower Design and Applications*; Gulf Publishing Co ,U.S., 1987.
(43) Tobiesen, F. A.; Svendsen, H. F.; et al. Experimental Validation of a Rigorous Absorber Model for CO2 Postcombustion Capture. *AIChE Journal* **2007**, *53* (4), 846–865. https://doi.org/10.1002/aic.11133.
(44) Tobiesen, F. A.; Juliussen, O.; et al. Experimental Validation of a Rigorous Desorber Model for CO2 Post-Combustion Capture. *Chemical Engineering Science* **2008**, *63* (10), 2641–2656. https://doi.org/10.1016/j.ces.2008.02.011.

(45) Towler, G.; Sinnott, R. Chapter 19 - Heat-Transfer Equipment. In *Chemical Engineering Design (Second Edition)*; Towler, G., Sinnott, R., Eds.; Butterworth-Heinemann: Boston, 2013; pp 1047–1205. https://doi.org/10.1016/B978-0-08-096659-5.00019-5.

(46) *GPSA Engineering Data Book*, 12th ed.; Gas Processors Suppliers Association, 2004.

(47) Herraiz, L.; Fernández, E. S.; et al. Selective Exhaust Gas Recirculation in Combined Cycle Gas Turbine Power Plants with Post-Combustion CO2 Capture. *International Journal of Greenhouse Gas Control* **2018**, *71*, 303–321. https://doi.org/10.1016/j.ijggc.2018.01.017.

(48) Amrollahi, Z.; Ystad, P. A. M.; et al. Optimized Process Configurations of Post-Combustion CO2 Capture for Natural-Gas-Fired Power Plant – Power Plant Efficiency Analysis. *International Journal of Greenhouse Gas Control* **2012**, *8*, 1–11. https://doi.org/10.1016/j.ijggc.2012.01.005.

(49) Fagerlund, J.; Zevenhoven, R.; et al. Performance of an Amine-Based CO2 Capture Pilot Plant at the Fortum Oslo Varme Waste to Energy Plant in Oslo, Norway. *International Journal of Greenhouse Gas Control* **2021**, *106*, 103242. https://doi.org/10.1016/j.ijggc.2020.103242.

(50) Magnanelli, E.; Mosby, J.; et al. Scenarios for Carbon Capture Integration in a Waste-to-Energy Plant. *Energy* **2021**, *227*, 120407. https://doi.org/10.1016/j.energy.2021.120407.

(51) Knudsen, J. N.; Jensen, J. N.; et al. Experience with CO2 Capture from Coal Flue Gas in Pilot-Scale: Testing of Different Amine Solvents. *Energy Procedia* **2009**, *1* (1), 783–790. https://doi.org/10.1016/j.egypro.2009.01.104.

(52) Moser, P.; Wiechers, G.; et al. Results of the 18-Month Test with MEA at the Post-Combustion Capture Pilot Plant at Niederaussem – New Impetus to Solvent Management, Emissions and Dynamic Behaviour. *International Journal of Greenhouse Gas Control* **2020**, *95*, 102945. https://doi.org/10.1016/j.ijggc.2019.102945.

(53) Knudsen, J. N.; Bade, O. M.; et al. Pilot Plant Demonstration of CO2 Capture from Cement Plant with Advanced Amine Technology. *Energy Procedia* **2014**, *63*, 6464–6475. https://doi.org/10.1016/j.egypro.2014.11.682.

(54) Freguia, S.; Rochelle, G. T. Modeling of CO2 Capture by Aqueous Monoethanolamine. *AIChE Journal* **2003**, *49* (7), 1676–1686. https://doi.org/10.1002/aic.690490708.

(55) Zhang, Y.; Chen, H.; et al. Rate-Based Process Modeling Study of CO2 Capture with Aqueous Monoethanolamine Solution. *Ind. Eng. Chem. Res.* **2009**, *48* (20), 9233–9246. https://doi.org/10.1021/ie900068k.

(56) Rao, A. B.; Rubin, E. S. A Technical, Economic, and Environmental Assessment of Amine-Based CO2 Capture Technology for Power Plant Greenhouse Gas Control. *Environmental Science and Technology* **2002**, *36* (20), 4467–4475. https://doi.org/10.1021/es0158861.

(57) Abu-Zahra, M. R. M.; Schneiders, L. H. J.; et al. CO2 Capture from Power Plants: Part I. A Parametric Study of the Technical Performance Based on

Monoethanolamine. *International Journal of Greenhouse Gas Control* **2007**, *1* (1), 37–46. https://doi.org/10.1016/S1750-5836(06)00007-7.
(58) Billet, R.; Schultes, M. Prediction of Mass Transfer Columns with Dumped and Arranged Packings: Updated Summary of the Calculation Method of Billet and Schultes. *Chemical Engineering Research and Design* **1999**, *77* (6), 498–504. https://doi.org/10.1205/026387699526520.
(59) Kvamsdal, H. M.; Rochelle, G. T. Effects of the Temperature Bulge in CO2 Absorption from Flue Gas by Aqueous Monoethanolamine. *Ind. Eng. Chem. Res.* **2008**, *47* (3), 867–875. https://doi.org/10.1021/ie061651s.
(60) Staab, G.; Fine, N.; et al. Modular Adaptive Packing for Integrally Cooled Absorbers. Rochester, NY November 28, 2022. https://doi.org/10.2139/ssrn.4288015.
(61) V. Figueiredo, R.; Srivastava, T.; et al. Impact of Dissolved Oxygen Removal on Solvent Degradation for Post-Combustion CO2 Capture. *International Journal of Greenhouse Gas Control* **2021**, *112*, 103493. https://doi.org/10.1016/j.ijggc.2021.103493.
(62) Nielsen, P. Oxidation of Piperazine in Post-Combustion Carbon Capture. Doctoral thesis, The University of Texas, 2018. https://repositories.lib.utexas.edu/bitstream/handle/2152/68015/NIELSEN-DISSERTATION-2018.pdf.
(63) Wu, Y. Mitigation Methods for Piperazine Oxidation in Post-Combustion Carbon Capture. Doctoral thesis, 2022. https://doi.org/10.26153/tsw/43500.
(64) Warudkar, S. S.; Cox, K. R.; et al. Influence of Stripper Operating Parameters on the Performance of Amine Absorption Systems for Post-Combustion Carbon Capture: Part I. High Pressure Strippers. *International Journal of Greenhouse Gas Control* **2013**, *16*, 342–350. https://doi.org/10.1016/j.ijggc.2013.01.050.
(65) Puxty, G.; Maeder, M. 2 - The Fundamentals of Post-Combustion Capture. In *Absorption-Based Post-combustion Capture of Carbon Dioxide*; Feron, P. H. M., Ed.; Woodhead Publishing, 2016; pp 13–33. https://doi.org/10.1016/B978-0-08-100514-9.00002-0.
(66) Voice, A. K.; Closmann, F.; et al. Oxidative Degradation of Amines With High-Temperature Cycling. *Energy Procedia* **2013**, *37*, 2118–2132. https://doi.org/10.1016/j.egypro.2013.06.091.
(67) Arnaut, L. Chapter 4 - Reaction Order and Rate Constants. In *Chemical Kinetics (Second Edition)*; Arnaut, L., Ed.; Elsevier, 2021; pp 93–138. https://doi.org/10.1016/B978-0-444-64039-0.00014-5.
(68) Sexton, A. J. Amine Oxidation in CO2 Capture Processes. Doctoral thesis, The University of Texas, 2008.
(69) Vevelstad, S. J.; Grimstvedt, A.; et al. Comparison of Different Solvents from the Solvent Degradation Rig with Real Samples. *Energy Procedia* **2017**, *114*, 2061–2077. https://doi.org/10.1016/j.egypro.2017.03.1341.
(70) Lepaumier, H.; da Silva, E. F.; et al. Comparison of MEA Degradation in Pilot-Scale with Lab-Scale Experiments. *Energy Procedia* **2011**, *4*, 1652–1659. https://doi.org/10.1016/j.egypro.2011.02.037.

(71) Knudsen, J. N.; Andersen, J.; et al. Evaluation of Process Upgrades and Novel Solvents for the Post Combustion CO2 Capture Process in Pilot-Scale. *Energy Procedia* **2011**, *4*, 1558–1565. https://doi.org/10.1016/j.egypro.2011.02.025.

Chapter 5: Article II: Additional Considerations

5.1 Validation of the Degradation Framework

The degradation framework is validated at two different scales by predicting degradation rates in a lab-scale cyclic degradation setup by SINTEF[1] and a capture plant pilot at the coal-fired power plant at Niederaussem[2]. Both processes expose the solvent to conditions at which both oxidative and thermal degradation of MEA is expected to occur. The solvent was analyzed in both campaigns and degradation rates were reported. The degradation model was able to make predictions that approximate reported numbers. Deviations are to be expected since limited information was available for the processes and several assumptions had to be made for the simulations. In addition, catalyzed degradation by dissolved metals is likely to play a role in the investigated processes.

5.1.1 Niederaussem Pilot Plant (RWE)

Based on the information available in the literature on the post-combustion capture plant at the coal-fired power plant at Niederaussem[2,3], the capture process has been simulated in Aspen Plus. The total column height is reported to be around 40 meters. Assuming between half and two-thirds of the column is packing and a water wash of 4 meters was used, around 20 meters of absorber packing is expected. The water wash has not been modeled as degradation is not expected to occur in this part of the plant. The process parameters used in this study are given in Table 5.1. Other process parameters, such as flue gas flow rate and composition, solvent flow rate, and process temperatures and pressures are given by Moser et al.[2]. Other residence times, such as those in pumps and pipes, are estimated similarly to the methods described in the article and are limited.

The specific degradation rate is predicted to be 140.12 g MEA/ton CO_2 captured. Moser et al.[2] observed a specific degradation rate of approximately 210 g/ton CO_2 after the first 55 days of operation. As the campaign progressed the degradation rate, concentration of degradation products, and the concentration of dissolved iron increased. Although the

Table 5.1: Process parameters for the simulation and degradation evaluation for the capture plant at Niederaussem. Parameter values are estimated unless a source is specified.

Parameter	Unit	Value
Column height	m	40
Packing height	m	20
Liquid distributors	-	4
Distributor residence time	s	15
Sump residence time[2]	s	438
Reboiler residence time	s	300
Heat exchanger residence time[2]	s	21 (per side)

concentration of dissolved iron was limited at the start of the campaign (< 3 mg/kg), catalyzed degradation is still expected to occur based on the work by Goff[4]. This would explain the under-prediction.

In the process, around 68% of the degradation is predicted to occur in the absorber (59% in the packing and 9.6% in the sump). Due to the relatively long residence time in the sump, nearly all of the dissolved O_2 is consumed before the rich solvent enters the heat exchanger and therefore degradation in this part is limited. Thermal degradation in the stripper accounts for 29% of the total degradation.

5.1.2 Solvent Degradation Rig at SINTEF

The Solvent Degradation Rig (SDR) is a laboratory test rig for studying solvent degradation at true operating conditions. The solvent is cycled between an absorber and stripper and is operated using a synthetic flue gas containing 12 vol-% O_2, 3.0 vol-% CO_2 and low ppmv levels of NO_x.[5] Vevelstad et al.[1] studied degradation of a 30 wt-% MEA solvent in the SDR over a period of 5 weeks. The rig was operated at standard conditions for 3 weeks, then 1 week with an increased temperature, and finally 1 week at standard temperatures but with a higher concentration of NO_x to study the formation of nitrosamines. The degradation of MEA as a result of the NO_x has not been included in the degradation model and is not accounted for.

Most of the rich solvent in the absorber sump is recycled (±70%), while the remaining solvent is temporarily stored in a buffer vessel before passing through the heat exchanger. A buffer vessel is also installed downstream of the stripper sump but there is no solvent recycle in the stripper. The stripped CO_2 is re-absorbed using the cooled lean solvent. The process parameters used in this study are given in Table 5.2. Other process

Table 5.2: Process parameters for the simulation and degradation evaluation of the Solvent Degradation Rig campaign. Parameter values are estimated unless a source is specified.

Parameter	**Unit**	**Value**
Absorber temperature[1]	°C	50
Packing height	m	0.20
Packing diameter	m	0.05
Packing solvent holdup	m^3/m^3	0.05
Absorber sump residence time	s	130
Stripper sump residence time	s	465
Buffer vessels residence time	s	620
Heat exchanger residence time	s	280 (per side)
Reboiler temperature[1]	°C	120/140
Total solvent volume[1]	L	5.0

parameters are given by Vevelstad et al.[1] The degradation model predicts an MEA degradation rate of 2.1 g/L/week for the overall campaign, whereas the observed degradation rate was 2.5 g/L/week. The uncertainty of the experimental results was estimated by the authors to be around 40% and the prediction appears to be accurate.

The rig is constructed mostly out of SS316 and although corrosion is limited, dissolved metals, such as iron, may still be present. The effect of the resulting catalyzed degradation is predicted to be limited, due to the small relative contribution of degradation in the absorber packing. The packing height is less than 1 m and the temperature is relatively mild, so degradation in the absorber is predicted to account for only 2% of the total degradation. An increase in the rate of consumption of dissolved O_2 in the sump and buffer vessel is not likely to have an impact on the total degradation, since all O_2 is already consumed without iron present, as is shown in Figure 5.1. It should be noted that this is under the assumption that the stoichiometry of the degradation reaction for O_2 is the same for the normal and catalyzed reactions.

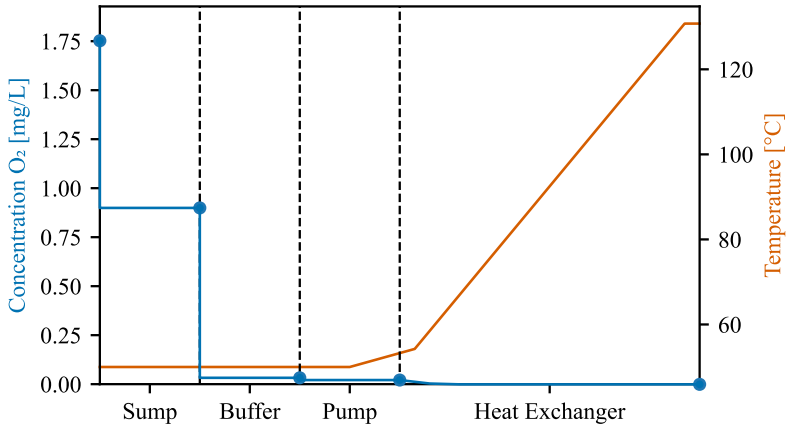

Figure 5.1: Predicted liquid temperature and concentration of dissolved O_2 in the rich solvent on the path from the absorber sump to the stripper inlet in the SDR.

At standard conditions, around 47% of the solvent degradation occurs in the absorber sump, and another 10% in the buffer vessel after the absorber sump. Figure 5.1 shows that the decrease in the concentration of O_2 in the buffer vessel is similar to the decrease in the sump. However, since the setup has a significant recycle of solvent from the absorber sump back to the top of the packing (78%), the solvent flow rate in the buffer vessel is smaller than the flow rate in the sump. As a result, less degradation is taking place in the buffer vessel. Thermal degradation in the stripper sump and buffer vessel is responsible for the remainder of the total degradation, with around 18.5% at standard conditions, and around 40% when operating with an increased stripper temperature.

5.2 Impact of Solvent Flow Rate

There are three main design variables for an absorption column: column height, liquid flow rate, and the stripper reboiler duty (influencing the lean CO_2 loading). Given a fixed capture efficiency (90% in this case) and a fixed height of the absorber packing (12 m), there is an infinite number of combinations of solvent flow rate and reboiler duties that satisfy these criteria. A selection of these are shown in Figure 5.2, where the specific reboiler duty is plotted as a function of the liquid-to-gas ratio, which is proportional to the solvent flow rate since the gas flow rate is kept constant. The corresponding lean and rich CO_2 loadings are given for the process designs in Figure 5.3.

The optimal specific energy duty balances the trade-off between higher energy duties needed to achieve a lower lean loading at low liquid flow rates and increased solvent circulation and heating at high liquid to gas ratios. As the solvent flow rate increases, so

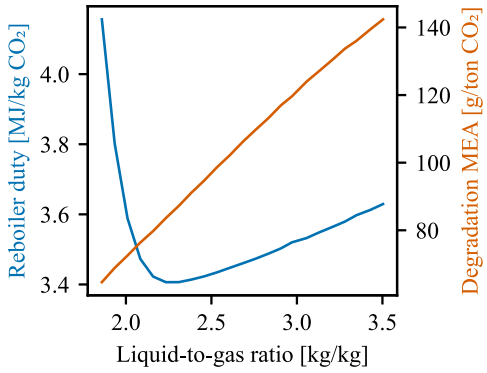

Figure 5.2: Specific reboiler duty and predicted overall degradation rate of MEA as a function of the liquid-to-gas ratio of the capture process

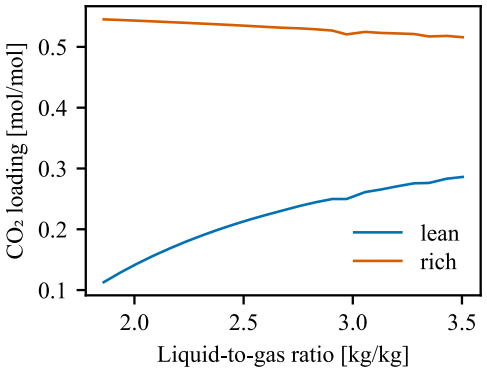

Figure 5.3: CO_2 loadings of the rich and lean solvent stream as a function of the liquid-to-gas ratio.

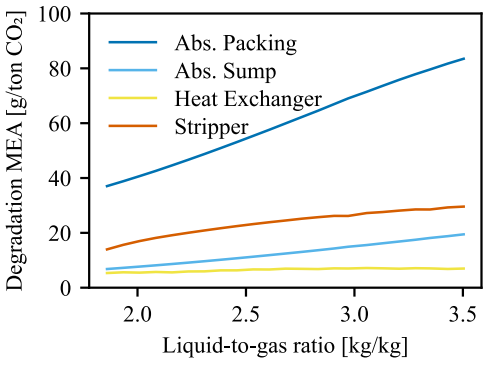

Figure 5.4: Degradation in the various parts of the capture process as a function of the liquid-to-gas ratio.

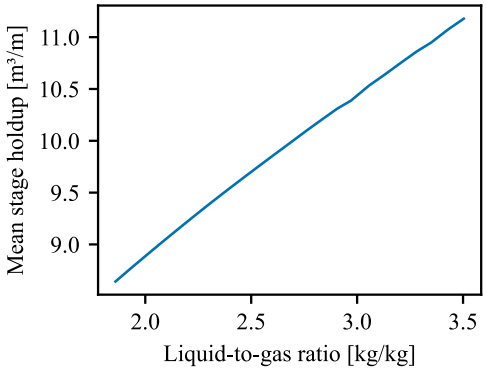

Figure 5.5: Average liquid holdup of the stages in the absorber packing per meter of packing.

does the degradation. The degradation rate is almost linearly proportional to the liquid to gas ratio. Figure 5.4 shows the effects of degradation in different parts of the process. Several factors affect the degradation rates in the absorber packing. One factor is the liquid holdup in the packing, which increases with the liquid flow rate at the same residence time, as shown in Figure 5.5. The liquid holdup is directly proportional to the degradation rate. Another factor is the CO_2 loading of the solvent because the O_2 solubility decreases when the solvent is loaded with CO_2. The low CO_2 loadings in the top of the absorber for the low liquid flow rate case increase the O_2 solubility. However, as Figure 5.6 shows, the CO_2 loading rises quickly as the solvent flows through the packing and soon exceeds the loading at high liquid to gas ratios. Nevertheless, the O_2 solubility remains higher in the low liquid to gas case, as shown in Figure 5.7. This is caused by the difference in temperature profiles, shown in Figure 5.8.

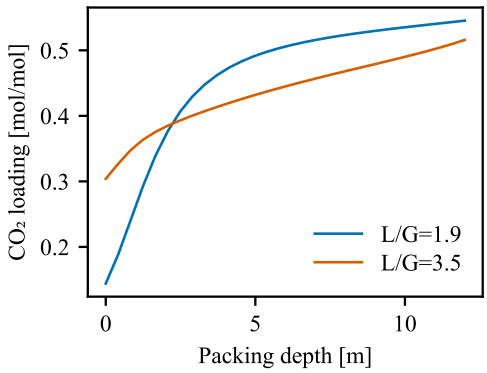

Figure 5.6: CO_2 loading as a function of the absorber packing for low and high liquid-to-gas ratios.

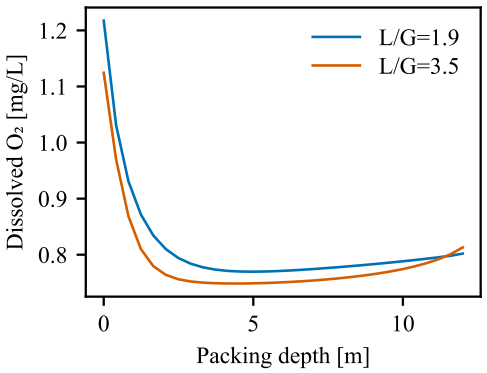

Figure 5.7: Concentration of dissolved O_2 as a function of the absorber packing for low and high liquid-to-gas ratios.

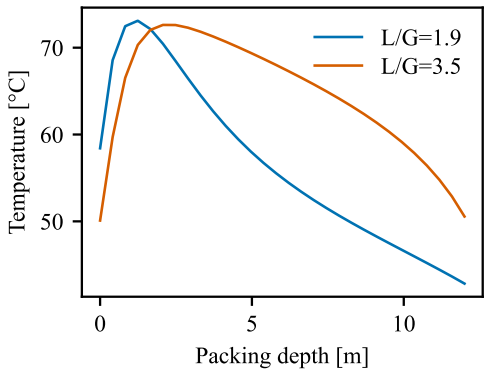

Figure 5.8: Liquid temperature as a function of the absorber packing for low and high liquid-to-gas ratios.

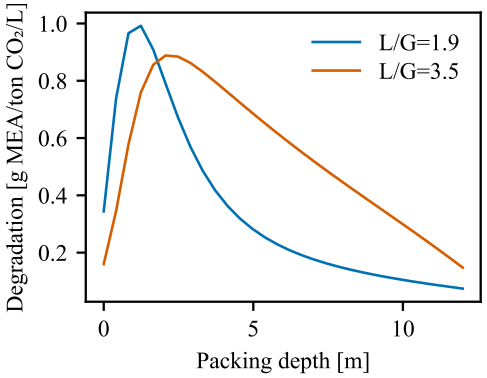

Figure 5.9: Local degradation rate as a function of the absorber packing for low and high liquid-to-gas ratios.

The liquid flow rates and CO_2 loadings, among others, determine what these temperature profiles look like. A low CO_2 loading, for example, causes significant absorption in the top of the absorber, resulting in a significant temperature bulge at this point. At higher liquid-to-gas ratios, on the other hand, this effect is less pronounced and the temperature bulge is more gradual. One would expect lower temperatures for the case with a high liquid-to-gas ratio because for the same amount of absorbed CO_2, and therefore roughly the same amount of heat produced, more liquid is available to absorb the heat. However, the simulations showed that significantly more water vapor was formed at the temperature bulge in the case with a low liquid-to-gas ratio. The heat of evaporation of the additional water vapor corresponds with the difference in energy absorbed in the liquid between both cases.

The higher temperatures in the lower part of the absorber in case of a high liquid-to-gas ratio reduce the solubility of O_2 slightly but lead to an increase in degradation rate due to the effect of temperature on the kinetic rate constant. The degradation rates across the packing are shown in Figure 5.9. The observed mechanisms in the absorber packing are in line with the mechanisms discussed in the article. Another result of the higher temperatures in the bottom of the absorber packing for the high liquid-to-gas ratio case is the reduced availability of O_2 in the absorber sump. This causes the extent of indirect oxidative degradation per volume of solvent to be less. An increase in solvent holdup, however, negates most of these effects. The higher temperatures lead to an increased degradation rate in the sump and, consequently, decreased degradation in the heat exchanger as a result of the limited availability of O_2. Degradation in the stripper sump and reboiler is linearly proportional to the solvent holdup volume. However, since the CO_2 loading of the lean solvent is higher for the high liquid-to-gas case, lower temperatures are required in the sump and reboiler. The observed increase in degradation in Figure 5.4 is therefore limited.

5.3 Formation of Thermal Degradation Products

The thermal degradation model for MEA that is used in the framework can also predict the concentration of degradation products, such as HEEDA or HEIA. Therefore the predicted concentrations of degradation products in the simulated post-combustion capture process for the coal-fired power plant case are given in Figure 5.10 and Figure 5.11. The concentration of HEEDA in the plant is higher than concentrations typically found in actual processes, for example in the results by Moser et al.[2] in the capture process from a coal-fired power plant. The authors observed a rapid increase in the concentration of HEEDA at the start of the campaign, but the concentration appears to stabilize around 350 mg/L. The concentration of HEIA was found to increase up to around 470 mg/L after around 140 days of operation, after which it also stabilized. Again, this is significantly lower than predicted by the degradation model. As discussed in more detail in section 2.4.6, the interaction between thermal and oxidative degradation

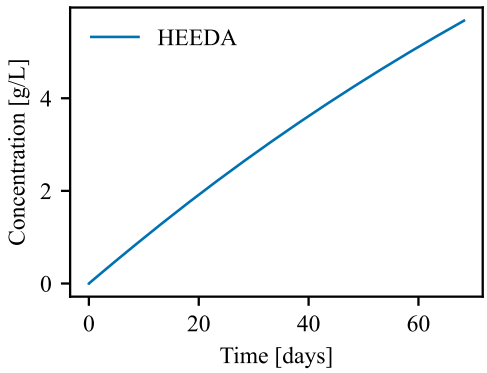

Figure 5.10: Concentration of HEEDA in the coal-fired power plant capture process as a function of time.

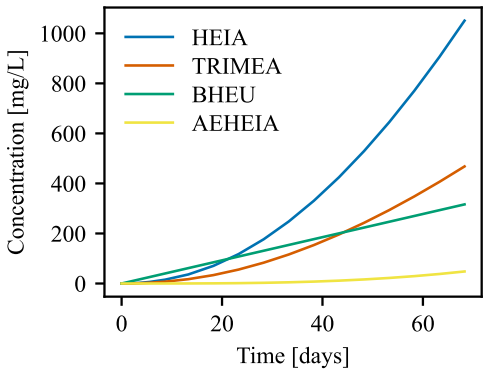

Figure 5.11: Concentration of other thermal degradation products in the coal-fired power plant capture process as a function of time.

mechanisms and the possible reaction of HEEDA with oxidative degradation products might explain the observed differences.

5.4 Combined Intercooling Effects: Temperature and Efficiency

The intercooling case studies discussed in section 4.3.6.1 did not consider the effect the intercooling has on the capture efficiency of the absorber. A reduction in temperature will also increase the solubility of CO_2 and the efficiency of the absorber. This would

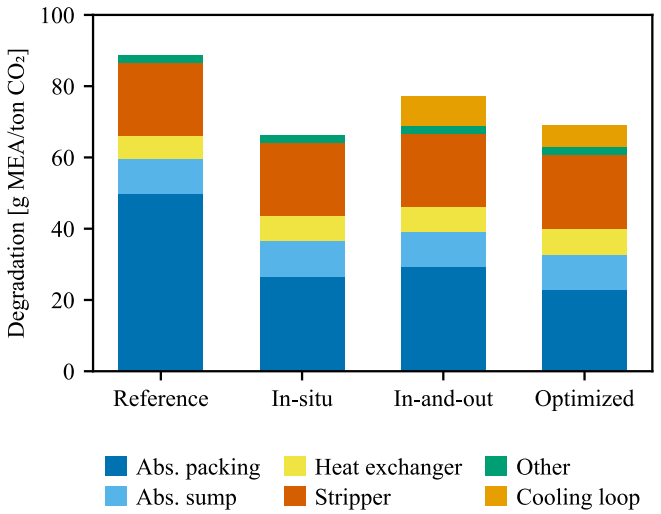

Figure 5.12: Predicted degradation in the coal case capture process (reference), the in-situ intercooled case, the in-and-out intercooled case, and the case with optimized in-and-out intercooling for the absorber efficiency (optimized).

allow for operation with smaller solvent flow rates or a reduced packing height. The intercooling was performed at the peak of the temperature bulge to result in the largest reduction in degradation. However, to increase the capture efficiency of the absorber, intercooling is typically applied at the CO_2 loading pinch, which is often located at the bottom of the column. Therefore, the single intercooling stage in the case study in section 4.4.3.1 at the top of the absorber column had a limited effect on the capture efficiency of the absorber. This can also be seen by looking at the temperature and CO_2 loading profiles throughout the absorber in Figure 4.27 and Figure 4.29.

In this section, another case study is considered, where a single intercooling stage is used with the purpose of increasing the efficiency of the absorber, thereby reducing the packing height. The solvent flow rate and overall capture efficiency of the process were kept constant at the same values that were used in the coal-fired base case. An optimization was then performed to optimize the intercooling location and at the same time minimize the packing height. The degradation framework was then used to evaluate

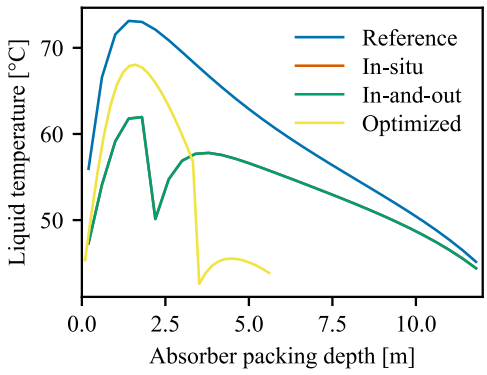

Figure 5.13: Temperature profiles in the absorber packing for the intercooling cases.

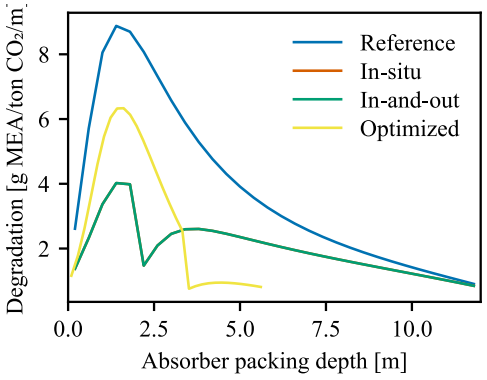

Figure 5.14: Degradation rates in the absorber packing for the intercooling cases.

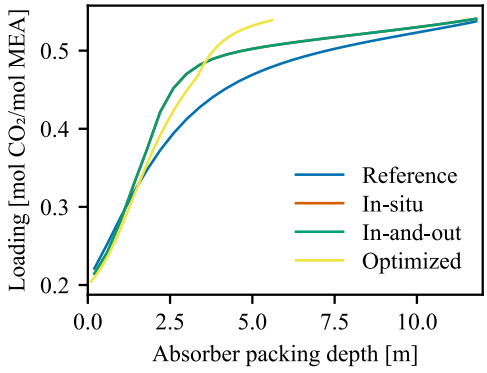

Figure 5.15: CO_2 loading profiles in the absorber packing for the intercooling cases.

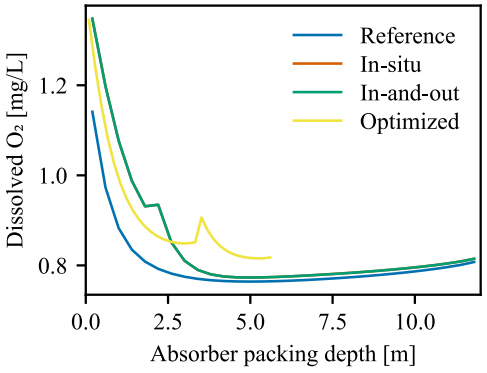

Figure 5.16: Dissolved O_2 concentration profiles in the absorber packing for the intercooling cases.

degradation in this process. In-and-out intercooling was also used in this case, as this is the most realistic implementation of the intercooling.

An overview of the predicted degradation rate in the process, compared to the reference case and the intercooling cases discussed in section 4.4.3.1, is given in Figure 5.12. Various profiles in the absorber packing are given in Figure 5.13 through Figure 5.16. Note that the profiles for the in-situ and in-and-out cases overlap. The minimum packing height for the case with the optimized intercooling for absorber capture efficiency is 5.7 m, and the intercooling is located closer to the bottom of the column. The effect of the intercooling on the temperature and CO_2 loading is demonstrated by Figure 5.13 and Figure 5.15. Although the temperatures and degradation rates in the top of the absorber are higher than those for the other intercooling cases, overall slightly less degradation is observed. The main reason for this is the reduction in absorber packing height since the solvent exposure time is reduced.

5.5 Flue Gas Entrainment in the Sump

An assumption within the degradation framework is that once the solvent exits the absorber packing and enters the sump, it is no longer in contact with O_2 from the flue gas. From this point onward, degradation occurs indirectly through previously dissolved O_2. However, in reality, it is anticipated that the solvent in the absorber sump will still have some exposure to the flue gas, either through contact at the interface or due to the introduction of entrained bubbles resulting from the splashing of the solvent. To assess the impact of this kind of exposure on the degradation rate in the process, the degradation rates were predicted under a worst-case scenario, where the solvent in the sump is fully

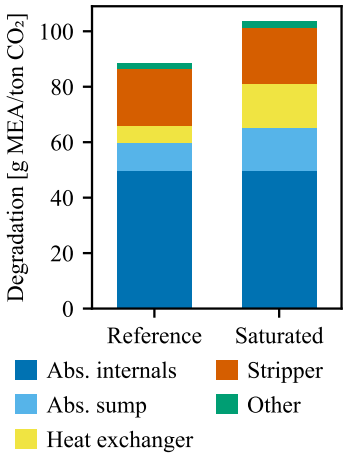

Figure 5.17: Predicted MEA degradation in the coal-fired case with and without O_2 saturation in the absorber sump.

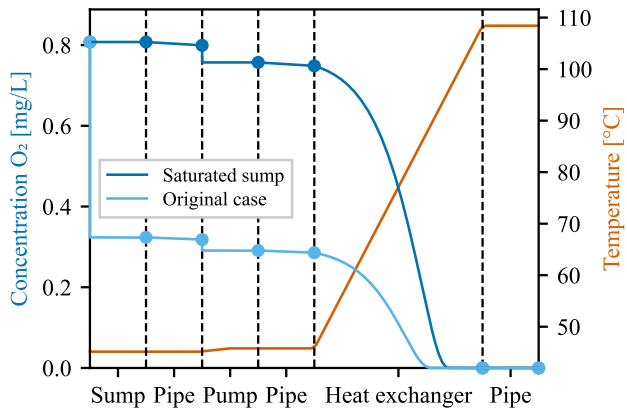

Figure 5.18: Liquid temperature and predicted concentrations of dissolved O_2 in the rich solvent from absorber sump to stripper inlet for the coal-fired case with and without O_2 saturation in the absorber sump.

saturated with O_2 throughout the entire residence time. The solvent leaving the sump is also fully saturated with O_2.

Figure 5.17 illustrates that the increase in total degradation is limited despite a significant relative increase in indirect oxidation in the sump and heat exchanger. Figure 5.18 shows the predicted concentration of dissolved O_2 for the two scenarios. In the original case study, most of the dissolved O_2 reacts in the absorber sump, which is modeled as a continuously stirred tank reactor with a residence time of 3.0 min. The remainder is consumed in the heat exchanger. In the case of a saturated sump, not only is the degradation rate higher in the sump due to the higher O_2 concentration, but also, more dissolved O_2 is carried downstream, leading to more degradation in the heat exchanger.

However, it is unlikely that the solvent will be entirely saturated with O_2 in the absorber sump because O_2 mass transfer limitations are also present in oxidative degradation experiments conducted in agitated bubble reactors (see also section 6.1 for a more detailed discussion on this topic). Nevertheless, it is important to consider this effect, especially when operating with long sump residence times or flue gasses rich in O_2, which result in high dissolved O_2 concentrations. Process modifications that mitigate prolonged contact between the solvent and the flue gas may be beneficial in such cases.

5.6 Dissolved O_2 Removal in the Natural Gas Case

Removal of dissolved O_2 in the capture plant for the coal-fired power plant flue gas had a limited effect on the overall degradation rate in the process. This was mainly due to the small contribution of indirect oxidative degradation since the concentration of dissolved O_2 was limited. A more significant effect is observed for dissolved O_2 removal in the natural gas case, where the concentration of O_2 is higher (11.8 vol% instead of 5.0 vol%). This is shown in Figure 5.19.

A reduction in the overall degradation of around 35% is predicted for the natural gas case if the removal occurs before the solvent enters the sump. However, in case removal occurs after the sump, the residence time in the sump determines the effectiveness of the mitigation strategy. In the case study a residence time of 180 seconds was selected, but in industrial pilots and full-scale capture plants higher residence times may occur[2,6]. Figure 5.20 shows the predicted concentration of dissolved O_2 in the rich solvent without dissolved O_2 removal and the results indicate that around 25% of the dissolved O_2 is already consumed in the sump.

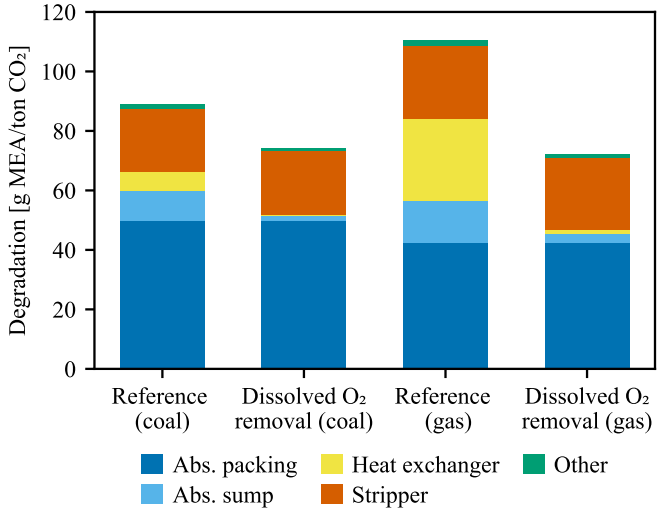

Figure 5.19: Predicted degradation in the capture process for the coal-fired and gas-fired power plant flue gas before and after 90% dissolved O_2 removal before the sump.

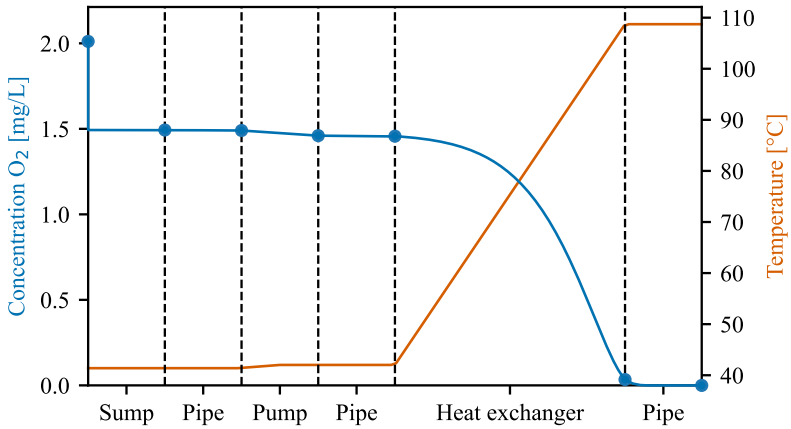

Figure 5.20: Solvent temperature and concentration of dissolved O_2 in the rich solvent from the absorber sump to the stripper inlet for the natural gas reference case study.

5.7 Degradation at High Capture Efficiency

In this section, work performed in collaboration with the University of Edinburgh and Sheffield (D. Mullen and Prof. M. Lucquiaud) is presented. D. Mullen and Prof. M. Lucquiaud are the main contributors and have been responsible for setting up the simulations, deciding the cases, and providing the motivation for this work, while the degradation evaluation related to these case studies has been part of this thesis. This section will give a brief overview of this collaborative effort and describe in more detail the work on evaluating degradation in the capture cases, and the discussions of these results. The work will be continued, and a joint publication is under preparation.

5.7.1 Overview of the Capture Cases

A selection of capture cases is considered based on the flue gas from a combined cycle gas turbine (CCGT), energy-from-waste (EfW), and steam-methane reforming (SMR). An overview of the case studies is given in Table 5.3 and more detailed information regarding the flue gas composition and the process parameters is given in Table 5.4. The capture processes closely resemble the process overview in Figure 4.2 and a 35 wt% aqueous MEA solvent is used here. The CO_2 is absorbed from the flue gas using two identical absorbers that operate in parallel. The reported degradation rates in the results are the combined rates of both absorbers. The rich solvent flows are combined and heated, after which the CO_2 is stripped in a single stripper.

Table 5.3: Overview of the studied capture cases for the CCGT, EfW, and SMR capture processes, where -95 and -99 indicate a capture efficiency of 95% and >99%. The application of in-situ absorber intercooling is indicated by I.

Case no.	**Lean loading [mol/mol]**	**Capture Efficiency [%]**	**Intercooler**	**SRD [MJ/kg CO_2]**
CCGT-99	0.1	99.2	-	3.67
CCGT-99I	0.1	99.2	1	3.74
CCGT-95	0.2	95	-	4.04
CCGT-95I	0.2	95	1	4.09
EfW-99I	0.1	99.7	1	3.63
EfW-95	0.2	95	-	3.65
EfW-95I	0.2	95	1	3.67
SMR-99I	0.1	99.8	2	3.64
SMR-95	0.2	95	-	3.61
SMR-95I	0.2	95	2	3.85

Table 5.4: Process parameters for the investigated capture cases.

Process parameters	**Capture cases**									
	CCGT-99	**CCGT-99I**	**CCGT-95**	**CCGT-95I**	**EfW-99I**	**EfW-95**	**EfW-95I**	**SMR-99I**	**SMR-95**	**SMR-95I**
Absorber packing height [m]	20	20	20	20	20	20	20	20	20	20
Absorber residence time [s]	358	352	259	262	200	190	189	180	153	169
Flue gas CO_2 content [v%]	4.7	4.7	4.7	4.7	11.1	11.1	11.1	19.5	19.5	19.5
Flue gas O_2 content [v%]	10.7	10.7	10.7	10.7	6.7	6.7	6.7	1.2	1.2	1.2
Liquid-to-gas ratio [kg/kg]	0.5	0.53	0.72	0.75	1.21	1.5	1.54	2.15	2.62	2.89
Abs. sump residence time [s]	351	351	265	257	160	133	130	93	79	72
Abs. sump temperature [°C]	45.4	45.3	45.4	45.4	45.9	46.1	46	40.9	51.2	36.6
Stripper packing height [m]	20	20	20	20	20	20	20	20	20	20
Stripper pressure [kPa]	275	275	155	155	275	155	155	275	155	155
Stripper inlet temperature [°C]	127.6	127.3	108.2	108.1	127.3	107.2	108.1	127.2	108.2	108
Stripper residence time [s]	88	87	96	93	85	96	94	86	97	95
Str. sump residence time [s]	266	252	193	187	115	96	94	67	57	52
Reboiler residence time [s]	112	107	87	87	109	90	89	109	89	87
Reboiler temperature [°C]	135.6	135.6	116.1	116	135.2	116.2	116	135.1	116.1	115.9
Total solvent inventory [m^3]	1501	1509	1576	1600	2250	2338	2352	3380	3256	3795
Lean solvent flow rate [m^3/s]	0.66	0.7	0.91	0.94	1.53	1.82	1.87	2.63	3.07	3.39

The capture processes are simulated using the MEA CCSI Aspen Plus (V10) steady state model, which was validated against NCCC data[7]. Both the absorber and stripper are modeled as rate based columns using Mellapak 250Y structured packing. The degradation models described in more detail previously in this chapter have been applied to predict the degradation of MEA. It is important to note that the degradation models are developed using experimental data only up to 30 wt% MEA. However, Høisæter[8] showed that the thermal degradation rates of aqueous solvents with higher MEA concentrations were comparable. With respect to oxidative degradation, the concentration of MEA is a parameter in the rate equation and, unless significant changes in the mechanism occur at 35 wt% compared to 30 wt%, the prediction is expected to be reasonable. Assumptions made in the original modeling work, such as neglecting mass transfer limitations for O_2 in the absorber packing are also applied here.

The capture efficiency of the processes is changed from 95% to 99.8% and the impact on solvent degradation is evaluated. Higher capture rates are obtained through increased stripper pressures and temperatures, which result in a lower CO_2 loading of the lean solvent. In addition the effect of absorber intercooling on the degradation rate is also studied. Either one or two in-situ intercooling stages are placed evenly throughout the absorber. This intercooling is assumed to occur instantly, without requiring additional solvent residence time. The solvent level height in the sump is assumed to be constant, which causes the residence time in the sump to change with the volumetric flow rate.

5.7.2 Predicted Degradation Rates

The predicted degradation rates for the investigated cases are given in Figure 5.21. The degradation rates are normalized by the CO_2 capture rate, so the absolute degradation rates are highest for the SMR process, since the flue gas for this process contains 19.5 vol-% CO_2 and the volumetric flow rates of the flue gasses are similar for all cases. Solvent degradation in the stripper occurs primarily due to thermal degradation, while in all other parts of the process, degradation is primarily of an oxidative nature. Degradation

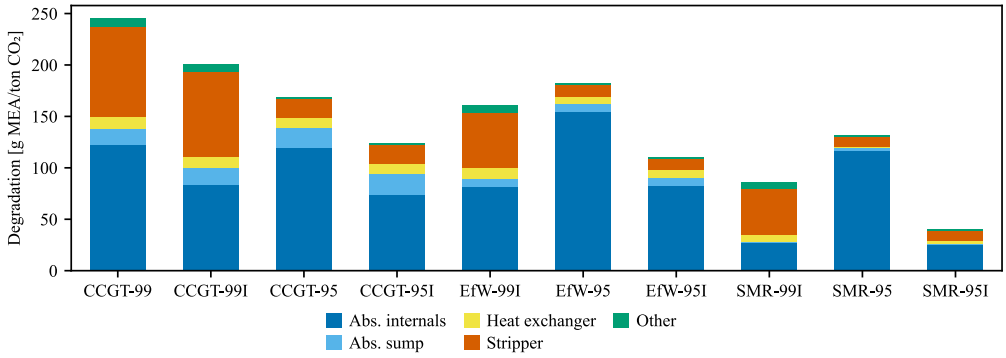

Figure 5.21: Predicted MEA degradation at different locations of the capture processes for the investigated case studies.

in the absorber internals is caused by direct oxidative degradation, where O_2 consumed by the degradation reaction is readily replenished from the gas phase. On the other hand, oxidative degradation in the absorber sump and heat exchanger is indirect and is caused by dissolved O_2 that has not yet reacted. As the rich solvent passes through the heat exchanger increasing the solvent temperature, the model predicts to exhaust all dissolved O_2 before the solvent enters the stripper.

The solvent degradation rates observed in pilot plant campaigns are higher than those predicted by the degradation models varying from 0.13 to 0.25 kg/ton CO_2. Solvent degradation rates in the range of 0.2 kg/ton CO_2 to 0.66 kg/ton CO_2 were reported by Moser et al.[2] in the 18-month capture campaign in the Niederaussem pilot plant using a lignite-fired power plant flue gas. Furthermore, a solvent loss of 1.6 kg/ton CO_2 was reported by Morken et al.[9] in a pilot campaign focused on carbon capture from a natural gas turbine flue gas[10]. One of the main reasons for the high degradation rates in these pilots compared with the model prediction is expected to be catalyzed solvent degradation by dissolved metals, such as iron. Due to a lack of experimental data, the degradation models do not consider the effect of dissolved metals. However, the effect may be significant, as Goff[4] showed that the evolution rate of NH_3 increased by a factor of three when dissolved iron was added in low concentrations (<5 mg/L) to a 30-wt% MEA solution at oxidizing conditions.

The deviation between the predicted rates by the degradation models and in pilot campaigns can also result from a difference in solvent residence times. The pilot plants use relatively long residence times that are useful for operation but may not necessarily realistically represent solvent holdup in the full-scale capture plants. As such, additional exposure of the solvent results in higher degradation rates. Finally, the degradation models do not take into account degradation by flue gas impurities, such as NO_x and SO_2. These impurities were present in the flue gasses used in the industrial pilots and may have resulted in additional degradation or deactivation of the solvent.

5.7.2.1 Differences Between Capture Cases

Although the process parameters, including flue gas composition and liquid-to-gas ratio, differ significantly between the three investigated capture cases, the predicted degradation rates in the absorber packing are similar. The profiles for the temperature, degradation rate, solvent holdup, and dissolved O_2 concentration as a function of packing depth are given in Figure 5.22 to Figure 5.27.

The CO_2 content in the CCGT flue gas is relatively low, resulting in lower temperatures in the absorber packing. The high concentration of O_2 and milder temperatures enhance the O_2 solubility of the solvent. The solvent holdup in the packing is primarily influenced by the solvent flow rate, but viscosity and temperature also play a role. Although the absolute degradation rates in the CCGT absorber are low, when normalized to the CO_2 capture rate, they are comparable to other cases. In contrast, the absorber conditions in

the SMR flue gas capture process differ significantly. The high CO_2 content in the flue gas results in higher liquid temperatures in the absorber. While elevated temperatures accelerate the degradation reaction rate, the limited availability of O_2 in the solvent due to the low O_2 content of the flue gas offsets this effect. Consequently, the degradation rates in SMR remain comparable to those in the EfW case. Surprisingly, the EfW case, despite not exhibiting the highest temperatures or the highest dissolved O_2 concentrations, is predicted to have the highest extent of degradation with respect to the CO_2 capture rate. This shows that oxidative degradation in the absorber packing is not solely dictated by a single process parameter but is influenced by multiple factors.

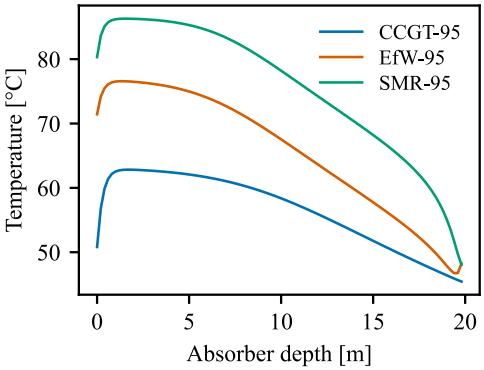

Figure 5.22: Temperature profiles for the cases with 95% capture and no intercooling as a function of the absorber packing depth.

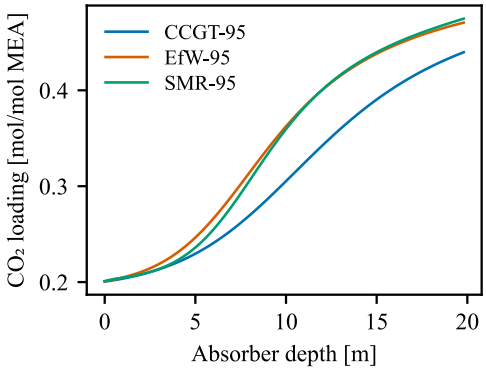

Figure 5.23: CO_2 loading profiles for the cases with 95% capture and no intercooling as a function of the absorber packing depth.

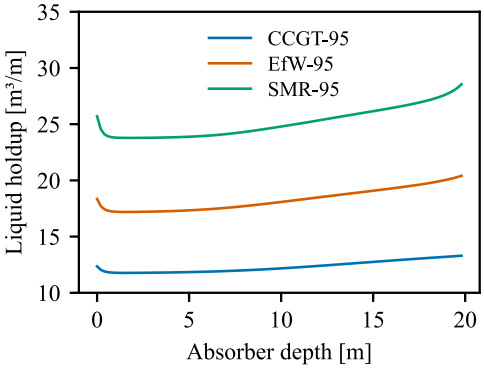

Figure 5.24: Solvent holdup profiles for the cases with 95% capture and no intercooling as a function of the absorber packing depth.

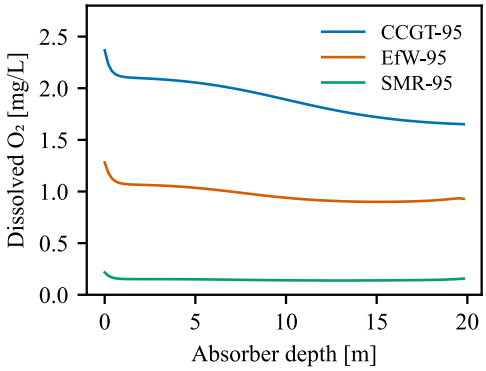

Figure 5.25: Dissolved O_2 concentration profiles for the cases with 95% capture and no intercooling as a function of the absorber packing depth.

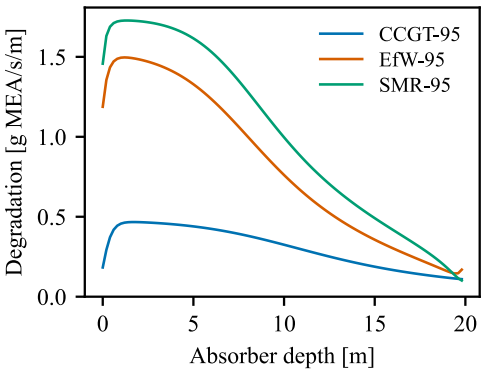

Figure 5.26: Absolute degradation rate profiles for the cases with 95% capture and no intercooling as a function of the absorber packing depth.

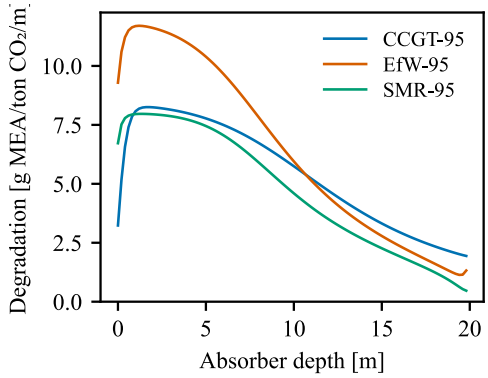

Figure 5.27: Degradation rate profiles for the cases with 95% capture and no intercooling as a function of the absorber packing depth.

5.7.2.2 Effects of High Capture Efficiency and Intercooling

The profiles in the absorber packing for all the studied CCGT cases are given in Figure 5.28 to Figure 5.31. When the process is operated to obtain a higher capture efficiency, in cases CCGT-99 and CCGT-99I, the CO_2 loading of the lean solvent is reduced from 0.2 to 0.1 mol CO_2/mol MEA. This change has a limited effect on the temperature profile in the absorber but leads to an increase in the O_2 solubility because the salinity of the solvent is reduced. Therefore, a slightly higher absolute degradation rate is predicted in the absorber when the capture efficiency is increased. However, when also considering the increased CO_2 capture rate, the relative degradation rates are comparable.

The oxidative degradation in the absorber packing is not limited by the availability of O_2 because it can be replenished from the flue gas. Therefore, as discussed in section 5.7.2.1, the solubility of O_2 and the temperature dictate the degradation rate. Proper temperature control in the absorber can thus be important to prevent excessive degradation. The introduction of a single intercooling stage has a significant influence on the temperatures and degradation rates in the upper part of the absorber, reducing the degradation rate at this position by nearly 50%. However, the temperature reduction also leads to higher concentrations of dissolved O_2 and thereby negates a small fraction of the benefits. For the CCGT cases with 95% capture, degradation in the absorber packing is reduced by 38% when in-situ intercooling is applied. Degradation in other parts of the process remains relatively constant and the reduction in overall degradation is thus 27%. Intercooling is also effective at reducing degradation in the SMR cases, where the temperatures in the absorber are relatively high. The use of two in-situ intercooling stages is predicted to reduce the overall degradation by 69%. Although more intercooling stages or isothermal operation can reduce the rate of oxidative degradation even further, the additional costs required for this implementation may outweigh the benefits.

To achieve lower lean loadings required in the high capture efficiency cases, the stripper is operated at a higher pressure and temperature. This temperature increase has a pronounced effect on the thermal degradation rates in the stripper sump and reboiler, as shown in Figure 5.21. When the contribution of thermal degradation to the overall degradation is limited, an increase resulting from higher operating temperatures may have a limited effect on the overall degradation rate. However, the contribution of thermal degradation can be more significant, for example when oxidative degradation is mitigated through intercooling, as is the case for SMR-99I. Temperature changes in the stripper will have a larger effect on the overall degradation rate, and the contribution of thermal degradation should not be disregarded.

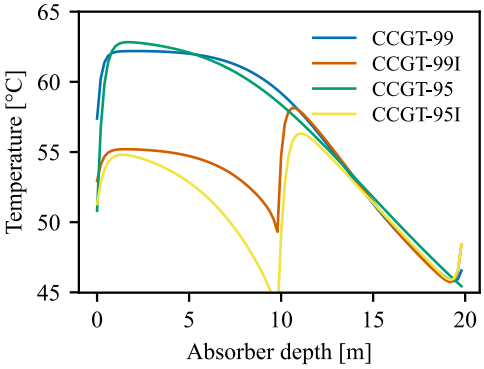

Figure 5.28: Temperature profiles for the CCGT cases as a function of the absorber packing depth.

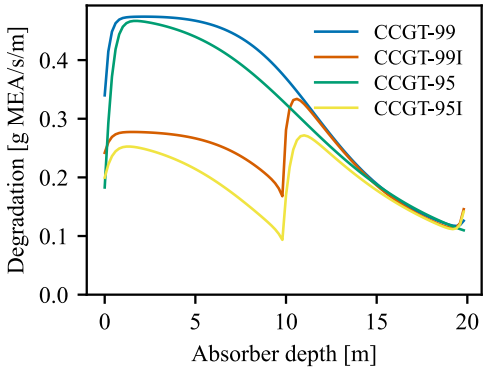

Figure 5.29: Degradation rate profiles for the CCGT cases as a function of the absorber packing depth.

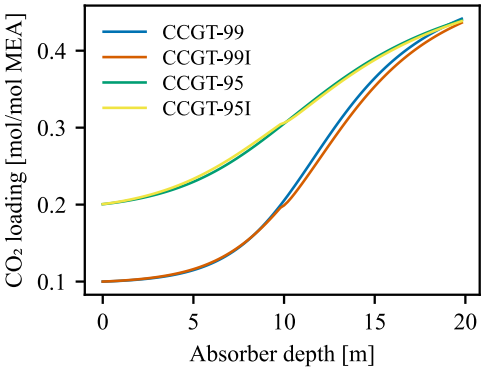

Figure 5.30: CO_2 loading profiles for the CCGT cases as a function of the absorber packing depth.

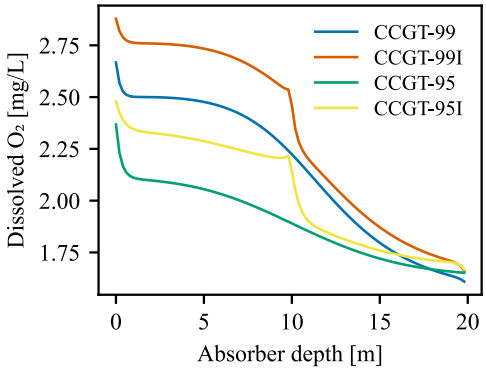

Figure 5.31: Dissolved O_2 concentration profiles for the CCGT cases as a function of the absorber packing depth.

5.8 References

(1) Vevelstad, S. J.; Grimstvedt, A.; et al. Comparison of Different Solvents from the Solvent Degradation Rig with Real Samples. *Energy Procedia* **2017**, *114*, 2061–2077. https://doi.org/10.1016/j.egypro.2017.03.1341.

(2) Moser, P.; Wiechers, G.; et al. Results of the 18-Month Test with MEA at the Post-Combustion Capture Pilot Plant at Niederaussem – New Impetus to Solvent Management, Emissions and Dynamic Behaviour. *International Journal of Greenhouse Gas Control* **2020**, *95*, 102945. https://doi.org/10.1016/j.ijggc.2019.102945.

(3) Moser, P.; Schmidt, S.; et al. Performance of MEA in a Long-Term Test at the Post-Combustion Capture Pilot Plant in Niederaussem. *International Journal of Greenhouse Gas Control* **2011**, *5* (4), 620–627. https://doi.org/10.1016/j.ijggc.2011.05.011.

(4) Goff, G. S. Oxidative Degradation of Aqueous Monoethanolamine in CO2 Capture Processes: Iron and Copper Catalysis, Inhibition, and O2 Mass Transfer. Doctoral thesis, 2005.

(5) Vevelstad, S. J.; Grimstvedt, A.; et al. Evaluation of Results from SDR Campaigns and Pilot Data. In *Trondheim Carbon Capture and Storage Conference (TCCS-11)*; Trondheim, 2021.

(6) Dhingra, S.; Khakharia, P.; et al. Understanding and Modelling the Effect of Dissolved Metals on Solvent Degradation in Post Combustion CO2 Capture Based on Pilot Plant Experience. *Energies* **2017**, *10* (5), 629. https://doi.org/10.3390/en10050629.

(7) Morgan, J.; Omell, B.; et al. *CCSI MEA Steady-State Model*. https://mea-ssm.readthedocs.io (accessed 2023-11-15).

(8) Høisæter, K. K.; Vevelstad, S. J.; et al. Impact of Solvent on the Thermal Stability of Amines. *Ind. Eng. Chem. Res.* **2022**, *61* (43), 16179–16192. https://doi.org/10.1021/acs.iecr.2c01934.

(9) Morken, A. K.; Pedersen, S.; et al. Degradation and Emission Results of Amine Plant Operations from MEA Testing at the CO2 Technology Centre Mongstad. *Energy Procedia* **2017**, *114*, 1245–1262. https://doi.org/10.1016/j.egypro.2017.03.1379.

(10) Flø, N. E.; Faramarzi, L.; et al. Results from MEA Degradation and Reclaiming Processes at the CO2 Technology Centre Mongstad. *Energy Procedia* **2017**, *114*, 1307–1324. https://doi.org/10.1016/j.egypro.2017.03.1899.

Chapter 6: Setup Development and Design

This chapter discusses the design of a new degradation setup to study solvent degradation in environments resembling those in the actual capture process. The results obtained from this setup should offer a more accurate representation of degradation mechanisms and reaction kinetics observed in reality, enabling the development of more precise degradation models and a more comprehensive evaluation of the degradation in the capture process.

First, the limitations and shortcomings of existing degradation setups are addressed. These include discrepancies in mass transfer characteristics compared to the actual process and the segregation of oxidative and thermal mechanisms, despite the observed interchange between these mechanisms in reality. Next, the setup's objectives are outlined and design options are explored, providing a comprehensive analysis and evaluation. Finally, this chapter discusses the results of several initial tests, highlighting shortcomings and proposing necessary improvements.

6.1 Limitations and Shortcomings of Traditional Reactors

Bench-scale solvent degradation experiments give valuable insight into solvent stability at various conditions in the capture process, which is required to prevent excessive degradation. Solvent degradation is often divided into two main reaction mechanisms: thermal and oxidative degradation (either autoxidation or oxidation in the presence of metals), and both degradation mechanisms are typically studied independently in different experimental setups. Thermal degradation is studied in closed batch cylinders, where the solvent is loaded and heated to stripper temperatures and above for days to weeks. More details on these experiments are given in chapter 2. Oxidative degradation, on the other hand, is studied in open batch reactors with a continuous gas flow or semi-open systems with a gas recycle, purge, and make-up. Dissolved O_2 is consumed in the degradation reaction and has to be replenished from the gas phase.

While oxidative degradation setups provide valuable insights into solvent stability and the impact of process variables such as temperature and oxygen concentration in flue gas, their utility in developing degradation models is limited. This is because the experiments do not replicate the mass transfer characteristics found in the structured packings commonly used in absorber columns. Goff[1] studied the mass transfer effects and reaction kinetics in a sparged reactor. The results indicated that the rate of NH_3 evolution primarily depends on O_2 absorption rates rather than degradation kinetics. Sexton[2] found that MEA degradation was controlled by the mass transfer rate of O_2 at catalyst conditions in an agitated reactor and recommends further characterization of the mass transfer conditions in the reactor. Léonard[3] also used an agitated bubble reactor and observed mass transfer limitations. At identical conditions, an increase in agitation rate resulted in significant increases in degradation rates.

A well-designed agitated bubble reactor has vigorous agitation to enhance liquid mixing and minimize mass transfer limitations and is characterized by small, uniformly sized bubbles that are evenly distributed to maximize the available interfacial area. While such a reactor can match or even outperform structured packings in mass transfer performance, its relatively high liquid holdup may still result in more pronounced mass transfer limitations. This is due to the increased reaction capacity and overall consumption rate of O_2. Therefore, structured packings are superior when considering mass transfer capacity per liquid volume.

6.1.1 Effect of Mass Transfer Resistance in Agitated Bubble Reactors

Mass transfer resistances can be accounted for by estimating the mass transfer coefficient (k_L) to determine the actual O_2 concentration within the solvent bulk. However, the uncertainty associated with estimating this coefficient can result in inaccuracies in the regressed kinetic parameters of the degradation model and the final predictions in the actual process. To illustrate the effect of this uncertainty, reaction kinetics for the oxidative degradation reactions have been regressed for several scenarios, as detailed below. The models were fitted using experimental data from Vevelstad et al.[4] for degradation without metals.

- Assuming no mass transfer resistance ($k'_L = \infty$)
- Mass transfer coefficient correlation ($k'_L = k_L$)
- Overestimation by the correlation ($k'_L = 0.7k_L$)

The first scenario assumes that there are no mass transfer limitations in the experiment and that the solvent is saturated with O_2 at all times. The mass transfer coefficient would approach infinity in this case, resulting in a negligible gradient between the interfacial

Table 6.1: Degradation reactions and reaction rate equations for the oxidative degradation model. The reference temperature for the oxidative rate coefficients is 338.15 K.

Reaction	**Reaction rate [mol/m^3/s]**	**Reaction rate coefficient**
$\mathrm{MEA} + 1.3\mathrm{O_2} \rightarrow \mathrm{Prod.}$	$R = k_r[\mathrm{MEA}][\mathrm{O_2}]^n$	$k_r = k_{\mathrm{ref}} \cdot \exp\left(\frac{-E_A}{R_{\mathrm{id}}}\left(\frac{1}{T} - \frac{1}{T_{\mathrm{ref}}}\right)\right)$

Table 6.2: Regressed kinetic parameters for the oxidative degradation reaction for the various mass transfer estimation scenarios.

Resistance scenario	k_{ref} [(m^3/mol)^n/s]	E_A [J/mol]	n [-]
No resistance ($k_L = \infty$)	$7.545 \cdot 10^{-7}$	$7.599 \cdot 10^4$	0.586
Base case ($k_L = k_L$)	$6.790 \cdot 10^{-7}$	$7.957 \cdot 10^4$	0.464
Overestimated ($k_L = 0.7k_L$)	$6.266 \cdot 10^{-7}$	$8.043 \cdot 10^4$	0.400

and bulk concentration of O_2. The second scenario considers the mass transfer effects and determines those using the correlation by Cussler et al.[5]. As this was the approach for the base cases, the results are identical to those presented in chapters 4 and 5. The final case study considers the uncertainty of the mass transfer coefficient correlation. Cussler et al.[5] mention that uncertainties of 30% are not uncommon when applying the correlation. This is due to the generalization of the correlation for a large set of fluids with different physical properties. Therefore, the third scenario assumes the actual mass transfer coefficient is 30% lower than the one predicted by the correlation, resulting in more prominent mass transfer limitation effects.

The reaction rate equations for oxidative degradation of MEA are given in Table 6.1, and the regressed kinetic parameters for each scenario are given in Table 6.2. Note that the concentrations for MEA and O_2 are specified in mol/m^3. As the estimated mass transfer resistance in the reactor increases, the calculated steady-state concentration of O_2 will decrease. For the model to match the observed degradation rates in the experiments, either a higher reaction order for O_2 (n) or a higher reaction rate coefficient (k_r) is required. The regression results in Table 6.2 agree with this hypothesis when looking at the reaction order, but appear to show an opposite trend for the reaction rate coefficient because the reaction rate coefficient at reference temperature (k_{ref}) decreases as the mass transfer coefficient decreases. However, the change in reaction rate coefficient is limited, as shown in Figure 6.1. The change in the oxygen concentration term shown in Figure 6.2, which is dictated by the reaction order n, is more significant. The reaction order for O_2 decreases as the estimated mass transfer coefficient decreases, which is as expected. The change in activation energy is limited.

The rate equations in Table 6.2 are also used to predict solvent degradation in the capture process for a coal-fired power plant flue gas, described in more detail in section 4.3.4. The overall degradation rates and distribution of degradation throughout the process for

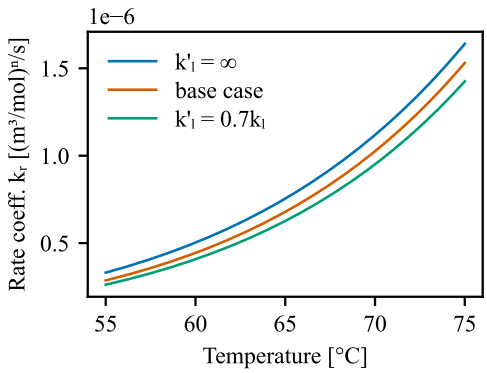

Figure 6.1: Reaction rate coefficient as a function of temperature for the mass transfer resistance scenarios.

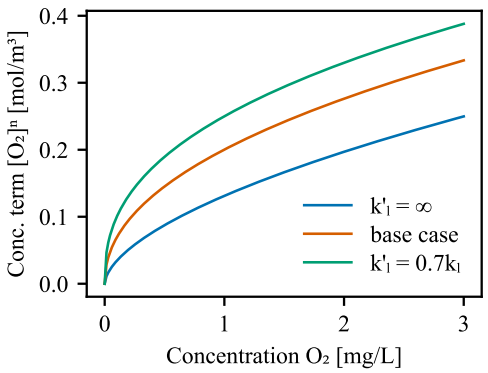

Figure 6.2: O_2 concentration term as a function of dissolved O_2 concentration for the mass transfer resistance scenarios

the scenarios are given in Figure 6.3, and the oxidative degradation rates in the absorber packing are shown in Figure 6.4. Note that the mass transfer resistance of O_2 is assumed to be negligible in the structured packing in the absorber. The kinetic model for thermal degradation is the same for each case, so the extent of thermal degradation, e.g. in the stripper and lean side of the heat exchanger, remains constant. In the case the mass transfer resistances are neglected when performing the regressions for the kinetic oxidative degradation model, oxidative degradation in the absorber packing is underpredicted (-28%). There is also less degradation in the absorber sump, however, the additional unreacted dissolved O_2 is now consumed in the heat exchanger.

Overestimation of the mass transfer resistance in the degradation experiments has a more limited effect on the predicted degradation rates, with an increase of only +18% in the absorber packing. It's important to note that the overestimation of 30% only considers the uncertainty in the mass transfer coefficient correlation but does not include the uncertainty in estimating experimental parameters, such as bubble size, stirring power, and diffusion coefficients. The examined scenarios demonstrate that mass transfer resistances likely impact degradation experiments conducted with agitated bubble reactors. Although correlations for mass transfer coefficients can be employed to address these effects, the associated uncertainties hinder the precise estimation of kinetic parameters, and may consequently diminish the accuracy of predictions in the process. A degradation setup in which mass transfer resistances are not present or can be accurately determined is required to improve the accuracy of the oxidative degradation models.

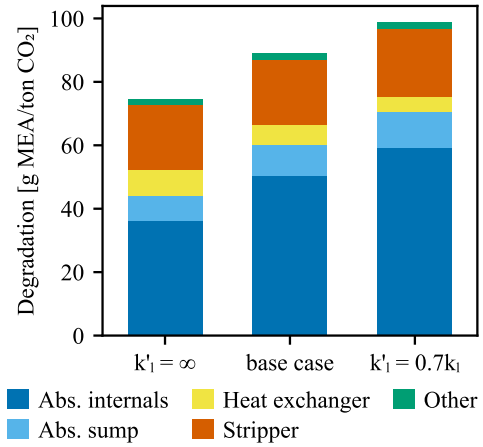

Figure 6.3: Impact of uncertainty in mass transfer resistance estimation in the degradation experiments on the predictions in a full-scale process.

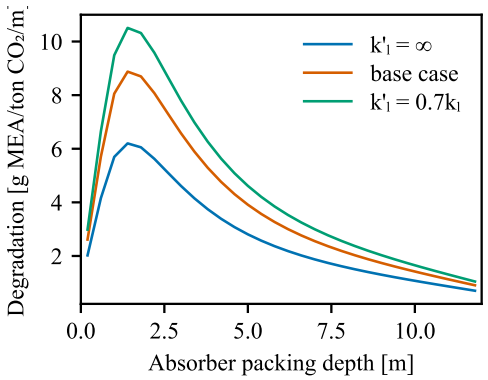

Figure 6.4: Impact of uncertainty in mass transfer resistance estimation in the degradation experiments on the predicted degradation rates in the absorber packing.

6.1.2 Effect of Iron on Mass Transfer Limitations

The experiments by Vevelstad et al.[4] that were used to develop the oxidative degradation model for MEA were conducted without dissolved metals. Some metals, such as copper and iron, are known to catalyze oxidative degradation and increase degradation rates significantly. Goff[1] showed that NH_3 evolution increased by a factor of three in their oxidative degradation experiments at dissolved iron concentrations around 10 mg/L. Here, the evolution of NH_3 is used as a surrogate for MEA degradation. Goff[1] observed that the rate of NH_3 evolution increased exponentially with the concentration of dissolved iron and flattened off when exceeding 10 mg/L. The authors argued that mass transfer limitations of O_2 caused this behavior.

To investigate the effect of accelerated degradation on the mass transfer limitations in experiments, liquid bulk concentrations of O_2 were predicted for steady-state oxidative degradation in the experiments by Vevelstad et al.[4]. The liquid mass transfer coefficients are estimated using the correlation by Cussler et al.[5] and more details on this estimation can be found in section 4.3.3.2. The mass transfer resistance of O_2 in the gas phase was considered to be negligible since gas absorption is commonly controlled by mass transfer in the liquid[5]. Therefore, the concentration in the liquid at the interface is equal to the saturation concentration.

The estimated liquid bulk concentrations in the agitated bubble reactor experiments are compared to the saturation concentrations in Figure 6.5. Additionally, a similar diagram is given in Figure 6.6, but in this diagram the regressed reaction rate coefficient is multiplied by a factor of 3 to simulate accelerated degradation due to the presence of iron. The results indicate a significant concentration gradient between the interface and

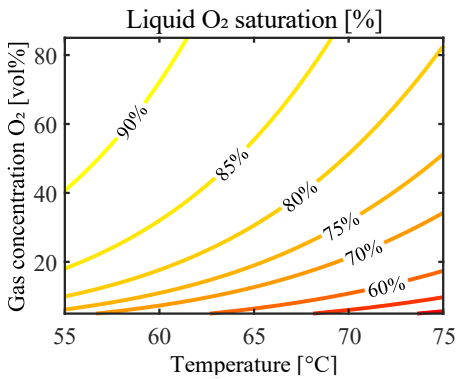

Figure 6.5: Estimated liquid-phase O_2 saturation (bulk over interfacial concentration) in the experiments by Vevelstad et al.[4] at various temperatures and gas-phase O_2 concentrations.

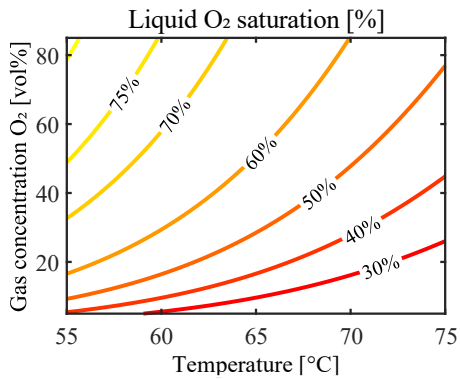

Figure 6.6: Estimated liquid-phase O_2 saturation (bulk over interfacial concentration) in the experiments by Vevelstad et al.[4] at various temperatures and gas-phase O_2 concentrations, assuming a 3x increase in reaction rates.

liquid bulk in the agitated bubble reactor experiments, especially at increased temperatures. Dissolved O_2, which is consumed by the degradation reaction, is not readily replenished by O_2 from the gas phase. As a result, the concentration drops, reducing the degradation rate and increasing the concentration gradient over the interface, increasing the mass transfer rate. A new equilibrium is then reached where the transfer and consumption rates are equal. Therefore, the concentration gradient indicates mass transfer limitations are at play, and reaction rates will be under-predicted if these limitations are not accounted for and O_2 saturation is assumed in the liquid bulk.

When reaction rates are increased due to the presence of dissolved metals, mass transfer limitation effects become even more pronounced. At a temperature of 75 °C and an O_2 concentration below 10 vol%, the liquid bulk concentration of O_2 is predicted to be well below 30% of the saturation concentration. Mass transfer effects can be taken into account by estimating mass transfer coefficients to approximate the actual liquid bulk concentrations. However, due to uncertainties in available correlations and correlation parameters in the experiment, such as bubble size and stirring power, it remains challenging to make accurate predictions. Therefore, the mass transfer effects will still be present, and the role of dissolved iron cannot be studied in isolation using agitated bubble reactors.

6.1.3 Interaction of Oxidative and Thermal Degradation Mechanisms

In the capture process, the solvent experiences both oxidative conditions at mild temperatures in the absorber and high temperatures in the stripper. Current lab-scale experiments typically focus on one of these degradation mechanisms, exposing the solvent to only one environment. Consequently, the interplay between oxidative and thermal degradation mechanisms remains unexplored. This interaction may manifest as the oxidation of thermal degradation products in the absorber. If these products readily oxidize, they could alter O_2 mass transfer dynamics or reduce the extent of purely oxidative degradation. Alternatively, oxidative degradation products might participate in thermal degradation reactions, resulting in the formation of new degradation products.

An example is the formation of 4-(2-hydroxyethyl)-2-piperazinone (4HEPO), which is one of the major degradation products of MEA typically observed in pilots[7]. Vevelstad

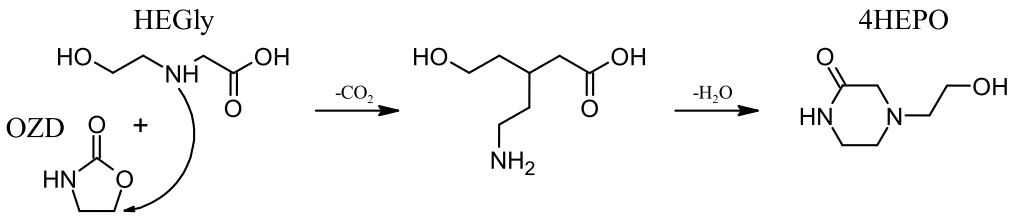

Figure 6.7: Mechanism for the formation of 4HEPO from HEGly and OZD as proposed by Gouedard[6].

et al.[4] reported relatively low concentrations of 4HEPO in the oxidative degradation experiments that cannot explain the observations in the pilots. Furthermore, concentrations of 4HEPO in thermally degraded MEA are negligible.[8] Significant 4HEPO formation occurs exclusively when the solvent is subjected to both oxidative conditions and elevated temperatures, as demonstrated by Vevelstad et al.[7] in the Solvent Degradation Rig (SDR). Gouedard[6] attributes this behavior to a reaction between oxidative and thermal degradation products and proposes two mechanisms: the reaction between HEGly (n-(2-hydroxyethyl)-glycine), obtained through the reaction of MEA with glyoxal or glyoxylic acid, and OZD (2-oxazolidinone) as shown in Figure 6.7, or the reaction between glyoxal and amino groups of HEEDA (n-(2-hydroxyethyl)-ethylenediamine).

Understanding the mechanisms arising from the interplay between oxidative and thermal degradation is important because they can change reaction kinetics and generate additional degradation products. These products may affect the solvent's properties, including viscosity, foaming, and corrosivity, which are relevant to the process. Moreover, if these products are volatile, it is essential to investigate their toxicity and emissions.

6.2 Objectives and Design Choices

This section gives an overview of the final design of the new degradation setup and provides a detailed insight into design challenges and considerations. To avoid the limitations of traditional lab-scale reactors, as discussed in section 6.1, the objectives are discussed and continuously considered during the design, construction, and operation of the new setup. The main objectives for the setup are given below:

- Achieve oxygen saturation of the solvent
- Study combined effects of oxidative and thermal degradation
- Control over concentrations of dissolved metals
- Regulating temperature, gas composition, and water losses

An overview of the setup design is given in Figure 6.8. The packed column, where the solvent and gas are brought into contact, is an important part of the setup. The solvent exits the packing and is collected in the sump, where the concentration of dissolved O_2 can be measured. The gas is fed between the sump and the packing and is collected at the top of the column, where a diaphragm pump is used to circulate the gas. A side stream is cooled down and the gas composition is analyzed. A small fraction of the analyzed gas is purged through the water lock, the rest is returned to the pump. Make-up gas is added to the gas flow to control the composition.

Both oxidative degradation and combined oxidative and thermal degradation can be studied using the setup. In case of only oxidative degradation, the solvent is pumped from the sump through a glass heating coil to the top of the column using a peristaltic

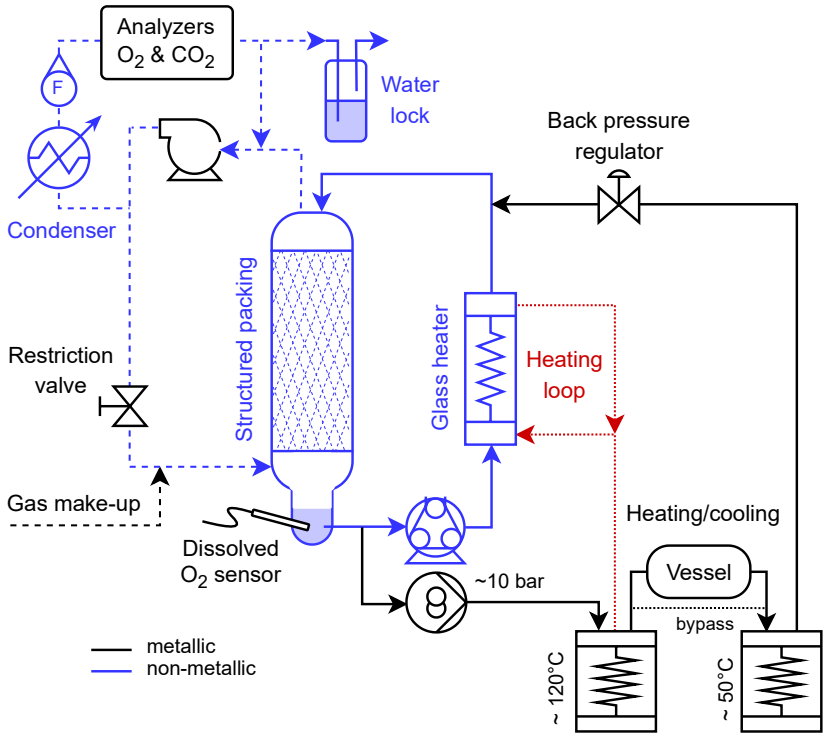

Figure 6.8: Schematic overview of the degradation setup.

tube pump. In this case, water from the heating bath is used to regulate the temperature of the solvent. When both oxidative and thermal degradation are studied, a gear pump is used to pump the solvent through the heating loop, composed of stainless steel (SS316) components. The solvent is pressurized before passing through the heating coil to prevent the stripping of CO_2. The solvent is then kept at this temperature in a buffer vessel before it is cooled down to the operating temperature of the column. A back pressure regulator is in place to control the pressure over the thermal loop.

6.3 Oxygen Saturation of the Solvent

6.3.1 Structured Packing

The column is equipped with a structured packing to facilitate the interfacial area between the gas and the liquid phase. The internal diameter of the column is 80 mm, and the packing height is 300 mm. Two packings are available for use: a Durapack borosilicate glass structured packing (3.3) and an SS316 Sulzer DX structured laboratory packing. The glass packing allows solvent degradation to be studied in the absence of dissolved metals, whereas the metallic packing features a high surface area of 900 m^2/m^3 for optimal mass transfer of O_2[9]. The solvent is distributed across the packing at the top

of the column using a perforated glass cup. In addition, both packings have fins at 2 to 3 locations on the side to collect liquid from the column wall and introduce it back into the packing.

As discussed in section 6.1, structured packings offer significantly more surface area per volume of liquid than bubble reactors and should reduce the effect of mass transfer limitations. Despite this reduction, it may still occur that mass transfer resistances play a role when the oxidative degradation rate is high, for example, as a result of high absorber temperatures or catalyzed degradation by metals. This is also shown in Figure 4.4 in section 4.3.5, where the estimated concentration bulk concentration of O_2 is slightly lower than the saturation concentration at the temperature bulge in the absorber.

However, there are several reasons why the remaining mass transfer effects are expected to have a significantly smaller impact on experimental uncertainties. Firstly, structured packings generally offer better-characterized mass transfer performance compared with custom agitated bubble reactors. Therefore, mass transfer coefficients and effective interfacial areas can be estimated with greater accuracy. Additionally, as the influence of mass transfer limitations is expected to be less pronounced, the associated uncertainties in parameter estimation are minimized. Furthermore, using structured packings in both the experiment and the actual process may lead to similar deviations in estimated mass transfer coefficients, potentially reducing some of the errors.

A spray tower type of design, which features small liquid solvent droplets that are dispersed in the gas phase, could be used as an alternative. The advantage of this type of contactor is the relatively high surface area to liquid volume ratio. This would address the mass transfer limitations and, at the expected degradation rates of MEA, ensure that the concentrations of O_2 throughout the droplet approach the saturation concentration. A drawback of having a relatively small liquid holdup volume is that only a small portion of the solvent inventory is in direct contact with the gas. The remaining solvent is located in the sump or is in transit as it moves from the sump toward the top of the column, and may not be saturated with O_2.

A venturi pump powered by gas with a spray nozzle at the outlet could be used to solve this problem. The inlet to the pump is then placed in the bottom of the reactor and sucks in a mixture of gas and collected solvent. This would not require significant liquid holdup in the sump, pump, and tubing due to the high speed of the air. However, it would be challenging to design and size such a venturi pump while ensuring the liquid is properly dispersed throughout the gas phase. Liquid sampling would be challenging and a single sample may make up a significant fraction of the total solvent volume. In addition, fine liquid droplets may be entrained in the gas phase and could enter the gas recycle or the water lock. For these reasons, a structured packing has been used in the current design.

6.3.2 Solvent Holdup Considerations

When the solvent enters the sump and is transported to the top of the column, either through the thermal loop or directly, intensive contact with the gas phase is no longer achieved. Since the O_2 that is consumed by the degradation reaction is not replenished, the concentration of O_2 in the solvent starts to decrease. Dissolved O_2 present in the solvent entering the thermal loop is likely to be completely consumed due to high temperatures, so a decrease in O_2 concentration is not an issue here. In the direct recycle through the glass heater, on the other hand, it is important to consider this decrease. In this case, the overall observed oxidative degradation rates may not correspond with those expected of a fully saturated solvent. Therefore, the setup has been designed to limit the holdup volume of solvent not exposed to O_2 and reduce the residence time in these sections.

One of the design decisions is to use a peristaltic tube pump to circulate the solvent in the oxidative loop. In contrast to many other types of pumps, this pump can operate when air is entrained in the solvent. As a result, the solvent holdup volume in the sump can be reduced, as occasional entrainment of bubbles is acceptable. The pump can to achieve rates of up to 2 L/min, so residence time in the tubing is limited. Additionally, since there is no direct contact between the pump and the solvent, corrosion and the dissolution of metals are no issue.

The solvent holdup in the oxidative parts of the setup has been determined for a typical experimental run with a solvent flow rate of 1.3 L/min, as shown in Table 6.3. A solvent holdup of 100 mL was selected. It is possible to run with lower solvent holdups, such as only 50 mL, but it is recommended to run with a little additional solvent as samples are taken and a small fraction of the water is lost via the purge. The approximate holdup of the Sulzer DX packing has been determined by measuring the static holdup and dynamic holdup at various flow rates using water. The 30 wt% MEA solvent will have a higher viscosity, and the solvent holdup in the packing is expected to increase.

Table 6.3: Determined required solvent holdup volumes and residence times for a typical experiment at a solvent recirculation rate of 1.3 L/min.

Equipment	**Holdup [L]**	**Residence time [s]**	**Contribution [%]**
Structured packing	0.195	9.0	48.1
Distributor	0.02	0.9	4.9
Sump	0.1	4.6	24.7
Glass heater	0.03	1.4	7.4
Tubing	0.06	2.8	14.8
Total	**0.405**	**18.7**	**100**

Approximately half of the solvent is expected to be in the structured packing, and around a fourth of the solvent is in the sump. The time the solvent spends outside the packing in the sump and tubing to be recycled is around 8.8 seconds. Despite this

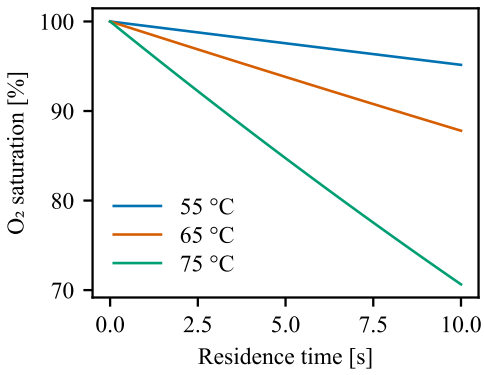

Figure 6.9: Estimated O_2 saturation of 30 wt% MEA as a function of residence time at different temperatures, with no replenishment of O_2.

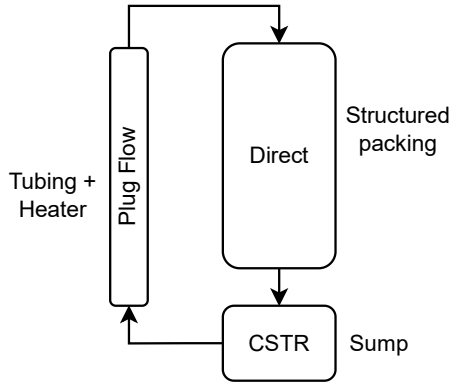

Figure 6.10: Proposed structure of reactor modeling approach for fitting reaction rate coefficients using the experimental data.

limited residence time, the concentration of O_2 is still expected to decrease when the solvent is transported from the sump to the top. This is shown in Figure 6.9, where the concentration of O_2 has been calculated as a function of residence time without replenishment of O_2 using the oxidative degradation model for 30 wt-% MEA developed in Article II (see section 4.4.1). The results show that up to around 30% of the dissolved O_2 can be expected to react at 75 °C.

The decrease in O_2 concentration is not necessarily a concern for developing a kinetic degradation model, as long as it is accounted for. Given a set of kinetic rate parameters, the extent of degradation can be evaluated in various parts of the setup separately, and the overall degradation rate can then be compared to experimental findings. An example is given in Figure 6.10. Degradation in the structured packing can be evaluated, assuming solvent is saturated with O_2, while the sump can be evaluated as a continuously stirred reactor (CSTR), and the tubing and heater can be considered a plug flow reactor (PFR).

6.3.3 Dissolved O_2 Measurements

An Endress Hauser optical oxygen sensor (COS81D) is installed to measure dissolved O_2 concentration in the solvent. The sensor features a permeable membrane layer containing marker molecules, which fluoresce when excited by light. The presence of O_2 molecules reduce the fluorescence intensity, which is measured using a light detector. At equilibrium, the partial pressure of O_2 in the membrane layer is equal to the pressure in the solvent.[10] The sensor is connected to a Liquiline Compact CM72 transmitter, which converts the measured signal into a 4-20mA signal. This signal is subsequently processed by a programmable logic controller.

There are several ways the dissolved O_2 measurements can be used. Firstly, the concentrations measured in the sump can be used to gain insights into the solubility data of O_2 in the solvent. The O_2 solubility model by Buvik et al.[11] that is currently used in the modeling work (see section 4.3.3.1) can be validated as the authors had challenges at increased temperatures due to rapid O_2 consumption. Although the residence time in the sump is low, the concentration may still decrease slightly due to degradation before it is measured at higher temperatures. This effect can be quantified by either changing the holdup volume in the sump and observing the difference or by calculating the expected decrease using a degradation model.

Measuring dissolved O_2 concentrations can also be valuable when using the thermal loop, as it provides insight into the extent of indirect oxidative degradation caused by dissolved O_2 in the heating loop and helps to quantify thermal degradation rates. Dissolved O_2 is typically completely consumed at the increased temperatures in the thermal loop. However, if the solvent is more resistant to oxidative degradation, the dissolved O_2 sensor could also be placed at the solvent inlet at the top of the column to measure the fraction of O_2 that is consumed. This will help to evaluate oxidative degradation rates at increased temperatures. Similarly, in oxidative-only experiments, measuring dissolved O_2 at the top of the column is useful for evaluating O_2 consumption in the tubing and heating coil.

6.4 Combined Oxidative and Thermal Degradation

Aside from oxidative-only experiments, combined oxidative and thermal degradation can be studied using the thermal loop. A side stream of solvent is taken from the sump and heated to typical stripper temperatures. In contrast to the actual process, CO_2 is not stripped from the solvent in the thermal loop. Therefore, an internal gear pump is used to pressurize the solvent to around 10 bara. The pump used in the setup is a type E/F 210 stainless steel gear pump by Linn-Pumpen GmbH. For this application, internal gear pumps have several advantages over other types of pumps: a relatively high differential pressure, a constant, non-pulsating discharge regardless of pressure conditions, good performance with viscous liquids, bidirectional operation for solvent discharge at the end of an experiment, and no need for priming because the pump can handle small quantities of gas.

An overview of the thermal loop and the control is shown in Figure 6.11. A temperature and pressure indicator are installed right after the gear pump. The pressure over the loop is controlled manually by adjusting the back pressure control valve. An alarm will be given (PI101) when the pressure exceeds operating pressure. Additionally, a pressure safety valve is installed after the gear pump which opens when a pressure of 12 bar is exceeded to protect the equipment’s structural integrity. This could occur due to a blockage in the loop or when the back pressure control valve is closed.

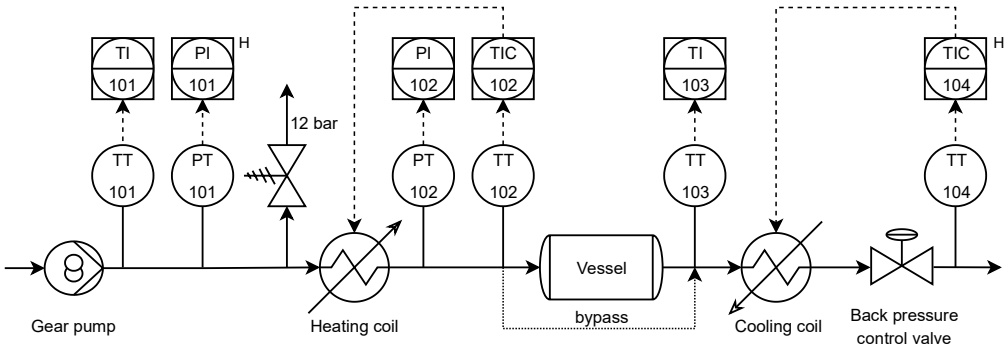

Figure 6.11: Schematic overview of transmitters, indicators, and control loops in the thermal loop.

The solvent is then heated by passing through a heating coil submerged in an oil bath. The temperature is measured after the heating coil, and this measurement can be used to control the temperature in the oil bath. The pressure is also measured here to ensure that the pressure drop over the heating coil is limited and the operating pressure is sufficient so the CO_2 is not stripped. The solvent can be stored in a buffer vessel to increase high-temperature exposure time. The buffer vessel has a volume of 2.5 L but a smaller buffer tank can be installed. The buffer vessel can be bypassed, allowing the solvent to enter the cooling coil directly.

In the cooling coil, the solvent is cooled to the column operating temperature. To control the solvent temperature, a temperature sensor is placed at the outlet to monitor and regulate the cooling bath temperature. If the temperature exceeds the normal operating range, an alarm is activated. Additionally, a bimetallic temperature switch is installed, and if the temperature surpasses 80 °C, it will disconnect the heating bath's electrical circuit. This safety measure prevents pressure buildup in the column, which can occur if the cooling bath fails and CO_2 is stripped or steam is produced.

6.5 Control of Dissolved Metals

The setup is designed such that oxidative degradation of a solvent can be investigated, without contact between the solvent and metallic surfaces. This prevents metals such as iron and copper to dissolve into the solvent and catalyze the oxidative degradation reactions. The column, liquid distributor, sump, packing (optional metallic packing), and the heater are made from glass. The different parts of the column are connected using PTFE seals. Silicone tubing is used to transport both the solvent and gas. Only the dissolved O_2 sensor and the two temperature sensors in the top and bottom of the structured packing are made from stainless steel, so the dissolution of metals in the solution should remain limited. Furthermore, controlled quantities of metals can be added to the solvent to study their effect on solvent degradation. Due to the temperature and pressure requirements in the thermal loop, stainless steel components were selected.

6.6 Regulating Temperature, Gas Composition, and Water Loss

In the initial design, the temperature of the solvent was controlled via a 400 W silicone heating mat surrounding the column. However, even when insulating the column and tubing, heat transfer through the glass column wall was insufficient to reliably operate at temperatures above 65 °C. Therefore, the heating mat has been replaced with a glass heater (a glass condenser), in which water from a heating bath is used to control the temperature of the solvent. As discussed in section 6.3.2, the solvent residence time in the heater is limited. The temperature of the solvent is measured at the top and bottom of the column, and a temperature gradient of approximately 2 °C is typically observed when the column is fully insulated. The temperature in the heating bath is currently adjusted manually since the temperatures in the column are stable, but there is the possibility of integrating the temperature regulation in the control loop.

Water losses are common for open batch setups as water vapor may be entrained in the gas exiting the reactor. Although a water makeup can be used to compensate for the losses, it remains challenging to quantify the loss of water and the changes in concentration of the components as a result. Degradation can be underestimated if water loss is not accounted for properly because the amine concentration increases as water disappears. For this reason, a closed system with a gas recycle is preferred. Regardless, a gas makeup is still required to have a continuous supply of O_2 and regulate the gas composition, as well as a purge to prevent the accumulation of volatile degradation products in the system, such as NH_3.

The composition of the gas phase is controlled using a continuous gas make-up and purge. Mass flow controllers are used to supply a mixture of O_2, CO_2, and N_2. In addition, CO_2 (Rosemount Binos 100, NDIR) and O_2 (Servomex 5200 Multipurpose, paramagnetic) analyzers are used in series to check the composition of the gas. A continuous side stream is taken from the main gas recycle, which is cooled to 7°C to condense water to prevent it from entering the analyzers. The condensate is reintroduced into the column. A rotameter is installed upstream of the analyzers to regulate the flow rate to the analyzers. In addition, a restriction valve is installed in the main gas loop to ensure sufficient gas passes through the analyzers. This restriction should not influence the pressure in the column because it is connected to the atmosphere via the water lock.

Since the water content of the analyzed gas is lower than in the reactor, the gas phase concentrations must be corrected to account for the partial pressure of water in the column at the operating temperature. After the analyzers, a fraction of the gas is purged and the remainder is reintroduced into the main gas loop. The water loss through the purge should be limited because the water content of the analyzed gas is low.

A measure to reduce the impact of water loss on the results is the use of a tracer. The tracer is an inert, non-volatile component not naturally present in the system. Water losses will cause the concentration of the tracer to increase over time and this difference

can be used to correct all other concentrations. Lithium carbonate has been considered due to its low natural abundance, but the salt has a low solubility and is difficult to handle and analyze accurately. Since the solvent holdup of the setup is relatively small, the amine can be dissolved in demineralized water so more common salts can be used because they are no longer naturally present.

The selected candidates are potassium hydroxide (KOH) and potassium carbonate (K_2CO_3). The solvent is alkaline and carbonates are abundant in the system, and the relatively low concentration of these tracer anions should have a negligible impact on the experiments. Furthermore, potassium was not found to affect the degradation significantly. Goff[1] reported that the addition of potassium chloride (KCl) weakly increased the degradation rates, whereas potassium bromide (KBr) acted as a weak inhibitor. In addition, Buvik et al.[12] found that the addition of 1.0 wt% potassium iodide (KI) significantly inhibited oxidative degradation of MEA. Therefore, it appears the anion is primarily responsible for the effect on the degradation rates. Furthermore, the concentrations of the salts employed in the experiments were higher than the intended tracer concentration in the new setup (5 mM K+), and Goff[1] observed no significant effect at concentrations around 10 mM. The concentration of potassium is orders of magnitude lower than that of CO_2 and other ionic species and will not influence the ionic strength and the solvent's capacity to absorb O_2. All in all, the potassium carbonate tracer is expected to have a negligible effect on the degradation rates.

6.7 Results, Experiences and Recommendations

6.7.1 Performance Analysis: Oxidative Degradation Experiments

After functional testing of the equipment and calibration of the analytical instruments, several oxidative degradation experiments were performed without using the thermal loop. The goal of these experiments was to test the continuous operation of the setup and compare the degradation results with those obtained using agitated bubble reactors. An overview of the performed experiments is given in Table 6.4. Note that the concentration of O_2 is given on a dry basis and that the partial pressure is expected to decrease in the reactor, where water vapor will be present.

For each experiment, a fresh 30 wt% MEA solution was prepared and pre-loaded with CO_2 to a loading of around 0.4. The tracer compound, either KOH or K_2CO_3, was added and the solvent was introduced into the setup after taking a sample of the initial solvent. Around 500 mL of solvent was added, such that the initial level in the sump was 200 mL upon circulation. The temperature of the heating bath was set to control the temperature of the solvent at the top of the absorber packing. Approximately one hour after the experiment was started and steady-state was achieved, the first solvent sample was taken for further analysis. Afterwards, solvent samples were taken at various intervals.

The total alkalinity of the samples was determined through amine titration with H_2SO_4. This is a quick and inexpensive way to estimate the amine concentration, however, some degradation products may also be alkaline, so the actual concentration of MEA may be lower[13]. In addition, total inorganic carbon (TIC) measurements were performed to determine the concentration of CO_2 in the solvent, and with these values, the CO_2 loadings can be determined. A Shimadzu TOCLCPH in TIC mode was used for this analysis.

Table 6.4: Overview of the performed experiments to test the setup and evaluate degradation rates at various conditions.

Exp. No.	**Temp. [°C]**	**Con. O_2 [vol%]**	**Equipment**	**Additives**	**Analysis**
1	75	98	Peristaltic pump Dissolved O_2 sensor	5 mM KOH	Total alkalinity, TIC, ICP-MS
2	65	19	Gear pump (SS316)	5 mM K_2CO_3, 0.5 mM $FeSO_4$	Total alkalinity, TIC
3	65	21	Peristaltic pump	2.5 mM K_2CO_3	Total alkalinity, TIC, ICP-MS, LCMS

Further quantitative analyses of the solvent samples were performed in collaboration with SINTEF Industry. Liquid chromatography combined with mass spectroscopy (LC-MSMS) was used to determine the concentration of MEA and a selection of degradation products and organic acids. For this, a UHPLC Agilent 1290 Infinity System with an Agilent 6495 triple quadrupole detector was used. Quantification of dissolved metals was performed by inductively coupled plasma mass spectrometry (ICP-MS) using an Agilent 8800 Triple Quadrupole from Agilent Technologies. For the first experiment, ICP-MS analyses were performed by the ICP-HR-MS Lab at the Department of Chemistry at NTNU, using an Agilent 8800 with a triple quadrupole detector. Samples were diluted to reduce the organic content and digested with 65% HNO_3. An overview of the analyzed compounds is given in Table 6.5.

Table 6.5: Degradation compounds and dissolved metals analyzed with LC-MS and ICP-MS in collaboration with SINTEF Industry and the ICP-HR-MS Lab at the Department of Chemistry at NTNU.

Method	**Compound name**	**Abb.**	**CAS**
LC-MS	Monoethanolamine	MEA	141-43-5
	N-(2-hydroxyethyl)glycine	HeGly	5835-28-9
	N-(2-hydroxyethyl)formamide	HEF	693-06-1
	N,N'-bis(2hydroxyethyl)ethanediamide	BHEOX	1871-89-2
	N-(2-hydroxyethyl)acetamide	HEA	142-26-7
	4-(2-hydroxyethyl)-2piperazinone	HEPO	23936-04-1
	1-(2-hydroxyethyl)-2imidazolidinone	HEIA	3699-54-5
	2-oxazolidinone	OZD	497-25-6

	1H-imidazole-1ethanol	HEI	1615-14-1
LC-MS: Acids	Glycolic acid		79-14-1
	3-OH propionic acid		503-66-2
	Lactic acid		50-21-5
	Formic acid		64-18-6
	3-OH Butyric acid		300-85-6
	Acetic acid		64-19-7
	Propionic acid		79-09-4
	Isobutyric acid		79-31-2
	Butyric acid		107-92-6
	Glyoxylic acid		298-12-4
ICP-MS	Iron	Fe	
	Copper	Cu	
	Chromium	Cr	
	Nikkel	Ni	
	Potassium	K	

6.7.2 Experiment 1: Extreme Conditions

The first experiment was performed at high temperature (75 °C) and high concentration of O_2 in the gas phase (98 v%, dry) to test operation at increased temperatures and obtain significant degradation in a relatively short time period. The remainder of the makeup gas was CO_2 (2 v%, dry) to keep the loading of the solvent constant. In addition, a potassium tracer was added in the form of 5 mM KOH to investigate how well water losses can be quantified.

A couple of operational challenges were encountered in the experiment. After three days of operation, the silicone tubing in the peristaltic pump failed, resulting in significant solvent leakage and the experiment was stopped. Failure of this tubing had not occurred earlier during test campaigns with water and air at similar conditions. Furthermore, the pump tubing was replaced before this first experiment with the MEA solvent. Therefore, the tube failure is expected to be caused by the reduced chemical resistance of the regular silicone pump tubing, which is likely not compatible with the alkaline conditions or the presence of degradation products, when combined with relatively high temperatures and continuous operation for several days. For this reason, Versilon 2001 pump tubing by Masterflex was selected for its chemical resistance and compatibility with comparable chemicals and was used for future experiments with the peristaltic pump. Regular silicone tubing was used in other parts of the setup as the tubing here would not be exposed to prolonged strain and no issues were observed here.

Other leaks were present during the experiment as some solvent leaked from one of the connections of the glass reactor. In addition, even though the make-up gas consisted of 98% O_2, the analyzed O_2 content of the gas stabilized around 89%, as shown in Figure

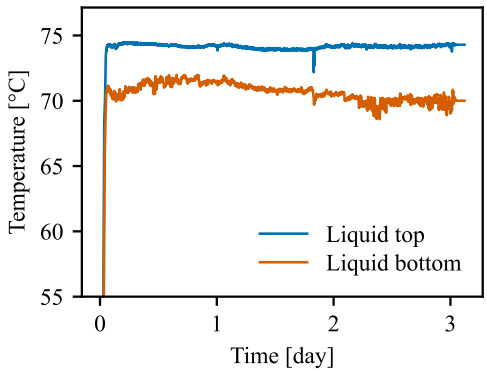

Figure 6.12: Temperature of the solvent inlet at the top and right below the structured packing over the course of experiment 1.

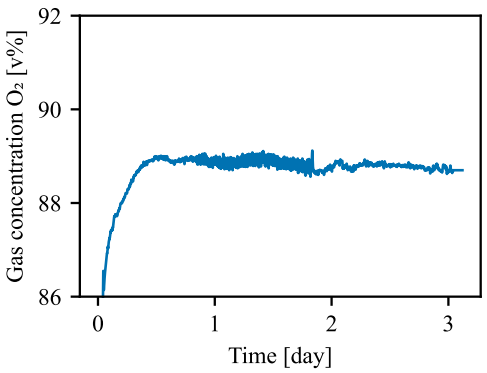

Figure 6.13: Analyzed concentration of O_2 in the gas phase over the course of experiment 1, after cooling the gas phase to condense H_2O.

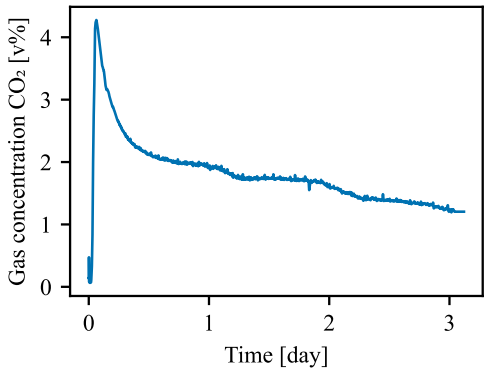

Figure 6.14: Analyzed concentration of CO_2 in the gas phase over the course of experiment 1, after cooling the gas phase to condense H_2O.

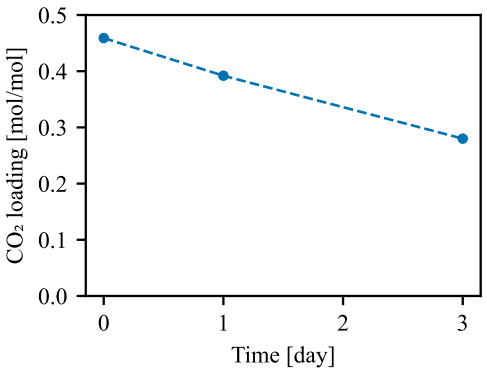

Figure 6.15: CO_2 loading of the solvent, determined using amine titration and TIC, over the course of experiment 1.

6.13. Note that the side stream of gas that was analyzed was cooled and passed through a bed of silica beads to condense and remove water, so a reading of 98% was expected.

Similar trends were observed for the concentration of CO_2, as shown in Figure 6.14. The solvent was pre-loaded with CO_2 above the expected saturation conditions in the reactor, and the gas-phase concentration of CO_2 increased during the first hours of the experiment due to stripping. Over the course of the experiment the CO_2 concentration of the gas phase reduced below the makeup concentration. In addition, a decrease in CO_2 loading is observed, see Figure 6.15. The absorbed CO_2 in the solvent is expected to act as a buffer and slow the decrease in CO_2 concentration due to the leakage. To prevent future problems with leakages, the reactor connections were tightened and hoses were checked and secured. Afterward, the setup was operated with water and a very small makeup of pure N_2. A proportional purge flow was observed in the water lock and no O_2 was

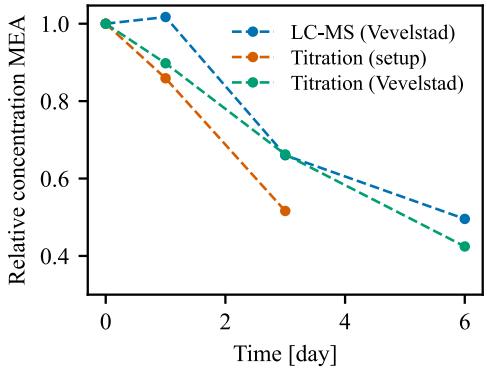

Figure 6.16: Normalized solvent alkalinity over the course of the experiment (65 °C, 21% O_2), compared to the results from the agitated bubble reactor experiment by Vevelstad et al.[4] at similar conditions.

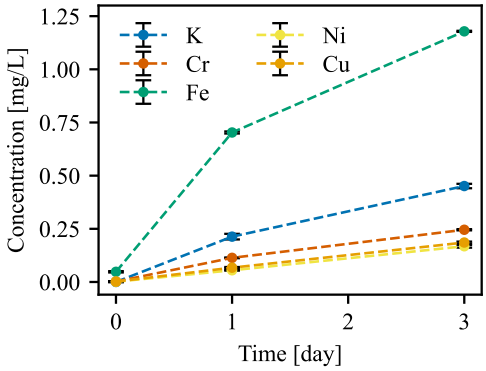

Figure 6.17: Concentrations of tracer and dissolved metals analyzed by ICP-MS over the course of the experiment.

detected by the gas analyzer, indicating that no gas leakages were present. This testing procedure was repeated each time the reactor was modified and reassembled.

The color of the solvent quickly changed from transparent to yellow/brown in the first hours of the experiment and continued to darken afterward. The liquid level in the sump had decreased from 200 mL at the start of the experiment to around 50 mL after 28 hours, indicating that significant water loss was occurring. Due to the solvent leakage, the final liquid level could not be determined. Furthermore, there was insufficient room for the gas to pass by the liquid distributor at the top of the reactor, causing some solvent to accumulate. This issue was not apparent from the tests with water but occurred when solvent was used. This was addressed by moving the distributor slightly higher above the packing, creating more space for the gas to pass. Although the dissolved O_2 sensor was installed in the sump during the experiment, the obtained data was not reliable. This is discussed in more detail in section 6.7.5.

The temperatures in the setup, shown in Figure 6.12, were stable and could be controlled well by manually adjusting the temperature of the water bath. The temperature sensor that was installed near the top of the packing was in good contact with the solvent and showed a constant reading. The other temperature sensor was right below the structured packing but was wetted only occasionally, resulting in a less stable response. Although the reactor was insulated, a temperature drop of around 3.5 °C was observed as a result of heat losses.

The samples were analyzed using amine titration to determine the total alkalinity, and the results are shown in Figure 6.16, where they are compared to the results by Vevelstad et al.[4], who ran an experiment at similar conditions in an agitated bubble reactor. Degradation rates appear to be higher in the new setup because the alkalinity is reduced by 50% in just 3 days, in contrast to 37% in the agitated bubble reactor. There appears

to be a discrepancy between the amine titration and LC-MS results by Vevelstad et al.[4] after 1 day. The authors state that the variation in the water balance is generally lower than 5% due to pre-saturation of the makeup gas and is not expected to significantly increase the MEA concentration profiles. Therefore, an increase in MEA concentration is unlikely and the LC-MS measurement is likely inaccurate.

The concentration of the KOH tracer in the prepared solvent was 5.0 mM, which would correspond with a concentration of 195.5 mg/L. The results from the ICP-MS analysis showed no potassium in the initial solvent sample and significantly lower concentrations for the solvent samples after 1 and 3 days than what was added (195.5 mg/L), as shown in Figure 6.17. The results have been discussed with the analytical lab but the reason for the discrepancy remains unclear. Given the accuracy of the scale in the laboratory and the direct addition of the KOH to the 600 mL of solvent, it is unlikely that there was an error during the preparation of the solvent. A dilution error is unlikely since this would also affect the concentrations of the other metals. The concentration of iron, for example, would approach 1.0 g/L, which is significantly higher than expected given the limited presence of metals in the reactor. For future experiments, K_2CO_3 was used as a tracer instead, and additional samples were taken, both of the initial solvent before entering use in the setup and a reference of 5.0 mM K in DI water.

Despite the unexpected results for the tracer, they can still be used to attempt to estimate the water loss during the experiment, by assuming that the analyzed concentrations of K are proportional to the total solvent volume. Because the analyzed concentration of K in the initial sample was zero, the absolute water loss during the last two days was used to estimate the water loss during the first day. Based on these assumptions, the water loss is estimated to be around 350 mL, which is around 80% of the water initially present. However, this estimate does not correspond with observations of the sump level during the campaign, which indicate a water loss of approximately 200 mL. Therefore, instead of the estimate based on the concentration of K, the sump level observations are used to correct the amine concentrations. The water loss is assumed to be constant during the experiment. More accurate tracer results are therefore needed to accurately quantify water losses.

The water loss-corrected results are given in Figure 6.18. The degradation rate is significantly larger than observed in the agitated bubble reactor experiments. Based on the estimated oxygen saturation data shown in Figure 6.5, the agitated bubble reactor experiment at 75 °C and with 98 v% of O_2 is expected to have a liquid bulk O_2 concentration that is 80% saturated compared to equilibrium. Considering the reaction order for O_2 in the reaction kinetics of the oxidative degradation model, $n = 0.469$ (see section 4.4.1), the degradation rate is then expected to be 90% of the degradation rate at O_2 saturation. The increase in degradation rates in the new setup compared with the results by Vevelstad et al.[4] is larger than the expected increase, even when considering the uncertainty in the mass transfer coefficient correlation.

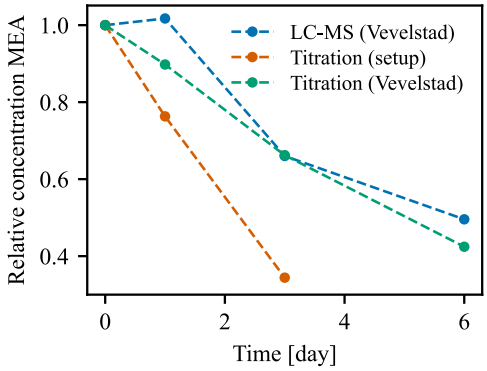

Figure 6.18: Water loss-corrected, normalized solvent alkalinity over the course of the experiment (65 °C, 21% O_2), compared to the results from the agitated bubble reactor experiment by Vevelstad et al.[4] at similar conditions.

Although the concentrations of dissolved metals are generally low, as shown in Figure 6.17, they are still significantly higher than those measured in the freshly prepared solvent (all analyzed metals < 0.005 mg/L). The increase in concentrations of the dissolved metals is relatively large between the samples taken at the start of the experiment and after 1 day. This is likely caused by metal impurities that remain in the setup from previous usage. Since the initial sample is taken when the system reaches steady-state after approximately one hour, not all metal impurities may have fully dissolved yet into the solvent. The concentrations of dissolved metals continued to increase during the last two days of the experiment, although at a slower rate. This increase could be caused by continued dissolution of remaining impurities, corrosion of the metallic temperature sensors, or water loss. Given the uncertainty in the water loss quantification, it is challenging to identify the reason for the increase.

A more thorough cleaning is recommended, since metals such as iron and copper may already catalyze oxidative degradation, even at these low concentrations[1,14]. This might thus also explain the relatively high degradation rates observed in the new reactor. Therefore, from this point on, the setup was cleaned more thoroughly in between experiments. DI water was repeatedly introduced and recycled right after the experiments to remove the remaining solvent. Afterward, the silicone tubing was replaced and the glass reactor was disassembled and cleaned. The glass parts were washed and scrubbed thoroughly with soap and water before being placed in an aqueous solution of 0.5 M H_2SO_4 overnight. The glass structured packing and heating coil, a glass condenser, could not be washed manually and were rinsed with DI water and placed in the H_2SO_4 solution overnight.

6.7.3 Experiment 2: Mild Conditions and Iron Addition

Based on the results of the first experiment the reactor was updated and prepared for a second experiment. This experiment was conducted at milder conditions that more closely resemble the actual capture process (65 °C and 19 v% O_2, dry). The concentration of O_2 was chosen such that the concentration in the reactor was 15 v% due to the presence of water vapor. The solvent was loaded with 0.4 mol of CO_2 per mole of MEA and the concentration of CO_2 in the makeup gas was set at 3.9 v%, resulting in 3.0 v% once saturated with water. At 65 °C this gas is in equilibrium with a 30 wt% MEA solution with a loading of 0.4[15]. Furthermore, 0.50 mM of iron was added to the solvent in the form of $FeSO_4$ to study the effect of the catalytic oxidation on the degradation rate and study how well the concentration of dissolved metals could be controlled.

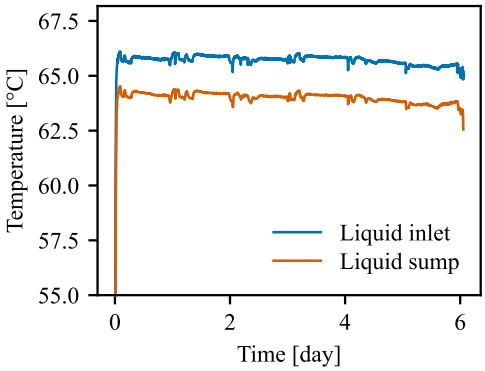

Figure 6.19: Temperature of the solvent inlet at the top and in the sump over the course of the experiment.

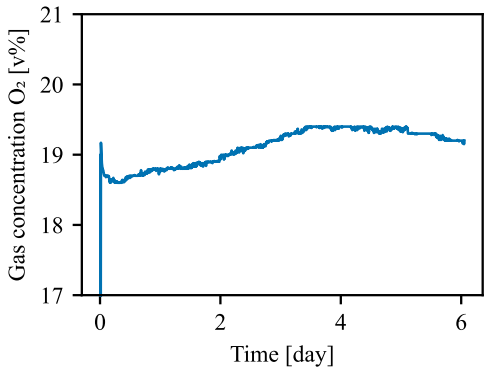

Figure 6.20: Analyzed concentration of O_2 in the gas phase over the course of the experiment, after cooling the gas phase to condense H_2O.

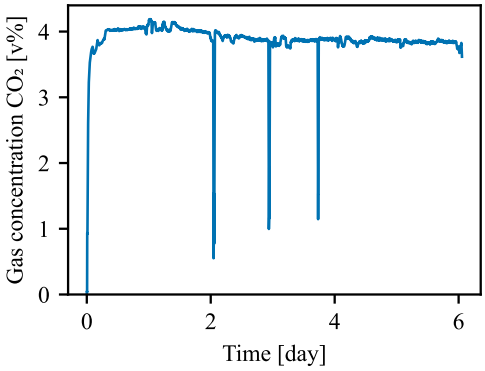

Figure 6.21: Analyzed concentration of CO_2 in the gas phase over the course of the experiment, after cooling the gas phase to condense H_2O.

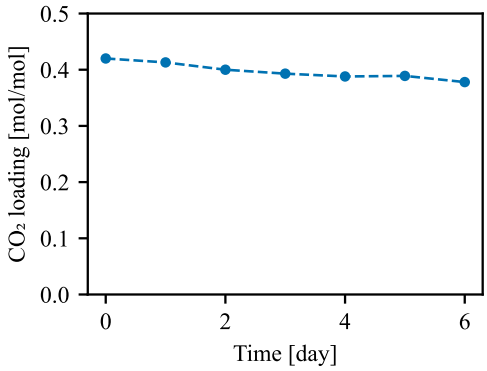

Figure 6.22: CO_2 loading of the solvent, determined using amine titration and TIC, over the course of the experiment.

The temperature sensor was moved from the bottom of the packing into the sump, where it was submerged in the solvent. Figure 6.19 shows the temperature profile over the course of the experiment. Due to continuous contact with the solvent, the reading of the lower temperature sensor was clearer and more precise compared with experiment 1, where it was only intermittently wetted. The temperature difference was constant and around 2.0 °C. The small fluctuations that are visible in the profiles are the result of opening the fume hood, refilling the water bath, and sampling.

The gas concentration profiles are given in Figure 6.20 and Figure 6.21. The concentrations are stable over the course of the experiment and correspond well with the concentrations of the makeup gas. The occasional dip in CO_2 concentration is caused by the temporary stoppage of the gas pump, for example during sampling. The CO_2 loading is also relatively constant and shows only a slight decrease over time. These results indicate that no gas leakages were present and that the tightening of the reactor connections was enough to prevent gas leakages.

Awaiting the arrival of the chemically resistant pump tubing, the SS316 gear pump was used to circulate the solvent in this experiment. This pump appeared to function well initially but solvent was continuously leaking along the motor shaft. This became apparent when the pump was inspected after the experiment, but also during the experiment because the solvent took on a blue/green color, which indicates the presence of copper. The copper is expected to originate from the brass motor coupling, which showed signs of corrosion when inspected after the experiment. Because of the contamination, the solvent samples were not analyzed in more detail. The seal in the pump should be replaced and tested to prevent future leaks and contamination. If this proves to be difficult, an alternative gear pump with a magnetic coupling could be used, since this eliminates the need for a seal. If the power of this pump is insufficient to pressurize the solvent for the thermal loop, several pumps in series could be used.

6.7.4 Experiment 3: Mild Conditions and Detailed Solvent Analysis

The final experiment was performed to compare the degradation rates in the new reactor with those reported by Vevelstad et al.[4] again, but this time at milder, more realistic conditions. The composition of the make-up gas was 21% O_2, 2% CO_2, and 77% N_2 (dry, volume basis) and the temperature at the top of the packing was kept at 66 °C to account for the temperature drop of 2.0 °C, which was found in the previous experiment. This corresponds well with the conditions in a similar experiment by Vevelstad et al.[4]. The temperature sensor in the bottom of the reactor was relocated to analyze the temperature of the gas entering the reactor.

No dissolved metals were added during the original agitated bubble reactor experiment, so a clean solvent was also used in the current experiment. The solvent was circulated with the peristaltic pump using the Versilon 2001 pump tubing with improved chemical resistance. However, not having tested this tubing before, and to avoid possible leakages,

the tubing in the pump was replaced daily right after a sample was taken. Both gas and liquid circulation were stopped for approximately 10 minutes when replacing the tubing. Pump tubing was analyzed after replacement and other than some wear marks, no signs of serious damage were observed. The peristaltic pump functioned well, providing a constant flow of liquid throughout the experiment and operating well in case of occasional gas entrainment.

The temperature and gas phase concentration profiles during the experiments are given in Figure 6.23, Figure 6.24, and Figure 6.25 respectively. The daily interruptions to replace the pump tubing are visible in the temperature and CO_2 concentration profile. The inlet temperature of the solvent was stable at around 66 °C over the course of the

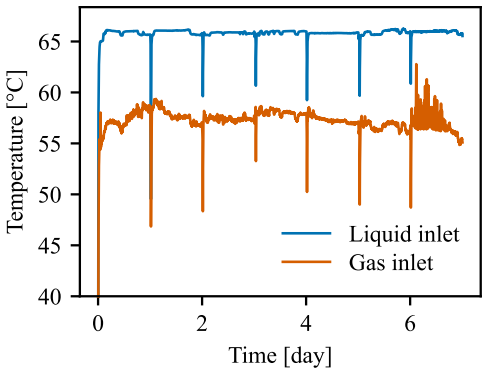

Figure 6.23: Temperature of the solvent inlet at the top and the gas inlet at the bottom of the reactor over the course of the experiment.

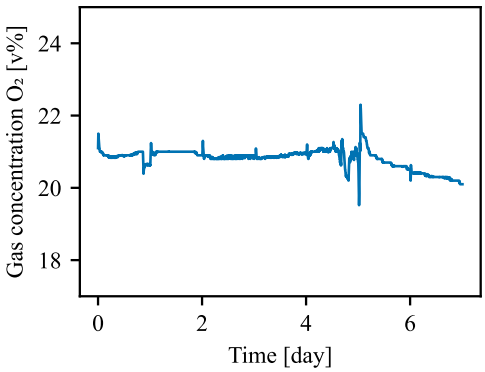

Figure 6.24: Analyzed concentration of O_2 in the gas phase over the course of the experiment, after cooling the gas phase to condense H_2O.

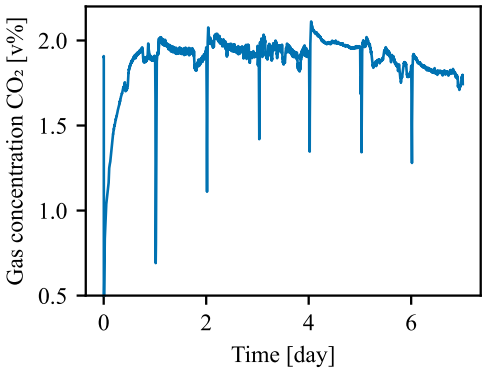

Figure 6.25: Analyzed concentration of CO_2 in the gas phase over the course of the experiment, after cooling the gas phase to condense H_2O.

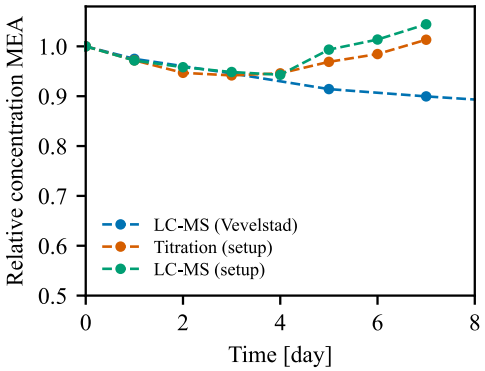

Figure 6.26: Normalized concentration of MEA over the course of the experiment (65 °C, 21% O_2, α=0.38), compared to the agitated bubble reactor experiment by Vevelstad et al.[4] at similar conditions.

experiment. The inlet temperature of the main gas recycle was slightly lower due to cooled gas flow through the analyzers and heat dissipation in the gas pump. The impact of the lower gas temperature on the temperature of the solvent is expected to be limited due to the large difference in heat capacity. The gas is also expected to heat up quickly when in contact with the solvent, but this should be tested in more detail when developing degradation models using the data. A lower temperature causes the water content of the gas to decrease, resulting in slightly higher partial pressures of O_2 and CO_2. The increase in fluctuations in gas inlet temperature during the final day is likely the result of the solvent occasionally coming in contact with the temperature sensor.

The solvent was pre-loaded with CO_2 but not yet fully saturated at the conditions in the reactor, for this reason, the concentration of CO_2 in the gas phase was relatively low during the first couple of hours of the experiment as the CO_2 that was supplied via the gas make-up was quickly absorbed. For future experiments, the solvent could be loaded with CO_2 up to the expected equilibrium concentrations in the reactor. Alternatively, the make-up rate could be increased at the start of the experiment to increase the supply of CO_2 and reach equilibrium sooner.

Around 5 days into the experiment, the cooling bath had turned off unexpectedly and uncondensed water had entered the analyzers. After briefly flushing the analyzers with N_2, normal operation was resumed. From this point on, both analyzers began to drift slightly. It is unlikely that this behavior is caused by a gas leakage since the concentration of O_2 would remain around 21% when outside air enters the system.

During the first couple of hours of the experiment, the clear fresh solvent quickly took on a yellow color. Over the course of the next couple of days, the color transitioned to orange and then to a dark red/brown near the end of the week. The decrease of the sump level over time was more significant than expected from daily sampling of 4 mL of solvent, and the viscosity of the solvent increased over time. These observations indicate that significant water loss had occurred. Further analysis using both amine titration and LCMS, as shown in Figure 6.26 appears to confirm these suspicions. The concentration of MEA decreases slightly during the first couple of days, after which it starts to increase and reaches concentrations above 30 wt%. The initial decrease in MEA concentration is similar to the observed rate by Vevelstad et al.[4] in the agitated bubble reactor experiment.

The quantification of the non-volatile potassium tracer in the samples, depicted in Figure 6.27, clearly shows the water loss in the system, as the concentration has nearly doubled at the end of the experiment. The solvent volume was reduced by 44%, meaning 63% of the water had evaporated, which amounts to approximately 220 mL. This corresponds with observations in the setup because the sump was nearly empty near the end of the experiment. However, the water loss is more significant than initially anticipated. Although the purge flow rate is only 400 mL/min, the flow rate through the analyzers is approximately 1.2 L/min. Before the gas enters the analyzers but after it is cooled, the gas is passed through a bed of silica beads to remove the remaining moisture. When the

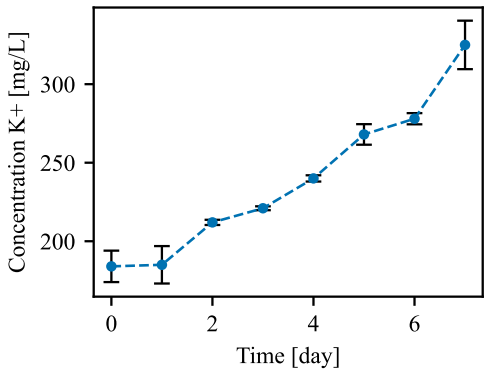

Figure 6.27: Concentration of the potassium tracer in the solvent over the course of the degradation experiment.

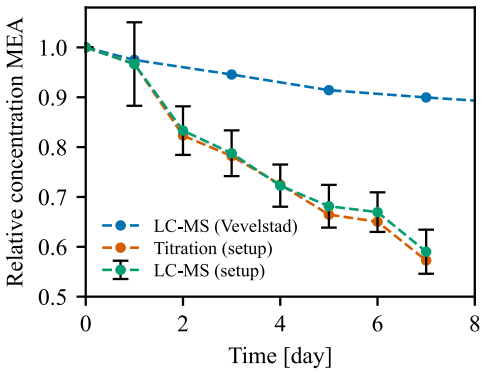

Figure 6.28: Tracer-corrected, normalized concentration of MEA over the course of the experiment (65 °C, 21% O_2, α=0.38), compared to the agitated bubble reactor experiment by Vevelstad et al.[4] at similar conditions.

gas flow is saturated with water at 7 °C, around 94.5 mL of water is expected to be adsorbed by the silica over the course of one week.

The difference in water loss could be caused by entrainment of liquid in the gas or insufficient cooling, as a gas temperature of 20 °C would result in the observed losses. Additional tests should be performed to measure the temperature of the condensed gas or the weight of the silica bed and more intense cooling of the gas should be tested. In addition, the make-up gas can be partially saturated with water to limit water losses. If cooling in the condenser is sufficient and additional water condensation does not occur in the analyzers, the silica beads could be removed. Otherwise, the setup can also be operated without continuously monitoring the gas phase concentrations, as the constant gas make-up and purge result in a stable gas composition. The gas phase can be checked intermittently, reducing water losses.

The potassium tracer results are used to correct the MEA concentrations and express the total amount of MEA as a function of the initial solvent volume, as shown in Figure 6.28. The degradation rate in the setup is significantly higher than those reported by Vevelstad et al.[4] in the agitated bubble reactor. After one week of continuous exposure, 42% of the MEA has degraded, compared with just 10% in the conventional reactor. The uncertainty for the LCMS concentration data has been estimated and is shown in the figure. Despite the lack of duplicates, the analytical uncertainty of the LCMS method is generally low, and a deviation of 2.0% has been assumed. The uncertainty in the corrected concentration is significantly higher since there is additional uncertainty from the potassium tracer, both from the initial and current concentration of potassium that are required to perform the correction. A reduction in uncertainty in the potassium tracer data will result in more accurate final concentrations of MEA. The initial tracer

concentration should be determined accurately since it is used to correct all MEA concentrations.

Similar to the approach for experiment 1, the increase in degradation rate compared to the agitated bubble reactor experiment can be estimated using the oxygen saturation data shown in Figure 6.5. The liquid bulk concentration in the agitated bubble reactor is estimated to be at 77% of the saturation concentration, resulting in a degradation rate of 88% the rate in case the solvent is saturated with O_2. The increase in degradation rates in the new setup compared with the results by Vevelstad et al.[4] is significantly larger than expected. Even when considering the uncertainty in the mass transfer coefficient correlation, the difference cannot be explained.

The concentrations of dissolved metals in the solvent, as quantified by ICP-MS and shown in Figure 6.29 and Figure 6.30. Both Fe and Cu are present in quantities that have been found to catalyze oxidative degradation, which may explain the high degradation rates[1,14]. No metals were initially added to the solvent and ICP-MS analysis of the prepared solvent showed negligible concentrations of these metals. Apart from the two stainless steel temperature sensors, no other metallic equipment was in contact with the solvent during the experiment and the metals. For this reason, the metals are expected to have remained from prior experiments and tests, despite the more thorough cleaning of the reactor parts and the use of 0.5M H_2SO_4. Discussions with colleagues and ICP-MS specialists in the department lead us to believe that the used dilute acid may not be potent enough to remove all the metal deposits and more concentrated solutions of HNO_3 are recommended to successfully eliminate all metal impurities from the system.

When the concentrations of the dissolved metals are corrected using the potassium tracer results, it becomes clear that the total amount of Fe, Cr, and Ni in the system is constant over the course of the experiment. The initial concentrations are lower because the

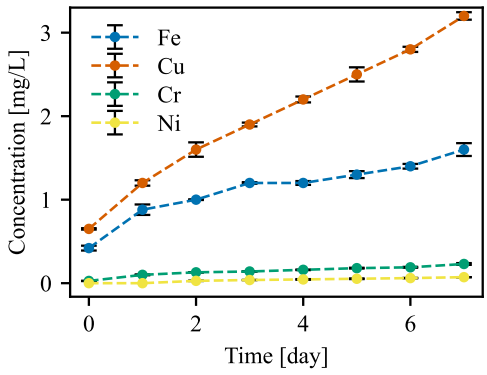

Figure 6.29: Concentrations of dissolved metals over the course of the experiment.

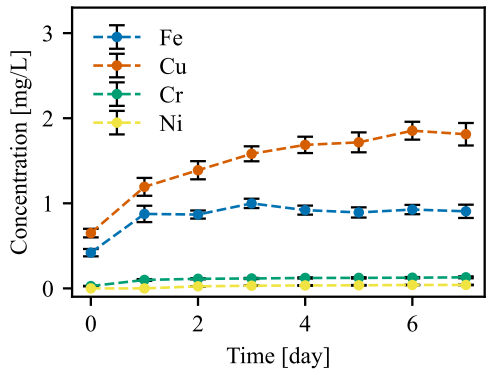

Figure 6.30: Tracer-corrected concentrations of dissolved metals over the course of the experiment.

system has had around an hour to equilibrate and not all of the impurities are dissolved. The total amount of Cu in the solvent appears to increase slightly over time.

The concentrations of degradation products that were quantified using LCMS are given in Figure 6.31 through Figure 6.34. These concentrations have been corrected for water loss using the tracer results. The concentrations of the degradation products are generally higher than those reported by Vevelstad et al.[4], which is expected because the extent of solvent degradation in these experiments is lower. The relative concentrations between the different degradation products are generally in agreement with the results by Vevelstad et al.[4]. HEF and HEI are the main degradation products in the experiment in the new setup, followed by formic acid, whose formation rate appears to increase over time. The concentrations of secondary degradation products, such as HeGly, BHEOX, and HEPO, are lower. Similar trends were observed in the concentrations of these by Vevelstad et al.[4], however, the concentration of HeGly was around 2.5X higher than that

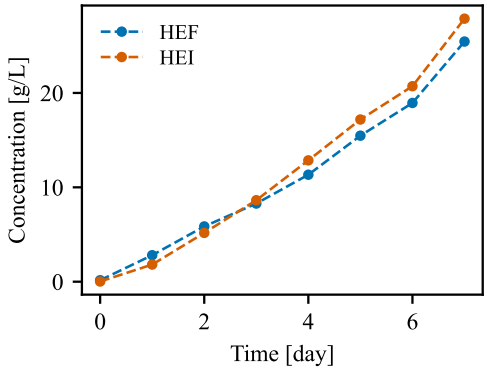

Figure 6.31: Tracer-corrected concentration profiles of the main degradation products over the course of the experiment.

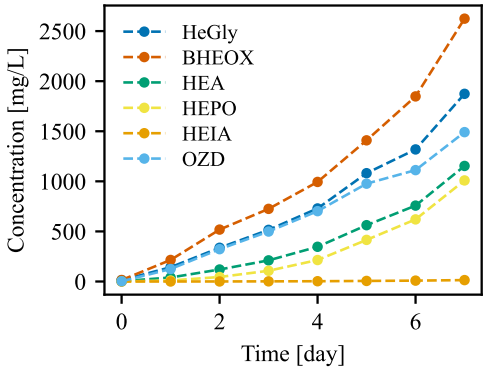

Figure 6.32: Tracer-corrected concentration profiles of other degradation products over the course of the experiment.

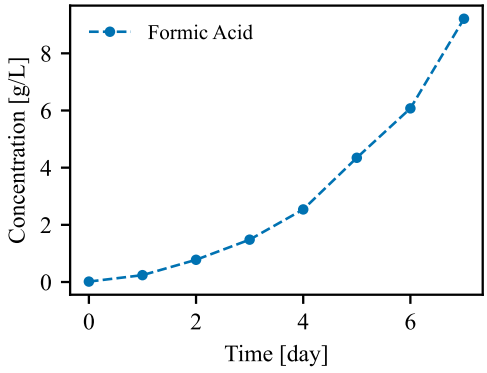

Figure 6.33: Tracer-corrected concentration profiles of formic acid over the course of the experiment.

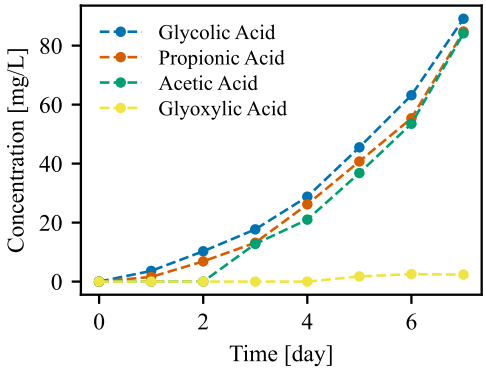

Figure 6.34: Tracer-corrected concentration of other acidic degradation products over the course of the experiment.

of BHEOX, whereas similar concentrations are found in the experiment in the new reactor. Degradation products that are mentioned in Table 6.5 but are not present in the figures were not measured in significant quantities and are left out.

6.7.5 Optical Dissolved O_2 Sensor

The optical sensor for measuring dissolved O_2 has undergone testing and has been used in the setup, although with limited success. The COS81D optical sensor, in combination with the CM72 transmitter, compensates for temperature and air pressure when determining the concentration of dissolved O_2. However, it does not account for the salinity of the solution, which is important to consider. This is because, with increasing salt concentration, gas solubility tends to decrease, a phenomenon known as the "salting-out effect" [16]. When CO_2 is introduced into an aqueous solution of MEA, it leads to the formation of significant quantities of salts, including MEA carbamate and protonated MEA. These salts lower the solubility of O_2, as also observed experimentally by Buvik et al.[11].

To evaluate the sensor's performance, it has been calibrated and tested using a range of solutions: water, saline water (30 g/L NaCl), 30 wt% unloaded MEA in water, and 30 wt% loaded MEA in water (α = 0.4). Each solution underwent testing at various temperatures (below 40 °C) and O_2 partial pressures. The measured O_2 solubility remained the same for all these solutions under identical conditions. This indicates the sensor's inability to account for dissolved salts.

Due to the sensor's operating principle, which involves the dissolution of O_2 molecules in a permeable membrane layer, it is expected to measure the activity of O_2 instead of its absolute concentration. When salt is introduced into the solvent, a new equilibrium is established between the gas, solvent, and the membrane. Consequently, the sensor effectively measures the partial pressure of O_2 in the gas phase. While the sensor can be used in conjunction with other transmitters that allow manual correction for solution salinity, such corrections are only valid for NaCl[11].

Despite its inability to measure the absolute solubility of O_2, the sensor still provides valuable insights into the oxygen concentration relative to saturation. This optical sensor has been applied similarly by Obute et al.[17], where it was used to measure O_2 consumption and compare degradation rates in the presence of iron and degradation products. Similarly, the sensor can be used in the new setup to monitor the rate of dissolved O_2 consumption.

When using the dissolved O_2 sensor in the sump, it is important to account for bubble formation, which can disrupt measurements. The setup currently features a 20 cm gap between the packing and the sump, causing solvent splashing and gas entrainment. To mitigate this issue in future degradation setups, consider reducing the gap between the

packing and the sump. To address the problem in the current setup, we have added a nylon fiber pad just above the sump to collect liquid without bubble formation.

6.7.6 Thermal Loop

Due to the seal leakage in the gear pump, the thermal loop could not be tested with solvent and the combined effect of oxidative and thermal degradation could not yet be studied. Tests with water were promising and showed good control over the temperatures and pressures in the loop. When the temperature difference between the oxidative reactor and the temperature loop was significant, the solvent flow rate had to be reduced, in order not to exceed the cooling duty of the cooler. A simple heat exchanger could be installed to lower the duty of both the heater and cooler of the temperature baths.

6.8 Conclusions

A new degradation reactor that addresses the shortcomings of traditional degradation reactors was designed, constructed, and tested. The reactor featured a glass or metal structured packing that was aimed at reducing O_2 mass transfer limitations and ensuring O_2 saturation of the solvent. Initial oxidative degradation experiments in the setup showed an increased degradation rate for operation at 75 °C and 98 v% O_2 as well as at 65 °C and 21 v% O_2. These increased degradation rates indicate the presence of mass transfer limitations in the agitated bubble reactor experiments and give a better representation of degradation in the actual process. Traces of metal impurities, such as iron and copper, were found in the samples using ICP-MS and, although these metals were present at low concentrations, they could have catalyzed degradation, causing the effect of mass transfer limitations to be overestimated. Therefore, a thorough cleaning of the setup, followed by another degradation experiment, is recommended to confirm the findings.

The control of the gas composition and temperatures in the reactor was good, and stable operation over the course of a week was achieved. Water loss during the experiments was significant and several setup modifications are suggested to reduce this loss, such as pre-saturation of the makeup gas or better cooling of gas before analysis. Water losses could be quantified using the K_2CO_3 tracer and the amine concentrations were corrected. However, the uncertainty in the quantification of tracer concentration using ICP-MS was relatively high, and a reduction in this uncertainty will yield more precise amine concentration results.

The optical dissolved O_2 sensor was found to be unable to measure the effect of CO_2 loading on the concentration of dissolved O_2 and thus gives a false representation of the actual concentration of O_2 in the solvent. The sensor can be used to monitor the relative O_2 concentration and can give insight into the extent of O_2 consumption in the sump, heating coil, or thermal loop. Bubble entrainment in the reactor sump should be prevented in future setup designs to obtain more reliable dissolved O_2 measurements.

6.9 References

(1) Goff, G. S. Oxidative Degradation of Aqueous Monoethanolamine in CO2 Capture Processes: Iron and Copper Catalysis, Inhibition, and O2 Mass Transfer. Doctoral thesis, 2005.

(2) Sexton, A. J. Amine Oxidation in CO2 Capture Processes. Doctoral thesis, The University of Texas, 2008.

(3) Léonard, G. Optimal Design of a CO2 Capture Unit with Assessment of Solvent Degradation. Doctoral thesis, Université de Liège, 2013.

(4) Vevelstad, S. J.; Johansen, M. T.; et al. Extensive Dataset for Oxidative Degradation of Ethanolamine at 55–75°C and Oxygen Concentrations from 6 to 98%. *International Journal of Greenhouse Gas Control* **2016**, *50*, 158–178. https://doi.org/10.1016/j.ijggc.2016.04.013.

(5) Cussler, E. L.; Cussler, E. L. *Diffusion: Mass Transfer in Fluid Systems*; Cambridge University Press, 2009.

(6) Gouedard, C. Novel Degradation Products of Ethanolamine (MEA) in CO2 Capture Conditions: Identification, Mechanisms Proposal and Transposition to Other Amines. Doctoral thesis, Université Pierre et Marie Curie, 2014.

(7) Vevelstad, S. J.; Grimstvedt, A.; et al. Evaluation of Results from SDR Campaigns and Pilot Data. In *Trondheim Carbon Capture and Storage Conference (TCCS-11)*; Trondheim, 2021.

(8) da Silva, E. F.; Lepaumier, H.; et al. Understanding 2-Ethanolamine Degradation in Postcombustion CO_2 Capture. *Ind. Eng. Chem. Res.* **2012**, *51* (41), 13329–13338. https://doi.org/10.1021/ie300718a.

(9) deMontigny, D.; Aboudheir, A.; et al. Modelling the Performance of a CO2 Absorber Containing Structured Packing. *Ind. Eng. Chem. Res.* **2006**, *45* (8), 2594–2600. https://doi.org/10.1021/ie050567u.

(10) Endress+Hauser. *Digital oxygen sensor Memosens COS81D*. https://www.endress.com/en/field-instruments-overview/liquid-analysis-product-overview/oxygen-optical-sensor-cos81d (accessed 2023-10-12).

(11) Buvik, V.; Bernhardsen, I. M.; et al. Measurement and Prediction of Oxygen Solubility in Post-Combustion CO2 Capture Solvents. *International Journal of Greenhouse Gas Control* **2021**, *104*, 103205. https://doi.org/10.1016/j.ijggc.2020.103205.

(12) Buvik, V.; Wanderley, R. R.; et al. Addition of Potassium Iodide Reduces Oxidative Degradation of Monoethanolamine (MEA). *Chemical Engineering Science: X* **2021**, *10*, 100096. https://doi.org/10.1016/j.cesx.2021.100096.

(13) Buvik, V. Stability of Amines for CO2 Capture. Doctoral thesis, NTNU, 2021. https://ntnuopen.ntnu.no/ntnu-xmlui/handle/11250/2777358 (accessed 2023-01-23).

(14) Chi, S. Oxidative Degradation of Monoethanolamine. Thesis, University of Texas Austin, 2000.

(15) Aronu, U. E.; Gondal, S.; et al. Solubility of CO2 in 15, 30, 45 and 60 Mass% MEA from 40 to 120°C and Model Representation Using the Extended UNIQUAC Framework. *Chemical Engineering Science* **2011**, *66* (24), 6393–6406. https://doi.org/10.1016/j.ces.2011.08.042.

(16) Weisenberger, S.; Schumpe, A. Estimation of Gas Solubilities in Salt Solutions at Temperatures from 273 K to 363 K. *AIChE Journal* **1996**, *42* (1), 298–300. https://doi.org/10.1002/aic.690420130.
(17) Obute, J. Effect of Impurities and Degradation Products on Dissolved Oxygen Consumption in Amine Scrubbing. In *Post Combustion Capture Conference (PCCC7)*; Pittsburgh, 2023.

Chapter 7: Role of Iron and Solvent Management

This chapter delves into the catalytic role of iron in oxidative solvent degradation and attempts to extend the oxidative degradation model to include this catalytic behavior. Several hypothetical scenarios are studied that focus on the potential effect of corrosion rate limitations, iron solubility limitations, and O_2 mass transfer limitations in the absorber packing. The predicted rate and concentration profiles over time are compared with observations in pilot plant campaigns and the likelihood of each scenario is evaluated. Knowledge gaps in the available experimental data are identified, and future experiments are proposed to better quantify the catalytic effect of iron.

7.1 Catalytic Effect of Iron

Various works in literature have discussed the role of dissolved metals, such as iron and copper, in accelerated oxidative degradation[1–6]. There is a focus on the influence of iron since it is a primary component in the carbon and stainless steels typically used in the construction of the capture plant[7]. When these materials come into contact with the solvent, they can undergo corrosion and dissolve into the solvent. Iron may also enter with the flue gas in the form of fly ash[8].

The concentration of iron and other dissolved metals is typically monitored in (pilot) capture plants during campaigns through solvent analysis[9–13]. Dhingra et al.[14] used data and trends observed in four pilot plants, including the concentrations of dissolved iron and degradation products, to develop an empirical model. This model is used to predict trends in ammonia emissions and dissolved iron concentration, offering insights into the effectiveness of solvent management strategies. However, it is important to note that this modeling approach lacks a catalytic mechanism as its foundation. Therefore, applying this model to extrapolate results to other carbon capture scenarios, characterized by different flue gasses, equipment configurations, and operational conditions, may be challenging.

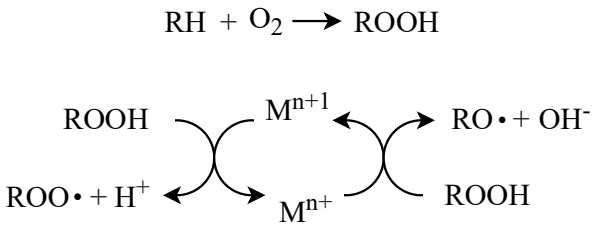

Figure 7.1: Proposed mechanism for the formation of hydroperoxides and the decomposition by dissolved metallic ions, adapted from Voice and Rochelle[15].

Despite the absence of consensus regarding the exact mechanism by which dissolved metals participate in and accelerate degradation reactions, several potential pathways have been proposed in the literature. The amine can be oxidized directly by the metal ion, forming an organic radical when exposed to elevated temperatures in the stripper. Reoxidation of the metal ion may lead to the formation of hydroxyl radicals[16]. Alternatively, in the presence of O_2, ferrous iron can react directly with it[6,7], creating other free radicals. These free radicals can subsequently participate in degradation reactions with the amine. Lastly, Chi[3] and Voice and Rochelle[15] suggest a mechanism in which dissolved metal ions decompose organic hydroperoxides that can be formed through a reaction between the amine and O_2. An overview of this mechanism is shown in Figure 7.1.

Although limited, some studies are available on quantifying the effect of iron on the degradation rate of solvents. In one study, Chi[3] used a sparged reactor to quantify the effect of iron on the oxidative degradation rate of MEA. Instead of analyzing the solvent to determine the degradation rate, an FTIR was used to measure the concentration of NH_3 in the gas phase, which acts as a surrogate for MEA degradation. At an iron concentration of 55.9 mg/L, the ammonia evolution rate was increased by roughly a factor of 4.8 compared with the evolution rate of the solvent without iron.

Goff[17] continued to study and quantify metal-catalyzed degradation rates. In addition to measurements in a sparged reactor, an agitated reactor was also used. This 1 L jacketed, glass reactor was equipped with a stirrer, capable of agitation speeds up to 1450 RPM. The bottom drain tube was used as a supply for the gas. An increase in the agitation speed of the reactor resulted in increased degradation rates, and the catalytic effect of both iron and copper was found to be more significant than previously observed in the sparged reactor.

NH_3 evolution was measured for loaded solvents with varying concentrations of iron in the agitated reactor. However, the reported uncertainty was high, and the author argues that most data points of this series should not be used for quantitative analysis due to problems with the mass balance and not reaching steady-state. For this reason, a series from the sparged reactor is used in this work to quantify the effect of iron on the degradation rate. However, it is important to take the effects of mass transfer limitations in these experiments into consideration.

The rate data from the air-sparged reactor experiments at 55 °C and with a CO_2 loading of 0.4 at varying concentrations of iron (0.0001 – 1.0 mM) from the work by Goff[17] was used to describe the catalytic effect of iron on the degradation rate. The reported experimental NH_3 production rates as a function of dissolved iron are given in Figure 7.2. Inspired by the rate equation proposed by Chi[3], the experimental points were fitted using a power law expression, which is given in Eq. 7.1.

$$R_{cat} = R(1 + 2.733c_{Fe}^{0.2696}) \quad \text{Eq. 7.1}$$

Here, R is the oxidative degradation rate of MEA without the presence of dissolved iron, and c_{Fe} is the concentration of iron in mol/m^3. Figure 7.3 shows the catalytic factor as a function of dissolved iron concentration, which describes the increase in NH_3 production, and as a surrogate also the MEA degradation. It is important to note that no experimental data was available for dissolved iron concentrations above 1.0 mM (55.85 mg/L) and catalytic factors at higher concentrations will be extrapolated and may deviate from reality.

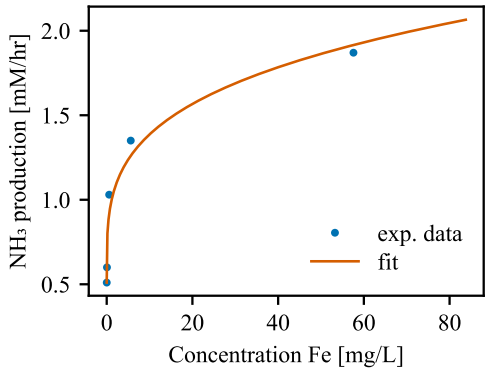

Figure 7.2: NH_3 production in the degradation experiments by Goff as a function of dissolved iron (Fe^{2+}/Fe^{3+}).

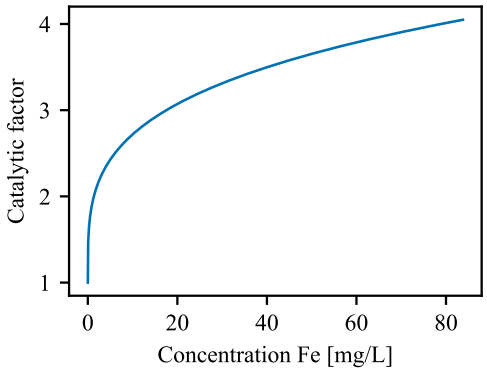

Figure 7.3: The catalytic factor, the increase in degradation rate, as a function of dissolved iron concentration.

7.2 Effect of Iron Concentration on Degradation in the Process

The effect of dissolved iron on the degradation rate in the coal-fired power plant flue gas capture case is shown in Figure 7.4. The coal-fired power plant case shown here is the same as discussed in section 4.3.4. Degradation in the stripper, which is caused by thermal degradation, is not influenced by iron and remains constant. A steep increase in degradation in the absorber packing is observed from around 50 g MEA/ton CO_2 without iron to around 160 g MEA/ton CO_2 at a concentration of 50 mg/L. As the solvent is assumed to be saturated with O_2 in the absorber packing, the degradation rate in the absorber packing closely resembles the ammonia evolution profile as a function of dissolved iron by Goff[17] in Figure 7.2.

The effect of dissolved iron on the solubility of O_2 is assumed to be negligible, and therefore the solubility in the absorber sump remains unchanged. As a result, the contribution of indirect oxidative degradation is constant. However, as the degradation rate increases due to the presence of iron, more degradation occurs in the absorber sump, and less dissolved O_2 is present in the heat exchanger. This shows that mitigation methods aimed at removing dissolved O_2 may become less effective as the concentration

of iron increases. The residence time of the solvent from the last contact with the flue gas until dissolved O_2 removal must therefore be limited.

7.2.1 Mass Transfer Limitations in the Absorber Packing

At increased reaction rates resulting from the iron catalysis, mass transfer limitations may occur in the structured packing despite its good mass transfer efficiency. In this case, a gradient appears between the liquid concentration at the interface and in the bulk, resulting in a lower oxidative degradation rate. To evaluate the impact of these limitations on the degradation rates, the mass transfer coefficients have been estimated for the structured packing in the absorber using the correlation by Billet and Schultes[18]. Mellapak 250Y by Sulzer was selected for this work. The packing-specific constants C_L and C_V are not specified in the original work by Billet and Schultes[18], but were taken from the work by Derichsweiler[19], in which the default constants were retrieved from ProMax and were found to be 0.992 and 0.337, respectively.

The effect of these liquid phase mass transfer limitations on the expected overall degradation rate is shown in Figure 7.5. Initially, with no iron present, the oxidative degradation rate in the absorber packing is low, and dissolved O_2 that is consumed by the degradation reaction is readily replenished from the gas phase. As a result, the concentration of dissolved O_2 is calculated to be close to the saturation concentration. As the concentration of iron increases and the degradation is accelerated, liquid phase mass transfer resistances of O_2 start to play a role. At a concentration of 50 mg/L, the overall degradation rate in the process may be overestimated by around 11% in case mass transfer limitations in the absorber are neglected. This is around 12.5% of the degradation in the absorber.

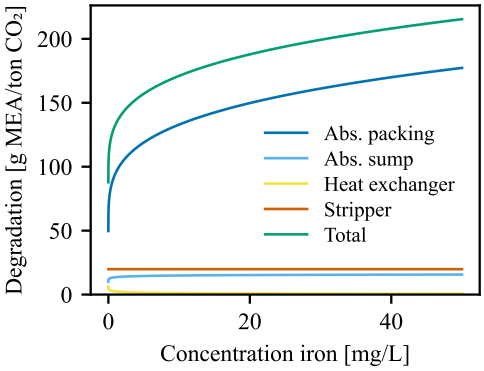

Figure 7.4: Degradation in the coal-fired power plant capture case as a function of dissolved iron concentration. Solvent in the absorber packing is assumed to be saturated with O_2.

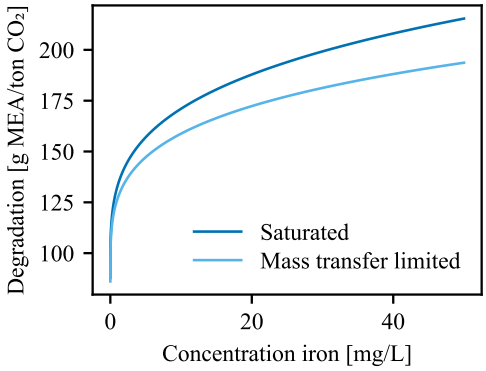

Figure 7.5: Degradation in the coal-fired power plant capture case as a function of dissolved iron, with and without mass transfer limitation in the absorber packing.

7.3 Dynamic Campaign Scenarios

Given the complex behavior in capture plants concerning catalyzed degradation, corrosion of equipment, and the solubility of metals combined with a limited understanding of their fundamental mechanisms, it is challenging to develop an accurate predictive model. Therefore, this section aims to model and investigate the dynamic behavior in a capture plant based on three hypothetical scenarios. A brief description of the investigated scenarios is given below and a more detailed discussion is given in the corresponding sections. The scenarios consider the coal-fired power plant capture process with a 30 wt% MEA solvent as discussed in section 4.3.4.

- Corrosion rate limited: the concentration of iron in the solvent is controlled by the overall corrosion rate, which is proportional to the concentration of degradation products.
- Iron solubility limited: the concentration of iron is controlled by the solubility of iron in the solvent, which is a function of the concentration of degradation products.
- Mass transfer limited: the concentration of iron in the solvent is not limited by the solubility, and the catalytic effect of iron is assumed to be linearly proportional to its concentration. Significant degradation occurs in the absorber, and mass transfer of O_2 is rate limiting.

The dynamic behavior of the scenarios is compared to typical observations in the pilot campaigns. Operation is stable initially, and the concentrations of dissolved metals and degradation products are low and increase steadily. After stable operation for some time, there is a deflection point after which the degradation rate and the concentrations of dissolved metals and degradation products start to increase exponentially. In the RWE campaign at Niederaussem[9], this deflection point occurs after around 200 days of operation, around 38 days in EnBW's campaign at Heilbronn[12], around 23 days during the campaign at Loy Yang[14,20], and around 108 days in the campaign at TNO[14].

Solvent degradation rates are determined by Moser et al. during the campaign at Niederaussem[9]. The initial solvent degradation rate was around 210 g MEA/ton CO_2. After 328 days of operation, right before the solvent was partially replaced and reclaiming was performed, the average degradation rate over the entire campaign was 660 g MEA/ton CO_2. Given the exponential profile of some of the degradation products, the degradation rate at the end of the campaign is expected to be higher than the average.

7.3.1 Scenario 1: Corrosion Rate Limited

In this scenario, the concentration of dissolved iron is governed by the rate at which iron is leached from metallic equipment in the plant. Dhingra et al.[14] proposed and investigated an auto-catalytic oxidative degradation mechanism, where products that are formed as a result of solvent degradation, for example, organic acids, cause the solvent

to become more corrosive. As a result, the corrosion rates and concentration of iron increase, leading to more degradation.

Although carbon steel can be used, the construction of some of the process equipment, parts exposed to rich solvents and/or high temperatures, such as the lean/rich heat exchanger and the stripper reboiler, are generally made from stainless steels to prevent excessive corrosion[21,22]. For this scenario, the equipment in the plant is considered to be made out of SS316, so a single expression can be used to describe the corrosion rates in the process.

7.3.1.1 Experimental Data on Corrosion Rates

Experimental data from literature is used to describe and model the corrosion rate in the process. Corrosion rates of metals in amine solutions are typically studied in lab-scale setups or in-situ in pilot plant campaigns. Lab-scale experiments, including electrochemical measurements and weight loss methods, are typically applied as screening tools and provide limited information on the impact of degradation products and flue gas impurities. Furthermore, it can be challenging to adequately replicate process conditions in the laboratory, for example, simulating high temperatures or conditions during plant stoppages.[11]

Most lab-scale corrosion experiments with 30 wt% MEA solutions investigate the corrosion resistance of carbon steels[23–26], as these are generally more prone to corrode than stainless steels. However, some works regarding the corrosion resistance of stainless steels are available in the literature. Stergioudi et al.[27] evaluated the corrosion behavior of SS304L and SS316L in 30 wt% MEA solutions as a function of the CO_2 loading and the solution temperature. The authors used electrochemical techniques, such as polarization curves, to determine the corrosion rates of the metals. The observed corrosion rates were notably higher than typical values obtained from coupon testing[24,28,29], but the authors did not offer any comparative analysis with other findings. The absence of O_2 in the reactor might hinder the formation of a stable passivation layer on the stainless steel, which could explain the elevated corrosion rates.

Tanthapanichakoon and Veawab[30] studied the influence of various common HSS on the corrosion rates of CS1018 and SS304 using electrochemical methods. The study revealed that the presence of HSS increased the corrosiveness of CS1018, and this increase was directly proportional to the concentration of these salts. In the case of SS304, the influence of HSS on corrosion was observed, although it was relatively limited and challenging to quantify. The results suggest that the presence of HSS does not compromise the corrosion resistance of stainless steel, but it may affect the total amount of metal leached by the solvent.

Corrosion rates were also measured in closed batch cylinders with 30 wt% MEA at stripper temperatures by Fytianos et al.[31] and Fisher[32]. Fytianos et al.[31] used ICP-MS to measure dissolved metal concentrations and concluded that the addition of some

degradation products increased solution corrosivity. However, the concentrations of iron, upon which the conclusions were drawn, remained stable over the course of the experiment, indicating potential solubility limitations. On the other hand, the nickel concentration increased linearly over time and it exhibited similar behavior under all conditions, regardless of the presence of degradation products. Fisher[32] quantified corrosion rates based on the weight loss of the cylinders during the experiment. Strikingly, carbon steel outperformed stainless SS316L in these experiments, and the author argued that the stagnant conditions in these experiments were not representative of the actual process.

Despite lab-scale experimental data is often preferable for model development due to well-controlled and steady conditions, the conditions in the experimental setups are not representative of those found in the process. Therefore, it will be challenging to accurately predict the corrosion rates of stainless steel in the process just using the lab-scale study results. Corrosion coupon studies in pilot plants may offer a better insight into the corrosion rates of stainless steel, despite occasional stoppages and fluctuations in process conditions.

Fischer[32] measured the weight loss of SS316L coupons also during the 2017 NCCC capture campaign with 30 wt% MEA. Coupons were installed at two locations in the absorber and at one location in the stripper sump. The corrosion rate of the stainless steel was measured in the range of 0-0.3 µm/yr in the absorber and 0.2-0.6 µm/yr in the stripper. Additionally, Hjelmaas et al.[29] studied the corrosion resistance of SS316L using coupons in the 2015 test campaign in the TCM DA Amine Plant in Mongstad. The results indicate acceptable levels of corrosion for the stainless steel but do not provide precise corrosion rates below 100 µm/yr likely because of uncertainties at lower concentrations.

Cousins et al.[28] performed a coupon corrosion study in the Tarong CO_2 capture pilot plant working with a coal-fired power plant flue gas. Coupons of various metals, including SS316L and SS316LW, were installed in 8 different locations in the plant, of which 5 in the absorber and 3 in the stripper. At each location, 3 coupons of the same metal were installed to assess the experimental variance. The plant was operated using 30 wt% MEA, and the coupons were exposed for 745 h. The average conditions over this period, such as temperature and CO_2 loading of the solvent, were reported for the locations. Weight analysis of the SS316L coupons shows that the corrosion rate is approximately 0.5 µm/yr to 3.0 µm/yr.

The observed corrosion rates in the Tarong pilot plant agree with those reported in the campaigns at NCCC and TCM. Given the comprehension of the corrosion study by Cousins et al.[28], it has been selected to model corrosion rates for SS316L as a function of temperature and CO_2 loading.

7.3.1.2 Modeling Approach

The corrosion rate prediction model is based on the multi-step approach by Roij et al.[21], in which the corrosion rate is initially estimated using isocorrosion curves. This initial estimate is then adjusted by applying a set of correction factors that account for the influences of temperature, CO_2 loading, wall shear stress, and impurities. The corrosion rates obtained from the Tarong pilot plant coupon campaign already include data regarding temperature and CO_2 loading. Additionally, the wall shear stress effects observed around the coupons can be considered representative for other equipment within the plant. As a result, only a correction factor for the impurities, degradation products in this case, has to be considered. A more detailed discussion regarding the determination of this correction factor is given in section 7.3.1.5.

An expression for the corrosion rate as a function of temperature and CO_2 loading can be developed, although some challenges remain. Replicates at each location revealed significant experimental uncertainty, and the observed trends regarding CO_2 loading and temperature are not convincing. A significantly higher corrosion rate is only observed near the bottom of the stripper. In addition, the data is correlated with loading and temperature, as high temperatures are linked with lower CO_2 loadings.

Due to these issues, it is challenging to create an accurate model that captures the actual corrosion mechanism. Therefore, a simple model with linear dependencies on both temperature and loading has been fitted, resulting in predictions resembling those of linear interpolation. It is important to note that linear behavior is not necessarily expected as experimental studies have identified an exponential relationship between the temperature and corrosion rate[27,33]. The regressed rate equation is given in Eq. 7.2. The corrosion rate is given in µm/yr, the temperature (T) in K, and the CO_2 loading (α) in mol CO_2/mol MEA. The corrosion rate in µm/yr can be expressed in mol/m^2/s using equation Eq. 7.3. Here f_{FE} represents the weight fraction of iron in stainless steel, typically 0.665 for SS316.

$$R_{C,\mu m} = -1.8 + 0.013\,T - 3.45\,\alpha \qquad \text{Eq. 7.2}$$

$$R_{C,\text{coupon}} = R_{C,\mu m} \cdot 10^{-6}\,\frac{m}{\mu m} \cdot \frac{1}{3600 \cdot 8766}\,\frac{yr}{s} \cdot \frac{\rho_{SS316}}{M_{W,SS316}} \cdot f_{FE} \qquad \text{Eq. 7.3}$$

7.3.1.3 Exposed Surface Area

The surface area exposed to the solvent is determined using characteristic lengths and areas for the equipment. The exposed surface area of the structured packings in the absorber and stripper columns is not expected to be equal to the interfacial area of the packing since complete wetting of the packing is likely not achieved. Therefore, the

exposed surface area is assumed to be equal to the apparent interfacial area. This area represents the actual contact area between the gas and liquid phases and is estimated using the correlation by Billet and Schultes[34] .

Since a plate heat exchanger is used to exchange heat between the rich and lean solvent flows, the exposed metallic surface area is assumed to be equal to twice the exchange area in the exchanger because each plate is exposed on both the lean and rich sides. The surface area in the reboiler has been estimated by roughly approximating the heat transfer area using the energy duty, an approach temperature of 10 °C, and an overall heat transfer coefficient of 3000 W/m^2/K[35]. Depending on the process and available heat sources, the reboiler design may differ.

7.3.1.4 Corrosion Rates in the Process

Using the corrosion model in Eq. 7.2 and the corrosion contact area estimates, the corrosion rates in the coal-fired base case capture plant can be evaluated. An overview of the distribution of corrosion is shown in Figure 7.6. Most iron is predicted to originate from the columns, and in particular, the structured packing. Most of the remaining iron originates from the heat exchanger.

Although temperatures are higher in the stripper and higher corrosion rates are expected, the absolute amount of corrosion in the stripper is lower than in the absorber. Figure 7.7 shows the predicted corrosion rate in both columns as a function of the packing depth. Corrosion rates in the stripper are generally higher, except at the top of the packing, where the stripper temperatures are low. However, a smaller overall surface area is exposed to the solvent in the stripper because the column diameter and packing height are smaller than those of the absorber column.

The total rate in the plant is predicted to be around 6.4 mg Fe/L/day. This rate is significantly larger than those observed in pilot plants. Cousins et al.[28] reported an iron

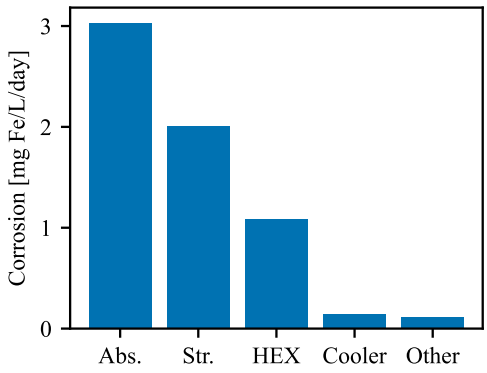

Figure 7.6: Predicted corrosion rates of iron in mg of iron per liter of solvent in various parts of the process.

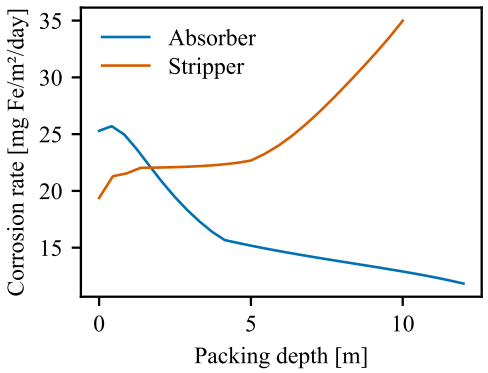

Figure 7.7: Predicted corrosion rates in the absorber and stripper packing as a function of the packing depth.

concentration of 1.5 mg/L of solvent after approximately 7 days of operation in the Tarong CO_2 capture pilot plant. Iron concentrations of around 60 mg/L were observed by Moser et al.[9] in the Niederaussem pilot capture plant after 300 days of operation. The solvent inventory in the pilot plants may have been relatively large to offer enough flexibility for running case studies, but even in this case, the model over-predicts the concentration of iron in the solvent significantly. It is also a possibility that the corrosion coupons were installed in locations with above-average exposure conditions, which resulted in relatively high corrosion rates.

Given that the simulated process is a pilot scale capture plant, the corrosion rate in a full-scale plant may be lower if the solvent holdup volumes scale faster with size than the surface areas of the equipment. However, this effect is expected to be limited since most of the corrosion is predicted to occur in the structured packings. The surface area exposed to the solvent in these packings should be proportional to the solvent flow rate.

7.3.1.5 Modeling the Influence of Degradation Products

The corrosion model, derived from the coupon results by Cousins et al.[28], reflects the average corrosion rate throughout the entire campaign. However, the hypothesis for this scenario suggests that corrosion rates will be initially low, gradually increasing as degradation products are formed. As the corrosion rates cannot be measured during the campaign, their dependency on the concentration of degradation products is unknown. For this reason, several dependencies are investigated to see if observations in pilot plant campaigns can be explained.

As HSS, such as organic acid degradation products, are considered to have the largest influence on the corrosivity[27], it is assumed only these affect the corrosion rates, and other degradation products are assumed to have no effect. The oxidative degradation model for MEA that is used in this work accounts for the depletion of MEA and dissolved O_2 but does not predict the rates of degradation compound formation. The complex nature of oxidative degradation mechanisms makes such predictions challenging. Therefore, we rely on experimental degradation data to estimate the formation rate of HSS. In the absence of flue gas impurities, the primary sources of HSS are the organic acids formed during oxidative degradation.

An analysis conducted by Vevelstad et al.[36] on the degraded solvent revealed that the identified organic acids, including formic and oxalic acid, constituted approximately 10% of the molar equivalent of degraded MEA in the experiment conducted at 65 °C and with an O_2 concentration of 21 vol-%. Similar stoichiometric ratios were reported by Sexton et al.[5] and da Silva et al.[37]. Therefore, this work assumes that 10% of the degraded MEA is converted into HSS. Given that formic acid is the most prevalent organic acid, the molar mass of formic acid is used to convert the molar concentration of HSS into weight fractions. This work does not include flue gas impurities, such as

SO_2 and NO_x, which could also lead to the formation of HSS and increase the corrosivity of the solvent.

To predict the corrosion rate of SS316 as a function of the concentration of HSS, Eq. 7.4 is proposed. The predicted corrosion rate that is based on the average coupon results ($R_{C,\text{coupon}}$) is multiplied with a correction factor (f_{HSS}). Given that the corrosion rate of the coupons is the average rate, a lower rate is expected for a clean solvent, and an above-average rate is expected for the degraded solvent. Optimally, the dependency of the correction factor on the concentration of HSS would be tuned such that the cumulative corrosion during the campaign matches the final weight loss of the corrosion coupons. However, since the concentration of HSS is only reported for the solvent at the end of the campaign, respectively 0.44 wt%[28], it is not possible to get an overview of the state of degradation of the solvent during the campaign. Therefore, it is assumed that the production rate of HSS is constant and its concentration will increase linearly. This assumption will be checked and discussed together with the results.

$$R_{C,\text{HSS}} = R_{C,\text{coupon}} \cdot f_{\text{HSS}} \qquad \text{Eq. 7.4}$$

$$f_{\text{HSS}} = a \cdot c_{\text{HSS}}^{n} + b \qquad \text{Eq. 7.5}$$

The HSS correction factor f_{HSS} is described by Eq. 7.5. Here n is the order that describes the dependency of the rate on the degradation products, a is a scaling factor, and b is the offset. The correction factor is assumed to be independent of other process conditions, such as temperature and CO_2 loading. Since no corrosion rate data is available for SS316 in the absence of degradation products, the initial corrosion rate is assumed to be negligible and the offset b is set to 0. This assumption maximizes the effect the

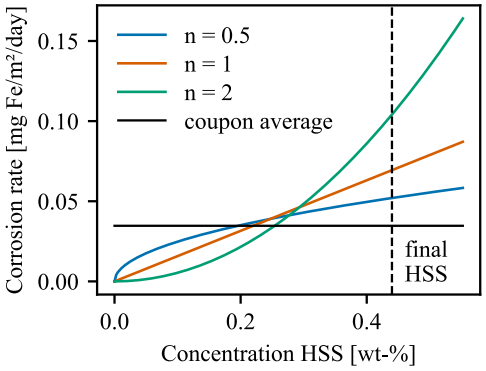

Figure 7.8: Predicted corrosion rates as a function of HSS concentration for SS316 for various orders (n) at 100 °C and a CO_2 loading of 0.2.

concentration of HSS has on the corrosion rate and should show a similar effect to those observed in pilot plants if the hypothesis of a corrosion rate-limited mechanism is correct. Next, for each investigated corrosion order, the scaling factor (a) is adjusted to ensure the average value for the correction factor over the HSS concentration range (0 – 0.44 wt-%) is equal to 1

The corrosion rates for the various corrosion orders (n) as a function of the concentration of HSS are given in Figure 7.8. When the corrosion order is larger than unity, the corrosion rate will be low when the concentration of HSS is low but it increases significantly as more HSS are formed. The area under each of the graphs from 0 to 0.44 wt-% is the same for every corrosion order and averages out at the corrosion rate based on the coupon results.

7.3.1.6 Dynamic Impact of Corrosion Rates

The degradation rate as a function of the campaign time is shown in Figure 7.9. The predicted degradation rates are significantly lower than those observed in the capture campaign at Niederaussem[9]. Consequently, the predicted concentration of degradation products is also lower than typically observed for capture campaigns with similar durations.

Initially, no dissolved iron is present and the degradation rate for each of the corrosion orders is similar. As degradation products are formed, corrosion begins to occur as shown in Figure 7.10. The corrosion rate of the case with corrosion order 0.5 shows a stronger initial reaction in the presence of degradation products. As a result, the concentration of dissolved iron (as shown in Figure 7.11) increased rapidly from the start of the campaign. This causes the oxidative degradation rate to increase and leads to more degradation in the absorber and in the overall plant. After around 500 h of operation, the additional iron that is dissolved into the solvent causes a smaller increase in the degradation rate, which starts to flatten out.

For the models with a higher corrosion order, the presence of the initial degradation products has a less pronounced effect on the corrosion rate and concentration of dissolved iron in the solvent. Therefore, more time is required before the degradation rates increase. However, the relative difference in degradation rate between the different corrosion order models is limited. For this reason, the concentrations of HSS are similar during the course of the campaign, as shown in Figure 7.12. The concentration profiles of the HSS are close to linear, which validates the assumption made in the model in section 7.3.1.5. These linear HSS concentration profiles do not correspond well with the observations in the pilots, where the concentration of degradation products only started to increase significantly when the concentration of dissolved iron also started to rise.

The steady increase in the concentration of dissolved iron for the cases with a corrosion order of 0.5 and 1 does also not correspond with observations in the pilots. Only the case with a corrosion order of 2 shows a mild deflection point after around 42 days of

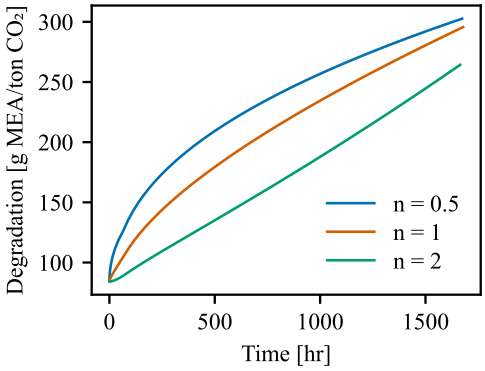

Figure 7.9: Predicted degradation rate over the course of the campaign for the different corrosion orders (n).

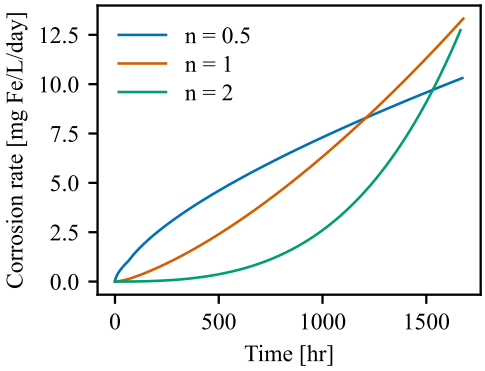

Figure 7.10: Predicted corrosion rate over the course of the campaign for the different corrosion orders (n).

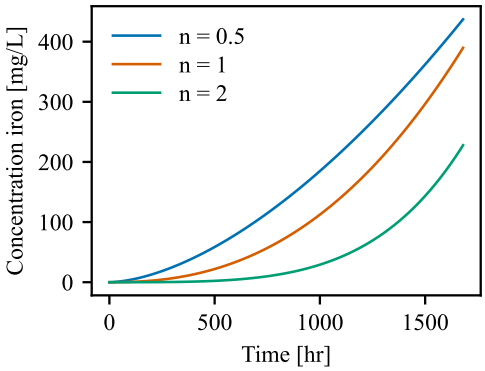

Figure 7.11: Predicted concentration of dissolved iron over the course of the campaign for the different corrosion orders (n).

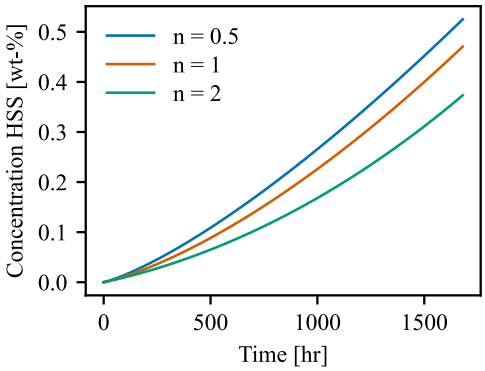

Figure 7.12: Predicted concentration of HSS over the course of the campaign for different degradation product orders (n).

operation. For this scenario to be viable, a high corrosion order would be required, meaning corrosion rates remain low initially and start to increase significantly once a certain threshold concentration of HSS has been reached. This could perhaps be explained by the change in sensitivity of the pH at different concentrations of HSS.

7.3.2 Scenario 2: Iron Solubility Limited

This scenario considers the potential corrosion rates in the plant to be significant but limits the concentration of dissolved iron based on its solubility in the solvent. Iron may precipitate in sections where the solubility of the solvent is limited. As the concentration of degradation products and HSS starts to increase due to flue gas impurities or solvent degradation, these components may act as chelating agents for iron. The products form a complex with dissolved iron, increasing the iron solubility[38]. The formation of the iron

complexes may reduce the catalytic activity of the metal for some chelates, thereby inhibiting degradation[39,40]. However, this effect is not considered in this case study. The coal-fired power plant capture process with a 30 wt% MEA solvent is also used to study this scenario.

7.3.2.1 Experimental Data on Iron Solubility

Fytianos et al.[41] studied the solubility of ferrous in several amine solvents, including MEA. Known quantities of $FeSO_4$ were gradually introduced into a stirred batch reactor containing the solvent at regulated temperatures between 25 °C and 60 °C. Samples were taken over the course of 72 h and analyzed using a spectrophotometer. The solubility of ferrous at 25 °C in MEA was found to be approximately 130 mg/L and decreased with an increase in temperature down to around 30 mg/L at 60 °C. The ferrous solubility was also measured at 40 °C in a synthetically, oxidatively degraded solution of MEA and an increase in solubility of approximately 1.5X was observed.

Fischer[32] performed solubility measurements comparable to those by Fytianos et al.[41]. Key differences were the duration of the experiments (up to 400 h) and the addition of Na_2CO_3 to facilitate the carbonate for the expected $FeCO_3$ precipitation. Concentrations were analyzed with ICP optical emission spectroscopy. Although the solubility concentrations obtained by Fischer[32] differed significantly, similar trends were observed with respect to temperature to those by Fytianos et al.[41]. The solubility of ferrous in MEA was found to be 780 mg/L at 25 °C and 8.4 mg/L at 60 °C. Fischer[32] also measured the solubility of Fe^{2+} in piperazine solvents that were degraded in the Separations Research Program pilot plant and the Tarong pilot plant. The solubility was observed to be 10-100X higher than in the clean solvent. The author suggests that amine degradation products can form complexes with iron, thereby increasing its solubility.

The experimentally determined solubility of iron is significantly higher than the concentrations typically observed in pilot plant campaigns. These high solubility limits should not restrict the dissolution of iron into the solvent, and the concentration of iron should be controlled by the corrosion rate. In case the solubility limit is reached, the concentration of iron is high and only a negligible change in degradation rate is observed according to the experimental data by Goff[17]. Consider two theories that can explain the discrepancy between experimental and pilot plant results.

Firstly, both experimental works indicate that the solubility of iron is negatively correlated with temperature but do not measure the solubility at temperatures above 60 °C. The log-transformed solubility appears to exhibit a linear relationship with temperature. When extrapolating up to 120 °C, the temperature typically expected in the stripper, the predicted solubilities are approximately 3.5 mg/L and $7.8 \cdot 10^{-3}$ mg/L for the data by Fytianos et al.[41] and Fischer[32], respectively. Even though the solubility of iron is higher in other parts of the plant, precipitation in the stripper may cause the effective

solubility of iron to be lower. Solubility experiments at increased temperatures could be performed to investigate this.

Secondly, recent in-house experiences indicate that the solubilities are significantly lower than predicted by Fytianos et al.[41] and Fischer[32]. The dissolution of 0.5 mM $FeSO_4$ (±28 mg/L) in a clean 30 wt-% MEA solvent for oxidative degradation experiments was challenging, and solid particles often remained suspended until the solvent started to degrade. Furthermore, recent experimental work on iron solubility by Stensås[42] showed significantly lower iron concentrations that were more in line with the observations in the pilot. Additionally, recent data from similar in-house solubility tests on synthetical, oxidatively degraded MEA showed an iron solubility of around 230 mg/L. At this point, 0.3 mol/L of the initial MEA had been degraded. Assuming a 10% conversion into HSS, as discussed in section 7.3.1.5, this equals an HSS concentration of 30 mol/m^3.

To investigate the effects of a solubility-limited system, several assumptions are made. The solubility in the initial solvent is low, starting at 1.0 mg/L, and increases with the concentration of degradation products. Similar to the corrosion limited scenario, several solubility orders will be evaluated to test the different dependencies using Eq. 7.6. Here n is the solubility order, b is the offset (1 mg/L), and a is the scaling factor that is adjusted to ensure the solubility at an HSS concentration of 30 mol/m^3, which is 230 mg/L.

$$c_{\mathrm{sol}} = a \cdot c_{\mathrm{HSS}}^{n} + b \qquad \text{Eq. 7.6}$$

Initially, the concentration of iron is dictated by the corrosion rate in the system. This rate is determined using Eq. 7.2, which describes the average corrosion rates according to the weight loss on the corrosion coupons by Cousins et al.[28]. When the solubility limit of the iron is reached, its concentration is now dictated by Eq. 7.6. The iron solubility is modeled to be independent of temperature. The solubility of iron as a function of the HSS concentration for the different solubility order cases is given in Figure 7.13.

7.3.2.2 Dynamic Impact of Iron Solubility

The predicted overall degradation rate in the process is shown in Figure 7.14. At the start of the campaign, the corrosion causes the concentration of iron to increase up to 1.0 mg/L, which is the initial solubility limit of the clean solvent. As a result, oxidative degradation is catalyzed, and the overall degradation rate increases to around 130 g MEA/ton CO_2. This rapid increase may partially explain the difference between the initial degradation rates in the Niederaussem pilot plant and those predicted by the degradation model in the absence of iron in section 5.1.1. Contamination of the solvent with a limited amount of iron may already significantly catalyze oxidative degradation.

As the solvent degrades and the iron solubility increases, it is no longer saturated with iron, and the corrosion rate becomes limiting. This transition is illustrated in Figure 7.15,

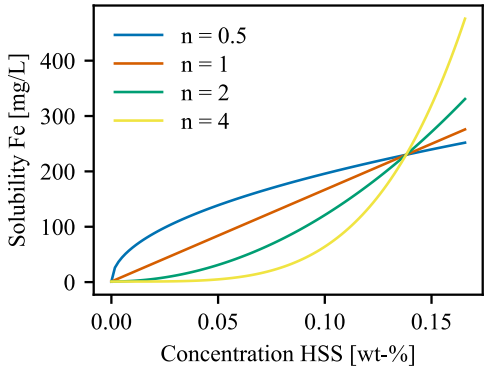

Figure 7.13: Predicted iron solubilities as a function of HSS concentration for various solubility orders (n).

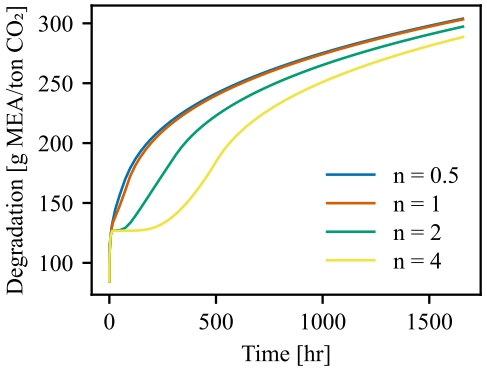

Figure 7.14: Predicted degradation rate over the course of the campaign for the different solubility orders (n).

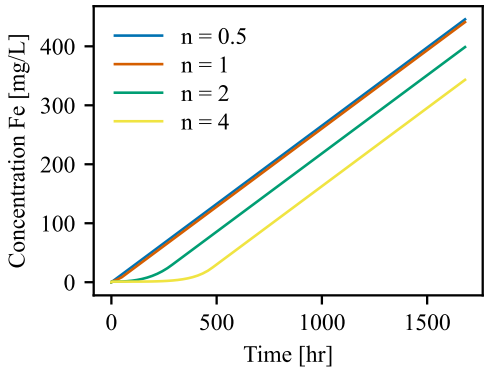

Figure 7.15: Predicted concentration of dissolved iron over the course of the campaign for the different solubility orders (n).

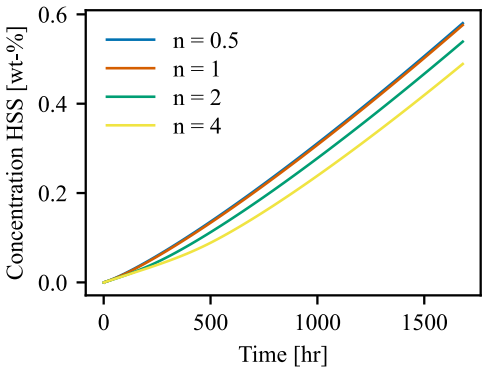

Figure 7.16: Predicted concentration of HSS over the course of the campaign for the different solubility orders (n).

where the increase in iron concentration is constant and the order case profiles are parallel after 500 hours of operation. In cases with a higher solubility order (e.g. $n = 4$), more degradation is required to increase the solubility limit, and the degradation rate is constant at the start of the campaign. For these cases, the sudden increase in iron concentration and degradation rate corresponds well with the observations in pilot plants. However, the following linear increase in iron concentration deviates from pilot observations.

Similarly, the linear concentration profiles for HSS in Figure 7.16 do not correspond well since a similar sudden increase would be expected. The difference between the initial and final degradation rates remains limited, resulting in a relatively constant gradient for these HSS concentration curves. To achieve comparable profiles for the degradation products, a more significant increase in the degradation rate is required.

7.3.3 Scenario 3: Mass Transfer Limited

The scenarios discussed up until now appear to predict significantly lower degradation rates than typically observed in capture plants [9,12,43]. A reason for this could be an underestimation of the catalytic potential of the dissolved iron. The increase in NH_3 emissions with increasing iron concentrations in the experiments by Goff[17], which formed the basis for describing the catalytic effect in the current model, may not reflect the actual catalytic dependence. As discussed in more detail in section 6.1, mass transfer limitations are expected to be present in sparged reactors, especially when degradation is catalyzed. Goff arrived at a similar conclusion when discussing the experimental results [17].

When mass transfer resistances are present, the concentration of dissolved O_2 in the liquid bulk is expected to drop and, if not accounted for, this will cause the degradation rate to be underestimated. Without more details about the experimental setup and operating parameters, it is difficult to estimate and compensate for the mass transfer limitations. Therefore, this scenario assumes that there is a linear dependency between the concentration of dissolved iron and the degradation rate. Based on the initial increase in NH_3 evolution rate, assuming mass transfer effects were less prominent here, the increase in degradation rate is described using Eq. 7.7. Here, R_{cat} is the catalyzed degradation rate, R is the degradation rate as predicted by the oxidative degradation model without the presence of iron, and c_{Fe} is the concentration of iron in mol/m^3.

$$R_{cat} = R(1 + 17.0c_{Fe}) \qquad \text{Eq. 7.7}$$

There is insufficient data and knowledge on the mechanism behind the catalytic effect to either justify or challenge the assumption of the linear dependence of iron with respect to the degradation rate. Chi[3] as well as Voice and Rochelle[15] suggest dissolved metal ions decompose organic hydroperoxides that are formed due to the presence of O_2, resulting in the formation of free radicals that can degrade the amine. An overview of these mechanisms is shown in Figure 7.1. If the concentration of iron is increased significantly, the production of the hydroperoxides may become limiting, reducing the effect of additional iron on the degradation rate. In such a case, the linear dependency of the degradation rate on iron concentration no longer applies.

When applying Eq. 7.7, the degradation rate increases substantially, approximately by a factor of 16, at an iron concentration of 50 mg/L. At this point, the accelerated degradation rate may result in the depletion of dissolved O_2 within the liquid bulk, despite the efficient mass transfer in the structured packing. Mass transfer limitations can become a significant factor, similar to those observed in agitated bubble reactor experiments detailed in section 6.1. Consequently, the oxygen supply from the gas phase into the solvent becomes the determining factor for degradation rates. This phenomenon has also been discussed Goff et al.[4] and Closmann[44].

7.3.3.1 Mass Transfer Metrics

A pair of metrics will be introduced to quantify and understand the mass transfer behavior in the structured packing. The dimensionless Hatta number (Ha)[45] is used to describe the maximum possible conversion in the liquid transfer film per m^2 over the maximum possible flux through the transfer film (in absence of a reaction) and is given in Eq. 7.8. Here R_{O_2} is the reaction rate of O_2 in mol/m^3/s, δ_L the thickness of the mass transfer layer in m, D_{O_2} the diffusion coefficient of O_2 in the solvent in m^2/s, k_r the reaction rate coefficient in $(m^3/mol)^n$/s, $c_{O_2,i}$ the concentration of O_2 in the solvent at the interface in mol/m^3, and k_L the mass transfer coefficient on the liquid side in m/s. A Hatta number that is larger than unity indicates a fast reaction as compared to the mass transfer rate, where mass transfer is enhanced and the bulk concentration approaches zero.

A second metric is the Hinterland ratio (Hi), which describes the ratio between the total solvent volume over the solvent volume in the mass transfer film at a location in the packing. The Hinterland ratio is given by Eq. 7.9, where V_L is the liquid volume in m^3, a_{int} the interfacial area in m^2/m^3, and V_{tot} the total volume that corresponds with the convention for the interfacial area. For cases where the Hatta number is small and the reaction primarily occurs in the bulk, the conversion capacity of the bulk can be evaluated by multiplying the ratio between the liquid volume in the bulk over the liquid volume in the film $(Hi-1)$ with Ha^2. A high result for $(Hi-1)Ha^2$ indicates sufficient bulk capacity and mass transfer limitations, whereas a result well below unity indicates the bulk is saturated with O_2.

$$Ha^2 = \frac{R_{O_2}\delta_L}{\frac{D_{O_2}}{\delta_L}\left(c_{O_2,i}-0\right)} = \frac{1.3k_r c_{MEA} c_{O_2,i}^n D_{O_2}}{k_L^2 c_{O_2,i}} \qquad \text{Eq. 7.8}$$

$$Hi = \frac{V_{L,\text{tot}}}{V_{L,\text{film}}} = 1 + \frac{V_{L,\text{bulk}}}{V_{L,\text{film}}} = 1 + \frac{V_{L,\text{bulk}} k_L}{V_{\text{tot}} a_{\text{int}} D_{O_2}} \qquad \text{Eq. 7.9}$$

7.3.3.2 Results

The predicted degradation rates in the capture process are given in Figure 7.17 as a function of the concentration of dissolved iron. The extent of oxidative degradation in the absorber packing increases significantly and is responsible for most of the degradation in the process. While oxidative degradation rates in the absorber sump and heat exchanger also rise, the dissolved O_2 availability in the rich solvent and the extent of degradation remain constant. With increasing degradation rates, a higher consumption of dissolved O_2 occurs in the sump, leading to lower concentrations of dissolved O_2 in the heat exchanger.

Although the oxidative degradation rate was modeled to be linearly proportional to the concentration of iron in the solvent, the oxidative degradation in the absorber packing flattens out with increasing iron concentration. This effect arises due to mass transfer limitations and is illustrated by Figure 7.18, which shows the predicted O_2 concentrations at the interface and in the liquid bulk at the temperature peak in the absorber. Due to the temperature effect on the reaction kinetics, mass transfer limitations are expected to be most prominent at this point in the absorber. Initially, the dissolved O_2 concentration in the liquid bulk closely mirrors the concentration at the interface, which is assumed to be in equilibrium with the gas phase. However, as iron concentration increases, a growing gradient emerges between these concentrations, indicating the growing significance of mass transfer limitations.

Although the reaction rate increases, the degree of reaction in the film remains limited as can be seen by the Hatta number at the temperature peak in Figure 7.19. The mass transfer capacity prevails over the reaction capacity in the liquid film, thereby limiting the potential for enhanced mass transfer due to O_2 consumption in the film. However, as the concentration of iron and degradation rate continue to rise, mass transfer enhancement is expected to become increasingly influential. The $(Hi - 1)Ha^2$ metric is shown in Figure 7.20 and illustrates the transition from a reaction rate limited (<< 1) to a mass transfer limited (>> 1) system.

The predicted degradation rates in the process are significantly higher than those predicted in the other scenarios and are more in line with observations in pilot plants. Moser et al.[9] quantified the amine loss by degradation in the lignite-fired power plant capture pilot at Niederaussem and found a rate of 210 g MEA/ton CO_2 at the start of the campaign, which increased to an average of 660 g MEA/ton CO_2. The concentration of dissolved iron was measured to be around 62 mg/L before the solvent was replaced. Although the public availability of process data, such as the type of structured packing and the packing height of the absorber, is limited, the predictions correspond relatively well with observed degradation rates.

The rate of thermal degradation is not dependent on the concentration of dissolved iron and remains constant. As a result, the contribution of thermal degradation to the overall degradation decreases significantly as the concentration of iron increases. Although the overall degradation rate is more in line with observations in the pilot, the distribution of oxidative and thermal degradation may no longer correspond. To illustrate, da Silva et al.[37] found that thermal degradation accounts for approximately 20% of the overall degradation.

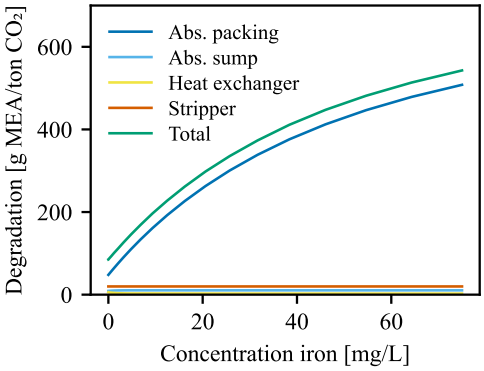

Figure 7.17: Degradation in the coal-fired power plant capture case as a function of dissolved iron concentration for the linear catalyzation profile.

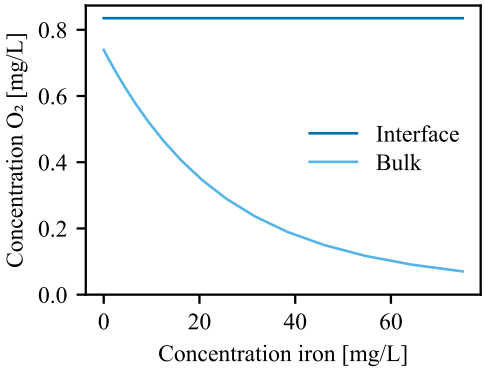

Figure 7.18: Concentration of dissolved O_2 at the interface and in the liquid bulk at the temperature peak in the absorber (at a depth of around 2 m).

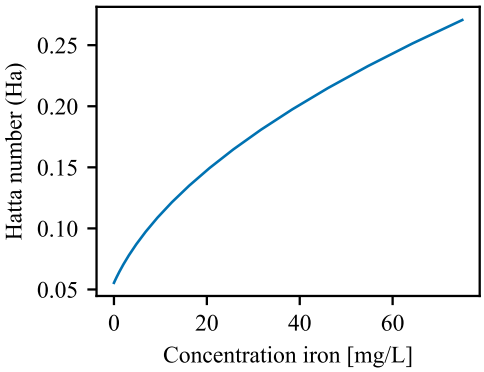

Figure 7.19: Hatta number at the temperature peak in the absorber (at a depth of around 2 m) as a function of the dissolved iron concentration.

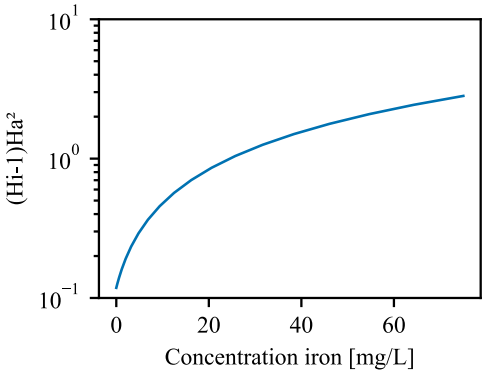

Figure 7.20: (Hi-1)Ha^2 metric at the temperature peak in the absorber (at a depth of around 2 m) as a function of the dissolved iron concentration.

7.3.3.3 Absorber Profiles

Figure 7.21 to Figure 7.24 show the mass transfer metrics in the absorber packing in the case with 75 mg/L of dissolved iron. The Hinterland ratio and volumetric mass transfer coefficient show a dependency on temperature, resulting in respectively a minimum and maximum around the temperature peak. The $(Hi-1)Ha^2$ metric changes significantly throughout the absorber column. The upper and lower segments, characterized by relatively low temperatures, are predominantly limited by reaction rate, while the remainder of the absorber packing is primarily constrained by mass transfer, which is also evident in Figure 7.25 and Figure 7.26.

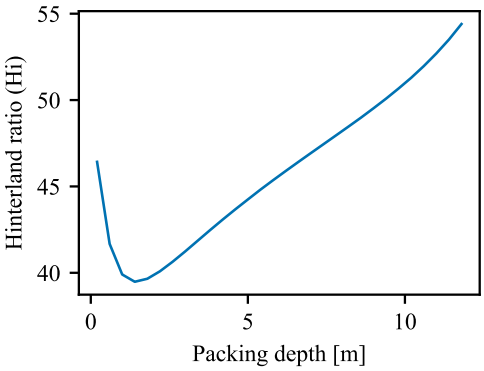

Figure 7.21: Hinterland ratio as a function of the absorber packing depth (not influenced by iron concentration).

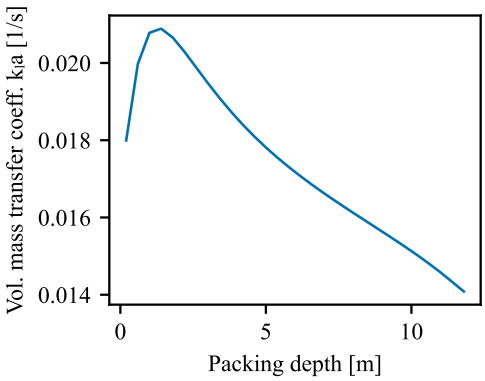

Figure 7.22: Volumetric mass transfer coefficient ($k_L a$) as a function of the absorber packing depth (not influenced by iron concentration).

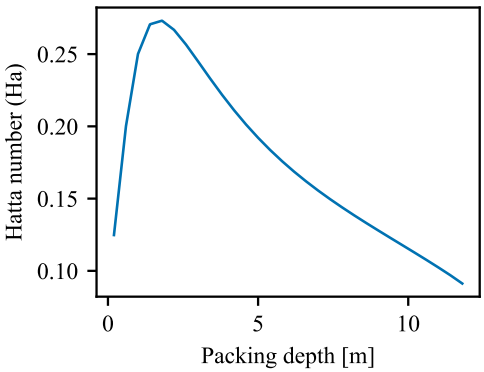

Figure 7.23: Hatta number as a function of the absorber packing depth at an iron concentration of 75 mg/L.

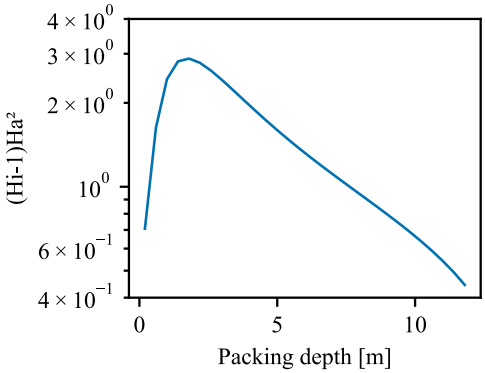

Figure 7.24: (Hi-1)Ha^2 metric as a function of the absorber packing depth at an iron concentration of 75 mg/L.

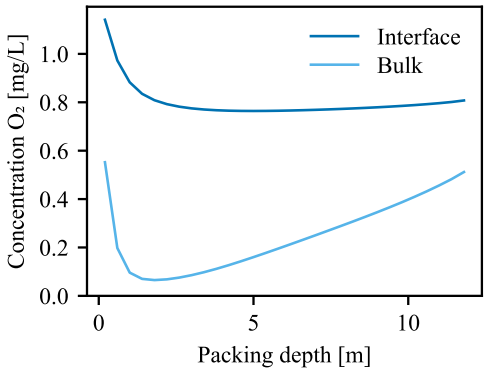

Figure 7.25: Concentration of dissolved O_2 at the interface and in the liquid bulk as a function of the absorber packing depth at an iron concentration of 75 mg/L.

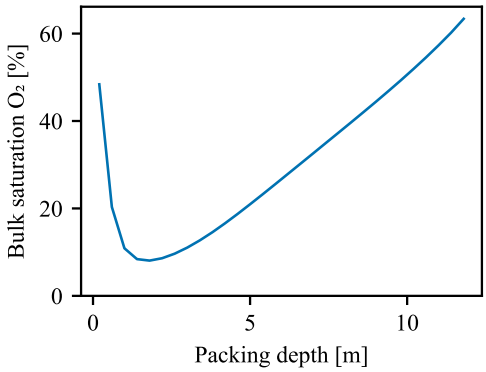

Figure 7.26: Liquid bulk O_2 saturation as a function of the absorber packing depth at an iron concentration of 75 mg/L.

7.4 Solvent Management and Reclaiming

To investigate the effectiveness of continuous reclaiming, a dynamic degradation model considering both scenarios 1 and 3 discussed in the previous sections is used. The corrosion rate is a function of the concentration of HSS in the solvent, and this dependency is described using a corrosion factor (n) of 2. The degradation rate is linearly proportional to the concentration of dissolved iron according to equation Eq. 7.7. Mass transfer effects in the structured packing in the absorber are accounted for and will limit degradation rates when high iron concentrations are present.

A continuous black-box reclaimer is modeled, which takes a solvent side stream and removes dissolved iron and degradation products, such as HSS. All iron is assumed to be removed, whereas a 5% carryover is taken for the degradation products. Overall, 95% of the MEA that enters the reclaimer, either free or part of a HSS is recovered. The turnover time is used to express the size of the side stream and denotes the time required for the entire plant solvent volume to pass through the reclaimer once. Operation with various turnover times has been investigated and the results are given in Figure 7.27 to Figure 7.30. A turnover time of 15 days is roughly equivalent to a 0.10% slip stream.

When the process is operated without continuous reclaiming, a deflection point is clearly visible after approximately 40 days. The corrosion rates and, consequently, the concentration of dissolved iron increase rapidly, resulting in significantly higher degradation rates and increased concentrations of HSS. The deflection point is more pronounced here than in scenario 1 (section 7.3.1) and corresponds well with the observed behavior in the pilot plants. The combination of HSS concentration-dependent corrosion rates and increased catalytic degradation rates may, therefore, give a good reflection of reality.

Continuous reclaiming reduces the degradation rates in the absorber both directly through the removal of dissolved iron and indirectly through the removal of HSS, which results in lower corrosion rates. When the turnover time is significant (50 or 30 days), the effect of reclaiming is visible, but a degradation run-away still occurs later in the campaign. Steady-state degradation appears only to occur when the turnover time is reduced to 10 days. At this point, the dissolution rates of iron and the production rates of HSS do not exceed the removal rates in the reclaimer. When the turnover time is increased (20 days), there seems to be no initial effect on the process dynamics. However, the imbalance in corrosion, degradation, and removal rates will eventually lead to a run-away.

With a turnover time of 50 h and a 95% MEA recovery in the reclaimer, around 1.2 kg MEA/ton CO_2 captured is lost in the reclaimer waste. This loss is proportional to the flow rate into the reclaimer and will be more significant at lower turnover times. Therefore, it is unlikely a short-term reduction in overall solvent loss is observed when the continuous reclaimer is active. The reclaiming will free some of the deactivated MEA

from the HSS and can keep the degradation rates in the process stable by removing products and dissolved metals.

The minimum turnover time needed for steady operation depends on the sensitivity of the corrosion rate on the concentration of HSS and the sensitivity of the degradation rate on the concentration of iron. Although similar trends are expected for real capture processes, the actual minimum turnover time is expected to deviate from the prediction in this case study. A good understanding and quantification of accelerated corrosion and catalytic degradation is required to determine these minimum reclaiming requirements.

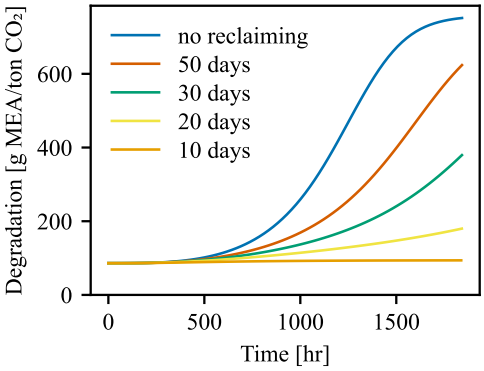

Figure 7.27: Predicted degradation rate in the capture process with continuous reclaiming, operated at varying turnover times.

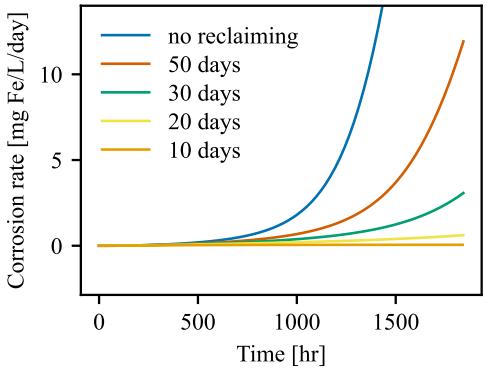

Figure 7.28: Predicted corrosion rate in the capture process with continuous reclaiming, operated at varying turnover times.

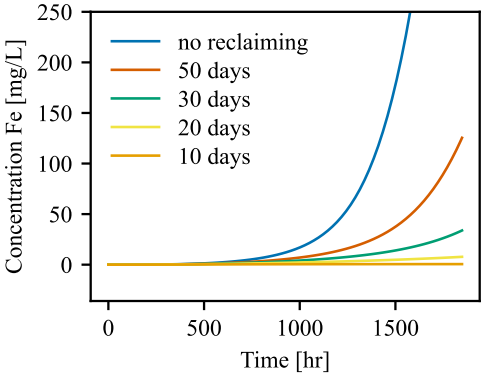

Figure 7.29: Predicted concentration of dissolved iron in the capture process with continuous reclaiming, operated at varying turnover times.

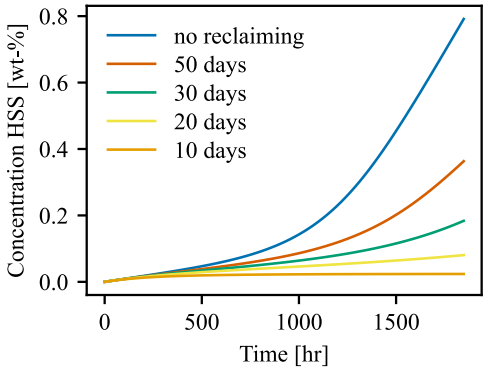

Figure 7.30: Predicted concentration of HSS in the capture process with continuous reclaiming, operated at varying turnover times.

7.5 Conclusions

It is unlikely that the corrosion rates limit the dissolution of iron into the solvent. Based on the corrosion rates determined by Cousins et al.[28] in the Tarong pilot plant based on corrosion coupon weight losses, the predicted average increase in iron concentration in a capture plant would be around 6.4 mg Fe/L/day, given that SS316 is used as a construction material. Despite the high observed corrosion rates, the concentration of dissolved iron remained around 1.0 mg/L in the solvent over the course of the campaign[28]. Furthermore, the predicted concentration profiles for HSS and dissolved iron do not have a clear deflection point and, therefore, do not correspond well with observations in pilot plants.

A low iron solubility in the fresh solvent could be an explanation for the stable and low concentration of dissolved iron in the Tarong pilot plant. The deflection point observed in other pilots could be explained by an increase in iron solubility, however, the order with respect to the concentration of HSS has to be large to obtain comparable profiles. Additional experimental research should be conducted to determine the solubility of metals at higher temperatures and in degraded solvents. Solvent from a capture plant would be preferred over an artificially degraded solvent as the composition of this solvent would be a better reflection of reality. The metal solubility should be measured as a function of solvent degradation or the concentration of several common degradation products.

When the degradation rate is assumed to continue to increase proportional to the concentration of dissolved iron, the degradation rates in the process become significant and come in the range of those observed in pilot plants. Mass transfer resistances for O_2 become more significant and begin to dictate degradation rates in the absorber packing. Due to the large increase in oxidative degradation, the contribution of thermal degradation to the overall degradation becomes negligible. This behavior is not observed in pilot plants, and the model, which is based on scenarios 1 and 3, may not fully represent the actual degradation mechanisms.

More detailed quantification of the catalytic effect of dissolved metals, in particular iron, should be a priority for further research since a better quantification of this relationship may result in a better understanding of the degradation rates and dynamics in the process. The high degradation rates that occur when iron is present lead to significant mass transfer limitations in the traditional sparged reactor experiments and accurate quantification of the degradation rates is challenging. Therefore, reactors that feature more intensive contact between the gas and liquid phases and substantially increase the available surface area per volume of solvent should be designed and used to quantify the catalytic effects of iron.

7.6 References

(1) Rooney, P. C.; Dupart, M. S.; et al. Oxygen's Role in Alkanolamine Degradation. *Hydrocarbon Processing* **1998**, *77*, 109–113.

(2) Bello, A.; Idem, R. O. Comprehensive Study of the Kinetics of the Oxidative Degradation of CO2 Loaded and Concentrated Aqueous Monoethanolamine (MEA) with and without Sodium Metavanadate during CO2 Absorption from Flue Gases. *Ind. Eng. Chem. Res.* **2006**, *45* (8), 2569–2579. https://doi.org/10.1021/ie050562x.

(3) Chi, S. Oxidative Degradation of Monoethanolamine. Thesis, University of Texas Austin, 2000.

(4) Goff, G. S.; Rochelle, G. T. Oxidation Inhibitors for Copper and Iron Catalyzed Degradation of Monoethanolamine in CO_2 Capture Processes. *Ind. Eng. Chem. Res.* **2006**, *45* (8), 2513–2521. https://doi.org/10.1021/ie0490031.

(5) Sexton, A. J.; Rochelle, G. T. Reaction Products from the Oxidative Degradation of Monoethanolamine. *Ind. Eng. Chem. Res.* **2011**, *50* (2), 667–673. https://doi.org/10.1021/ie901053s.

(6) Voice, Alexander K. Amine Oxidation in Carbon Dioxide Capture by Aqueous Scrubbing. Doctoral thesis, University of Texas Austin, 2013. https://sites.utexas.edu/rochelle/files/2015/02/Voice-2013-Amine-Oxidation-in-Carbon-Dioxide-Capture-by-Aqueous-Scrubbing.pdf.

(7) Sexton, A. J. Amine Oxidation in CO2 Capture Processes. Doctoral thesis, The University of Texas, 2008.

(8) Reynolds, A. J.; Verheyen, T. V.; et al. Monoethanolamine Degradation during Pilot-Scale Post-Combustion Capture of CO2 from a Brown Coal-Fired Power Station. *Energy Fuels* **2015**, *29* (11), 7441–7455. https://doi.org/10.1021/acs.energyfuels.5b00713.

(9) Moser, P.; Wiechers, G.; et al. Results of the 18-Month Test with MEA at the Post-Combustion Capture Pilot Plant at Niederaussem – New Impetus to Solvent Management, Emissions and Dynamic Behaviour. *International Journal of Greenhouse Gas Control* **2020**, *95*, 102945. https://doi.org/10.1016/j.ijggc.2019.102945.

(10) Buvik, V.; Høisæter, K. K.; et al. A Review of Degradation and Emissions in Post-Combustion CO2 Capture Pilot Plants. *International Journal of Greenhouse Gas Control* **2021**, *106*, 103246. https://doi.org/10.1016/j.ijggc.2020.103246.

(11) Pearson, P.; Cousins, A. Assessment of Corrosion in Amine-Based Post-Combustion Capture of Carbon Dioxide Systems. In *Absorption-Based Post-combustion Capture of Carbon Dioxide*; Elsevier, 2016.

(12) Rieder, A.; Unterberger, S. EnBW's Post-Combustion Capture Pilot Plant at Heilbronn–Results of the First Year's Testing Programme. *Energy Procedia* **2013**, *37*, 6464–6472. https://doi.org/10.1016/j.egypro.2013.06.576.

(13) Khakharia, P.; Mertens, J.; et al. Online Corrosion Monitoring in a Postcombustion CO_2 Capture Pilot Plant and Its Relation to Solvent Degradation and Ammonia Emissions. *Ind. Eng. Chem. Res.* **2015**, *54* (19), 5336–5344. https://doi.org/10.1021/acs.iecr.5b00729.

(14) Dhingra, S.; Khakharia, P.; et al. Understanding and Modelling the Effect of Dissolved Metals on Solvent Degradation in Post Combustion CO2 Capture Based on Pilot Plant Experience. *Energies* **2017**, *10* (5), 629. https://doi.org/10.3390/en10050629.
(15) Voice, A. K.; Rochelle, G. T. Inhibitors of Monoethanolamine Oxidation in CO_2 Capture Processes. *Ind. Eng. Chem. Res.* **2014**, *53* (42), 16222–16228. https://doi.org/10.1021/ie500996z.
(16) Bedell, S. A. Oxidative Degradation Mechanisms for Amines in Flue Gas Capture. In *Energy Procedia*; Elsevier, 2009; Vol. 1, pp 771–778. https://doi.org/10.1016/j.egypro.2009.01.102.
(17) Goff, G. S. Oxidative Degradation of Aqueous Monoethanolamine in CO2 Capture Processes: Iron and Copper Catalysis, Inhibition, and O2 Mass Transfer. Doctoral thesis, 2005.
(18) Billet, R.; Schultes, M. Prediction of Mass Transfer Columns with Dumped and Arranged Packings: Updated Summary of the Calculation Method of Billet and Schultes. *Chemical Engineering Research and Design* **1999**, *77* (6), 498–504. https://doi.org/10.1205/026387699526520.
(19) Mathew T. Derichsweiler. Development and Application of Mass Transfer Correlations for CO2 Absorption in Packed Columns., Texas A&M University, 2020.
(20) Reynolds, A. J.; Verheyen, T. V.; et al. Primary Sources and Accumulation Rates of Inorganic Anions and Dissolved Metals in a MEA Absorbent during PCC at a Brown Coal-Fired Power Station. *International Journal of Greenhouse Gas Control* **2015**, *41*, 239–248. https://doi.org/10.1016/j.ijggc.2015.07.004.
(21) 7 - Corrosion Modeling in Lean and Rich Amine Systems. In *Corrosion in Amine Treating Units (Second Edition)*; van Roij, J., Ed.; European Federation of Corrosion (EFC) Series; Woodhead Publishing, 2022; pp 55–66. https://doi.org/10.1016/B978-0-323-91549-6.00007-1.
(22) Billingham, M. A.; Lee, C.-H.; et al. Corrosion and Materials Selection Issues in Carbon Capture Plants. *Energy Procedia* **2011**, *4*, 2020–2027. https://doi.org/10.1016/j.egypro.2011.02.083.
(23) Gunasekaran, P.; Veawab, A.; et al. Corrosivity of Amine-Based Absorbents for CO2 Capture. *Energy Procedia* **2017**, *114*, 2047–2054. https://doi.org/10.1016/j.egypro.2017.03.1339.
(24) Kittel, J.; Gonzalez, S. Corrosion in CO2 Post-Combustion Capture with Alkanolamines – A Review. *Oil Gas Sci. Technol. – Rev. IFP Energies nouvelles* **2014**, *69* (5), 915–929. https://doi.org/10.2516/ogst/2013161.
(25) Kladkaew, N.; Idem, R.; et al. Corrosion Behavior of Carbon Steel in the Monoethanolamine−H2O−CO2−O2−SO2 System: Products, Reaction Pathways, and Kinetics. *Ind. Eng. Chem. Res.* **2009**, *48* (23), 10169–10179. https://doi.org/10.1021/ie900746g.
(26) Saiwan, C.; Supap, T.; et al. Part 3: Corrosion and Prevention in Post-Combustion CO_2 Capture Systems. *Carbon Management* **2011**, *2* (6), 659–675. https://doi.org/10.4155/cmt.11.63.

(27) Stergioudi, F.; Baxevani, A.; et al. Corrosion Behavior of Stainless Steels in CO2 Absorption Process Using Aqueous Solution of Monoethanolamine (MEA). *CMD* **2022**, *3* (3), 422–438. https://doi.org/10.3390/cmd3030025.
(28) Cousins, A.; Ilyushechkin, A.; et al. Corrosion Coupon Evaluation under Pilot-Scale CO2 Capture Conditions at an Australian Coal-Fired Power Station. *Greenhouse Gases: Science and Technology* **2013**, *3* (3), 169–184. https://doi.org/10.1002/ghg.1341.
(29) Hjelmaas, S.; Storheim, E.; et al. Results from MEA Amine Plant Corrosion Processes at the CO2 Technology Centre Mongstad. *Energy Procedia* **2017**, *114*, 1166–1178. https://doi.org/10.1016/j.egypro.2017.03.1280.
(30) Tanthapanichakoon, W.; Veawab, A.; et al. Electrochemical Investigation on the Effect of Heat-Stable Salts on Corrosion in CO_2 Capture Plants Using Aqueous Solution of MEA. *Ind. Eng. Chem. Res.* **2006**, *45* (8), 2586–2593. https://doi.org/10.1021/ie050575a.
(31) Fytianos, G.; Ucar, S.; et al. Corrosion and Degradation in MEA Based Post-Combustion CO2 Capture. *International Journal of Greenhouse Gas Control* **2016**, *46*, 48–56. https://doi.org/10.1016/j.ijggc.2015.12.028.
(32) Fischer, K. Corrosion of Stainless and Carbon Steel in Aqueous Amine for CO2 Capture. Doctoral thesis, The University of Texas at Austin, 2019.
(33) Kittel, J.; Fleury, E.; et al. Corrosion in Alkanolamine Used for Acid Gas Removal: From Natural Gas Processing to CO2 Capture. *Materials and Corrosion* **2012**, *63* (3), 223–230. https://doi.org/10.1002/maco.201005847.
(34) Billet, R.; Schultes, M. A Physical Model for the Prediction of Liquid Hold-up in Two-Phase Countercurrent Columns. *Chemical Engineering & Technology* **1993**, *16* (6), 370–375. https://doi.org/10.1002/ceat.270160603.
(35) Towler, G.; Sinnott, R. Chapter 19 - Heat-Transfer Equipment. In *Chemical Engineering Design (Second Edition)*; Towler, G., Sinnott, R., Eds.; Butterworth-Heinemann: Boston, 2013; pp 1047–1205. https://doi.org/10.1016/B978-0-08-096659-5.00019-5.
(36) Vevelstad, S. J.; Johansen, M. T.; et al. Extensive Dataset for Oxidative Degradation of Ethanolamine at 55–75°C and Oxygen Concentrations from 6 to 98%. *International Journal of Greenhouse Gas Control* **2016**, *50*, 158–178. https://doi.org/10.1016/j.ijggc.2016.04.013.
(37) da Silva, E. F.; Lepaumier, H.; et al. Understanding 2-Ethanolamine Degradation in Postcombustion CO_2 Capture. *Ind. Eng. Chem. Res.* **2012**, *51* (41), 13329–13338. https://doi.org/10.1021/ie300718a.
(38) *GPSA Engineering Data Book*, 12th ed.; Gas Processors Suppliers Association, 2004.
(39) Léonard, G.; Voice, A.; et al. Influence of Dissolved Metals and Oxidative Degradation Inhibitors on the Oxidative and Thermal Degradation of Monoethanolamine in Postcombustion CO_2 Capture. *Ind. Eng. Chem. Res.* **2014**, *53* (47), 18121–18129. https://doi.org/10.1021/ie5036572.
(40) Fytianos, G.; Vevelstad, S. J.; et al. Degradation and Corrosion Inhibitors for MEA-Based CO2 Capture Plants. *International Journal of Greenhouse Gas Control* **2016**, *50*, 240–247. https://doi.org/10.1016/j.ijggc.2016.05.003.

(41) Fytianos, Georgios. Corrosion and Degradation in Amine Based Post-Combustion CO2 Capture. Doctoral thesis, Norwegian University of Science and Technology, Trondheim, 2016.
(42) Stenså, A. A.; Knuutila, H. K. Solubility of Metal Ions in 30wt% MEA (Aq.) and Their Influence on Oxidative Degradation. Thesis, Norwegian University of Science and Technology, 2023.
(43) Flø, N. E.; Faramarzi, L.; et al. Results from MEA Degradation and Reclaiming Processes at the CO2 Technology Centre Mongstad. *Energy Procedia* **2017**, *114*, 1307–1324. https://doi.org/10.1016/j.egypro.2017.03.1899.
(44) Closmann, F. B. Oxidation and Thermal Degradation of Methyldiethanolamine/Piperazine in CO2 Capture. Doctoral thesis, University of Texas Austin, 2011.
(45) Hatta, S. Tohoku Imperial University Technical Reports; 10; 1932; p 119.

Chapter 8: Conclusions and Future Research

This thesis focused on the development of kinetic degradation models to describe solvent degradation in amine-based CO_2 capture plants. The work predominantly involved models for 30 wt% aqueous MEA, as it is one of the most well-studied and characterized solvents in the field. In this chapter, a general overview of the conclusions is given, but a more detailed discussion can be found at the end of the respective chapters.

In chapters 2 and 3, a kinetic model was successfully developed to predict the thermal degradation of MEA. The degradation model was found to have an average relative deviation of 17.5%, most of which was caused by uncertainty in the experimental data. As such, an increase in model parameters had a limited effect on the performance of the model, and a reduced experimental uncertainty is required to improve its accuracy. This can be achieved by more detailed reporting of experimental conditions, measured or expected uncertainties, and solvent composition, both initially and during the experiment. Overall, the degradation model made sensible predictions for the formation and consumption of reaction intermediates and products, with trends that are in agreement with experimental observations. The concentrations of some degradation products deviate significantly from measurements in cyclic systems, indicating that interactions between oxidative and thermal mechanisms are most likely at play. These interactions should be studied in more detail in future experiments.

Chapters 4 and 5 focused on the development of an oxidative degradation model for MEA and the evaluation of degradation in various carbon capture processes. The use of agitated bubble reactors to measure oxidative degradation was discussed and the mass transfer coefficient of O_2 in these reactors was estimated. The results showed that mass transfer resistances play an important role and may limit degradation rates, especially at higher temperatures or in the presence of dissolved metals that catalyze degradation. In addition, the influence of CO_2 loadings on the solubility of O_2 was found to significantly influence the predicted degradation rates. Therefore, it is important to consider these effects when developing degradation models and using experimental data to make predictions in the actual process, where the exposure conditions and role of mass transfer limitations can differ.

Considering these effects, an oxidative degradation model for MEA was developed, and, combined with the thermal degradation model, solvent degradation was predicted in typical capture processes. This evaluation showed that most of the amine was consumed through oxidative degradation, which was most prevalent in the absorber packing. The composition of the flue gas has an important influence on the degradation rates and distribution throughout the process. An increase in CO_2 content will lead to increased absorber temperatures, resulting in higher degradation rates. An increase in O_2 concentration, on the other hand, will result in a higher concentration of dissolved O_2 in the rich solvent that causes more indirect oxidation upon heating in the heat exchanger.

Absorber intercooling is found to be one of the most effective mitigation strategies, as long as it can be realized without significantly increasing solvent residence times in the absorber. Dissolved O_2 removal can be a viable mitigation strategy, but its effectiveness depends on the initial contribution of indirect oxidation and the residence time and temperature of the solvent before removal. A reduction in solvent residence times only resulted in reduced thermal degradation and had a limited effect on the overall degradation. The catalytic effect of dissolved metals is anticipated to primarily increase degradation rates in the absorber packing and the effectiveness of intercooling is expected to increase in case catalytic degradation occurs.

Absorption-based capture processes that operate at higher capture efficiencies are expected to experience increased solvent degradation. This is caused by increased oxidative degradation, as a result of an increased packing height or solvent flow rate, and by increased thermal degradation, when higher stripper temperatures are required to obtain lower lean loadings. The discussed process modifications aimed at reducing degradation, such as absorber intercooling or a reduction in stripper and reboiler residence time, can help to limit the extent of degradation in high-efficiency capture processes.

Chapter 6 discussed the design, construction, testing, and initial operation of a new type of degradation reactor that aims to address the shortcomings of agitated bubble reactors and provide data to develop more accurate degradation models. Experiments in the new reactor showed that oxidative degradation rates were significantly higher than those observed in agitated bubble reactors at identical temperatures and gas compositions. This is expected to be caused by lower mass transfer resistances in the new reactor resulting in higher concentrations of O_2 in the solvent. However, traces of metal impurities were found in the analyzed solvent samples, which could have catalyzed the degradation reaction, despite their low concentrations. Therefore, a more thorough cleaning of the setup is recommended to prevent contamination in future experiments.

Oxidative degradation experiments could be run at stable conditions for extended periods and both solvent degradation and the production of degradation products could be quantified. Water loss was significant and, despite good quantification using a potassium carbonate tracer, improvements that limit the extent of water loss are recommended. Promising results were obtained when using inerts to test the thermal loop, which serves the purpose of also exposing the solvent to thermal degradation. However, operational challenges were encountered when solvent was introduced. These challenges should be addressed with some minor modifications and the combined oxidative and thermal degradation should be studied in more detail. In addition, the effect of the concentration of metals on the oxidative degradation rate should be studied through the controlled addition of metals.

Chapter 7 focused on different aspects related to the role of dissolved iron in capture processes. An overview was presented of the available data in the literature on the

catalytic effect of iron on degradation, as well as on the influence of the concentration of degradation products and HSS on the corrosion rates and iron solubility. Several hypothetical scenarios that describe the presence and role of iron were proposed and investigated using models developed based on the available data in the literature. None of these scenarios can fully describe the observed behavior in pilot plants alone but a combination of several scenario models is able to reproduce profiles and trends in pilot plants. The effect of the concentration of HSS on corrosion rates and iron solubility, as well as mass transfer limited degradation rates in the absorber packing, are expected to play a role. More research is required to gain a better understanding of these effects and quantify them to develop models that can be used in the framework.

Overall, it has proven challenging to develop a degradation framework that can capture the many complexities related to solvent degradation in absorption-based capture processes. Although this work has provided insight into the distribution of degradation in processes and the effect of various process modifications and mitigation strategies, more research and experimental studies are required to better capture these complexities and describe the mechanisms at play in the capture plant. The development of accurate degradation models for other solvents or blends, whose degradation has been studied to a lesser extent than MEA, the case study solvent for this work, will prove challenging, and the predictive accuracy of these models will be limited. The characterization of these solvents should be performed thoroughly and with both process conditions and model development requirements in mind.

ISBN 978-82-326-7708-5 (printed ver.)
ISBN 978-82-326-7707-8 (electronic ver.)
ISSN 1503-8181 (printed ver.)
ISSN 2703-8084 (online ver.)

NTNU

Norwegian University of
Science and Technology